Structural Diversity in Antibody Interactions with HIV-1 Env Immunogens

Thaddeus M. Davenport

A dissertation
submitted in partial fulfillment of the
requirements for the degree of:

Doctor of Philosophy

University of Washington
2013

Reading Committee:
Kelly K. Lee, Chair
Jaisri Lingappa
Shiu-Lok Hu

Program Authorized to Confer Degree:
Pathobiology

University of Washington

Abstract

Structural Diversity in Antibody Interactions with HIV-1 Env Immunogens

Thaddeus M. Davenport

Chair of the Supervisory Committee:
Asst. Professor Kelly K. Lee
Medicinal Chemistry

Due to the impressive diversity of human immunodeficiency virus type 1 (HIV-1), control of the HIV-1 pandemic will likely depend on the design of a vaccine that can elicit broadly neutralizing antibodies (bNAbs) that can prevent transmission of diverse HIV-1 isolates. Although bNAbs have been observed in HIV-infected individuals, we are currently unable to elicit them through vaccination. The difficulty associated with eliciting broadly reactive antibodies is rooted in the exceptional sequence, structural, and conformational diversity of the HIV-1 Envelope glycoprotein (Env), the sole target of neutralizing antibodies. In addition, we have an incomplete understanding of the factors that govern Env-antibody interactions, and we are poorly equipped to rationally manipulate these interactions in order to obtain desired antibody specificities through vaccination. This thesis explores structural heterogeneity in purified soluble Env immunogens and the antibodies that recognize them, in order to understand how structural diversity – generated through post-translational modifications or conformational flexibility – impacts Env-antibody interactions.

First, I measured soluble Env ectodomain immunogen binding to the antibodies PG9 and PG16, which were reported to preferentially recognize the native Env trimer. I tested the impact of glycosylation, proteolysis, and oligomerization state on exposure of the PG9/PG16 epitope and demonstrated that PG9/PG16 are less specific for the native trimer than previously reported. Next, I used small angle x-ray scattering (SAXS) and hydrogen-deuterium exchange with mass spectrometry (HDX-MS) to characterize the solution structure and conformational

dynamics of soluble monomeric gp120 Env proteins from four diverse HIV-1 isolates. This work showed that while the overall subunit morphology is similar among diverse gp120 proteins, there are distinct differences in conformational dynamics. I observed that more dynamic gp120 proteins were poorly recognized by conformation-dependent antibodies. Finally, to examine the potential influence of antibody conformational dynamics on Env recognition, I measured changes in antibody paratope stability over the course of affinity maturation for the bNAbs VRC03 and VRC26, which target the CD4-binding site and a V2-quaternary epitope, respectively. I observed that paratope stability does not increase uniformly or linearly over the course of affinity maturation for either antibody, although germline antibodies were relatively more dynamic than mature antibodies. Altogether, this work provides useful insight into the structural heterogeneity of purified Env immunogens and the role of conformational dynamics in modifying Env-antibody interactions. These data suggest that targeted stabilization may facilitate rational manipulation of Env-antibody interactions during vaccination.

Table of Contents

Table of Figures

List of Tables

Acknowledgements

Thank you to:

Kelly Lee for being an incredible advisor and an exceptionally wise human being. I've learned so much from you about science, the practice of research, clarity in communication through images and words, how to interact with other researchers and people in general, and how to appreciate (and perhaps even enjoy) the challenges associated with scientific research (and other somewhat frustrating endeavors). These are valuable skills that I will carry with me throughout the rest of my life.

Leo Stamatatos, who taught me an enormous amount about the field of HIV. He had the unenviable task of introducing me to the world of "real" scientific research, so I apologize for any difficulty or irreversible hair loss that experience may have caused him. I am, without a doubt, a better person as a direct result of the time I spent in the Stamatatos lab. Thank you, Leo, Zane, George, Noah, and Zach for being great teachers.

My committee members: Jaisri Lingappa, Michael Emerman, Shiu-Lok Hu, Bill Atkins, Nancy Maizels, and (unofficially) Julie Overbaugh who was a valuable source of support throughout graduate school. Thank you to Jais and Shiu-Lok for taking the time to read through my thesis. Thank you, Jais, for helping me to become a better writer. Thank you Michael and Jais for being exceptional professors; you have a real skill for teaching. Thank you for finding that skill, and thank you for using your life to improve the lives of your students.

Lee Ann Campbell, Rachel Reichert, and the Pathobiology Program for your help in navigating graduate school and for working so hard on behalf of the students.

Peggy Daugherty and Sunhee Choi, my research and academic advisors at Middlebury College, respectively. Peggy provided such a wonderful, nurturing environment for developing my curiosity, and Sunhee Choi taught me to believe in myself, to “be committed” like the ham on the breakfast plate, and to appreciate the colorful world around me. Thank you to all of the great chemistry/biochemistry professors at Middlebury College: Roger Sandwick, Rick Bunt, Jeff Byers, Steve Sontum, Jim Larrabee, Bob Cluss, and Steve Oster.

My lab-mates: Natalie Garcia, Long Gui, James Williams, Mike Guttman, Yu Liang, Javier Aguilera, and Jamie Ebner. Special thank you to Mike for being so patient in teaching me everything I know about mass spectrometry. Thank you to lab-neighbor Ryan Seguin for his inspirational quotes and his feedback on my new inventions. These people all feel like family, and I feel lucky to have gotten to meet such good, interesting, and funny people along the way.

My classmates: Leslie Goo, Maxwell Majiwa-Omenda, Melanie Gasper, Sara Murray, Jess Brownell, Alison Kell, and Tara Brinck who have been great company throughout graduate school.

My greatest friends: Eli Berman, Hayden Thomsen, Matt Griswold, Loren Bienvenu, Miles Farmer, and Brooks Saucedo-McQuade. You are some of the funniest people I have ever met. Thank you for helping me explore the world.

Seattle housemates: John Compton, Julia Hon, Bonnie Strelitz, JJ Stein, JigHan Jeong, Joe Meredith, Kyle Minch, Emily Knouf, Kate Souza, Nisha Duggal, and Leslie Goo who have made Seattle such a wonderful place to live.

Leslie Goo, who, as I have said before, and will maintain as long as I am able, is responsible for my finishing graduate school. You inspire me to be a good human being (you are one of the best ones I know). Thank you for being my best friend. Thank you for fighting for me - sometimes fighting for me against me, as I resist change and new things.

My grandparents: David, Fran, Pops, Effie, and Kim. Thank you for leading the way, and for teaching me about cowboys, carpentry, red light-green light, and card games. I would like to thank my grandma, Effie Kimball, who very generously gave me the opportunity to go to Middlebury College. This allowed me the freedom to explore the things that interested me, and I almost certainly could not have reached this point without your support. Thank you also to Mary Moreno, who treated me as her *jito* and who is a living example of the patience, compassion, and love that are frequently discussed but rarely achieved in a life's work.

My family: Dave, Beth, Davey, and Abby Davenport who taught me how to be a human. Thank you for encouraging me to be myself and nothing more, for inspiring my curiosity in the natural world, and for guiding me through the confusion of life. You are angels, and I love you all endlessly. Never doubt that you have changed the world.

Dedication

To my wonderful parents who
Taught me to
Shower, Measure, Cut,
Focus, Listen, Observe
And Breathe.

Introduction

Overview:

Human immunodeficiency virus (HIV), the causative agent of acquired immunodeficiency syndrome (AIDS), was discovered in 1983 (1, 2), following reports of unusual clusters of opportunistic infections in seemingly healthy demographic groups (3, 4). In the time since the virus' discovery, over 70 million people have become HIV-infected, and 35 million have died as a result of AIDS-related complications (5). There are currently around 35 million people living with HIV worldwide (5). As a result of a concerted, global effort to stem the pandemic through education and increased access to anti-retroviral therapy (ART), the incidence of new HIV infections has fallen from 3.4 million in 2001 to 2.3 million in 2012 (5). As will be reviewed in the following paragraphs, there are limitations to these strategies, and successful control of the HIV pandemic will likely depend on novel interventions, among which, an effective HIV vaccine is of the highest priority. The design of a vaccine that is capable of preventing transmission of diverse HIV-1 isolates has been complicated by the enormous global diversity of HIV, our limited understanding of the detailed structural differences among isolates, and our poor understanding of the molecular processes that determine immunogenicity. At its very essence, the goal of vaccine design is to educate the immune system to recognize and bind to foreign antigens with high affinity. All macromolecular interactions are governed by the same forces, but the interactions at the core of antibody-based HIV vaccine design – between antibodies and the HIV-1 Envelope glycoprotein – are distinguished by the unique structural diversity of the molecules involved. This thesis is focused on understanding how structural diversity – within HIV and the humoral immune response that counteracts it – impacts antibody recognition of HIV and immunogens designed to elicit protective immunity against the virus.

Virion Structure:

Based on its life cycle, virion structure, genome structure, and characteristically slow pathogenesis, HIV is categorized as a lentivirus within the retrovirus family (6). It is an enveloped virus that carries two copies of a positive-stranded RNA genome. Because of the possibility that these two copies may not be identical as a result of error-prone replication or co-infection of a single cell by two viruses, HIV is often described as having a "pseudo-diploid" genome (7). Like other retroviruses, HIV possesses genes that code for structural proteins (Gag), replication enzymes (Pol), and a surface protein required for cell entry (Env). Gag is cleaved post-translationally in the budded virion by the viral protease to generate the membrane-associated matrix protein (MA, p17), the capsid protein (CA, p24), which condenses to form the conical shell containing the viral RNA, the nucleocapsid protein (NC, p7) which coats the viral RNA, and the p6 protein, which appears to play a critical role in virus budding and release (8). Similarly, the poly-protein encoded by the Gag-Pro-Pol transcript, and which contains the viral protease (Pr) undergoes auto-proteolysis to produce the RNA-dependent DNA polymerase known as reverse transcriptase (RT), the protease itself (PR), and the integrase enzyme (IN), which facilitates integration of the viral cDNA genome into the host genome (9). The Env gene product is also translated as a pre-protein, which is cleaved post-translationally by the cellular protease, furin, to produce the gp120 surface protein and the gp41 transmembrane protein (10-13). It is estimated that there are roughly 10-20 Env spikes on the surface of each virus particle (14). The Env glycoprotein is central to the work presented in this thesis, and will be discussed in greater detail below. In addition to these central proteins, HIV possesses a number of accessory genes including Tat, Rev, Nef, Vif, Vpr, and Vpu, which are required for productive infection in humans (15, 16). All of these viral proteins, with the exception of Tat, Rev, and Vpu are incorporated into the mature virus particle (8).

Structural Overview of HIV-1 Envelope Glycoprotein (Env):

HIV-1 Env exists as a trimer of non-covalently associated gp120-gp41 heterodimers on the virus surface (17-19). Env plays a central role in the viral lifecycle and HIV-1 vaccine design because it is required for viral entry into the host cell (20), and it is also the sole target of HIV-1 neutralizing antibodies (nAbs) (11, 21). Env mediates viral entry following sequential interactions with the virus receptor, CD4, and co-receptor, commonly CCR5 or CXCR4 (20). Interactions between gp120 and CD4/CCR5 trigger a conformational change in Env, which exposes the metastable pre-fusion gp41 transmembrane subunit. Subsequently, the gp41 fusion peptide inserts into the host cell membrane, and a large-scale, highly-favorable refolding event in gp41 leads to the formation of a stable, post-fusion six-helix bundle, which drives fusion of the host and virus membranes (22). It is likely that more than one Env trimer is necessary for this process, but it is unknown exactly how many spikes are required to efficiently open a fusion pore (23, 24).

The gp120 surface subunit exhibits the most diversity of any gene in the HIV-1 genome, and most of this sequence diversity is concentrated within five hypervariable regions (V1-V5), which protrude from five relatively conserved sequences (C1-C5) that fold together to form the gp120 core (18, 25, 26). With the exception of V3, the variable loops are heavily glycosylated. Loops V1/V2 and V3 occupy density at the crown of the Env trimer where they likely participate in inter-subunit quaternary interactions (27-30). Loops V4 and V5 are thought to project away from the trimer's three fold axis, shielding conserved elements of the Env trimer (18, 19). The gp120 core contains nine highly-conserved disulfide bonds (31), which direct folding of the gp120 core into two distinct domains: a relatively conserved inner domain, composed of three mobile "layers" protruding from a seven-stranded beta sandwich at the base of gp120, and a conformationally inert outer domain, which is heavily glycosylated (25) (Figure 1). The domains are named according to their hypothesized positions in the mature trimer. The inner domain faces the center of the spike and interacts with gp41, while the outer domain faces outward and

would be vulnerable to neutralizing antibodies, but for its dense glycosylation (18). A third "micro-domain", known as the bridging sheet, forms upon CD4 binding. This CD4-induced structure is a four-stranded antiparallel beta sheet made up of strands beta 2 and 3 in the V1/V2 stem protruding from the inner domain and beta strands 20 and 21, which are proximal to the CD4-binding site on the gp120 outer domain (25). The CD4 binding site is a conformational epitope within gp120 that involves residues from the inner and outer domains as well as the bridging sheet (18, 25). Similarly, the co-receptor binding site is a highly conserved conformational epitope involving elements of V3 and the bridging sheet that is only briefly exposed following the CD4-induced conformational change that leads to bridging sheet formation (18, 25, 36).

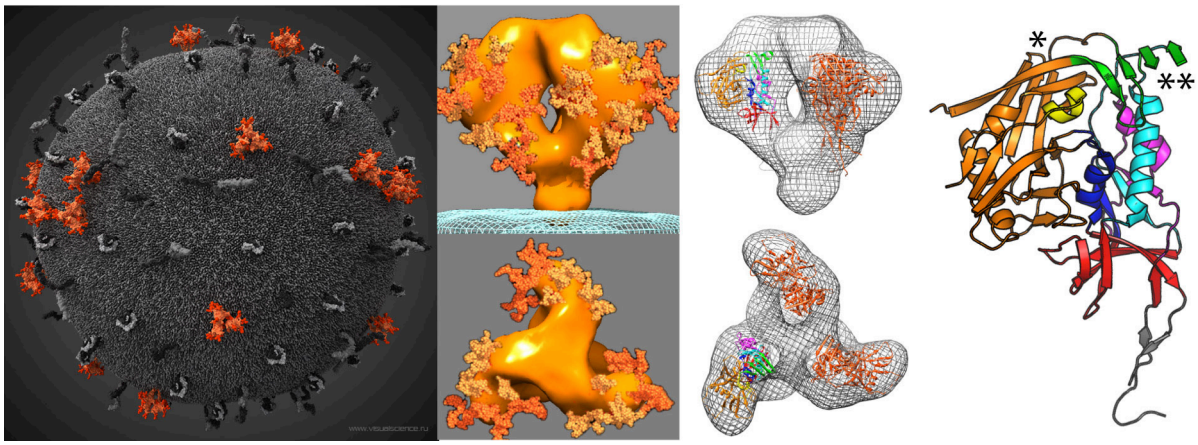

Figure 1. Structural overview of the HIV-1 Envelope Trimer. Model of an HIV-1 virion with Env trimers highlighted in orange from www.visualscience.ru (32)(left panel). Side (top center panels) and top (bottom center panels) views of the Env trimer observed by cryo-electron tomography (33). The approximate position of gp120 core glycans in the context of the trimer are modeled according to (34)(orange, left center panels). The x-ray crystal structure of gp120 core with N and C-terminal extensions (PDB 3JWD) (35) is docked into the density of the Env trimer (33). Two gp120 subunits are colored orange, and one is colored to match the structure on the right (gray mesh, center-right panels). The PDB 3JWD structure is colored to highlight the N- and C-termini (gray), 7-stranded beta sandwich (red), layers 1, 2, and 3 of the inner domain (pink, cyan, and blue, respectively), bridging sheet (green), CD4-binding loop (yellow), gp120 outer domain (orange) (right panel). The position of the V1/V2 and V3 loops, which are absent from the structure are indicated with the asterisks (** and *, respectively). These variable loops likely occupy the empty density at the top of the trimer within its three-fold axis (28), as shown in the center-right panels.

The pre-fusion structure of the gp41 transmembrane subunit is poorly understood. The only crystallographic data that is available for this region is from a post-fusion six-helix bundle containing the N- and C-terminal gp41 helices (37), which likely adopt a distinct conformation in the pre-fusion structure of gp41 (38). These helices are separated by a disulfide-linked, glycosylated loop, known as the immunodominant loop of gp41. Two regions of gp41 have a preponderance of hydrophobic amino acid residues, which facilitate membrane interactions: the fusion peptide proximal region (FPPR) at the N-terminus of gp41, just downstream of the furin cleavage site, and the membrane proximal external region (MPER) just prior to the gp41 transmembrane helix (13). The cytoplasmic tail of gp41 is quite long, and likely interacts with the matrix (p17) layer beneath the membrane. Truncations of the cytoplasmic tail alter levels of Env expression on the virus surface and Env sensitivity to neutralizing antibodies (13). As will be discussed in depth below, the Env glycoprotein is structurally heterogenous, which makes it a challenging target for the humoral immune system, structural study, and HIV-1 vaccine design.

Strategies for the Control of HIV-1

Antiretroviral Therapy, Low-Tech Interventions, and The Need for a Vaccine:

In contrast to Env, the Pol gene products - reverse transcriptase, protease, and integrase - are quite well conserved (39). Small molecule inhibitors of these enzymes, broadly grouped under the umbrella of antiretroviral therapy (ART), have been incredibly effective in controlling viremia, extending the lifespan and improving the quality of life for HIV-infected individuals (40). Anti-retroviral therapy administered to the infected individual, and to the uninfected partner of an HIV-infected individual, has also proven to be effective in limiting transmission (41-46). In combination with low-technology interventions such as male circumcision (47), education, counseling, and condom usage, ART has played a critical role in limiting the spread of the HIV-1 pandemic (5). These strategies are not perfect: circumcision,

education, and condom usage are only as effective as the level of participation, and even with complete participation, these methods are not completely effective in blocking transmission (43, 48). Additionally, ART is expensive and not everyone who needs it has access to it (5). There are also issues with drug resistance (49), and toxicity as a result of prolonged use (50). These issues become especially complex in considering the use of ART in pre-exposure prophylaxis. Can we justify providing ART to healthy people when HIV-infected individuals do not have access? What amount of toxicity is tolerable for preventing progression to AIDS? What amount of toxicity is tolerable for a healthy individual who may never become infected?

All of these considerations highlight the need for novel interventions against HIV. Among the many possible strategies, it is believed that an effective vaccine will be critical in halting the HIV-1 pandemic. This belief is rooted in the success of vaccines against other viral pathogens, including poliovirus (51), measles (52), and human papilloma virus (53), among others. One major advantage to immunization is that, in contrast to pre-exposure prophylaxis with ART, which would require life-long adherence, immunization, at its best, would require only one or a few administrations to achieve life-long protection. An effective vaccination series against HIV could be highly cost-effective, replacing potential costs of life-long ART, hospital fees, as well as drugs to manage the toxicity of long-term ART usage (54). This consideration is not irrelevant, given that the burden of the HIV pandemic is disproportionately placed on developing countries. It is, therefore, a central priority to identify, through rational design or empirical testing, a vaccine that is capable of eliciting protective immunity against the enormously diverse pool of global HIV-1 variants.

HIV-1 Vaccine Design:

Although there is still no effective vaccine against HIV-1, human clinical trials have provided valuable information about the type of immune response that will be required of an effective vaccine. Because live-attenuated HIV-1 vaccines are thought to be unsafe, and whole-

inactivated HIV-1 vaccine showed little efficacy in non-human primates, all human clinical trials to date have focused on subunit vaccines (55). In light of early studies, which showed that chimpanzees immunized with recombinant gp120 were protected against infection by both homologous and heterologous HIV-1 isolates (56, 57), two HIV-1 vaccine trials, VAX003 and VAX004 (among others) were designed to test the ability of gp120 proteins to elicit neutralizing antibodies and protect against HIV-1 infection in humans. Although the vaccines elicited nAbs, they provided no protection against infection (58, 59), likely due to the inability of those antibodies to neutralize diverse primary isolates (60, 61). Indeed, the variability of the Env glycoprotein is thought to be a major impediment to the design of an effective antibody-based HIV-1 vaccine. In contrast, T cell-based vaccines have the potential to focus the CD8+ T cell response against functionally conserved epitopes within the HIV-1 genome (39). The Step clinical trial was designed to test the ability of T cells targeting conserved HIV-1 genes – gag, pol, and nef – to protect against HIV-1 infection. While this vaccine was immunogenic, it did not protect against infection, and the clinical trial was stopped early based on evidence that the vaccine increased risk of infection in vaccinees with pre-existing antibodies to the adenovirus serotype 5 (ad5) vector used in the vaccine (62).

The RV144 “Thai Trial” was designed to test the role of cell-mediated immunity in combination with antibodies in protection against HIV-1 infection. This trial made use of a DNA-prime/protein boost strategy, in which, participants were primed with canarypox vectors containing genes for gag, protease, and the gp41 portion of Env, and boosted with monomeric gp120 proteins from clades B and E (63). Although protection was modest (~31%), and the significance of the protection was sensitive to the specific statistical analysis used, it was the first clinical trial to show that it may be possible to elicit protective immune responses against HIV-1 acquisition through vaccination (64). Notably, binding antibodies to the V1/V2 loop of gp120 correlated with protection in RV144, while levels of neutralizing antibodies were similar in protected and non-protected vaccinees (65-67). This observation suggests that both

neutralizing and non-neutralizing (e.g. antibody-dependent cellular cytotoxicity (ADCC)-active) antibody responses may be protective. In the context of previous HIV-1 vaccine studies, the RV144 trial highlights the likely importance of eliciting a balanced immune response that incorporates both humoral and cell-mediated immunity.

The Role of Antibodies in HIV-1 Infection:

The goal of vaccination is to induce long-lasting immunity against a pathogen in the absence of, or while mitigating, symptoms of a true infection. Understanding the immune response to natural infection and other effective vaccines is, therefore, informative for vaccine design. There is substantial evidence that cell-mediated immunity plays a critical role in controlling acute HIV-1 infection and progression to AIDS (68, 69), and a large fraction of HIV vaccine research is devoted to T-cell-based vaccines (70), however, there will be little presented on these topics here. In this thesis and elsewhere, a major focused is placed on antibodies as a critical component of an HIV-1 vaccine for a number of reasons: 1) because HIV-1 is integrated into the host genome and establishes a pool of latently-infected cells that is difficult to clear (71), it would be desirable to prevent infection altogether, and this would only be possible through neutralizing antibodies; 2) passive immunization of non-human primates with neutralizing antibodies can prevent SHIV (an HIV-1 Env gene in an SIV genome backbone) infection (72-75); 3) high antibody titers are the primary correlate of protection in most licensed vaccines against other viral pathogens (76); and 4) binding antibodies against HIV-1 Env V1/V2 were correlated with the modest protection observed in the RV144 trial (65).

Antibodies are elicited against nearly all HIV-1 gene products during natural infection, but only Env-specific antibodies are capable of blocking HIV-1 entry (77). There is evidence that antibodies may exert selective pressure on the infecting HIV-1 population as early as two weeks post-infection (78). The earliest measurable anti-Env antibodies are typically non-neutralizing antibodies targeting gp41, which emerge at roughly four weeks post-infection. Neutralizing

antibodies appear to develop more slowly, reaching measurable levels at around ten weeks of infection (79). Although these antibodies may effectively neutralize the infecting HIV-1 isolate (also known as the "autologous" virus), they are typically unable to recognize antigenically diverse - so-called "heterologous" – isolates that the immune system has not previously encountered (79).

While nearly all HIV-infected individuals develop autologous neutralizing antibodies, only 10-20% of infected individuals will develop "broadly neutralizing antibodies" (bNAbs) that are capable of neutralizing heterologous isolates (80, 81). These antibodies target structurally-conserved epitopes on HIV-1 Env and typically only develop after 2-3 years of infection (80). In most cases, broad serum neutralizing activity can be attributed to a single bNAb specificity (81). The development of breadth is associated with high viral load and viral diversity within the infected host (82-86), and recent evidence suggests that features of the infecting virus and its evolutionary trajectory may contribute to the development of bNAb specificities (87). Thus, prolonged exposure to diverse antigenic structures seems to be critical for bNAb development. In light of the enormous global diversity of HIV-1 (discussed below), it is believed that a truly effective antibody-based vaccine against HIV-1 would need to elicit bNAbs, and it is of great interest to understand the factors that contribute to bNAb development.

Antibody-Based Protection Against HIV-1 Transmission:

In agreement with the ease of Env escape from neutralizing antibodies (88-91), most evidence indicates that even broad and potent nAbs do not control viral replication or delay disease progression in patients who develop such responses (92-95). The inability of antibodies to control viral replication is likely due to the late development of antibody responses - after the establishment of a pool of latently infected cells and substantial viral diversification as a result of weeks of error prone replication in the infected host, which complicate viral clearance and facilitate immune escape. In contrast, viral diversity is extremely low in the early stages of

infection, with the majority of infections initiated by a single HIV-1 isolate (96-98). Thus, pre-existing antibodies, such as those elicited through immunization have the potential to block infection, with little opportunity for viral escape.

The potential protective efficacy of pre-existing neutralizing antibodies has been demonstrated clearly in non-human primate models of HIV-1 infection. Chimpanzees immunized with gp120 or passively immunized with nAbs from HIV-infected individuals were protected from HIV-1 infection by the neutralization sensitive isolates HIV-1 IIIB (56, 99). Similarly, rhesus macaques passively immunized with high concentrations of broadly neutralizing antibodies were protected from infection following challenge with chimeric simian-human immunodeficiency viruses (SHIVs) sensitive to neutralization by the same antibodies (73-75). In contrast, macaques immunized with weak or non-neutralizing antibodies were just as likely to become infected following challenge (100). This latter scenario likely reflects the lack of efficacy observed in antibody-based HIV-1 vaccine clinical trials, such as VAX003, in which the antibody response was not sufficiently broad to neutralize, and therefore, prevent the transmission of, diverse circulating isolates. Thus, the enormous diversity of circulating viruses in natural HIV-1 transmission presents an additional challenge not captured in these proof of concept animal models, and a vaccine capable of eliciting high titers of neutralizing antibodies may still be effective in limiting HIV-1 transmission.

Two natural models of vaccination – mother-to-child transmission (MTCT) and superinfection – provide insight into the ability of pre-existing antibodies to protect against the transmission of diverse viral variants. In MTCT, an HIV-infected mother can passively transfer neutralizing antibodies to her infant in utero and during breast-feeding (101), which may prevent the infant from becoming infected by the virus circulating in the mother. There appears to be little impact of passively transferred antibodies on the likelihood of HIV-1 transmission to the infant (101), but viral variants that are transmitted from mother to infant are typically resistant to neutralization by maternal antibodies, which suggests that these antibodies limit transmission

and select against neutralization sensitive viruses (102). Similarly, in superinfection, an HIV-infected individual develops antibodies against the infecting virus, and these antibodies have the potential to prevent transmission of a second isolate to the same individual. Recent work suggests that primary HIV-1 infection reduces the likelihood of superinfection (103), although it remains uncertain whether this partial protection is antibody-mediated (104-106). Thus these two natural models of vaccination provide evidence that pre-existing antibodies may be effective in limiting transmission of diverse HIV-1 isolates. However, because protection is incomplete in these settings, these models further illustrate that if an antibody-based vaccine is to be truly effective in preventing infection, it must elicit antibodies with sufficient potency and breadth to prevent transmission of diverse isolates at even low antibody titers.

HIV-1 Immune Evasion Strategies:

In spite of the host immune responses described above, HIV is a highly effective pathogen. Its success depends critically on its slow pathogenesis, which is characteristic of other lentiviruses, and its facile evasion of host immunity (6). For many pathogens, the disease state is linked to transmission, and this is true for HIV as well. HIV infection is effectively permanent following integration into the host cell genome and the establishment of latency (107, 108), and it has evolved to moderate its pathogenesis and evade host immunity in order to maximize its chances of transmission (71, 109, 110). Whereas a virus that induced rapid onset of disease might prevent an infected individual from interacting with other potential hosts, the long asymptomatic phase of HIV infection increases its likelihood of transmission from an active, long-lived and social carrier.

Active Immune Evasion and Passive Antigenic Drift

In order to persist over the course of a chronic infection HIV must continually evade host immunity. It accomplishes this through both active and passive mechanisms of evasion. For

example, HIV actively disrupts host adaptive immune responses by targeting CD4 T-cells for infection and killing (111). Additionally, the HIV accessory proteins Nef, Vif, Vpr, and Vpu facilitate immune evasion by counteracting host restriction factors and down-regulating cellular immune receptors (109). In addition to these active mechanisms of counteracting the host immune response, HIV escapes immune recognition by antigenic drift, a passive process of diversification and selection by the host immune system. This immune evasion strategy, which is common to many pathogens, occurs rapidly in HIV as a result of error-prone replication by reverse transcriptase and RNA pol II and the mutagenic activity of APOBEC3G, which, altogether, yield an error rate of ~3 x 10^{-5} mutations/base pairs/replication cycle, or roughly one incorrect nucleotide for every three HIV genomes in each round of replication (112). Because of the chronic nature of HIV infection, the large number of new virus particles produced every day (estimated to be ~10^{11}), and the constant selective pressure of host immunity, exceptional diversity emerges within the HIV population (113). Bette Korber and colleagues placed this diversity in context, noting that the diversity of HIV-1 Env sequences isolated from an HIV-infected individual at a single time point is greater than the global diversity of all influenza hemagglutinin sequences isolated in a given year (26). This substantial intra-host diversity increases the likelihood that viral variants persist in spite of host adaptive immune responses.

Global HIV-1 Diversity:

Just as HIV diversity within an infected individual poses a challenge to the host adaptive immune response, so does the global diversity of HIV present a challenge for the design of an effective intervention to block transmission of diverse circulating variants. The majority of the ~35 million individuals currently infected with HIV-1 were infected with viruses descended from a single simian immunodeficiency virus (SIVcpz) that was transmitted from the chimpanzee species *Pan troglodytes troglodytes* to humans, likely during the slaughter of a chimpanzee for food sometime before 1930 (114-116). This single transmission event gave rise to the 'main'

group of HIV-1 viruses (HIV-1 group M) that has diversified through error-prone replication into 9 subtypes (A, B, C, D, F, G, H, J, K) and through recombination into over 55 circulating recombinant forms (CRFs) (117). Subsequent, independent cross-species transmission events initiated smaller outbreaks of HIV-1 (groups N, O, and P) (118). In contrast, the less-pathogenic HIV-2 is descended from SIVsm transmitted from sooty mangabeys to humans (118).

The subtypes of HIV-1 group M are now globally distributed in a manner that reflects the founder virus that initiated each regional epidemic (119). The greatest subtype diversity is observed in the Democratic of Congo, which supports the hypothesis that the virus originated in this region (70). Within a given HIV-1 group M subtype, Env amino acid sequence diversity is typically around 17%, however 35% of the *Env* sequence may differ among isolates from two distinct subtypes (26). Korber and colleagues place this level of diversity in context, again, through a comparison with influenza, which exhibits comparatively low levels of sequence diversity in hemagglutinin at around 2% (120). And yet, they point out, that even this level of diversity generates sufficient antigenic variability to disrupt antibody recognition and require yearly influenza vaccinations with the most current circulating isolate (26, 120).

Env Structural Diversity:

The sequence diversity of HIV-1 Env generates impressive functional differences among HIV isolates, including variable sensitivity to neutralizing antibodies (121), co-receptor usage (122), and dependence upon CD4 (123, 124). Such functional diversity presumably reflects isolate-specific structural differences, but the underlying structural basis for Env functional diversity remains poorly defined, and this is a motivation for the work presented in chapter 2. In addition, there is dramatic structural heterogeneity even within a single HIV-1 Env isolate, due to the glycoprotein's intrinsic flexibility and fragility and the inherent variability associated with post-translational modification and protein folding. Not only does this heterogeneity complicate the

elicitation of broadly-protective immune responses, but it also hinders detailed structural studies of the native Env trimer.

Glycosylation:

Glycans account for approximately fifty percent of the mass of the gp120 surface subunit (10, 125). Depending on the primary sequence of a given Env isolate, there may be twenty to thirty potential N-linked glycosylation sites (PNGS; encoded by the N-x-S/T motif, where "x" is any amino acid besides proline) per gp120 subunit (77, 126). The relatively well-conserved gp41 transmembrane subunit typically encodes 4 PNGS (126). Although a number of PNGS are highly conserved among Env isolates and appear to be critical for viral fitness, the majority of PNGS are variable among isolates (127). Due to their large size, glycans have the potential to dramatically alter epitope exposure, in a way that amino acid mutations cannot. By adding, subtracting, or shifting potential N-linked glycosylation sites within the primary sequence during evolution, Env is able to introduce exceptional antigenic variability, that would not be possible by simply changing amino acid side chains. In addition, some regions of Env contain PNGS that are closely spaced within the primary sequence, which leads to variability in PNGS occupancy presumably because the large glycan moiety of an occupied PNGS hinders oligosaccaridetransferase enzyme access to neighboring sites (128). In regions with many densely-spaced PNGS, not all sites will be glycosylated (128-130).

In addition to this heterogeneity in PNGS occupancy, there is also site-specific variability in glycosylation pattern. It is possible for a given site to exhibit either high-mannose or complex-type glycans. Patterns ranging from Man5 to Man9 may all be observed at a site that commonly possesses high-mannose glycans, whereas sialylated, fucosylated, bi-antennary, tri-antennary patterns may all be present at a site that commonly presents complex-type glycans (128-130). High-mannose glycans appear to be the major glycoform, on HIV-1 Env(131), although diverse glycoforms exist on the native Env trimer (132). The specific glycosylation pattern of HIV-1 Env

has been shown to be critical for bNAb recognition(133) and modifies Env antigenicity and immunogenicity (134). Because there are 20-30 glycosylation sites per trimer, 10-20 Env trimers per virus particle and billions of virus particles circulating within a host, it is likely that all of these possible glycosylation patterns exist simultaneously, generating substantial heterogeneity and complicating Env recognition by neutralizing antibodies.

Furin Cleavage and Disulfide Bonding:

Because of the stochastic nature of protein-protein interactions within the crowded environment of the cell, all post-translational modifications exhibit a degree of heterogeneity. Soon after the discovery of HIV, it was noted that Env undergoes incomplete cleavage into gp120 and gp41 (10, 11, 135). Uncleaved gp160 Env expressed on the virus surface is not functional for fusion (136), because the fusion peptide is not free to enter the target membrane, and it appears to be antigenically distinct from cleaved Env trimers (137). In addition, it is common for non-native, unintended intra and intersubunit disulfide linkages to form during Env maturation (31). Many of these incorrect bonds are resolved by disulfide isomerases (31, 125) although some bonding heterogeneity remains in virion-associated Env (138). Aberrant disulfide bonding patterns are frequently observed in soluble Env and generate substantial conformational heterogeneity (139-141). Both cleavage and improper disulfide bonding have complicated the design, expression, and purification of soluble Env immunogens that mimic the native trimer.

Conformational Mobility:

The intrinsic mobility of the Env glycoprotein contributes to its heterogeneity as well (19, 142). It has been hypothesized that the trimer naturally “breathes” between its unliganded “closed” conformation and an “open” conformation similar to that observed following CD4-binding (33, 38, 143). The equilibrium between the “open” and “closed” trimeric forms appears

to vary in an isolate-specific manner (28), but a given Env isolate is likely to sample all of the conformational intermediates between “open” and “closed” over time. Transitions between multiple quaternary conformations would limit the sustained exposure of potential neutralizing epitopes on the Env trimer (143). In addition to this quaternary structural mobility, there appears to be substantial conformational flexibility within the gp120 subunit itself (142, 144, 145), which generates structural heterogeneity at a finer scale. It has been proposed that this disorder is unfavorable for antibody-gp120 interactions because it imposes a large entropic cost on antibody binding (145). Additionally, by fluctuating among multiple conformations, gp120 may limit its presentation of potential neutralizing epitopes (142).

Disassembly:

One consequence of the dynamic nature of the Env glycoprotein is that it is a highly labile molecule (12). Non-covalent interactions between gp120 and gp41, and between protomers within the trimer, are broken with relative ease, and this fragility introduces additional heterogeneity within the Env population. It is common for gp120 to be shed from the trimer (10, 146), yielding monomeric and trimeric gp41 stumps. Unincorporated protomers may also be present as monomers in the viral membrane (147, 148). Dissociation of subunits from the Env trimer not only decreases the number of “native” Env spikes on the viral surface, it also increases exposure of immunodominant epitopes that have been shown to be irrelevant and inaccessible in the context of the native Env trimer, including the gp120 inner domain and regions of gp41 (147, 149). Similarly, monomeric gp120 is likely to be differentially stabilized relative to gp120 in the context of the trimer. Therefore, although shed gp120 monomers are immunogenic, the antibodies elicited may not recognize the conformation of gp120 in the context of the trimer (150, 151). In this way, the sequence diversity of HIV-1 Env is compounded by heterogeneity due to glycosylation, disulfide bonding, proteolysis, conformational flexibility, and relatively labile non-covalent interactions.

"Self" Antigen Cloak:

In addition to their role in generating structural heterogeneity, glycans restrict antibody access to the underlying, potentially immunogenic, protein surfaces of Env (152). Because Env glycans are manufactured by host glycosylation machinery, they are largely – though not completely - indistinguishable from the glycans on host glycoproteins. Immunological tolerance to "self" antigens - molecules expressed naturally by the host - reduces the immunogenicity of the glycans on the surface of HIV-1 Env (153), although a number of antibodies have been identified, which target glycan-specific epitopes on Env (30, 154, 155). Similarly, the MPER region of gp41 is targeted by the broadly neutralizing antibodies 2F5 and 4E10 (156, 157). These antibodies exhibit cross-reactivity with lipid, and their MPER binding and neutralization activity appear to depend on this cross-reactivity (158, 159). Such cross-reactivity with lipid, another "self" antigen, complicates the development of 2F5 and 4E10-like antibodies, because the self-reactive germline antibodies are deleted during B cell maturation (160). Through its close association with "self" antigens, HIV-1 Env reduces the exposure of surfaces that might be recognized as "non-self" and decreases the immunogenicity of nearby epitopes.

Low Levels of Env Expression on the Virus Surface:

It has been proposed that the low levels of Env expression on the virus surface prevent bivalent antibody binding to the virus particle (161). In contrast to influenza, which is densely coated with hemagglutinin molecules, it is estimated that there are only 10-20 Env spikes per virus particle. Assuming that these spikes are randomly distributed over the virus surface, the distance between Env trimers would be great enough that the F(ab) arms of an IgG molecule could not crosslink two adjacent trimers. Thus, in contrast to anti-influenza antibodies, which may bind with high avidity to two adjacent spikes, anti-Env antibodies must develop higher affinity monovalent interactions if they are to remain bound at equilibrium (161). This would

impose a more stringent requirement on the degree of affinity maturation for anti-Env antibodies than for antibodies targeting other viruses that present their spike proteins at a high density.

Weak Interactions with "Germline" Antibodies:

It was recently observed that most Env proteins interact poorly with the predicted germline precursor B cell receptors of bNAbs (162, 163). As will be discussed below, mature bNAbs typically undergo extensive somatic hypermutation to increase their binding affinity and their potency and breadth of neutralization (164, 165). If these mutations are reverted to the germline sequence, Env binding and neutralization activities are lost (162, 163). Although there is some uncertainty in predicting the germline ancestor sequence, if true, these observations suggest that many HIV-1 isolates may have evolved to occupy a sequence and structural space that cannot be recognized by the germline precursors of broad and potent antibodies. This would significantly hinder bNAb development and the ability to elicit bNAbs through vaccination using purified Env proteins. Altogether, these strategies for avoiding activation of the humoral immune response in combination with the exceptional sequence and structural diversity of Env yield an immensely variable molecule, which is a uniquely challenging target for humoral immunity, vaccine design, and structural study.

Antibody Structural Diversity:

In spite of its great sequence, structural, and conformational heterogeneity, HIV-1 Env is vulnerable to neutralizing antibody recognition. The humoral immune system is able to recognize a nearly infinite array of potential foreign antigens, including the variable surface of HIV-1 Env, because of the immense diversity of the naïve B cell receptor (BCR) repertoire. This diversity is generated through the random recombination of gene segments, non-templated addition of nucleotides at gene segment junctions during recombination, and pairing of heavy and light chains, which undergo these processes separately (166). The human genome

contains more than 40 heavy chain variable (V_H), 25 diversity (D_H), and 6 joining (J_H) gene segments, and one of each gene segment is randomly recombined with the heavy chain constant gene segments to produce a full-length heavy chain gene (167, 168). A similar process of recombination occurs separately for the light chain, in which one variable (V_L) and one joining (J_L) segment are recombined from a number of possible V_L and J_L gene segments with a constant gene segment to produce the full-length light chain. Random addition of non-templated nucleotides between gene segments during recombination further expands the diversity of the BCR repertoire (166, 167, 169). The majority of antibody sequence diversity is concentrated in the complementarity determining regions (CDR) 1, 2, and 3 on both the heavy and light chains, which typically make contact with the antigen. The CDR1 and CDR2 loops are encoded by each V_H and V_L gene segment, while the CDR3 loop is encoded at the junction of VDJ recombination in the heavy chain and the site of VJ recombination in the light chain. The heavy chain CDR3 (CDRH3) typically plays a critical role in antigen binding (167).

Following recombination, junctional diversification, heavy and light chain pairing, and elimination of autoreactive B cells, the remaining mature naïve B cells express “germline” encoded B cell receptors. It has been proposed that germline BCR are uniquely dynamic and polyreactive (170), and that this conformational and functional diversity increases the likelihood that a germline BCR will recognize a foreign antigen (171). This hypothesis motivates the work presented in chapter 3. Should the germline B cell encounter antigen and receive T cell help, the BCR will diversify further through somatic hypermutation and affinity maturation to optimize its affinity for the target antigen (167). In this way, the human B cell repertoire achieves dramatic sequence and structural diversity that facilitates recognition of unknown pathogens and the exceptionally variable Env glycoprotein. Broadly neutralizing antibodies against HIV-1 commonly possess unusual features, including exceptionally long CDRH3 loops, extensive somatic hypermutation, and even moderate levels of autoreactivity with self-antigens (164, 165). These rare features reflect the difficulty of identifying and accessing conserved features on HIV-

1 Env, and the importance of sequence, structural, and functional diversity in antibody recognition of an antigen like HIV-1 Env, that is itself, so uniquely variable.

Challenges of Rational Antibody-Based HIV-1 Vaccine Design:

In the context of non-human primate studies, which showed that neutralizing antibodies can block transmission of neutralization sensitive isolates, the lack of protection afforded by nAbs in human clinical trials suggest that these vaccines did not elicit the correct "type" of neutralizing antibodies. The goal of rational antibody-based vaccine design is not only to elicit neutralizing antibodies, but to generate select broad and potent antibody specificities through vaccination (172, 173). This ambitious goal depends on a detailed structural understanding of conserved epitopes on the native Env trimer and soluble Env immunogens, and the recognition of these epitopes by neutralizing antibodies. While there has been considerable progress in these areas, significant gaps remain in our understanding of soluble Env immunogen structure, the accuracy with which these immunogens recreate the structure of the native Env trimer, and the factors governing their immunogenicity.

Epitopes Targeted by HIV-1 Broadly Neutralizing Antibodies:

By screening sera from HIV-infected individuals for broad neutralizing activity and isolating monoclonal antibodies from these individuals, we have gained a detailed appreciation of highly conserved and vulnerable epitopes on the Env trimer that are targeted by naturally-occurring bNAbs (174). The first broadly neutralizing antibodies that were identified were found to target three separate regions within Env: the CD4-binding site (bound by IgG1-b12) (175, 176), a conserved cluster of mannose sugars on the gp120 outer domain (bound by 2G12) (155), and the conserved, linear epitope in the gp41 MPER (bound by 2F5 and 4E10) (177, 178). In addition to these epitopes, two other regions of Env were observed to be bound by less-broadly neutralizing antibodies: a CD4-induced epitope overlapping the co-receptor binding

site (bound by 17b and 48d, among others) and the conserved tip of the V3 loop (bound by 447-52D) (179-181). These early bNAbs, exhibit modest breadth - neutralizing ~40% of isolates - and weak potency, requiring high concentrations of antibody to achieve neutralization (30).

Recent advances in technologies for isolating monoclonal antibodies(174) led to the discovery of a new panel of bNAbs with greater breadth and potency than the early bNAbs: neutralizing up to 91% of viruses at high concentrations in the case of VRC01 (182), and neutralizing 50% of viruses at concentrations less than 0.1 ug/mL for PGT128 (154). The "second generation" bNAbs recognize epitopes including the CD4-binding site (VRC01, NIH45-46, and PGV04, among others) (182-185), conformational, glycan-dependent epitopes involving the V2 loop that are preferentially exposed in native trimeric Env (PG9, PG16, PGT141-145), and glycan-dependent epitopes overlapping that of 2G12 at the base of the V3 loop (PGT125-128, 130-131) (30, 154). These antibodies have dramatically improved our understanding of conserved structures on trimeric Env and mechanisms of antibody neutralization, providing important targets for rational vaccine design.

Limitations in Our Structural Understanding of HIV-1 Env:

The flexibility and heterogeneity of HIV-1 Env discussed above, make it difficult to study by x-ray crystallography because this technique requires large amounts of stable, homogenous material. To achieve this high level of conformational purity, nearly all gp120 crystal structures focus on truncated, deglycosylated gp120 "core" proteins stabilized with soluble two-domain CD4 and/or the antigen-binding fragment of an antibody (Fab) (25, 35, 186-192). Because of their flexibility and dense glycosylation, the large V1/V2 loops are truncated in all gp120 crystal structures, and the V3 loop is frequently truncated as well, although it has been resolved in a crystal structure of gp120 core in complex with CD4 and the co-receptor binding site antibody X5 (187). Although structures have been solved for gp120 core proteins from diverse isolates, these structures are highly convergent, possibly as a result of the modifications required for

crystallography (192). Therefore, we have little understanding of the structural features that distinguish Env isolates, generate substantial functional diversity (121, 193, 194), and complicate the development of broadly reactive neutralizing antibodies. This critical gap in our understanding motivates the work presented in chapter 2.

In addition, there is currently no high resolution crystal structure available for the Env trimer (although, a moderate resolution structure was recently reported for a highly stable soluble Env trimer from the clade A isolate BG505 at the AIDS Vaccine 2013 conference by Ian Wilson and colleagues), so it is unclear whether the structures described for the gp120 core reflect the conformation of gp120 in the context of the trimer. In light of the functional diversity of the native Env trimer, and the heterogeneity of the molecule as discussed above, it is likely that, as with the gp120 core structures, static crystal structures may select for uniquely stable constructs and underrepresent the structural variability within and across isolates of HIV-1 Env. Complementary structural techniques have provided valuable information about the structure and dynamics of unmodified, trimeric Env and soluble Env constructs. Cryo-electron microscopy (Cryo-EM) revealed the likely position of the variable loops at the trimer apex and quaternary structural rearrangements within the trimer upon sCD4-binding (28, 33). Small-Angle X-ray scattering (SAXS) has facilitated study of the subunit morphology of unmodified soluble Env immunogens in solution (142, 195). Hydrogen-deuterium exchange with mass spectrometry (HDX-MS) is a technique central to this thesis, which provides information on the local stability of protein secondary structure and the degree of solvent accessibility (142, 196, 197). Previous studies of full-length glycosylated gp120 by HDX-MS indicated that the protein is quite disordered in solution and provided insight into potential mechanisms by which CD4-binding may allosterically trigger gp41 reorganization prior to fusion (142). In combination with x-ray crystallography, these techniques critically expand our capacity to study unmodified, conformationally-heterogenous Env constructs, which better reflect the structure and diversity of the “native” Env trimer.

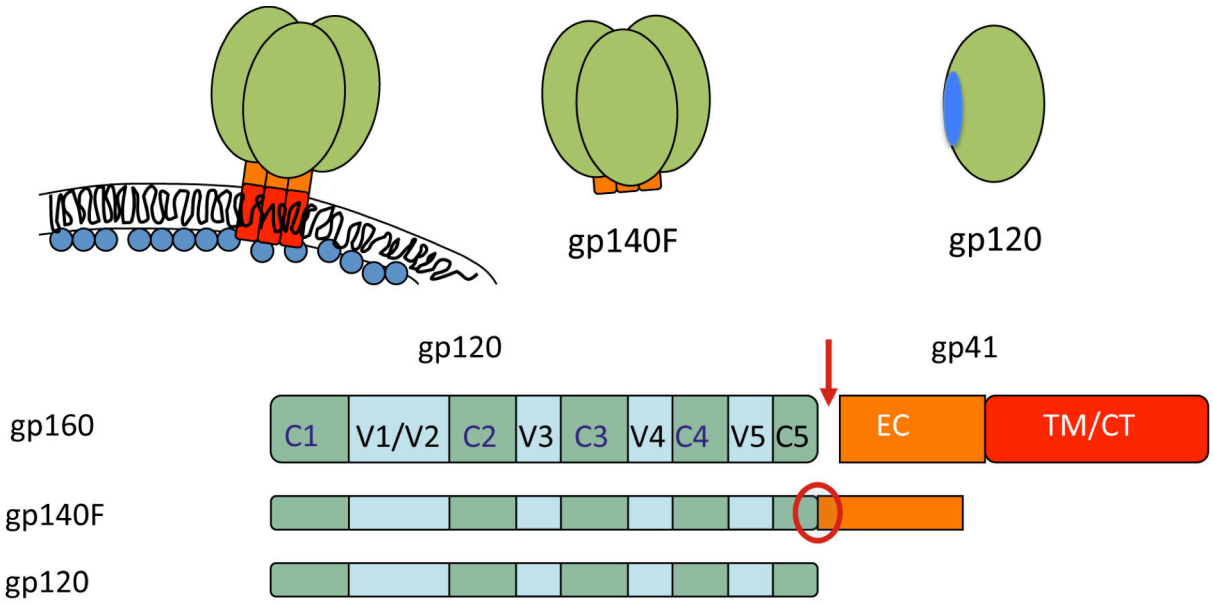

Figure 2. Diagram of Soluble Env Immunogens. Full-length, membrane-associated, trimeric gp160 Env is shown in the top left corner, and a linear representation of the gp160 sequence including the variable (V1-V5), and conserved regions (C1-C5) is shown directly beneath it. An ideal, soluble trimeric gp140 Env ectodomain immunogen is illustrated in the middle panel, with a linear representation below. The furin cleavage site, indicated with the red arrow, is mutated to prevent furin cleavage in gp140F constructs. A soluble monomeric gp120 immunogen is illustrated on the right, with a linear representation below. The blue oval indicates an epitope that is typically buried in the context of the native trimer.

Design of Authentic Env Immunogens:

With no detailed structure of the native Env trimer or the Env immunogens used to elicit antibodies against it, it is difficult to assess the authenticity of commonly-used Env immunogens. One common explanation for the lack of efficacy observed in antibody-based vaccine trials is that Env immunogens do not accurately reflect the structure of the native trimer (55). For example, gp120 immunization typically elicits antibodies highly specific for the immunogen isolate variable loops or the sparsely-glycosylated gp120 inner domain, which is not accessible in the native trimer (55). Therefore, antibodies elicited by such immunogens target irrelevant or isolate-specific epitopes, and it is to be expected that these antibodies would be poorly

neutralizing and poorly cross-reactive. In light of this, substantial work has been done towards identifying Env immunogens that accurately reflect the native Env trimer (149, 198).

To better mimic the native Env trimer and hopefully improve the quality of the antibodies elicited through vaccination, researchers tested the ability of soluble oligomeric gp140 Env ectodomain constructs to focus the antibody response on epitopes that are only exposed in the trimer (Figure 2) (55). These immunogens elicited improved antibody titers as compared to gp120 proteins but showed little improvement in breadth of the neutralizing response (55, 199). Recent work suggests that the weak antibody response to oligomeric gp140 may be partially explained by the fact that many gp140 oligomers do not accurately reflect the structure of the native Env trimer, and rather resemble non-native, disulfide-linked dimers (141). This structural dissimilarity is especially problematic because an important class of bNAb, the PG9/PG16-like antibodies, are some of the most potent and broad antibodies that have been identified, but they do not bind to many soluble Env constructs, including many gp140 constructs designed to better mimic the native trimer (30). Thus, many oligomeric gp140 immunogens appear to be inauthentic, with distinct antigenic profiles compared to that of the native trimer. These observations inspired the work in chapter 1, to improve the exposure of the PG9/PG16 epitope in soluble gp140 constructs, in order to develop a more native mimic of the Env trimer.

The Missing Link between Antigenicity and Immunogenicity:

It has been repeatedly demonstrated that antigenicity does not predict immunogenicity (200-202). Many commonly used immunogens bind with high affinity to bNabs, but these immunogens do not elicit bNAbs through vaccination. Perhaps the largest bottleneck in HIV-1 vaccine design stems from our limited ability to rationally manipulate antibody-based immune responses to an epitope of interest. It is still beyond the reach of the scientific community to predict the antibody response to an immunogen, and still further out of reach lies an ability to design an immunogen that would elicit a specific monoclonal antibody. This problem is

sufficiently challenging even for relatively simple, discrete protein epitopes, such as the MPER helix that is targeted by bNAbs 2F5 and 4E10 (201, 202). However, most of the epitopes recognized by bNAbs are far more complex than the linear, helical epitope targeted by 2F5 and 4E10 – all of the other bNAb epitopes are discontinuous, conformational epitopes, and many of them involve both protein and carbohydrate residues – making them exceptionally challenging targets for rational vaccine design. Among the many factors that may influence immunogenicity is the ability of germline antibodies to bind immunogens and activate B cell affinity maturation. In chapter 3, I explore the role that antibody conformational dynamics may play in modifying antigen binding.

Goals of This Dissertation:

Sequence, structural, and conformational diversity are essential for antibody recognition of HIV-1 Env and Env escape from humoral immunity. Post-translational modifications and conformational dynamics contribute to the structural diversity of HIV-1 Env immunogens and the antibodies that recognize them. The goal of this thesis is to explore the influence of these factors on interactions between antibodies and HIV-1 Env immunogens. In chapter 1, I test the impact of sequence, glycosylation, proteolytic cleavage, and oligomerization on PG9/PG16 binding to gp140 proteins, with the goal of identifying modifications to improve the presentation of the PG9/PG16 epitope in order to design more authentic gp140 immunogens. In chapter 2, I explore structural variability among a panel of four full-length glycosylated gp120 proteins and test the relationship between conformational dynamics and antigenicity. In chapter 3, I studied changes in conformational stability over the course of affinity maturation for two broadly neutralizing antibodies, VRC03 and VRC26. With an improved understanding of the molecular factors that influence antibody-Env interactions, it may be possible to design enhanced Env immunogens that are able to effectively stimulate the development of broad and potent antibodies that will be required of a protective antibody-based HIV-1 vaccine.

Chapter 1

Binding interactions between soluble HIV envelope glycoproteins and quaternary-structure-specific MAbs PG9 and PG16*

*This work was performed in the laboratory of Dr. Leonidas Stamatatos. He has graciously allowed me to include it in this thesis.

The text in this chapter has been modified slightly from © American Society for Microbiology, Journal of Virology, Vol. 85(14), 2011, p.7095-107. doi: 10.1128/JVI.00411-11

Introduction

It is currently widely accepted that an effective vaccine against HIV must elicit broad anti-viral neutralizing antibody responses: antibodies that can prevent infection from diverse circulating primary HIV-1 isolates (55, 203). Such broad anti-HIV neutralizing antibody responses have not yet been achieved by immunization (204-218). Initially, it was thought that such anti-viral responses are extremely rare, even in the context of natural HIV-1 infection, and therefore, their elicitation by vaccination would be extremely difficult, if not impossible. However, recent evidence suggests that approximately a third of those infected with HIV-1 develop broad and potent neutralizing antibody responses (83, 84, 86, 92, 219). Such responses typically develop within the first 2-3 years of infection, and as early as the first year of infection (80).

The neutralizing antibody response against HIV-1 exclusively targets the viral envelope glycoprotein (Env), which is the only virally-encoded protein on the surface of viral particles. Env is initially expressed as a 160 kDa precursor protein (gp160), which is cleaved post-translationally into two non-covalently associated subunits: the extracellular subunit gp120 and

the transmembrane subunit gp41. This cleavage is performed by furin-like cellular proteases. On the surface of infectious virions, the functional Env is expressed as a trimer of gp120/gp41 heterodimers. Gp120 is responsible for binding to the CD4 and CCR5/CXCR4 cell surface proteins, while gp41 mediates fusion of the virion and host cell membranes.

The earliest Env-based immunogens that aimed at the elicitation of anti-HIV NAbs were based on the gp120 subunit alone and derivatives of that protein (61, 212, 220-228). This type of immunogen elicited binding antibodies that were largely non-neutralizing or primarily displayed neutralizing activity against the virus from which the Env immunogen was derived, but not heterologous primary isolates. The elicitation of non-neutralizing antibodies by such immunogens is due to the exposure on soluble gp120 immunogens of epitopes that are normally occluded within the functional HIV Env trimer. The elicitation of strain-specific NAbs is primarily due to the natural immunodominance of variable epitopes (i.e., epitopes that are not conserved among diverse HIV isolates) on soluble gp120 proteins but also due to improper presentation of more conserved neutralization epitopes (i.e., epitopes that are present on diverse isolates (see reviews, (172, 229)).

Second generation soluble HIV Env immunogens were based on the entire extracellular part of gp160, i.e., not only the gp120 subunit but also the extracellular part of the gp41 subunit. These constructs are commonly referred to as gp140s and can be trimeric. Soluble trimeric gp140 Env immunogens were shown by several groups to elicit antibody responses with broader neutralizing activities than those elicited by soluble monomeric gp120 immunogens (204, 218, 230). Overall, however, gp140s elicit NAbs with a breadth that is much narrower than those antibodies we wish to elicit by vaccination and those that are generated by approximately a third of those infected with HIV-1 (83, 84, 86, 92, 219). It was hoped that the trimeric nature of soluble gp140 constructs would better present epitopes that are also present on the virion-associated gp160 Env trimer. However, even in the context of soluble gp140 trimers, the presentation of conserved neutralization epitopes differs from that on the native virion-

associated gp160 Env trimers. This is particularly true for gp140 constructs on which the gp120-gp41 cleavage site was artificially eliminated in order to increase the stability of these soluble gp140 trimers (137, 230). The imperfect design of soluble gp140 trimers became even more evident recently, with the isolation of several anti-Env monoclonal antibodies (MAbs) that potently neutralize diverse HIV-1 isolates, but do not bind soluble versions of Env. These MAbs include 2909, a human MAb, which has a very narrow breadth of neutralization (neutralizes the clade B SF162 isolate) (29), several MAbs, 1.6F, 2.2G, 2.3E, 2.5B, 2.8F, and 3.10E, isolated from SHIV-infected macaques (collectively referred to here as “RhMAbs”) that also display exclusive neutralizing activity against SF162 (231), and PG9 and PG16, both human MAbs, which neutralize diverse HIV-1 isolates (30). Despite the distinct neutralizing properties of PG9/PG16, 2909 and the RhMAbs, these antibodies recognize overlapping epitopes. Several recent studies have discussed key differences in the epitopes recognized by these antibodies (232, 233). For example, neutralization by PG9 and PG16 requires the presence of an asparagine at position 160 within the V2 loop, while neutralization by 2909 and the RhMAbs requires a lysine at that same position (231). The vast majority of circulating viruses possess an asparagine at position 160, while SF162 is among a minority of viruses which possess a lysine at that same position (30). The epitopes recognized by these MAbs are currently referred to as ‘quaternary’ and, at least in the cases of PG9 and PG16, appear to exist on individual protomers that form the functional trimeric Env (30). Whether this is also true for 2909 and the RhMAbs is currently unknown.

The fact that all of the above-mentioned MAbs can neutralize virions but bind inefficiently, if at all, to recombinant soluble gp120 or gp140 Env, provides additional evidence of structural dissimilarities between these soluble constructs (that are routinely used as immunogens to elicit broad anti-HIV NAbs) and the functional, virion-associated Env spike. The engineering of soluble Env proteins whose structure more accurately mimics that of the virion-associated Env trimer could improve the immunogenic properties of soluble Env proteins,

specifically their ability to elicit broadly neutralizing antibodies with quaternary epitope specificities. Recent studies indicate that broadly neutralizing antibody responses with quaternary epitope specificities, similar to those of PG9 and PG16, appear within the first 1-3 years of infection and are not infrequent among those patients who develop broad anti-HIV neutralizing antibodies (80, 81). These observations suggest, therefore, that the elicitation of similar types of NAbs by immunization may be feasible once appropriate immunogens are designed.

Here, we identified several soluble gp140s that are recognized by MAbs PG9 and PG16 and factors that are important for that recognition. Specifically, we investigated the effect of Env trimerization, the requirement for specific amino acids at position 160 within the V2 loop, and the importance of proper gp120-gp41 cleavage for MAb-binding to soluble gp140s. Finally, we investigated whether and how the kinetics of PG9 and PG16 binding to soluble gp140 correlates with the neutralizing potency of these MAbs.

Materials and Methods

Cell Lines

Human embryonic kidney 293T and 293F cells were cultured as previously described (234). The HeLa-derived TZM-bl cell line (David Montefiori, Duke University, Durham, NC) expressing CD4, CCR5, and CXCR4 and containing B-Gal and Luciferase reporter genes under the control of the HIV LTR promoter was cultured in Dulbecco's Modified Eagle's Medium (DMEM) supplemented with 10% FBS, Penicillin, Streptomycin and L-glutamine, as previously described (235).

Antibodies and HIV+ sera

Human MAbs PG9 and PG16 (30)were provided by Matthew Moyle (Theraclone). Human mAb 447-52D (236) was provided by Susan Zolla-Pazner and Mirek Gorny (New York

University, New York, NY). The Fab versions of the antibodies 447-52D, PG9, and PG16 were provided by Pamela Bjorkman and Paola Marcovecchio (CalTech, Pasadena, CA). A plasma pool from 30 primarily clade A-infected individuals (between 1998-2000) in Mombasa, Kenya (237) was provided by Julie Overbaugh and Catherine Blish (University of Washington, Seattle, WA).

Env-Expressing Plasmids and Mutagenesis

The HIV-1 gp160 Env gene of four clade A isolates (Q168a2, Q259d2.17, Q461e2, and Q769h5) (237), and that of the clade B SF162 isolate (238), were previously cloned in the pEMC* mammalian DNA vector for pseudovirus production (239). Gp140 versions of these Envs were generated by introducing stop codons immediately upstream from the transmembrane region (240). As these constructs possess a wild-type gp120-gp41 furin cleavage site, these constructs are referred to as “cleaved” or gp140C. We also generated the corresponding cleavage-defective gp140 constructs, on which the gp120-gp41 furin cleavage site was eliminated by mutagenesis (241). These constructs are termed as “non-cleaved” or gp140F for ‘fused’. Codon-optimized versions of the gp140F clones were synthesized by Genscript and cloned into the pTT3 vector for high-level mammalian expression (242).

The K160N mutation was generated on the gp160, gp140F, and gp140C versions of SF162 Env. Mutagenesis of the gp160, of the non-codon-optimized gp140F and of the non-codon-optimized gp140C constructs was performed with primers previously described (231). Introduction of the K160N mutation into the codon-optimized SF162 gp140F construct was performed using the forward primer: K160NF (5’-CAA AAA CTG CAG CTT TAA CGT GAC AAC GAG CAT TAG -3’) and reverse primer: K160NR (5’-CTA ATG CTC GTT GTC ACG TTA AAG CTG CAG TTT TTG -3’). The inverse mutation, N160K, was introduced on the codon-optimized Q259d2.17 gp140F construct using the forward primer: Q259N160K (5’-AAG AAC TGT AGC TTC AAG ATT ACA ACA GAG CTG-3’) and the reverse primer: Q259N160K-r (5’-CAG CTC

TGT TGT AAT CTT GAA GCT ACA GTT CTT-3'). Mutagenesis of Q259d2.17 gp140F was performed to create Q259d2.17 gp120. The primers used for this reaction were: 259gp120stopF (5'-CCC TAC ACG GGC CTA GTA AAT TTC CTC TGT G-3') and 259gp120stopR (5'-CAC AGA GGA AAT TTA CTA GGC CCG TGT AGG G-3'). The reaction mixture contained 60 ng of gp140F template (Codon optimized), 125 ng of each respective primer, and 22 µL AccuPrime™ Pfx SuperMix (Invitrogen) for a total reaction volume of 25 µL. The reaction conditions consisted of 1 hold at 95° C for 30 s, followed by 18 cycles of successive denaturation, annealing, and elongation steps performed at 95° C for 30 s, 60° C for 1 min, and 68° C for 8 min, respectively, and 1 final hold at 68° C for 10 min. All reactions were digested with Dpn-I for 3 hr at 37° C. The mixture was purified and concentrated to 10 µL using the MinElute PCR Purification Kit (Qiagen), and was subsequently used to transform competent cells (One Shot MAX Efficiency DH5α-T1R; Invitrogen). Successful mutagenesis was confirmed by sequencing.

Expression and purification of soluble Env gp140

Small-scale transient transfection of 293T cells with plasmids expressing gp120 and gp140 proteins was performed as previously described (234), with minor modifications. Briefly, $3x10^5$ 293T cells per well of a 6 well plate were transfected for 4 hours with 2 µg of plasmid DNA using GeneJuice and Optimem serum free-medium. After transfection, the media were replaced with fresh media and the cells cultured for 48 hours. The culture supernatants were harvested and clarified by centrifugation at 2000 RPM for 5 min. Protease inhibitors Pepstatin A, E-64, Aprotinin, and EDTA were added to final concentrations of 2 µM, 2 µM, 0.6 µM, and 2 mM, respectively. Supernatants were then aliquoted and frozen at -20° C until further use.

Large-scale expression and purification of gp140F Env constructs was performed as previously described in detail (234). Briefly, the cell transfection supernatants were concentrated and buffer exchanged using a 30kDa mwco TFF membrane cassette (Pall Life

Sciences, CA) and lectin purified (GNA, Vector Laboratories). The eluate was concentrated using a 30kDa mwco Amicon Ultra centrifugal concentrator (2,500 x g) and loaded on to a Superdex 200PG size exclusion column (GE Healthcare) and run at 1 ml/min in 1 x PBS. Eluted fractions were analyzed by Native PAGE using the Invitrogen NativePAGE system. Fractions containing monomeric gp140 were pooled separately from those fractions containing trimeric gp140 Env. Q461e2gp140 is almost exclusively expressed as a trimer and we were unable therefore to investigate the interactions of PG9 and PG16 with the corresponding monomeric gp140 from of that protein. Protein concentration was determined by BCA or by absorbance at 280 nm.

Quantification of gp140 Env in Transfection Supernatants by Odyssey Western

Licor Odyssey Western blotting was used to quantify the concentration of gp140 Env in transfection supernatants, using the protocol described previously (243). Samples were prepared using 4x loading buffer and 10x reducing agent and were heated at 95° C for 10 min. Gels-NuPAGE 4-12% Bis-Tris gel (Invitrogen) - were run in 1X MOPS buffer with antioxidant at 200V for 60 min. Quantification was performed using purified SF162 gp140 (25, 75, and 150 ng) to establish a standard curve. Transfection supernatants were loaded at two volumes (7.5 µL and 15 µL) and the integrated intensity of protein bands was determined.

Transfer of the proteins from the SDS gels to nitrocellulose membranes (Pall) was performed by applying current at 375 mA (constant current) for 90 minutes in 2X NuPAGE transfer buffer (Invitrogen) with 15% methanol and antioxidant. The membranes were air-dried briefly, then blocked for 1 hour in Odyssey Block Buffer (Licor) at room temperature. The membrane was then incubated in PBS with 50% Odyssey Block Buffer, 0.2% Tween-20, and pooled rabbit polyclonal anti-Env sera (diluted 1:8000) for 1 hour shaking at room temperature. The membrane was washed in Odyssey Wash Buffer (PBS with 0.1% Triton X-100). After washing, the membrane was incubated with the secondary antibody mixture containing PBS

with 50% Odyssey Block Buffer, 0.2% Tween-20, 0.02% SDS, and goat anti-rabbit IR Dye680 (diluted 1:15,000) at room temperature, protected from light. The membrane was washed again and scanned using a Licor Scanner at a wavelength of 700 nm. Quantification was performed using Licor Software.

Immunoprecipitation and Western Blotting of gp140 Env

Immunoprecipitations of soluble Env present in transfection supernatants (SF162 or SF162 K160N as gp140F or gp140C, as well as Q259d2.17 or Q259d2.17 N160K gp140F), or of size-exclusion purified gp120 Env (SF162, SF162 K160N, Q259d2.17, and Q461e2) and monomeric and trimeric gp140 Env proteins (Q168a2, Q259d2.17, Q461e2, Q769h5, SF162 and SF162 K160N) were performed as follows. In all cases, to 100 µL of DMEM supplemented with 10% FBS and containing 100 ng Env, MAbs PG9 and PG16 were added to a final concentration of 10 µg/mL. No antibody was added to the negative control samples ('beads alone'). Incubations took place at room temperature for 1.5 hours before adding 50 µL of protein G-agarose beads resuspended in PBS with 0.3% Tween-20 and incubated for an additional hour, rotating at room temperature. The beads were then pelleted by centrifugation at 4,000xg and washed seven times in 1 mL cold PBS with 0.2% Tween-20. Finally, the proteins were eluted from the pelleted beads by resuspension in 60 µl of 2x SDS-PAGE loading buffer with BME and heating at 95° C for 10 minutes. After re-pelleting the beads at 13,000xg for 5 min, 20 µL of eluted and denatured protein sample was loaded onto a 4-12% Bis-Tris NuPAGE gel (Invitrogen).

The proteins were transferred from the SDS-PAGE gels to PVDF membranes as described above (Pall). The PVDF membranes were incubated for 1.5 hours in PBS with 10% non-fat milk, and 0.6% Tween-20. The membrane was probed for 1 hour with a polyclonal goat anti-Env sera raised against denatured SF2 gp120 (diluted 1:1000). Following an intermediate

wash, the membrane was incubated with protein-G-horseradish peroxidase (1:10,000) for one hour. The membrane was then washed and developed using Amersham ECL-plus (GE) and Amersham Hyperfilm Chemiluminescence film (GE) or a Storm Phosphoimager.

Enzyme Linked Immunosorbant Assay (ELISA)

Purified gp120 monomers, gp140 monomers or gp140 trimers were adsorbed onto 96 well ELISA plates at a concentration of 0.75 µg/mL in 100 mM $NaHCO_3$, pH 9.6 by an overnight incubation at 4° C. Plates were then washed 4x in a plate washer and blocked for 2 hours at room temperature in PBS with 10% NFM, and 0.3% Tween-20. After blocking, the plates were washed 4x, and the primary antibodies (PG9, PG16, 447-52D, or VA plasma pool) were titrated into the wells starting at a concentration of 20 µg/mL for mAbs or 1:1000 for VA plasma pool, and making 5-fold serial dilutions (or 10-fold dilutions for 447-52D and plasma pool) into PBS with 10% NFM and 0.03% Tween-20. Plates were incubated at 37° C for 1 hour, washed 4x, and the secondary goat anti-human (whole molecule) IgG was added to each well at a dilution of 1:3,000 and incubated at 37° C for an additional hour. Following a final wash, the plates were developed with SureBlue Reserve TMB microwell peroxidase substrate (KPL) for 3 minutes and stopped using 1N H_2SO_4. Plates were read on a Versamax microplate reader, and analysis was performed using the Prism package (GraphPad Software). Binding was measured in duplicate in two independent experiments.

Surface Plasmon Resonance Analysis

Surface plasmon resonance (SPR) measurements were carried out on a Biacore T100 instrument at 25° C. Gp140F constructs were immobilized on CM5 sensor chips using standard amine-coupling chemistry immediately following repurification by size-exclusion chromatography (SEC) to remove any contaminating degradation or oligomerization products. Flow cell 1 on each chip was activated/deactivated and left blank as a reference surface. Analyte (PG9,

PG16, 447-52D Fabs) and buffer blank injections were randomized and run in duplicate at 50 μL/min in HBS-EP (10 mM HEPES, 150 mM NaCl, 3 mM EDTA, 0.005% Surfactant P20, pH 7.4). Specific immobilization conditions, analyte concentrations and interaction parameters are summarized in Appendix A, Supplemental Table 1. Surfaces were regenerated with 10 mM glycine, pH 1.5 at 50 μL/min for 5 seconds. Where fitting was possible, double-referenced data were fit with 1:1 interaction models by global analysis with BiaEvaluation 2.0 software. SPR responses to surfaces coupled with Q259d2 trimers and Q769h5 monomers and trimers were too low to permit quantitative analysis (Appendix A, Table S1).

In order to confirm the validity of the numbers derived from experiments performed by amine-coupling gp140F constructs, a capture assay was also performed in which goat anti-human Fcγ IgG was amine-coupled to two flow cells of a CM5 chip. Approximately 115 response units (RU) of PG9 IgG was captured by flowing a 1 μg/mL stock over one anti-IgG surface for 60 seconds at 10 μL/min leaving the other anti-IgG surface as a reference. Duplicate injections of buffer and 300 nM monomeric or 100 nM trimeric Q168a2 gp140 were used as analytes at 50 μL/min, with an association time of 7 minutes and a dissociation time of 30 or 60 minutes, respectively. The surface was regenerated by injecting two 30 second pulses of 10 mM glycine, pH 1.5 at 50 μL/min. Double-referenced data was fit globally with a 1:1 binding model using BiaEvaluation 2.0 software.

Production of single round competent virions

Single round competent virions (pseudoviruses) expressing the gp160 of interest were produced as previously described by co-transfection of 293T cells with a pNL4-3 Luc+Env-Rev- backbone and a mammalian expression vector containing the gp160 gene (239). Transfection supernatants were harvested 72 hours later, clarified at 2000xg, aliquoted and stored at -80° C until further use.

Neutralization Assays

Neutralization assays were performed in a TZM-bl reporter cell line as previously described (207, 239). Briefly, cells were plated at a density of $3x10^3$ cells/well in 96 well flat-bottom plates 24 hours prior to the addition of pseudovirus and antibodies. Antibodies or Fabs were serially diluted six-fold and were incubated with virus for 1 hour at 37° C. Predetermined amounts of viruses to produce roughly 10^5 RLU after infecting TZM-bl cells in the absence of antibody were used. The virus/antibody mixture (as well as virus in the absence of any antibody as a positive control) was then added to TZM-bl cells that had been treated with polybrene at 2 μg/mL for 30 minutes at 37° C. Infection was allowed to proceed for 72 hours at 37° C. Virus-entry and percent neutralization were measured by luciferase activity using Steady-Glo Luciferase reagent (Promega). Neutralization was measured in duplicate in two independent experiments by determining the cell-associated luciferase activity in the absence and presence of antibodies using the following mathematical equation: [(RLUpos-RLUmab)/RLUpos]*100, where RLUpos is the average RLU measured for cells infected with pseudovirus in the absence of any antibody, and RLUmab is the average RLU measured for cells infected with pseudovirus that had been pre-incubated with MAb.

Results

PG9 and PG16 Bind Preferentially to Soluble Monomeric gp140 by ELISA

PG9 and PG16 were isolated from an HIV-1-infected subject based on their ability to neutralize diverse HIV-1 isolates without binding to soluble Envs in ELISA experiments (30). In the original study by Walker and colleagues, a limited number of soluble gp120s or gp140s were evaluated for PG9/PG16 recognition and it was reported that none of these Envs were recognized by PG16, while PG9 weakly recognized gp120 from the DU422 and ADA isolates and the gp140-foldon protein from the YU2 virus.

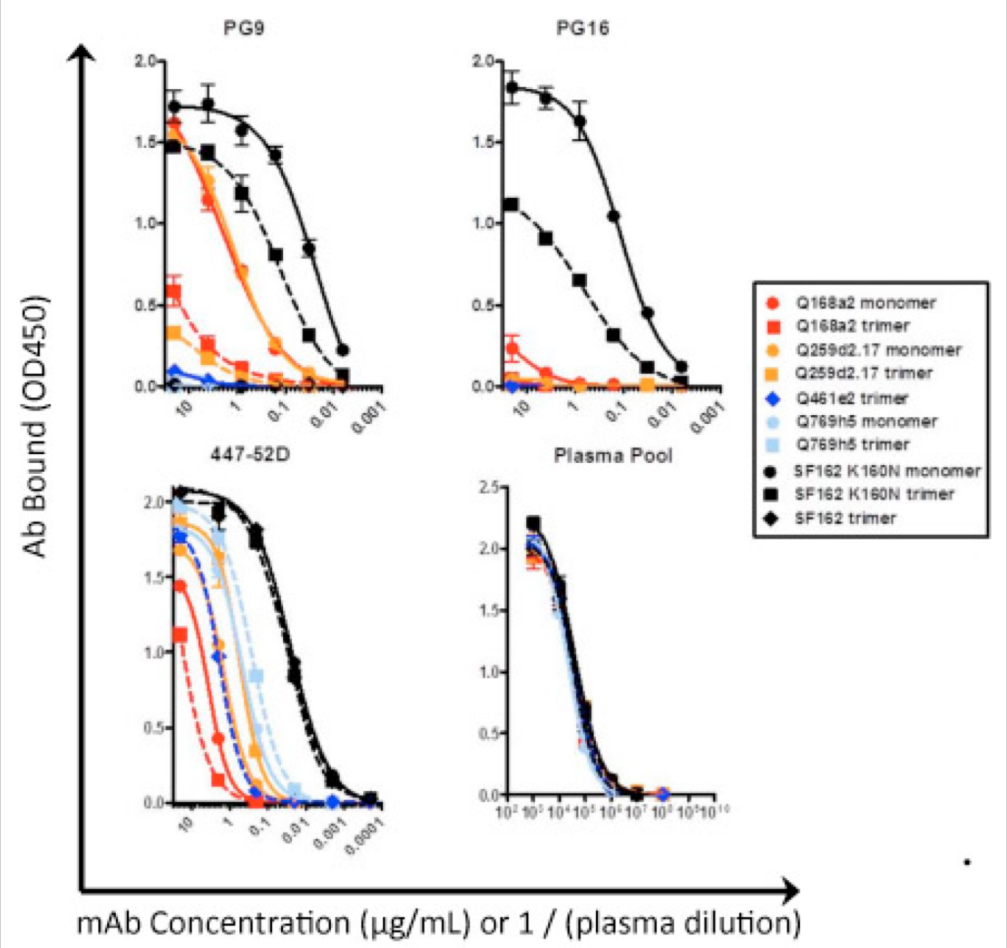

Figure 1.1. PG9 and PG16 binding to monomeric and trimeric gp140 by ELISA. Binding of PG9, PG16, 447-52D, and pooled plasma binding (as indicated in the inset) to SEC purified trimeric (squares and diamonds, dashed lines) and monomeric (circles, solid lines) gp140 molecules for the indicated Env is shown. Only trimeric gp140 Env was available for Q461e2 and SF162.

With the goal of identifying previously unreported strong binding interactions between PG9 / PG16 and soluble Env, we examined whether PG9 and PG16 were capable of binding to four well-characterized clade A gp140 Envs (Q168a2, Q259d2.17, Q461e2 and Q769h5), isolated between 28 and 75 days post-infection (244). As PG9 and PG16 were isolated from a clade A HIV-1-infected individual, we hypothesized that these MAbs may display a favored recognition of soluble Envs derived from clade A viruses. In addition to these clade A Envs, we also evaluated the binding of PG9 and PG16 to gp140 constructs derived from a clade B isolate,

SF162, which is resistant to neutralization by these two antibodies, as well as the SF162 K160N mutant, which is sensitive to neutralization by these two MAbs (30). Importantly, the clade A Envs express an asparagine at position 160 within the V2 loop, while the clade B SF162 expresses a lysine at that position (which is mutated to an asparagine in the case of the SF162 K160N construct). The presence of an asparagine at position 160 creates a potential N-linked glycosylation site, which is absent from the Env of SF162.

We first investigated the binding of PG9 and PG16 to this panel of gp140 Envs by ELISA. We observed that PG9 bound to both the monomeric and trimeric forms of Q168a2, Q259d2.17 and SF162 K160N gp140, although the binding to the monomeric forms was superior to that of the corresponding trimeric forms (Figure 1.1). Interestingly, PG9-binding to SF162K160N was superior ric forms of SF162 K160N gp140 and weakly to the monomeric form of Q168a2 gp140. As observed for PG9, PG16 preferentially recognized the monomeric gp140 forms and more efficiently bound SF162K160N than Q168a2. To our knowledge, this is the first evidence of PG16 binding to a soluble gp140 molecule (SF162 K160N gp140).

In some cases, such as PG9 binding to monomeric Q168a2, Q259d2.17, and SF162 K160N gp140s and trimeric SF162 K160N gp140, or PG16 binding to monomeric SF162 K160N gp140, the affinities of PG9/PG16 binding were comparable (within 1.5 fold) to that of the V3-specific MAb 447-52D. It appears, therefore, that the PG9 / PG16 epitope is not universally absent from soluble Env proteins, rather, as with other antibody epitopes, it is presented on soluble gp140 Env in an isolate-dependent manner.

Binding of PG9 and PG16 to several monomeric and trimeric gp140s in solution

Binding interactions in an ELISA format occur on a solid surface, with the antigen (in this case, gp140 Env) non-specifically adsorbed on the well surface. This may lead to occlusion of certain epitopes or alter the conformation of Env in such a way that antibodies, which may bind well to the native protein molecules in solution, fail to bind or bind very inefficiently to the ELISA-

adsorbed protein molecules. To determine whether the selective binding of PG9 and PG16 to a subset of the gp140 molecules tested here was due to the absence of the appropriate epitopes on the constructs that did not bind, or due to artifacts of the ELISA assay, we characterized the interaction of PG9 and PG16 with monomeric and trimeric gp140 in solution (Figure 1.2). During those experiments, the antibodies and the Env proteins are allowed to interact in solution and then the antibodies (and any bound Env molecules) are immunoprecipitated. Any immunoprecipitated Env is then detected by Western blot analysis.

Results from the immunoprecipitation experiments confirmed those obtained by ELISA,

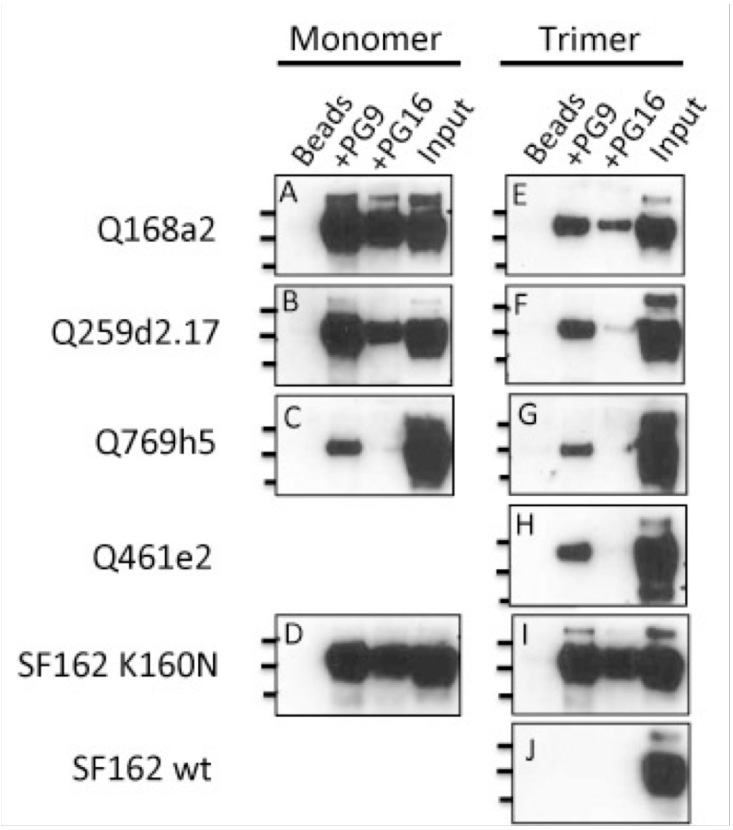

Figure 1.2. In solution interaction of PG9 and PG16 monomeric and trimeric gp140 . Shown are Western blots, with protein bands corresponding to gp140 Env immunoprecipitated by PG9 and PG16. Immunoprecipitations of purified monomeric (A-D) and trimeric (E-J) gp140 molecules for Q168a2 (A and E), Q259d2.17 (B and F), Q769h5 (C and G), Q461e2 (H), SF162 K160N (D and I), and SF162 (J) are indicated in the inset. Lines designate molecular weights (250, 130, and 100 kDa for the Top, Middle, and Bottom lines, respectively). Beads: Env was incubated with Protein G-Agarose beads in the absence of MAb. Input: 10 ng of protein were directly applied to the SDS-PAGE gels.

in that PG9 recognizes Q168a2, Q259d2.17 and SF162 K160N and that PG16 recognizes the SF162 K160N envelope. However, additional weak interactions became evident during immunoprecipitation experiments. For example, PG9 bound to Q461e2 and Q769h5 in solution. Also, PG16 bound to Q168a2 and to a lesser extent, Q259d2.17 in solution. The relative levels of PG9 and PG16 binding to gp140 Env were similar in the case of SF162 K160N, however, for Q168a2 and Q259d2.17, PG9 appeared to bind at a higher level than PG16 (especially in the cases of trimeric Q168a2 and Q259d2.17 gp140).

Similar to what we observed by ELISA, here too, the monomeric gp140 forms of Q168a2 and Q259d2.17 were more efficiently recognized by PG9 than the corresponding trimeric gp140 forms. Overall these results confirm the observations made by Walker et al., (30) that the epitope of PG9 is present on the protomer forming the Env trimeric spike, but also indicate that the PG9 / PG16 epitope is either partially occluded in the context of soluble trimeric gp140 molecules, or that monomeric and trimeric gp140 represent distinct populations of Env that are differentially recognized by PG9 / PG16, perhaps as a result of distinct post-translational modifications between the two populations, as will be discussed further in the following sections.

During these immunoprecipitation experiments, 100 ng soluble gp140s were first incubated with MAbs and the MAb-gp140 complexes were then immunoprecipitated with the use of agarose beads. The beads were resuspended in loading buffer, and a third of the resuspension volume was loaded on the SDS-PAGE gel. In parallel, 10 ng of gp140 was directly applied to the same gel, as an internal control. Based on the intensity of the protein bands shown in Figure 1.2, it appears that in most cases, PG9, and especially PG16, were able to immunoprecipitate only a fraction of the available gp140 molecules in solution. This was particularly true for the trimeric gp140 forms. Potentially, this is related to poor accessibility of the PG9 and PG16 epitopes on soluble trimeric gp140s by the IgG versions of these antibodies. However, it is also seems likely that only a fraction of the gp140 molecules produced in 293

cells display the necessary glycosylation profiles that are required for the binding of PG9 or PG16, as recently reported (131, 133).

PG9 and PG16 Binding to gp120 and gp140 proteins

Given that PG9 and PG16 IgGs preferentially bound to monomeric Q259d2.17 gp140 as compared to the trimeric gp140 form, we examined the possibility that these antibodies would also interact with monomeric Q259d2.17 gp120 molecules. To test this hypothesis, we again performed immunoprecipitation experiments and compared the binding of PG9 and PG16 to purified Q259d2.17 gp120 and the corresponding monomeric and trimeric gp140s (Figure 1.3A). We observed that PG9 bound better to monomeric gp140 than it did to the monomeric gp120 form. PG16 bound the monomeric gp140 but not gp120. Similarly, PG9 did not recognize the Q461e2 gp120, while it weakly recognized the trimeric gp140 form. We were unable to investigate the binding of PG9 to the monomeric Q461e2 gp140 form, since (as discussed above) this Env is predominantly expressed as a trimer. In contrast to these two examples, the predominant recognition of the gp140 over the gp120 form was not evident in the case of the SF162K160N Env. In that case, PG9 (and PG16) recognized with an apparent equal efficiency the gp120, monomeric gp140 and trimeric gp140 forms. As expected, the SF162 gp120 or trimeric gp140 forms were not recognized by either PG9 or PG16. These results were confirmed by ELISA (Figure 1.3B). Here we also examined the binding of PG9 and PG16 to monomeric gp140 as well and observed that PG9 binds more efficiently to the monomeric gp140 form than the corresponding monomeric gp120 form.

Proper gp120-gp41 cleavage is not required for PG9 and PG16 binding to gp140

Because immunoprecipitation appears to be a more sensitive test of the ability of PG9 and PG16 to recognize soluble gp140 constructs, we used this method to characterize PG9 and PG16 binding to a series of mutated gp140 Env proteins. This allowed us to investigate 1)

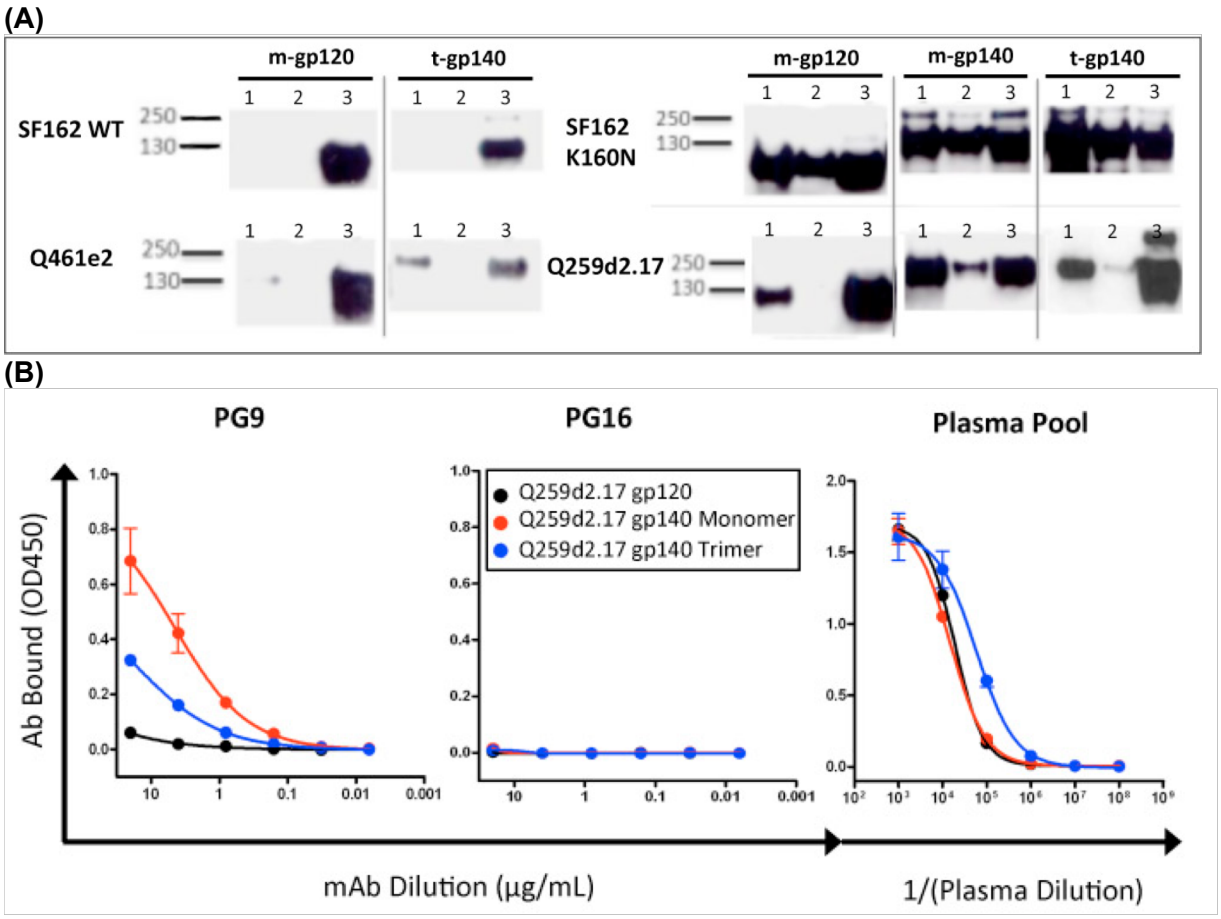

Figure 1.3. PG9 and PG16 binding to gp120 and gp140 proteins. (a) Purified monomeric gp120 (m-gp120), monomeric gp140 (m-gp140) or trimeric gp140 (t-gp140) were incubated with PG9 or PG16 and immunoprecipitated as described in Materials and Methods. Molecular weight markers are indicated. Lane 1: PG9; lane 2: PG16; lane 3: 10 ng of protein were directly applied to the SDS-PAGE gels. (b) ELISA binding curves are shown for monomeric gp120 as well as monomeric gp140 and trimeric gp140 derived from Q259d2.17. HIV+ plasma pool was used as control to confirm the presence of equal amounts of gp120 and gp140 on the ELISA plates.

whether Asn 160 is required for PG9 and PG16 recognition of gp140 Env examined here (as reported in the case of virion-associated Envs) (30), and 2) whether cleavage of Env at the gp120-gp41 furin cleavage site impacts the binding of PG9 and PG16 to soluble gp140 constructs (Figure 1.4).

Our immunoprecipitation and ELISA results discussed above, indicated that the replacement of the lysine by an asparagine at position 160 in the V2 loop of the SF162 Env,

(A)

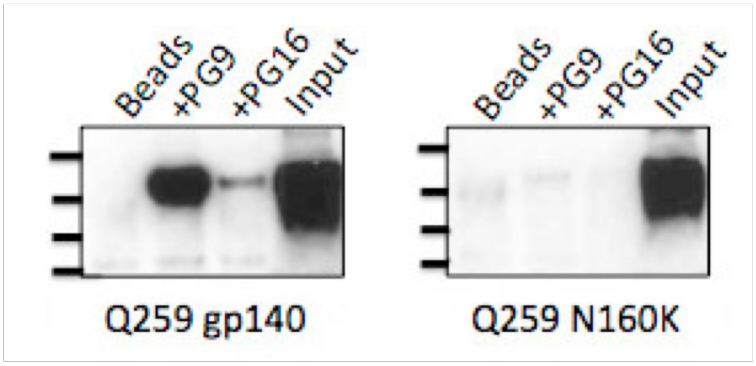

(B)

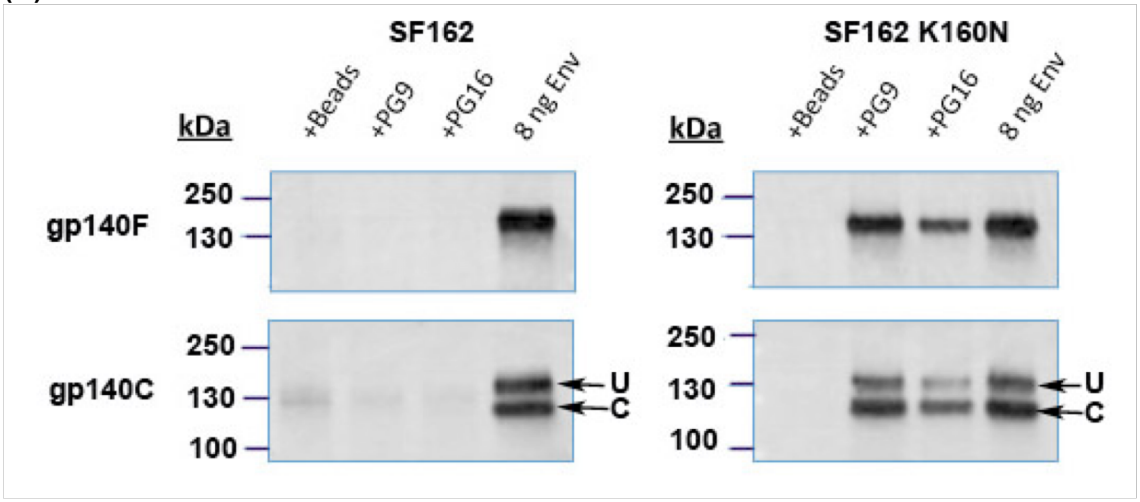

Figure 1.4. Post-translational modifications affecting the binding of PG9 and PG16. (a) Western blot of gp140 Env immunoprecipitated by PG9 or PG16, from transfection supernatants containing Q259d2.17 or Q259d2.17 N160K gp140. Input: supernatant was directly loaded onto the indicated wells. Beads: supernatants were incubated with protein G agarose beads in the absence of MAb. (b) Western blot of either uncleaved (gp140F; Top) or cleaved (gp140C; Bottom) gp140 Env proteins immunoprecipitated from transfection supernatants containing either SF162 or SF162 K160N. Molecular weights are indicated on the vertical axis.

was sufficient to confer very efficient binding by both PG9 and PG16 (Figure 1.2). The reverse mutation (N160K) on the backbone of the Q259d2.17 gp140, abolished recognition of that Env by PG9 and PG16 (Figure 1.4A). These results indicate that, as reported for the case of virion-associated Env gp160, the recognition of soluble gp140 constructs by PG9 and PG16 depends on the presence of an asparagine at position 160 (30).

Intracellular enzymatic cleavage of HIV-1 Env gp160 into gp120 and gp41 optimizes the presentation of certain neutralization epitopes (137, 245-247). Apparently, gp160 cleavage into gp120 and gp41 alters the conformation of Env. The gp140 constructs used in the above-discussed experiments were artificially modified so that the natural gp120-gp41 cleavage site was removed, to increase the stability of the expressed trimeric gp140 (248, 249). We reasoned that potentially, PG9 and PG16 may recognize properly cleaved gp140 molecules more efficiently than the above-discussed non-cleaved gp140 molecules. To address this, we compared the binding of PG9 and PG16 to two versions of SF162 K160N gp140: one containing the REKR furin cleavage site (denoted gp140C) and one with a mutated cleavage site (denoted gp140F) (Figure 1.4B).

Gp140C and gp140F were expressed in the supernatant of transiently transfected cells, and the MAbs were added to those supernatants. It is well established that during transient transfection of cell lines with plasmids expressing the 'cleavable' form of gp140 (gp140C) a mixture of cleaved gp140s as well as non-cleaved gp140s can be found in the cell supernatant due to insufficient intracellular amounts of endogenous furin-like enzymes (250). Assuming that both cleaved and non-cleaved gp140s are recognized by MAbs PG9 and PG16, then two protein bands will be visible after western blotting (when anti-gp120 antibodies are used as the detecting reagent): a band of approximately 140kDa, corresponding to the uncleaved gp140 (designated as ' U' in Figure 1.4B) and a second band of approximately 120kDa (designated as 'C' in Figure 1.4B), corresponding to the gp120 part of the cleaved gp140 (during sample denaturation prior to SDS electrophoresis, the gp120 subunits dissociate from their gp41 counterparts).

PG9 and PG16 recognize both the cleaved and non-cleaved versions of SF162 K160N gp140 (Figure 1.4B). Based on the intensity of the Env bands, it does not appear that PG9 and PG16 recognized the 'cleaved' Env significantly more efficiently than the corresponding non-cleaved Env.

Quantitative determination of PG9 / PG16 binding to gp140 Env by SPR

ELISA and immunoprecipitation methodologies do not provide 'real time' binding information. The relatively inefficient binding of PG9 and PG16 to certain constructs, such as the clade A gp140s, and the more efficient binding to the SF162K160N gp140, could be due to differences in the dissociation, association, or both binding rate constants. To better understand the binding kinetics between gp140 and PG9 and PG16 we used SPR to determine equilibrium dissociation constants (K_D), association rate constants (k_a) and dissociation rate constants (k_d) (Figure 1.5). In cases where no binding of PG9/PG16 to specific gp140s was detected by ELISA or immunoprecipitation, SPR may reveal transient and weak interactions. The V3 loop-specific MAb 447-52D (236) was used as an internal control to confirm the activity of Env on SPR sensor chips.

Despite high densities of amine-coupled gp140 monomer or trimer ligands (~1500 RU and ~3000 RU, respectively), the SPR responses by PG9 and PG16 Fabs were low (Figure 1.5). PG9 and PG16 Fab binding to Q168a2 or Q259d2.17 monomeric or trimeric gp140 was less than 50 RU, while in the case of the SF162K160N gp140 it reached approximately 115 RU. These responses were substantially lower than that of 447-52D Fab, which commonly approached RU values 1.3 - 50 times greater than that of PG9 Fab after 7 minutes of association (Appendix A, Table S1). The observed lower activities of gp140 ligands to PG9/PG16 than 447D binding could be due to several reasons. For example, as discussed above, only a fraction of gp140 molecules may express the PG9/PG16 epitopes due to heterogeneity in glycosylation. Also, coupling conditions may stochastically interfere with gp140 binding selectively, for instance by a greater number of lysine residues at or near PG9 or PG16 binding sites than 447-52D binding site. This would lead to inaccessibility of the PG9 and PG16 epitopes on the chip, while not affecting the accessibility to the 447D epitope.

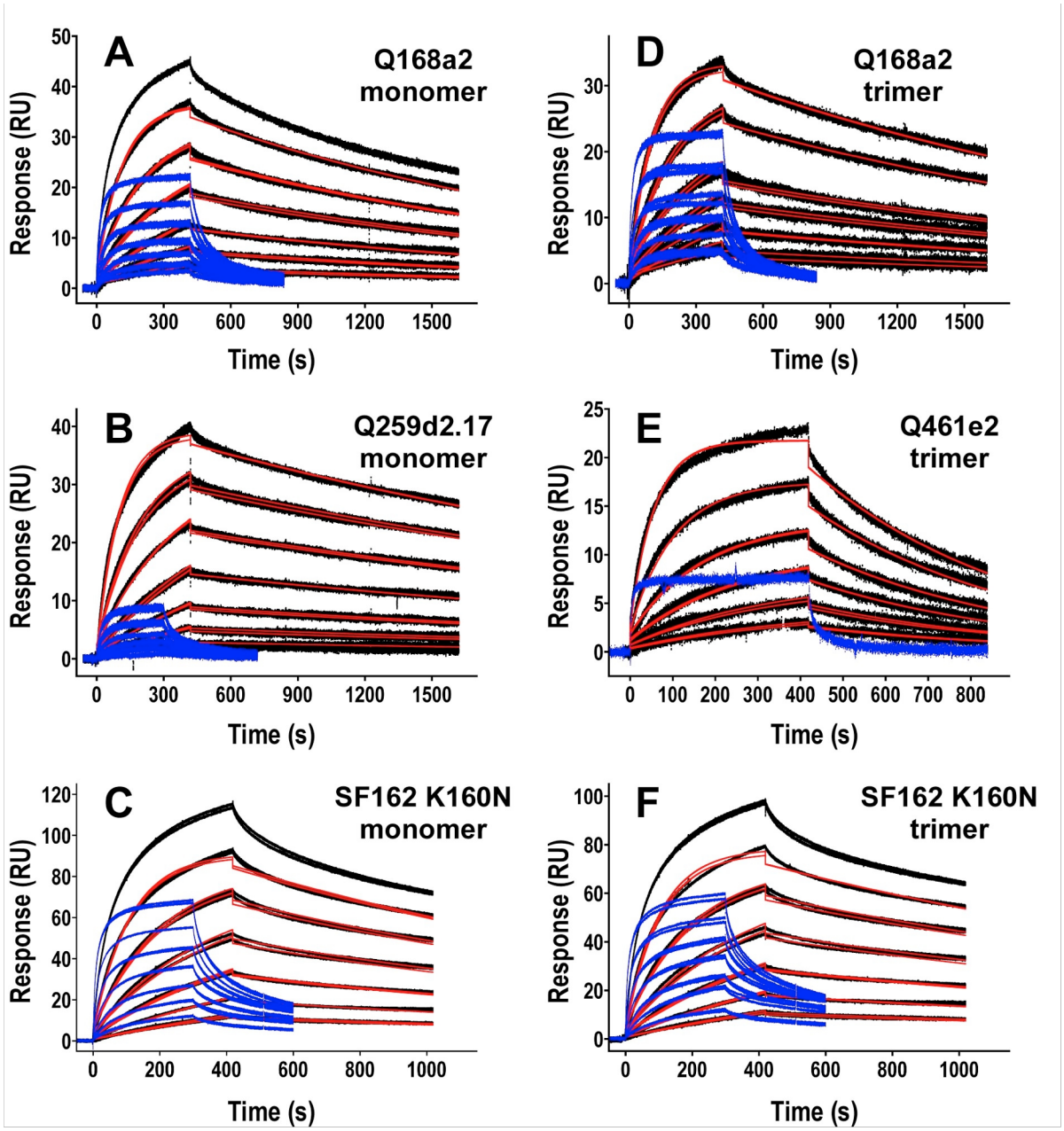

Figure 1.5. PG9 and PG16 Fab binding to gp140 by SPR. Sensorgrams of PG9 and PG16 Fab analyte series binding to immobilized gp140 ligands. PG9 binding curves are shown in black with corresponding kinetic fits in red; superimposed PG16 binding curves are shown in blue. Serial two-fold dilutions of analytes were used, starting at 1 μM for PG9 Fab in panels A through C, E and F and 500 nM for PG9 Fab in panel D. PG16 Fab concentration ranges started at 1 μM in panels A through C and F and 2 μM in panel D. A single PG16 Fab concentration of 2 μM was run in panel E.

In all cases, for any given gp140 construct, the maximum observed response for PG16 Fab was less than that of PG9 Fab. In addition to distinct levels of binding, the PG9 and PG16 Fab sensorgrams were qualitatively different, in that most PG9 Fab binding curves could be well-approximated by a 1:1 binding model whereas the binding curves for PG16 Fab deviated significantly from a 1:1 model and could be better approximated by two-state binding interaction, heterogenous analyte, or heterogenous ligand models.

As summarized in Table 1.1, the K_D values for PG9 Fab binding to gp140s were typically on the order of 25 nM for both monomeric and trimeric gp140 constructs, with the exception of the Q461e2 trimer (K_D ~ 130 nM). A K_D value could be determined for the interaction between PG9 Fabs and Q259d2.17 monomers (29 nM), but not the trimer, because SPR responses of PG9 Fab analytes to trimeric Q259d2.17 gp140 ligands were too low (<10 RU) to confidently parameterize. In contrast, the K_D values for PG9 Fab binding to monomeric Q168a2 and SF162 K160N (27 nM and 33 nM, respectively) were similar to those observed for PG9 Fab binding to the trimeric versions of each isolate (20 nM and 26 nM, respectively). K_D values of qualitatively the same order of magnitude were observed when reverse SPR experiments were performed by capturing PG9 IgG on the chip and using Q168a2 gp140 as the analyte, though this flipped arrangement could not be used for precise, quantitative measurements (data not shown).

Therefore, despite the observation that the IgG versions of PG9 and PG16 recognize monomeric gp140s more efficiently than the trimeric gp140s by ELISA and immunoprecipitation

Table 1.1 PG9 Fab Binding to gp140 by SPR

	gp140 monomer			gp140 trimer		
gp140	K_D (nM)	k_a ($M^{-1}s^{-1}$)	k_d (s^{-1})	K_D (nM)	k_a ($M^{-1}s^{-1}$)	k_d (s^{-1})
Q168a2	26.81(3)	$1.731(2) \times 10^{4}$	$4.640(2) \times 10^{-4}$	20.21(3)	$1.950(2) \times 10^{4}$	$3.940(2) \times 10^{-4}$
Q259d2.17	29.30(3)	$9.658(9) \times 10^{3}$	$2.830(2) \times 10^{-4}$		Signal < 10 RUs	
Q461e2		ND		130.3(2)	$1.557(2) \times 10^{4}$	$2.029(2) \times 10^{-3}$
Q769h5		Signal < 10 RUs			Signal < 10 RUs	
SF162 K160N	33.24(4)	$1.746(2) \times 10^{4}$	$5.805(4) \times 10^{-4}$	26.46(4)	$1.855(2) \times 10^{4}$	$4.910(4) \times 10^{-4}$
SF162		ND			Did not bind	

*Standard error on the last significant figure is reported in parentheses
ND: not determined

(as discussed above), this preferential binding to gp140 monomers was not observed in SPR measurements, when the Fab versions of these antibodies were used, though quantitative analyses for only two monomer/trimer pairs (Q168a2 and SF162 K160N) were available for direct comparison.

Correlation between PG9 and PG16 neutralizing activities and binding affinities to soluble trimeric gp140

We performed neutralization experiments with the IgG and the Fab versions of PG9 and PG16 against viruses expressing the Envs described above, including those Envs that were not recognized by these antibodies as gp140 molecules (Figure 1.6). The results are summarized in Table 1.2. With the exception of SF162, all the other viruses tested were susceptible to neutralization by PG9 and PG16 (Figure 1.6). Therefore, even in cases where binding of PG9 or PG16 to the soluble trimer was not observed, neutralization of the corresponding virus took place, similar to previous reports (30, 81). This was the case, for example, with PG16, which neutralized Q769h5 and Q461e2, but did not bind to these soluble Envs (Figures 1.1, 1.2 and 1.6).

There was no instance where PG9 or PG16 bound to a given soluble gp140 Env but did not neutralize the corresponding virus. This was observed, however, for the control MAb, 447-52D, which binds to an epitope within the V3 loop of gp120 and interacts very efficiently with monomeric gp120. MAb 447-52D bound to all clade A Env gp140 tested (Figure 1.1 and additional data not shown) but did not neutralize the corresponding viruses (Figure 1.6). As previously reported, 447-52D neutralized the clade B SF162 virus (239), but interestingly the anti-SF162 neutralizing activity of 447-52D decreased when the lysine at position 160 was replaced by an asparagine. The presence of an asparagine at that position creates an N-linked glycosylation site and the presence of sugar molecules on that site may partially occlude the epitope of 447-52D on the virion-associated Env spike. Alternatively, the presence of the amino

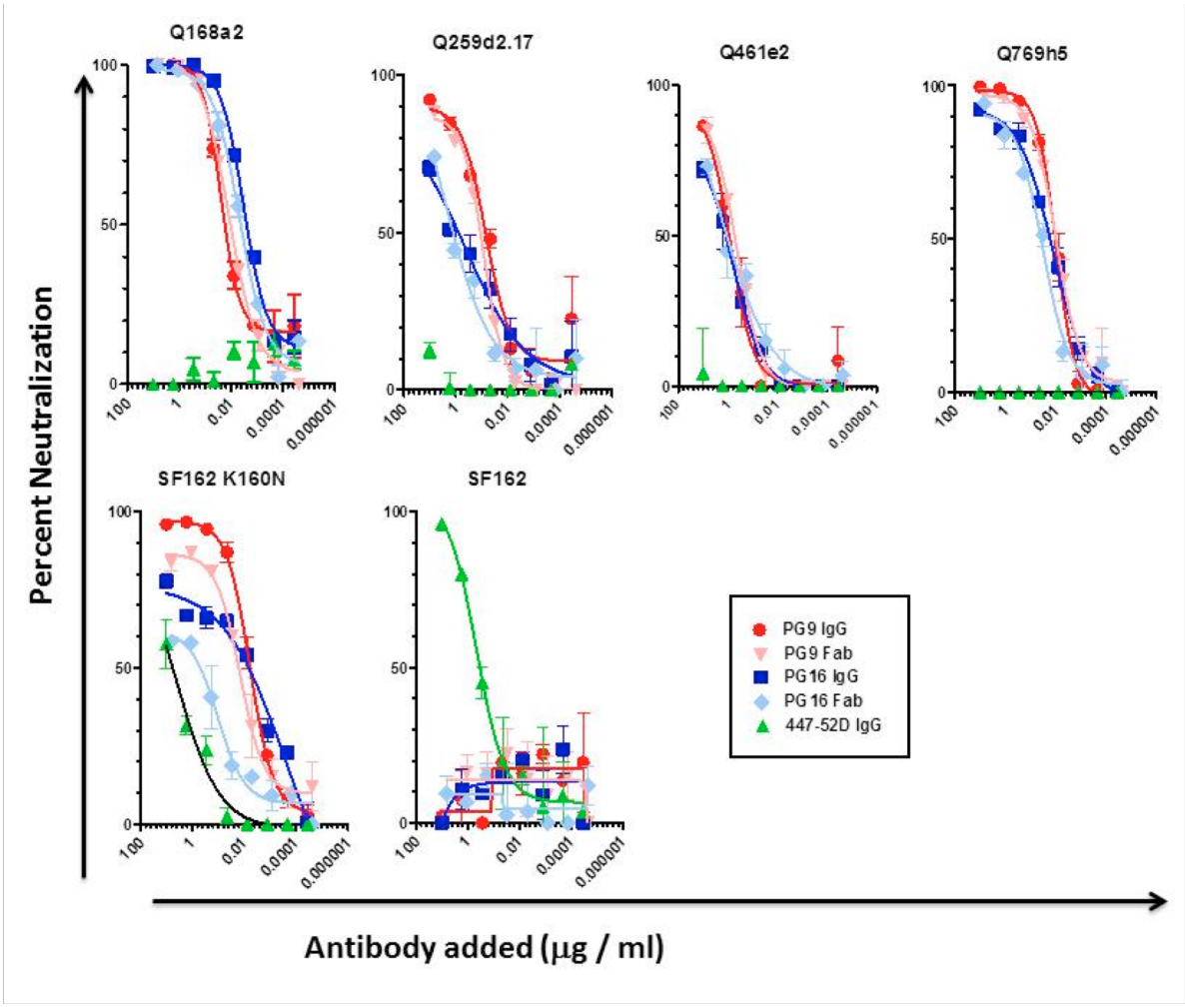

Figure 1.6. Neutralization by the IgG and Fab versions of PG9, PG16, and 447-52D. Shown are neutralization curves representative of two independent experiments. The form of antibody used, IgG or Fab, is indicated in the inset. The target virus is indicated above each insert.

acid asparagine, and/or the attached sugars, may alter the conformation of Env in a way that reduces the accessibility of the V3 loop.

PG9 and PG16 IgG neutralized with similar potencies, overall. Across the panel of isolates, the IC50 values for PG9 and PG16 neutralization each spanned a 2 Log_{10} range. In contrast, the binding affinities measured by SPR were quite similar between isolates for which data was available (Table 1.1). Additionally, PG9 and PG16 potently neutralized the isolate Q769h5, despite their poor recognition of soluble gp140 in ELISA, IP and SPR experiments (where estimation of PG9 Fab binding affinity was not possible due to its low specific activity).

Despite the fact that a correlation between PG9 / PG16 neutralizing potency and binding affinity to soluble Env was not observed in all cases examined here, in certain instances the pattern of neutralization potency and binding affinity were similar. For example, Fab PG9 bound to the trimeric Q461e2 gp140 with approximately 7 fold lower affinity than to the trimeric Q168a2 gp140 (Table 1.1) and neutralized the Q168a2 virus approximately 2 Log_{10} more efficiently than the Q461e2 virus (Figure 1.6). Also, Fab PG9 bound to the trimeric Q168a2 gp140 with a similar affinity to the trimeric SF162K160N gp140, and neutralized both viruses with very similar potencies.

The Role of Avidity in Neutralization by PG9 and PG16

Our binding results indicate that the epitopes of PG9 and PG16 are present on each protomer within the trimeric spike and that trimerization of Env is not required for their formation, although it may decrease their relative exposure. Anti-HIV antibodies that bind to epitopes on Env that are present and are readily exposed on monomeric gp120, appear to neutralize the virus by binding to the Env spike without cross-linking protomers within that spike (161). It is unknown whether this is also true for PG9 and PG16 whose epitopes appear to be preferentially exposed on the virion-associated Env spike. To test whether avidity plays any role in the neutralization properties of PG9 and PG16, we compared the potency of neutralization by the IgG and Fab versions of these two antibodies, using a Molar Neutralization Ratio (MNR = [Molar IC50 Fab]/[Molar IC50 IgG]), which has been previously used to assess the role of avidity in the potency of neutralization by other HIV-1 and influenza-specific antibodies (161). A large MNR value indicates that more Fab is required to produce the same amount of neutralization (50% in this case) as a smaller quantity of IgG, potentially due to the absence of avidity effects in the Fab. For all isolates tested, the molar IC50 neutralization value for Fab was greater than that observed for IgG, and MNR values typically ranged between 2 and 10 (Figure 1.7A). These values are very similar to those reported for other broadly-neutralizing antibodies, including 2F5,

(A)

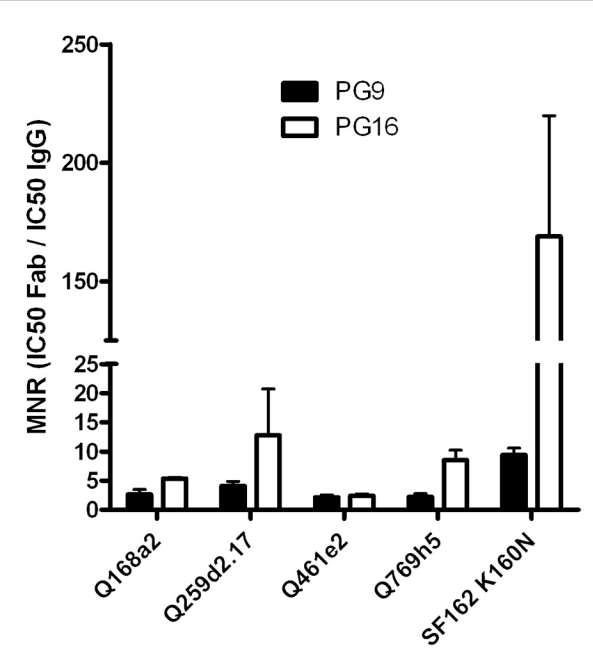

(B)

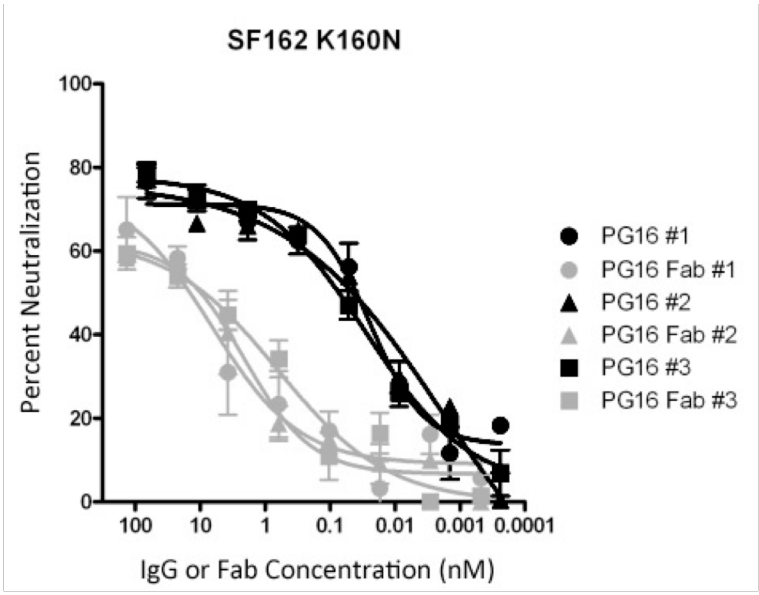

Figure 1.7. Contribution of avidity to the neutralizing activity of PG9 and PG16. (A) Neutralization assays were performed as described in materials and methods, using IgG or Fab versions of PG9 or PG16. The neutralization data was transformed as x=Log[x], and fit using a sigmoidal-dose response curve to calculate IC50 neutralization values. MNR = [IC50 Fab] / [IC50 IgG]; an MNR value >1 indicates that a higher molar concentration of Fab is required to achieve 50% neutralization as compared to IgG. (b) Neutralization curves of SF162K160N by the IgG and the Fab versions of PG16 from three independent experiments (each conducted in duplicate) are shown.

Table 1.2: Neutralizing potencies of the IgG and Fab forms of PG9, PG16 and 447-52D (nM)

Isolate	PG9	PG16	447D
Q168a2	0.094 ± 0.028(IgG) 0.232± 0.035 (Fab)	0.013 ± 0.004(IgG) 0.07 ± 0.017(Fab)	---
Q259d2.17	0.35 ± 0.15(IgG) 1.5 ± 1(Fab)	2.6 ± 3.5(IgG) 14 ± 15.5(Fab)	---
Q461e2	6.07 ± 0.17(IgG) 13.26 ± 3.61(Fab)	6.31 ± 2.53(IgG) 15.8 ± 9.12(Fab)	---
Q769h5	0.063 ± 0.01(IgG) 0.147 ± 0.067(Fab)	0.07 ± 0.05(IgG) 0.567 ± 0.27(Fab)	---
SF162 K160N	0.041 ± 0.003(IgG) 0.39 ± 0.095(Fab)	0.058 ± 0.02(IgG) 9.15 ± 0.85(Fab)	537.8 (IgG)
SF162	---	---	2.3 (IgG)

The IC50 neutralizing titers for the IgG and Fab forms are shown. The values shown are the mean and standard deviation for the mean, of two independent experiments each performed in duplicate. (--): neutralization was not recorded.

4E10, and b12, that are thought to bind with one Fab per Env spike (161). Interestingly, however, the MNR of PG16 for SF162 K160N was 150. To our knowledge, this is the highest reported MNR observed for an HIV-specific neutralizing antibody, and it is on the order of some anti-influenza NAbs, for which, avidity is thought to play an important role in neutralization. We note however that the Fab neutralization curves do not reach complete saturation, which renders the determination of the IC50 values difficult (Figure 1.7B). Overall, these results suggest that in most cases avidity likely does not play a major role in the potency of PG9 / PG16 neutralization, but our data suggest that there is a possible role for avidity in the potency of PG16 neutralization of SF162 K160N.

Discussion

The discovery of PG9 and PG16 expanded our understanding of the epitopes targeted by broadly neutralizing antibody responses which develop during natural HIV-1 infection and spurred an active investigation into the design of Env-based immunogens that better mimic the functional virion-associated HIV-1 Env spike. The characterization of binding and neutralizing

properties of these two MAbs provided direct evidence of the dissimilarities between soluble Env-based immunogens and the corresponding virion-associated Env form. Neutralizing antibody specificities similar to those of PG9 and PG16 have been recently identified in numerous HIV-1+ sera (80, 81). These observations potentially suggest that the corresponding epitopes are immunogenic in the setting of natural HIV-1 infection. This last point provides hope that PG9- or PG16-like neutralizing antibody specificities may be more easily elicited by vaccination than other types of broadly neutralizing antibody specificities, which are rarely identified in HIV-1-positive sera. The absence, or inefficient presentation, of epitopes similar to those of MAbs PG9/PG16 on soluble Env immunogens, is however a significant obstacle in the elicitation of the corresponding antibodies by immunization.

With the goal of furthering our understanding of the overlapping epitopes recognized by PG9 and PG16, we used multiple, complementary techniques, including ELISA and immunoprecipitation methodologies, to identify a number of soluble gp140 Env proteins which are recognized by PG9 and PG16. It was previously reported that while PG9 and PG16 efficiently recognized cell surfaced expressed Env, they rarely recognized the corresponding soluble monomeric gp120 by ELISA (30, 81). Here we report that, in some cases, binding interactions between PG9 / PG16 and soluble Env (gp120 or gp140) that are not observed by ELISA, may be detected through other binding assays such as immunoprecipitation or SPR. Our data also indicate that the presence of the extracellular part of gp41 on some (but not all) gp140 constructs, improves the recognition of the PG9 and PG16 epitopes on the gp120 subunit. Potentially, gp120 and gp140 molecules undergo distinct post-translational modifications, such as glycosylation, which greatly influences the binding of PG9 and PG16 (133). Alternatively it is possible that the gp41 ectodomain of certain Envs stabilizes the conformation of the PG9 / PG16 epitopes. We note, however, that the comparison of PG9/PG16-binding to gp120 and gp140 was only made with a small number of Envs, and among these, SF162 K160N gp120 bound at a high level to both PG9 and PG16. Similar

studies with a greater number of Envs derived from other isolates are required to better define the contribution of the gp41 ectodomain in the proper formation of the PG9/PG16 epitope in the context of soluble gp140.

Our observation that PG9 and PG16 recognize the monomeric form of gp140 supports the initial observation made by Walker et al., (30), that the epitopes for PG9 and PG16 exist on the individual protomers forming the Env trimer. Our current data however also reveal that the PG9 / PG16 epitope is poorly presented in soluble, trimeric gp140 Env as compared to monomeric gp140 Env. When considered simultaneously, the ELISA/IP results and the binding affinities estimated by SPR can be interpreted in at least two ways. By one interpretation, Env trimerization may restrict the accessibility of these two overlapping epitopes to the full-length IgG versions of PG9 and PG16 used in IP/ELISA experiments. Such accessibility restrictions appeared to be eliminated when the smaller, Fab versions of these antibodies were used in SPR. Alternatively, it may be that PG9 IgG (like Fab) binds to monomeric and trimeric gp140 Env with equal affinity, but the fraction of Env proteins that are capable of binding to PG9 / PG16 within the population of trimeric gp140 molecules is smaller than that within the population of monomeric gp140. This may be explained by differences in post-translational modification (e.g. glycosylation or disulfide bonding) between the monomeric and trimeric populations. Further studies will be required to differentiate between these two possibilities. These observations may be important for the design of soluble Env immunogens that aim at the elicitation of PG9- and PG16-like antibody responses. If epitope-immunogenicity is positively associated with epitope-exposure on the surface of an immunogen, then our data suggest that appropriately designed soluble monomeric gp140s may be more appropriate for the elicitation of PG9- or PG16-like neutralizing antibody specificities than soluble trimeric gp140s.

From the small number of soluble gp140 Envs tested here, the one most efficiently recognized both by PG9 and PG16 was the modified SF162 Env, SF162K160N. The SF162 virus is susceptible to neutralization by numerous antibodies; including antibodies against the

variable as well as antibodies to conserved regions of Env (239). Presumably the virion-associated SF162 Env trimeric form has an 'open' configuration, that is unlike the 'closed' configuration of Envs from typical tier 2 primary isolates. The only reason for the absence of SF162-neutralizaiton by PG9 or PG16 is the presence of a lysine at position 160 instead of an asparagine. Once the K to N mutation is introduced, the virus becomes very susceptible to PG9 and PG16 and the MAbs very efficiently recognize the soluble gp140 versions of that Env. It appears therefore that the trimeric SF162 K160N Env adopts a configuration that is not dissimilar to that of Envs from viruses that are susceptible to PG9 or PG16.

PG9 and PG16 recognize overlapping epitopes and display very similar breadths and potencies of neutralizing activities, although differences in both binding and neutralizing activities have been reported (30). We observed that PG16 recognized a smaller number of gp140s tested here than PG9. Potentially, despite the overlapping nature of the PG9 and PG16 epitopes, any structural differences between the virion-associated Env form and the soluble gp140 form, have a greater impact on the PG16 epitope than the PG9 epitope.

Although ligand specific activities were low in SPR experiments, the kinetics of association and dissociation of PG9/gp140 interactions revealed a relatively tight binding: K_D values on the order of 25 nM. This affinity is comparable to values previously reported for the anti-V3 loop antibody 447-52D Fab binding to SF162 gp140 molecules (K_D values in the order of 90 nM) (251). The SPR analysis also revealed that only a fraction of Env molecules that were available for antibody binding were engaged by PG9 (low ligand specific activities). Explanations for low activities include ligand heterogeneity (for instance, differential Env glycosylation (131, 133) or temporal fluctuations in the exposure of the PG9 epitope on gp140 (either soluble monomers or within the context of soluble trimers), and incomplete stochastic ablation of analyte binding sites during primary amine coupling, potentially reflecting the presence of lysine residues at or near PG9 and PG16 binding sites.

PG16 sensorgrams are only adequately modeled by higher-order binding models including additional fitting parameters. While multiphasic sensorgrams are common, they are not necessarily biologically relevant and are often the result of heterogeneous or oligomeric analytes (though oligomers are unlikely the problem because of careful SEC purification just prior to analysis) or chemically or conformationally heterogeneous ligand surfaces (252). PG16 exists in both sulfated and non-sulfated forms and the extent of PG16-sulfation greatly affects the neutralizing potential of this antibody (253) and potentially the interaction kinetics with gp140s. However, PG9 also exists in sulfated and non-sulfated forms, and yet the PG9-gp140 SPR sensorgrams are adequately fit with simple 1:1 binding models. Therefore the multiphasic PG16-gp140 binding curves may not be related to the relative proportion of the sulfated and non-sulfated antibody molecules in our preparation. Another explanation for the observed SPR binding curve shapes for PG16 could be related to the glycosylation heterogeneity of our gp140 preparations. The neutralizing activity of PG16, and presumably the efficiency with which it binds its epitope, is sensitive to changes in the type and extent of Env glycosylation (133). Gp140 glycosylation heterogeneity in our preparations could lead to a wide range of binding kinetics. Since Env glycosylation is known to affect PG9 neutralizing activity as well (133), Env glycosylation heterogeneity must affect PG9 binding to a lesser degree, consistent with the very distinct overall binding properties of these two related antibodies. The combination of heterogeneity in antibody-sulfation and gp140-glycosylation may be responsible for the observed differences in binding kinetics between PG9 and PG16.

It is proposed that, due to the scarcity of functional Env spikes on HIV-1 viral particles, antibodies that neutralize HIV, do so without cross-linking Env spikes, but rather by one antibody binding to one Env spike (161). The binding of an antibody to an individual Env spike is mediated by only one of the two antibody arms. In other words, the antibody binds to a single protomer within the spike, without cross-linking two protomer within that spike. Therefore, avidity does not appear to play a major role in antibody-mediated neutralization of HIV. Our data

indicate that PG9 and PG16 neutralize with a similar mechanism. Only in the case of the PG16/SF162K160N virus combination, we observed a significant contribution of avidity in neutralization. It is unclear whether this effect would be unique to the PG16 / SF162 K160N combination, or a similar observation will be made once additional viruses are examined in this manner. At this time it is not known why avidity does not appear to be involved in the neutralization of SF162K160N by PG9. The distinct manner in which SF162K160N is neutralized by PG9 and by PG16, is another indication that these two antibodies may differ structurally, that their post-translational modification differs, and that their epitopes, despite significant similarities, display important differences.

In summary, the results presented here indicate that the epitopes of PG9 and PG16 are presented in the context of some, but not all, soluble gp140s. The identification of several soluble gp140 Env constructs that are recognized by PG9 and by PG16 is important because it facilitates studies to better define similarities and differences in the epitopes of these two MAbs. It will also allow us to investigate how post-translational Env modifications affect the formation and exposure of these two overlapping epitopes. Such studies are crucial to our efforts that aim at engineering soluble Env-based constructs that would accurately express conserved HIV neutralization epitopes which are naturally immunogenic.

ACKNOWLEDGEMENTS

This study was supported by NIH grant AI47708 (LS) and by a grant from the Bill & Melinda Gates Foundation, as part of the CAVD program. We would like to thank all those who contributed reagents that were used in our study.

Chapter 2

Isolate-Specific Differences in the Conformational Dynamics and Antigenicity of HIV-1 gp120

The text in this chapter has been modified slightly from © American Society for Microbiology, Journal of Virology, Vol. 87(19), 2013, p.10855-73. doi: 10.1128/JVI.01535-13.

Introduction

The HIV-1 Envelope glycoprotein (Env) facilitates viral entry into host cells through a series of receptor-mediated conformational changes that lead to fusion of the viral and host membranes. Env is a heavily glycosylated trimer of gp120 surface subunit and gp41 transmembrane subunit heterodimers. As the primary target of the humoral immune response against HIV-1 (11, 21, 254), Env is the focus of intensive vaccine design efforts (203). HIV-1 escape from neutralizing antibodies generates exceptional diversity within the Env gene, which is particularly concentrated within the variable loops of gp120 (V1-V5) (26, 88-90). It is widely believed that an effective antibody-based HIV-1 vaccine would need to elicit antibodies capable of recognizing diverse Env isolates, ideally including “broadly” neutralizing antibodies (NAbs) as well as non-neutralizing antibodies with antibody-dependent cellular cytotoxicity (ADCC) effector functions that appeared to correlate with protection in the RV144 HIV-1 vaccine trial (65). Indeed, the hopeful results of the RV144 trial, which provided evidence that vaccine-induced protection against HIV-1 may be possible (64), suggest that monomeric gp120 is a relevant HIV-1 vaccine immunogen and highlight the importance of understanding the structural features that distinguish gp120 proteins and influence gp120 reactivity with neutralizing and ADCC-active antibodies (66, 134, 255).

Although the sequence and functional diversity of HIV-1 Env have been well-described (26, 121, 193), the degree of structural variability among global Env isolates, which must be overcome by broadly cross-reactive neutralizing and ADCC-active antibodies, is poorly understood. Similarly, it is unclear what structural features are associated with improved antibody recognition of Env immunogens and how these features vary among immunogens derived from distinct HIV-1 isolates. Cryo-electron microscopy studies have provided evidence that trimeric Env from distinct isolates can adopt different quaternary conformations on the virus surface (28, 33), but the detailed structural differences underlying these large-scale morphological rearrangements have not been resolved. Crystal structures of HIV-1 gp120 core, with variable loops and glycosylation largely removed, have been determined for a number of Env isolates from multiple clades (25, 35, 186-192). The available structures indicate that the gp120 core is organized into a conserved inner domain composed of three layers (35), a heavily-glycosylated outer domain, and a bridging sheet subdomain that forms upon CD4 binding (25). Furthermore, these truncated gp120 structures revealed a striking degree of structural conservation in the gp120 core across clades (19, 192). This conservation contrasts with the significant functional variability among diverse Env isolates, including differences in sensitivity to neutralizing antibodies (121), co-receptor usage (122, 256), CD4-reactivity (257), dependence upon CD4 (123, 124), antigenicity (193) and immunogenicity (194). This discrepancy between the functional diversity of Env and the apparent structural conservation of gp120 has often been attributed to quaternary structural differences in trimeric Env, which may not be apparent in monomeric gp120 (28, 188). However, differences in the antigenicity (193) and immunogenicity (194) of gp120 proteins from diverse isolates suggest that there is substantial conformational heterogeneity among isolates even in the context of monomeric gp120.

The apparent homogeneity of the available gp120 core structures is rooted in the fact that the most divergent features of gp120, the variable loops and glycans (258) are truncated in

order to facilitate crystallization. This is problematic for understanding the relationship between gp120 structure and antigenicity because these elements are the primary regulators of antibody binding to Env (259-261). Variable loop truncation has also been reported to allow the core to adopt the receptor-bound state even in the absence of receptor, potentially favoring uniformity among the core structures (192). Additionally, most structures feature gp120 core in complex with a stabilizing ligand such as sCD4 or antigen binding antibody fragments (Fabs) which may influence the observed core structure (188). The available crystal structures of truncated core constructs thus provide a detailed picture of how antibodies and receptors recognize the conserved elements of gp120, but the structural basis for isolate-specific antigenic and immunogenic differences among gp120 proteins remain poorly characterized.

To better understand the structure-function relationship that governs gp120 Env antigenicity, it is necessary to study constructs with intact variable loops (V1-V5) and glycosylation under native conditions. The critical importance of characterizing gp120 in solution is supported by previous work, which suggests that the global disorder of gp120 Env may disfavor antibody and receptor binding (145). Conformational flexibility is difficult to assess by x-ray crystallography, however, and requires complementary approaches, such as hydrogen-deuterium exchange with mass spectrometry (HDX-MS) that can elucidate the dynamic character of proteins in solution. HDX-MS was used in two recent studies to examine disorder and structural flexibility in gp120 and to demonstrate that regions throughout the subunit, including the CD4 and co-receptor binding sites, are disordered in unliganded minimal core and full-length gp120 in solution (142, 144). Additionally, a recent study used molecular dynamics modeling to identify isolate-specific differences in residue communication networks within gp120 that contribute to differences in coupled motions among isolates. The study highlighted the role that molecular movements may play in generating conformational diversity among isolates, even within the conserved gp120 core (262).

Here, we investigate the extent of isolate-specific structural differences in a panel of full-length gp120s in their unliganded and CD4-bound forms, and we examine whether site-specific differences in dynamics relate to differences in association with sCD4 and antibodies directed against a variety of linear and conformational epitopes. Four Env isolates with widely divergent phenotypes were compared (Table 2.1): SF162 (263), HXB2 (264), 1084i (265), and 1157ip (266). These isolates are derived from clades B and C, exhibit differences in co-receptor usage, vary in their sensitivity to neutralization by the CD4-binding site-directed antibody IgG1-b12, and exhibit a range of variable loop lengths and number of potential N-linked glycosylation sites (PNGS) (Table 2.1). Of these, HXB2 and 1084i are the most divergent isolates with a sequence identity of 71.4% based on 486 overlapping amino acids. Given the functional diversity of these Env isolates and the variability of their gp120 amino acid sequences, we hypothesized that there would be measurable isolate-specific differences in solution structure and stability among the gp120s, and that differences such as these might contribute to the antigenic variability of gp120 proteins.

We used complementary biophysical methods to characterize the structure of full-length, glycosylated gp120 monomers in solution: small angle x-ray scattering (SAXS) and HDX-MS. SAXS provides a low-resolution structure for proteins in solution (267-269) and can identify the location of the large V1/V2 loops relative to the conserved core (142). HDX-MS provides complementary information on solvent accessibility and local structural dynamics by measuring

Table 2.1. Characteristics of the four Env isolates

Isolate	Source	Clade	Co-R***	b12 IC50	Loop Length (# AA)							Number of PNGS (#)						
				(μg/mL)	V1	V2	V3	V4	V5	C1	V1/V2	C2	V3	C3	V4	C4	V5	C5	Total
1157ip	Plasma	C	CCR5[a]	0.7[d]	21	43	35	28	13	1	6	8	1	3	4	2	2	0	27
1084i	Plasma	C	CCR5[b]	20[e]	16	44	35	21	10	1	6	6	1	3	4	2	1	0	24
HXB2	TCLA*	B	CXCR4[c]	0.01[f]	26	40	36	34	11	1	5	8	1	3	4	1	1	0	24
SF162	CSF**	B	CCR5[c]	<0.01[f]	25	40	35	28	12	1	3	6	1	3	5	1	1	0	21

* T-cell line adapted, ** Cerebrospinal fluid, *** Coreceptor usage, From references [a] (266), [b] (265), [c] (271), [d] (272), [e] (273), [f] (274)

the rate of deuterium incorporation into the amide groups of the protein backbone (197). Amide groups that are buried deep within a protein's hydrophobic core or that participate in stable hydrogen bond networks, such as those in protein secondary structures, take on deuterium slowly, while those in solvent-accessible, flexible or dynamic regions of the native protein take on deuterium rapidly (270).

We observe that while the overall architecture of full-length, glycosylated gp120 is similar among diverse isolates, there are clear isolate-specific differences in the conformational dynamics of both unliganded and CD4-bound gp120, particularly within the gp120 inner domain. Our results provide insight into the structural factors that contribute to naturally-occurring antigenic differences among full-length, glycosylated gp120 proteins and suggest that conformational dynamics should be considered in the selection and design of enhanced HIV-1 Env immunogens.

Materials and Methods

Antibodies and CD4 constructs

Antibodies IgG1-b12 (175, 176, 275, 276), 17b (18, 25, 179, 180, 259), VRC01 (182), A32 (259, 277) and soluble two-domain CD4 (278) and CD4-IgG2 were obtained from the NIH AIDS reagents program. The antibodies N5i5, B18, and C4 were generously provided by Yongjun Guan and George Lewis (U. Maryland) (279, 280). Antibody M90 was purchased from Advanced BioScience Laboratories, Inc. (Rockville, MD) (281). Antibody CA13 (ARP3119) was obtained through the Programme EVA Center for AIDS Reagents of the National Institute for Biological Standards and Control (NIBSC,Hertfordshire, UK).

Expression and Purification of gp120 glycoproteins

Full-length gp120 glycoproteins HXB2, SF162, 1084i, and 1157ip K197N (referred to simply as 1157ip throughout this text) were expressed in African green monkey kidney cells

(BSC40) infected with vaccinia virus encoding the corresponding gp120 sequence within the thymidine kinase locus as described previously (282). Plasmids encoding Env sequences for HXB2 and SF162 were kindly provided by Leo Stamatatos, while those for 1157ip and 1084i were kindly provided by Ruth Ruprecht. All gp120 constructs possessed the same signal sequence derived from HXB2. Briefly, cells were maintained at 37^{o}C and 5% CO_2 in Dulbecco's Modified Eagle's Medium (DMEM) supplemented with 10% fetal bovine serum (FBS) and 1% penicillin/streptomycin (pen/strep). Infection of BSC40 cells was carried out using a multiplicity of infection of 3, after which the cells were cultured in DMEM with 5% FBS and 1% pen/strep for 48 hours. The culture supernatant was clarified by centrifugation and Empigen BB was added to a final concentration of 0.25% to inactivate virus particles. After clarification, gp120 was purified by *Galanthus nivalis* lectin affinity, DEAE ion exchange, and size-exclusion chromatography on a HighLoad 26/600 Superdex 200 column (GE Healthcare). Purified monomeric gp120s were homogenous as determined by denaturing and reducing as well as blue native polyacrylamide gel electrophoresis (PAGE) (Appendix B, Figure B.S1).

Hydrogen-Deuterium Exchange with Mass Spectrometry

HDX-MS was carried out as described previously (142) with a few modifications. Specifically, full-length, glycosylated gp120 proteins were diluted into a D_2O-based phosphate buffer (10 mM phosphate, 144 mM sodium chloride, 85% D_2O, pH 7.4) to a final gp120 concentration of 100 µg/mL. The sCD4-complexes of 1084i, 1157ip, and HXB2 were formed by incubating gp120 with a 3-fold molar excess of sCD4 for 1084i and HXB2 or both 3-fold and 5-fold molar excesses of sCD4 for 1157ip at room temperature for 1 hour and 4^{o}C overnight. Soluble CD4-bound SF162 expressed in CHO cells was previously studied by HDX-MS (142). CD4-bound gp120 samples were diluted to a final gp120 concentration of 100 µg/mL and were deuterated under conditions that were identical to the unliganded gp120 samples. Exchange reactions were quenched at 12 seconds, 1 minute, 5 minutes, 30 minutes, and 4 hours by

adding an equal volume of ice cold 1M tris(2-carboxyethyl)phosphine (TCEP) in 0.2% formic acid, titrated with sodium hydroxide such that the pH of the final solution was 2.5. The quenched exchange reaction was digested with pepsin (2:1 mass ratio) on ice for 5 minutes prior to flash freezing in liquid nitrogen. In addition to these experimental samples, three control samples were prepared in parallel as previously described (142): an undeuterated sample, a "zero" exchange sample to correct for H-to-D exchange during pepsin digestion, and a fully-deuterated sample to correct for D-to-H back-exchange during digestion and chromatography. Quenched and digested HDX samples were frozen in liquid nitrogen and stored at -80^{o}C.

Deuterium uptake was monitored by LC-MS using a Waters ACQUITY UPLC system connected to a Waters Synapt HDMS Q-TOF instrument. HDX samples were thawed on ice rapidly and loaded onto a 100-µL injection loop within a closed, insulated box with all lines and columns kept on melting ice to minimize back exchange. Peptides were trapped on an ACQUITY UPLC BEH Shield Reverse-Phase C-18 guard column (2.1 x 5mm, 1.7 µm particle size, Waters) in a running buffer of 0.1% TFA. Peptides were eluted from the guard column and further resolved on a Hypersil Gold Reverse-Phase C18 UPLC column (50x1mm, 1.9 µm particle size) (Thermo Scientific) using a 15-minute linear gradient from 5%B to 80%B (A: 5% ACN 0.05% TFA; B: 80% ACN 0.05%TFA). To minimize sample carryover between runs, three "sawtooth gradients" from 5% to 80% acetonitrile over the course of 1 minute were used to wash the main column while the trap column was washed with successive injections of 10% formic acid, 80% methanol, 2:1 isopropanol:acetonitrile, and 80% acetonitrile between samples (283). Mass shifts were analyzed using HX Express (284) and percent deuteration was calculated as shown in Equation 1 (where m is the peptide mass centroid at a given time point, $m_{0\%}$ is the "zero" time point peptide mass centroid, and $m_{100\%}$ is the fully deuterated peptide mass centroid):

$$\%D = 100 * \frac{(m - m_{0\%})}{(m_{100\%} - m_{0\%})} \quad \text{(Equation 2.1)}$$

Estimated standard deviation on percent deuteration values was calculated from independently prepared duplicate deuteration experiments using Equation 2 as implemented in Microsoft Excel (where n is the number of replicates, x_i is the measured value, and $\bar{x}$ is the average value):

$$s = \sqrt{\frac{1}{(n-1)}\sum_{i=1}^{n}(x_i - \bar{x})^2} \quad \text{(Equation 2.2)}$$

Peptic fragments were identified using a combination of MS/MS and exact mass with the aid of Protein Prospector (http://prospector.ucsf.edu) as previously described (142). While glycan moieties on glycopeptides can retain deuterium, potentially affecting the observed rate of deuterium uptake (285), we observed that variability in site-specific glycosylation patterns (changes in the number of mannose, galactose, and fucose groups) had only a minor impact on the rate of deuterium exchange. Therefore, glycopeptide deuteration plots reflect the average deuterium uptake values for all available glycoforms. Heat map figures were generated in Pymol (286).

Surface plasmon resonance

All surface plasmon resonance (SPR) experiments were carried out on a Biacore T100 instrument (GE Healthcare) at 25^{o}C in HBS-EP+ buffer (10 mM HEPES, 150 mM NaCl, 3 mM EDTA, and 0.05% P-20 at pH 7.4). Interactions between each gp120 isolate and sCD4 were measured by immobilizing sCD4 (1-2 µg/mL in 10 mM sodium acetate pH 5.5) to densities of 85 RU and 185 RU on a CM5 chip by standard-amine coupling with EDC/NHS. Flow cell 1 was activated with EDC/NHS and capped with ethanolamine as the reference surface. After testing a variety of analyte flow rates to minimize potential mass transfer effects, gp120 injections were performed at 30 µl/min with a 4 min association phase and an 11 min dissociation phase. Duplicate gp120 samples were prepared independently with a 2-fold dilution series ranging from

1 μM to 15 nM. Regeneration of the sCD4 surface was performed with a 30 second injection of 10 mM glycine pH 1.5 at 10 μl/min.

Interactions between gp120 isolates and gp120-specific antibodies were measured using an antibody capture method. The four flow cells of a CM5 chip were immobilized with either goat anti-human or goat anti-mouse Fc-specific antibodies (Jackson Immunoresearch Laboratories, Inc.) at 30 μg/mL in 10 mM sodium acetate buffer (pH 5.5) to a final density of ~15,000 RU by amine coupling. Flow cell 1 was used as a reference surface, and flow cells 2, 3, and 4 were used to capture gp120-specific antibodies by injecting antibodies (diluted to 0.1-2 μg/mL in HBS-EP) at a flow rate of 10 μl/min with empirically-determined contact times to achieve the desired surface density (typically around 60 RU). Independently prepared duplicate samples of gp120 were then injected over the captured antibody surface. The specific conditions for capture and gp120 injection, including flow rates, contact and dissociation times, and analyte concentrations are summarized in Appendix B, Table B.S1. Injections of sCD4-bound gp120 were performed using gp120 concentrations from 125 – 1.9 nM all in the presence of 625 nM sCD4 (a 5-fold molar excess at minimum). Blank injections contained the same concentration of sCD4. The goat anti-human or goat anti-mouse surface was regenerated with a 30-40 second injection of 10 mM glycine pH 1.5 at 10 μl/min. All data was double reference-subtracted and curves were fit using a 1:1 langmuir binding model in Biacore Evaluation software. The dissociation of gp120 from 17b and N5i5 was too slow to obtain a reliable fit of the off rate, even after more than an hour of dissociation. However, by fixing the dissociation rate to zero in a custom binding model within the Biacore Evaluation software, it was possible to obtain estimates of the association rate. Fits of the experimental data using the 1:1 binding model and the fixed off-rate model produced comparable results as judged by similar chi^2 values (Appendix B, Table B.S2). Estimated error on rates and dissociation constants was calculated from independently prepared duplicate concentration series for each analyte-ligand pair using Equation 2.

Enzyme-Linked Immunosorbance Assay (ELISA)

ELISA assays were performed by immobilizing 50 ng of gp120 per well of an Immulon 2HB plate (Thermo Scientific) in PBS at 4°C overnight. The following day, plates were blocked in a solution of PBS with 2% BSA and 0.01% Tween-20 for two hours at room temperature and washed with TBS with 0.02% Tween-20. Primary antibody was added at a starting concentration of 10 μg/mL for human antibodies or 5 μg/mL for mouse antibodies, diluted with a four-fold dilution series into antibody dilution buffer (PBS with 1% BSA and 0.01% Tween-20) and allowed to incubate at room temperature for 1 hour. Plates were washed, and secondary horseradish peroxidase (HRP)-conjugated goat anti-human or goat anti-mouse secondary antibodies (Jackson Immunoresearch) were added to wells at 1:5000 in antibody dilution buffer for 1 hour at room temperature. After a final set of washes, the plates were developed with SureBlue Reserve TMB (KPL, Inc.), stopped with 1M HCl, and absorbance at 450 nm was measured on a Tecan Infinite M200 plate reader. Methods used in the peptide competition ELISA (Appendix B, Figure B.S19) are described in Appendix B.

Small angle x-ray scattering

Small-angle X-ray scattering (SAXS) measurements were conducted on Beam Line 4-2 at the Stanford Synchrotron Radiation Laboratory (287). In-line size-exclusion with SAXS was used to generate high quality data sets for each gp120 protein. In these experiments, 100 μL of each sample at 3-5 mg/mL was injected onto a highres Sepharose 200 column (GE Healthcare) with a flowrate of 50 μL/min in PBS. The focused 11 keV X-ray beam irradiated the eluted sample flowing through a thin-wall quartz capillary cell, placed at 1.7 m upstream of the Rayonix MX 225HE detector (Evanston, IL). One second exposures were collected every 5 seconds through the course of each run. The detector pixel numbers were converted to the momentum transfer $q=4\pi*\sin\theta/\lambda$, where $2*\theta$ is the scattering angle and λ the X-ray wavelength of 1.127 Å,

calibrated with silver behenate powder at the capillary position. Protein scattering data were processed by *MarParse* and scaled for the transmitted beam intensity integrated for each exposure, and azimuthally averaged (287). A buffer blank was obtained from the average of the first 100 data points (before the void volume) and subtracted from the subsequent protein scattering data. Rg and I(0) for each frame were batch analyzed using autoRg (288), and frames with a stable Rg values were merged in Primus (289). The 1-D SAXS curves were

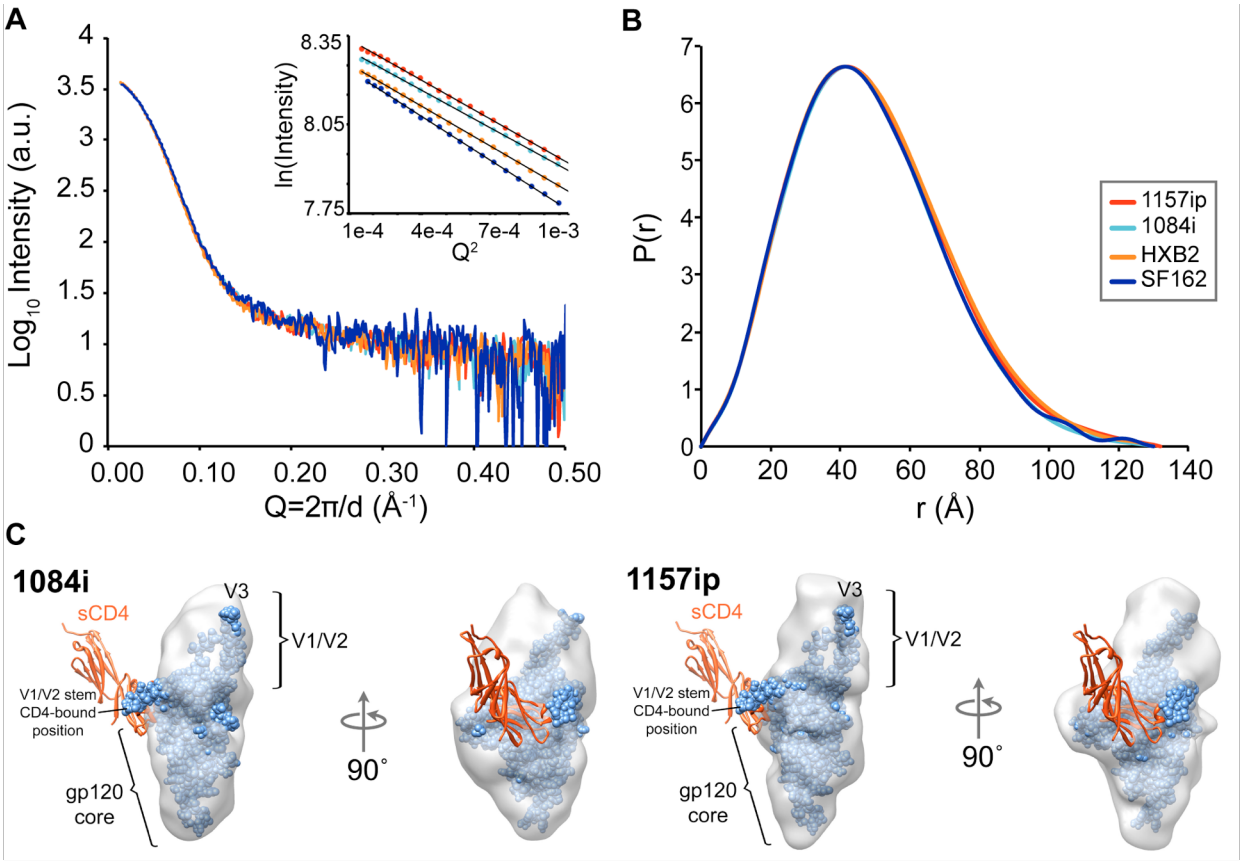

Figure 2.1. Similar architecture of gp120 across isolates by Small-Angle X-ray Scattering (SAXS). **(A)** SAXS curves and **(B)** Pairwise distance distribution, P(r), plots show that the four full-length gp120s are similar in shape and size. Guinier plots (A, inset) indicate the gp120 specimens did not exhibit aggregation or inter-particle effects, which would complicate analysis **(C)** DAMMIN shape reconstructions of unliganded 1084i (left) and 1157ip (right) full-length gp120 (gray envelopes) with gp120 extended core from 3JWD.pdb and containing V3 loop from 2B4C.pdb (blue spheres) docked into the SAXS shape envelope. The V1/V2 stem in CD4-bound conformation does not fit into the unliganded SAXS density. Instead a lobe of mass atop the gp120 core is attributed to V1/V2 proximal to the likely V3 position in unliganded full-length gp120 (142). Two-domain sCD4 was not present in the SAXS experiment, however it is shown in red ribbon to aid in the interpretation of the SAXS envelopes.

processed using GNOM to determine Rg and Dmax values from the P(r) plots, the pairwise distance distribution functions (290-292). Low-resolution shape reconstructions were performed following the procedure described previously (142). In brief, DAMMIN (293) was used to generate a set of bead models, which were then aligned with each other. Positions of low-occupancy were filtered using DAMAVER and DAMFILT to generate the final model (294).

Results

Full-Length, glycosylated gp120s exhibit similar morphologies by SAXS

Small angle X-ray scattering was used to study large-scale structural differences among the four isolates. Previous studies have used this technique to observe changes in the position of V1/V2 loops upon sCD4 binding (142). If any of the isolates exhibited a distinct difference with regard to variable loop position, we would expect to observe this by SAXS. Because minor populations of dimeric contaminant can lead to large changes in the scattering profile, scattering data was collected with on-line size exclusion chromatography to ensure that only the homogenous monomeric population was sampled. The averaged scattering patterns for the four gp120s are shown in Figure 2.1A and are essentially superimposable. The Figure 2.1A inset shows that the Guinier plots for each gp120 sample are linear, confirming that the SAXS data from SEC-eluted samples were free of artifacts due to aggregation or interparticle effects, and hence suitable for further analysis (195). Radii of gyration (Rg) - the root-mean squared distance from the molecules' center of mass - calculated from the slope of the Guinier plot and from the P(r) pairwise distance distribution histogram (195) (Figure 2.1B) were in excellent agreement. The SAXS data suggest that only slight differences in radius of gyration and maximal dimensions exist among the four gp120s examined, with general dimensional trends mirroring the expected increases in size based upon V1/V2 size and degree of glycosylation (Tables 2.1 and 2.2). *Ab initio* shape reconstruction was also performed for the gp120 monomers in their unliganded state. A comparison of reconstructions for 1157ip and 1084i

Table 2.2. SAXS-derived gp120 dimensions

	Rg (Å) Guinier	Rg (Å) GNOM	Dmax (Å)
1157ip	37.4 +/- 0.1	37.7 +/- 0.1	132
1084i	36.6 +/- 0.1	36.8 +/- 0.1	130
HXB2	37.7 +/- 0.1	37.9 +/- 0.1	130
SF162	36.6 +/- 0.1	367. +/- 0.1	130

gp120 is shown in Figure 2.1C; all four gp120 reconstructions are compared in Appendix B, Figure B.S2A. Overall the raw SAXS data and reconstructions indicate that the gp120 monomers possess similar morphologies. Additionally, the subunit organization observed for these gp120s matched previous observations with SF162 gp120 from Chinese hamster ovary (CHO) and 293E cell expression systems, with a prominent bulge positioned atop the gp120 core proximal to the likely V3 loop position. We infer that this bulge corresponds to the position of V1/V2 in unliganded gp120 (142). The Porod-Debye region of the scattering curve along with Kratky plots were also compared (Appedix B, Figures B.S2B and B.S2C) as these can report differences in the degree of globular character and compactness (195, 295). These plots are nearly superimposable for the isolates indicating that they exhibit similar degrees of globular structure. Therefore, it appears that on a global scale, the four gp120s are similar in their overall architecture, and the differences in deuterium uptake observed by HDX-MS (presented below) largely reflect local differences in structural stability and dynamics.

Isolate-specific differences in unliganded gp120 conformational dynamics measured by HDX-MS

For the set of gp120s studied here, observable peptides provided deuteration information for 62-69% of the residues in the mature gp120 sequences: 62% for 1157ip, 67% for HXB2, and 69% coverage for both 1084i and SF162 (Appendix B, Figures B.S3-B.S6). There was excellent peptide coverage of the gp120 inner domain sequence (~98%, on average). In contrast, coverage of the outer domain and variable loops was lower and differed substantially among the isolates due to greater sequence variability and abundant glycosylation in these

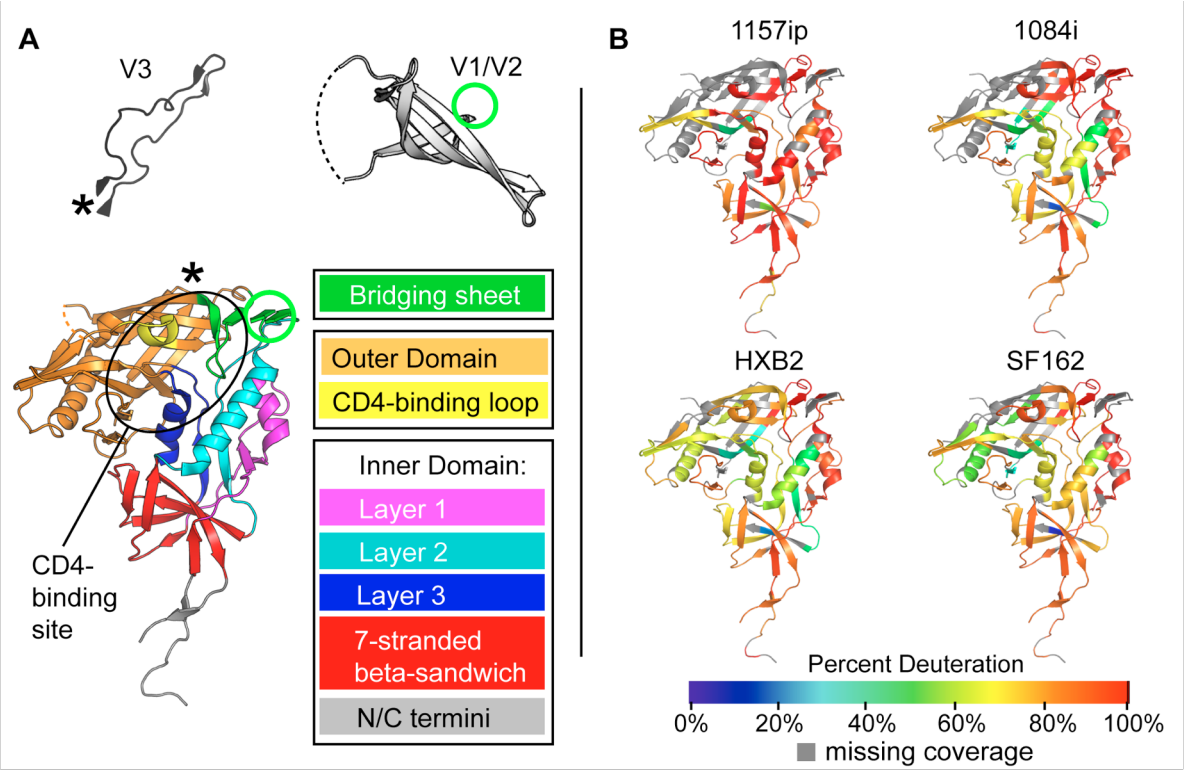

Figure 2.2. Summary of isolate-specific differences in unliganded gp120 conformational dynamics. (A) The organization of monomeric gp120 into inner, outer, and bridging sheet domains is indicated by color on the gp120 core with N- and C-terminal extensions (PDB ID: 3JWD). The inner domain is further divided into mobile layers 1, 2, and 3 (magenta, cyan, and blue, respectively) that protrude from the 7-stranded beta sandwich (red) (35). Variable loops V1/V2 and V3 (from PDB 3U4E and PDB 2B4C respectively) are included for reference. The position of these elements in the context of the gp120 core is indicated by an asterisk for V3 and a green circle for V1/V2. The approximate location of the CD4-binding site is indicated with a black oval. The structures shown here and throughout the text reflect that of gp120 in a receptor-bound conformation because no structure is currently available for full-length, unliganded gp120. These structures may not necessarily reflect the unliganded structure of full-length gp120 in solution. **(B)** Heat maps of HDX-MS data for unliganded gp120 conformational dynamics reveal the general profile of isolate-specific differences in structural dynamics. Colors mapped onto gp120 core (PDB ID: 3JWD) indicate percent deuteration of peptides after 1 minute of incubation in a deuterated buffer for the panel of gp120s; warm colors correspond to high levels of deuterium uptake (dynamic regions) and cool colors correspond to low levels of deuteration (ordered or "protected" regions). Regions where peptide information is missing are indicated in gray.

regions (Appendix B, Figure B.S7). For example, an L369P mutation between the clade C and B isolates likely disrupted a potential pepsin cleavage site (296) in the clade B isolates and yielded differential coverage of the CD4 binding loop across clades. Similarly, peptides spanning V1 and V4, the most densely glycosylated regions of gp120, were not observed for any isolates.

Overall, differences in peptide coverage limited, but did not eliminate, our ability to characterize the stability of certain regions of gp120 and to compare the stability of those regions across isolates (Appendix B, Figure B.S8).

In order to measure the local dynamics of each full-length, glycosylated gp120, we quantified deuterium incorporation for every observable peptide in each isolate as a function of deuteration time (Appendix B, Figures B.S9-B.S12). This data is summarized in the form of heat maps (Figure 2.2 and Appendix B, B.S13) in which the percent deuterium uptake values for each peptide are indicated by color on the gp120 core crystal structure with N- and C-terminal extensions (35). These heat maps make it possible to identify regions of order and disorder within full-length gp120 in solution. Notably, a number of peptides from layer 1 and the bridging sheet, which map to ordered alpha helices and beta-sheets in core crystal structures (Figure 2.2A), were found to be rapidly deuterated in HDX-MS analysis of unliganded, full-length gp120s in solution (Figure 2.2B). Such discrepancies illustrate that secondary structures within the core regions of gp120 may be quite dynamic in the context of full-length gp120 in solution.

Heat maps also enable a qualitative comparison of overall differences in stability among the four isolates. Figure 2.2B shows that there are many similarities among the isolates, for example, the CD4 binding loop, bridging sheets, and portions of the inner domain exhibit a relatively high degree of structural dynamics in all isolates. Additionally, similar regions of gp120 are protected in all four isolates (e.g. portions of the outer domain and the seven-stranded beta-sandwich, Figures 2.2, 2.3, and 2.4). While there are general similarities, there are also abundant differences that can be observed among the four gp120s. Of the four isolates, 1157ip stands out as being the most dynamic, however, additional apparent differences in deuterium uptake over time (Appendix B, Figure B.S13) among the other gp120s suggest that each isolate may have a unique stability profile.

Specific comparison of peptides that are common to multiple isolates reveals increased disorder within the inner domain of 1157ip gp120

A more focused, direct comparison of individual peptides that are similar or identical among the isolates is shown in Figures 2.3 and 2.4. Excluding glycoform variants, we identified 60, 49, 51, and 53 unique peptides for 1084i, 1157ip, HXB2, and SF162, respectively. Of these peptides, 29 were present in all four isolates, 9 were common to three isolates, and 10 were common to 2 isolates. Altogether, these peptides allowed us to compare deuterium uptake for 91% of residues within the inner domain and 42% of residues within the outer domain, bridging sheet, or variable loops across at least two isolates. However, it was only possible to compare deuterium uptake among four isolates for 81% of the inner domain residues and 17% of the residues in the outer domain, bridging sheet, or variable loops (Appendix B, Figure B.S8).

The stability of the gp120 inner domain varied substantially among the four isolates (Figure 2.3). Layer 1 peptides were saturated with deuterium at the earliest time point in every isolate (Figure 2.3A), indicating that this region is poorly-ordered in the solution structure of full-length gp120. Because the deuterium uptake was so fast for these peptides, we could not detect differences among the isolates in this region. In contrast, layer 2 peptides (AA 96-104, 105-111, and 211-222) showed varying degrees of protection from deuterium uptake at early time points in 1084i, HXB2, and SF162 but the corresponding peptides from 1157ip gp120 were nearly fully-exchanged at matched time points (Figures 2.3B and Appendix B, B.S14). Layer 3 peptides (AA 227-258, and 467-483) (Figure 2.3C) and peptides from the 7-stranded beta sandwich (AA 84-95, 223-225, and 484-501) (Figure 2.3D) showed a similar trend, in which 1157ip peptides were rapidly deuterated relative to those derived from other isolates. Therefore it appears that inner domain secondary structures, which exhibit similar, though not identical, stabilization in the other three isolates, are substantially more dynamic in the context of 1157ip gp120.

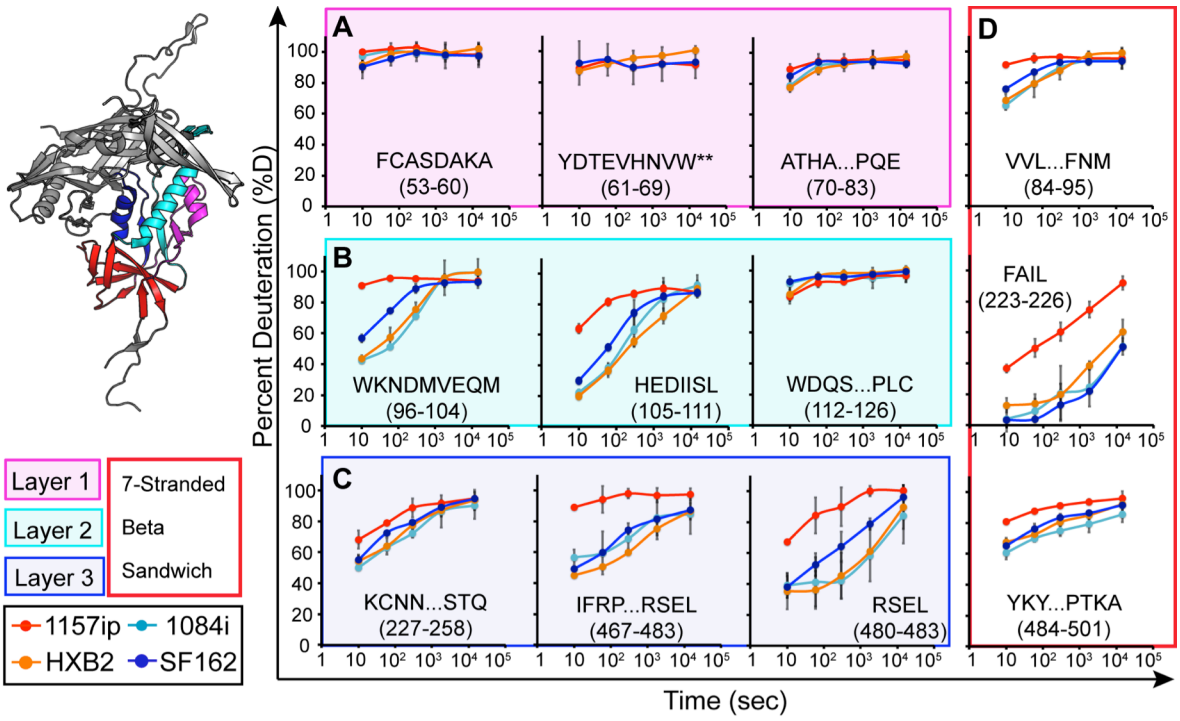

Figure 2.3. Deuterium exchange profiles of homologous inner domain peptides. Each graph shows the deuterium uptake (% deuteration) over time for peptides throughout the gp120 inner domain, which are either identical or homologous among the four gp120s. Each line in the graph reflects the deuterium uptake for that peptide in the context of a different isolate as indicated in the figure legend. The peptide sequence and amino acid position (HXB2 numbering) are indicated for each graph. **(A-C)** Peptides from layers 1, 2, and 3 are color-coded in the ribbon diagram and deuteration uptake plots are grouped within the magenta, cyan, and blue boxes, respectively. **(D)** Peptides from the 7-stranded beta-sandwich are bounded by a red box. A comparison of the deuterium uptake curves for a given peptide from multiple isolates reveals differences in stability, for example, the WKNDMVEQM peptide is more dynamic in 1157ip as compared to the other isolates. (**) indicates deuteration data obtained by subtraction of overlapping peptides. Error bars reflect standard deviation calculated as described in materials and methods.

Although few outer domain peptides could be directly compared across all four isolates, much of the outer domain sequence was comparable between at least two isolates (Figures 2.4 and Appendix B, B.S15). Most peptides from the outer domain were similarly stabilized among those isolates for which comparable peptides were available (e.g. AA 270-283 and 446-453). However, the LLLNGSL peptide (AA 259-265), which is directly linked to the inner domain, was deuterated more rapidly in 1157p as compared to the other isolates (Figure 2.4A). The CD4-binding loop peptide (AA 369-382) was only slightly more dynamic in 1157ip as compared to

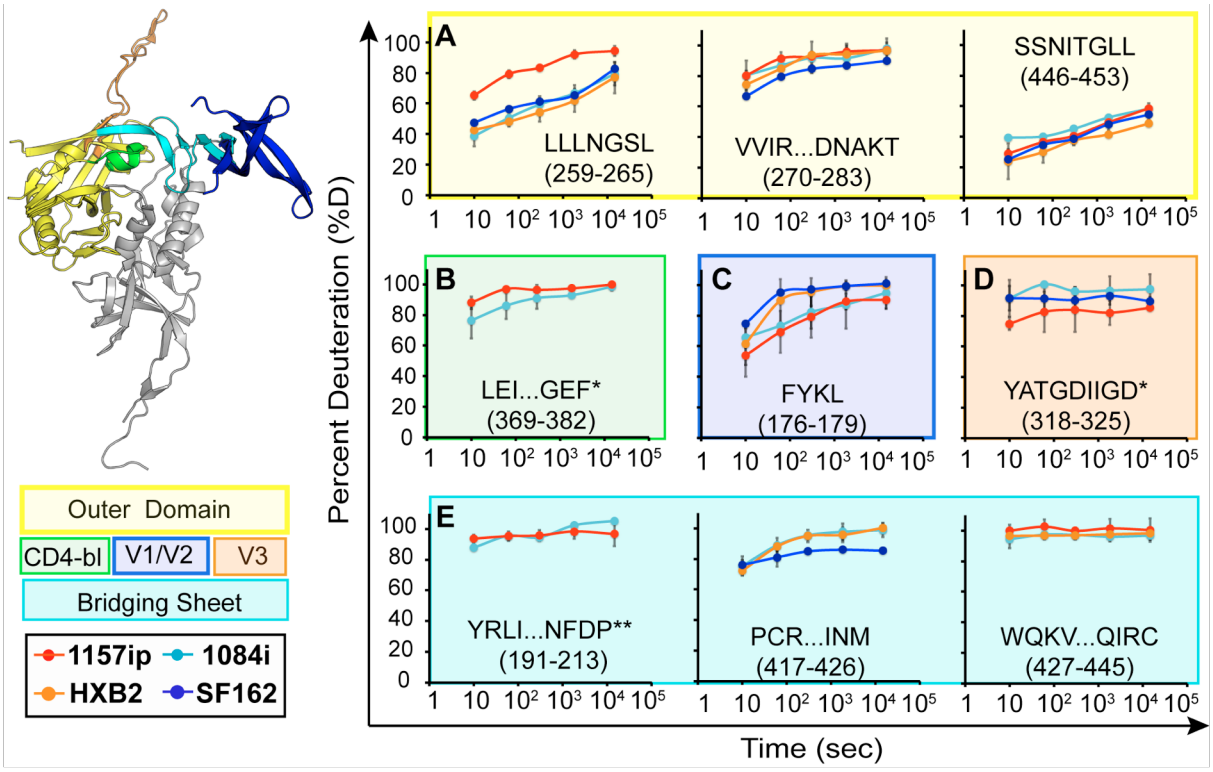

Figure 2.4. Deuterium exchange profiles for homologous outer domain, bridging sheet, and variable loop peptides. Each graph shows deuterium uptake (% deuteration) over time for peptides in **(A)** the gp120 outer domain **(B)**, CD4-binding loop (CD4-bl, **(C)**, variable loop V2 and **(D)** V3, **(E)** and bridging sheets. Each line on the graph corresponds to deuterium uptake for that peptide in the context of a different isolate, as indicated in the figure legend The peptide sequence and amino acid position (HXB2 numbering) are indicated for each graph. Each graph is color-coded according to the position of the peptide in the gp120 structure as indicated in the ribbon diagram and legend to the left. (*) indicates that the listed peptide sequence is from an isolate other than HXB2, because peptide coverage was missing for HXB2 (**) indicates deuteration data obtained by subtraction of overlapping peptides. Error bars reflect standard deviation calculated as described in materials and methods.

1084i (Figure 2.4B). Interestingly, the CD4-binding site-proximal peptide (AA 350-361) was significantly more stable in SF162 as compared to HXB2 (Appendix B, Figure B.S15). Overall, these results reveal conformational variation of the outer domain across isolates, although the extent of this variation appears limited relative to that observed for the inner domain.

Peptides from the variable loops and bridging sheet that were common to multiple isolates revealed few isolate-specific differences in deuterium uptake, partially due to the fact that these peptides were typically saturated with deuterium at the earliest time point of deuteration (Figure 2.4C-2.4E). The peptides FYKL (Figure 2.4C) and YATGDIIGD (Figure

2.4D) from V2 and V3, respectively, showed subtle differences in protection across isolates but more complete coverage of these regions is needed to better characterize the extent of structural differences in the variable loops. Peptides within bridging sheets beta 2, 3, and 21 (AA 112-127, 191-213 and 427-445, respectively) exhibited rapid deuterium uptake that was similar among all available isolates (Figure 2.4E and Appendix B, B.S15). The PCRIKQIINM peptide (AA 417-426), which reports on beta strands 19 and 20 of the bridging sheet, showed slight protection at early time points in all available isolates (Figure 2.4E) perhaps due to hydrogen bonding with beta sheet 17, downstream of the CD4 binding loop as observed in the core crystal structure (35).

In summary, significant isolate-specific differences in stability could be observed throughout gp120. Most notably, peptides mapping to the gp120 inner domain were consistently more disordered in 1157ip as compared to matched peptides from other isolates. Many (but not all) peptides from the outer domain were similarly protected among the isolates that could be directly compared. Peptides mapping to the variable loops and bridging sheets were typically disordered, but poor peptide coverage and rapid saturation with deuterium made it difficult to discern differences in dynamics in these regions.

Isolate-specific differences persist in CD4-bound gp120

Because CD4-binding has been shown to stabilize gp120 (145, 297) and induce ordering of the conserved CD4 and co-receptor binding sites (142, 144) we hypothesized that the CD4-bound form of gp120 might be more structurally similar among isolates than unliganded gp120. To test this, we performed HDX-MS on pre-formed sCD4-gp120 complexes for each isolate (Figure 2.5). Overall, sCD4-bound gp120s were stabilized relative to their unliganded forms, taking on less deuterium than unliganded gp120s at matched time points (Appendix B, Figures B.S9-B.S11). This is likely a result of multiple factors including solvent occlusion, hydrogen bonding between sCD4 and the gp120 backbone, and a conformational

change within gp120 that leads to the formation of more stable secondary structures. For regions of gp120 outside of the CD4-binding site, for example, the bridging sheet and layers 1 and 2 of the inner domain, CD4-induced HDX protection is likely to be explained entirely by stabilization of secondary structures. The impact of sCD4 binding on deuterium uptake by gp120 is shown in the difference maps of Figure 2.5A, in which blue colors indicate protection relative to unliganded gp120. Similar patterns of protection were observed among the four isolates - most notably in the CD4-binding loop, the bridging sheet, and layers 1, 2 and 3 of the inner domain (Figure 2.5A and Appendix B, B.S16). However, the degree of protection as a result of sCD4-binding - the downward shift in deuterium uptake between unliganded and sCD4-bound gp120 - varied among the isolates (Figure 2.5B). Deuterium uptake plots for matched peptides from the sCD4-bound gp120s revealed that in contrast to 1084i and HXB2, 1157ip was poorly stabilized in the presence of sCD4 (Figure 2.5B, and Appendix B, B.S17, B.S18). For example, 1084i and HXB2 peptides from the inner domain (e.g. AA 61-83, 105-111, 454-483), bridging sheet (e.g. 112-126 and 427-445), and the CD4-binding loop for 1084i (AA 369-382) were dramatically stabilized in the presence of sCD4 relative to 1157ip. Notably, the sCD4-induced stabilization of 1084i and HXB2 was comparable to that observed for CHO-cell expressed SF162 gp120 (dark blue lines, Figure 2.5B) from previous work (142). Increasing sCD4 in the 1157ip-sCD4 mixture from a 3-fold to a 5-fold molar ratio did not increase the apparent protection of sCD4-stabilized peptides (data not shown), which suggests that sCD4 was present at saturating concentrations, and all available gp120 was bound by sCD4. Thus, it appears that while similar regions of gp120 are stabilized as a result of sCD4-binding to diverse isolates, the sCD4-bound gp120s maintain different levels of structural dynamics and, as in the unliganded state, 1157ip gp120 remains relatively dynamic even with sCD4 bound.

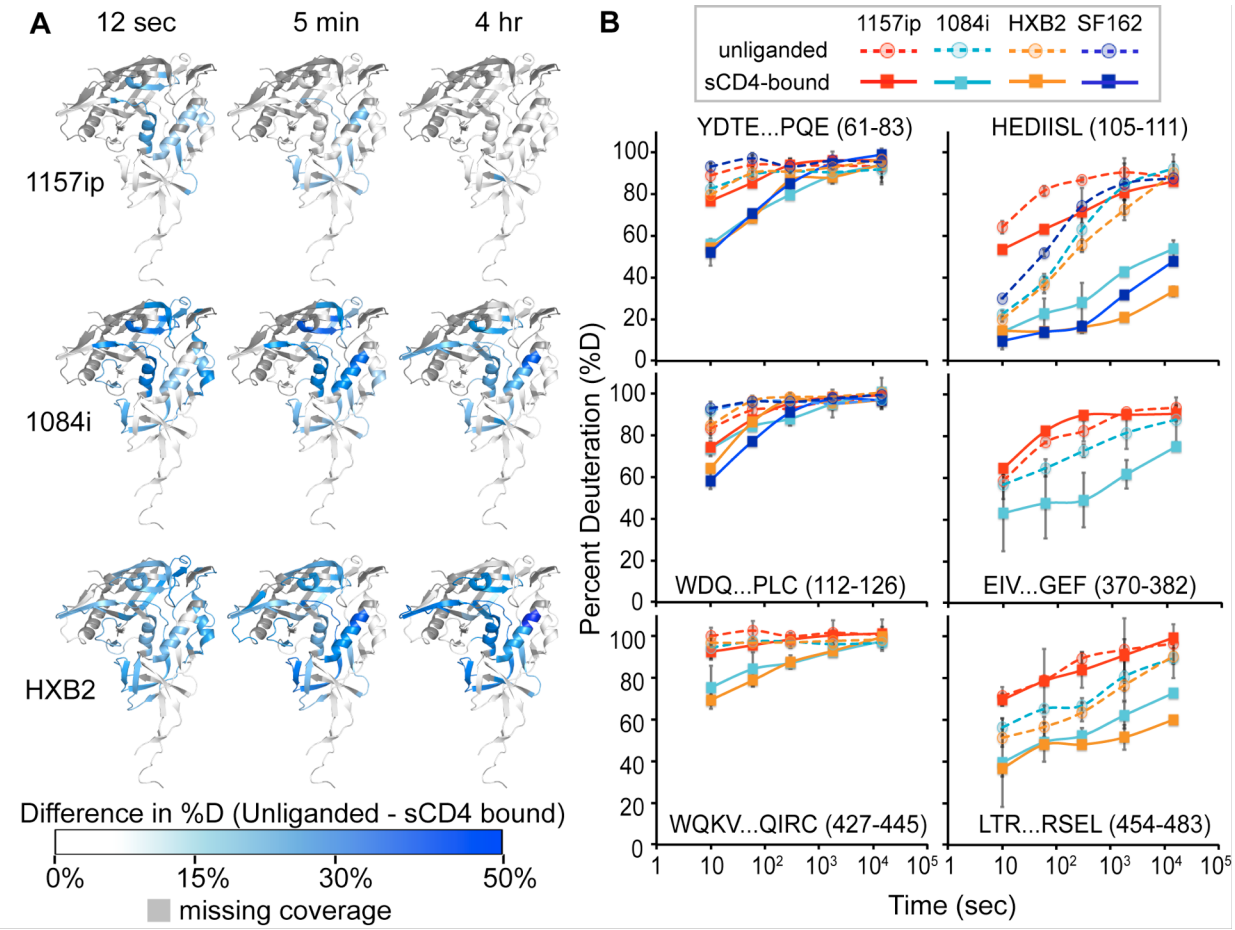

Figure 2.5. Isolate-specific differences in sCD4-induced stabilization of gp120. (A) Difference heat maps show the spatial profile of sCD4-induced stabilization of gp120. The colors mapped onto the 3JWD structure indicate the quantitative difference in percent deuteration between unliganded and CD4-bound full-length gp120s. Darker blue colors correspond to greater CD4-induced stabilization. Missing peptide coverage is shown in gray. Difference heat maps for 12 sec, 5 min and 4 hr time points are shown. **(B)** Deuterium uptake plots (% deuteration vs time) for identical or homologous peptides that are stabilized upon sCD4-binding. The peptide sequence and amino acid position (HXB2 numbering) are indicated for each graph. Dashed lines with circles show data for unliganded gp120, solid lines with squares show deuterium uptake for sCD4-bound gp120. The traces are color-coded by isolates as defined in the figure legend. Stabilization as a result of sCD4-binding is observed as a downward shift in the deuterium uptake curve. Error bars reflect standard deviation calculated as described in materials and methods.

Epitope stability and antigenicity: linear-epitope specific antibodies

In order to determine whether differences in structural dynamics observed by HDX-MS affect ligand association with gp120, we used surface plasmon resonance (SPR) to quantify the

kinetics of sCD4 and antibody binding to the four gp120s and enzyme-linked immunosorbance assays (ELISA) to measure the levels of antibody stably bound to gp120. The determinants of antigenicity are complex and include the minimal requirements that 1) the residues that make up the antibody epitope be present in the primary amino acid sequence, and 2) these residues, which form the antibody epitope, must be exposed or accessible for antibody recognition (298). Beyond these basic requirements, we hypothesized that the local conformational stability of an antigen might also impact the kinetics and/or the affinity of an antibody's interaction with its epitope, as has been previously proposed (298).

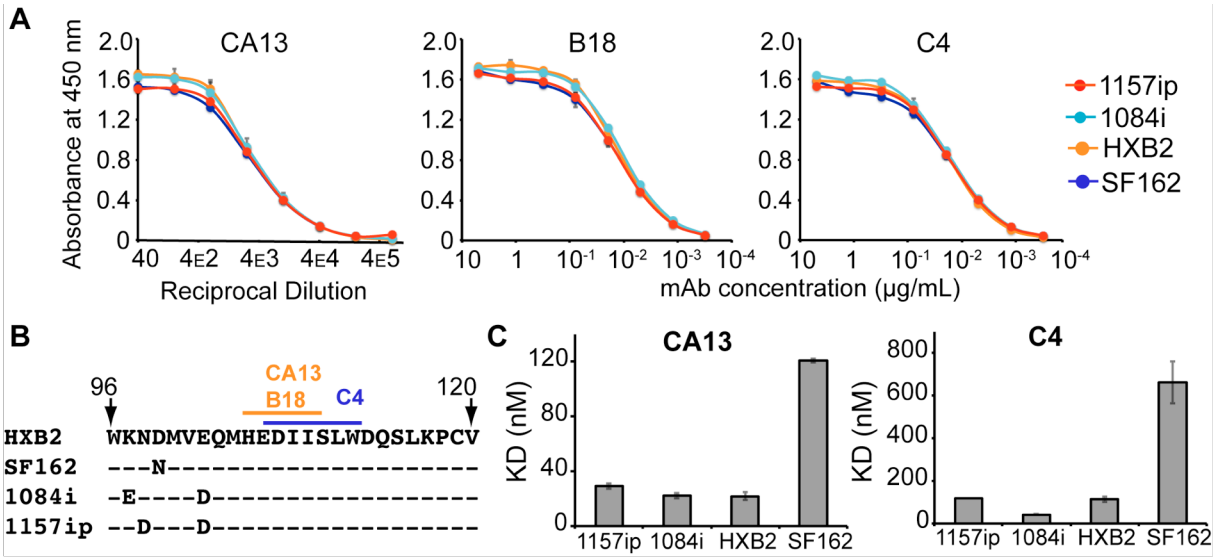

Figure 2.6. Linear epitope-specific antibody binding to a region of gp120 differentially stabilized across isolates (A) Linear-epitope-specific antibody (CA13, B18, and C4) binding to gp120 proteins by ELISA. The curves are color-coded by Env isolate as defined in the figure legend. Concentrations of monoclonal antibody are shown on the x-axis for C4 and B18, reciprocal dilution of antibody supernatant is shown on the x-axis for CA13. Curves are representative of at least two independent experiments; error bars indicate standard deviation from duplicate measurements. **(B)** The primary sequence recognized by antibodies CA13, B18, and C4 is absolutely conserved among the four gp120 isolates; (-) indicates that the residue is conserved in a given isolate, amino acid differences are indicated. This region is differentially stabilized in the four gp120s by HDX-MS (see Figure 2.3B) **(C)** Summary of SPR-derived binding constants for CA13 and C4 binding to the four gp120 isolates. Raw and fitted SPR curves are shown in Figure B.S20. The B18-gp120 SPR binding curves did not fit well to a 1:1 binding model, therefore estimates of affinity are not available, although qualitative isolate specific differences in binding to B18 were similar to that observed for CA13 and C4 (Figure B.S20). Error bars indicate standard deviation calculated as described in materials and methods.

Table 2.3. SPR binding parameters for linear-epitope specific antibodies

		1157ip	1084i	HXB2	SF162
CA13	ka (1/M-s)	$1.8(1) \times 10^4$*	$1.96(9) \times 10^4$	$0.9(1) \times 10^4$	$0.36(1) \times 10^4$
	kd (1/s)	$5.31(4) \times 10^{-4}$	$4.3(2) \times 10^{-4}$	$2.03(1) \times 10^{-4}$	$4.32(9) \times 10^{-4}$
	KD (nM)	29(2)	22(2)	22(3)	121(1)
C4	ka (1/M-s)	$2.6(2) \times 10^4$	$3.2(1) \times 10^4$	$1.1(1) \times 10^4$	$0.42(5) \times 10^4$
	kd (1/s)	$3.1(2) \times 10^{-3}$	$1.34(1) \times 10^{-3}$	$1.29(3) \times 10^{-3}$	$2.8(1) \times 10^{-3}$
	KD (nM)	118(1)	42(2)	110(10)	600(100)

*Error on the last significant figure is presented in parentheses (for example, $1.9(1) \times 10^4$ is equivalent to 19000 +/- 1000)

The antibodies B18, C4, and CA13 were reported to recognize linear epitopes within helix 1 of gp120 (280, 299), and we confirmed their specificity by peptide competition ELISA (Appendix B, Figure B.S19). The core epitopes of the three antibodies were absolutely conserved in all four isolates (Figure 2.6B), yet exhibited significant differences in conformational dynamics by HDX-MS (Figure 2.3B). There was no detectable difference in linear epitope-specific antibody binding to the four gp120 isolates by ELISA (Figure 2.6A). We also investigated isolate-specific differences in the kinetics of gp120 binding to captured B18, CA13, and C4 by SPR (Appendix B, Figure B.S20). Although 1157ip stood out among the four isolates with a more dynamic helix 1 by HDX-MS, it was not distinguished by substantially different rates of association with or dissociation from these linear epitope-specific antibodies (Table 2.3). Furthermore, the affinities of C4 and CA13 for 1157ip were comparable to those observed for 1084i and HXB2, both of which feature a more ordered helix 1(Table 2.3 and Figure 2.6C). In contrast, SF162, which was similar to 1084i and HXB2 in helix 1 stability, had an affinity for CA13 and C4 that was at least 4-fold weaker than those of the other isolates. This suggests that the weaker recognition of SF162 by this panel of helix 1-specific antibodies may be due to factors other than the conformational stability of helix 1 (e.g. tertiary structural differences).

Dynamics and conformational epitope antigenicity: CD4-binding site

Because the majority of broadly cross-reactive HIV-1 NAbs and ADCC-active antibodies target discontinuous epitopes within gp120, we sought to determine whether differences in the stability and structural dynamics of gp120 correlated with differences in the antigenicity of conformational epitopes such as the CD4 binding site. A summary of the differences in the primary sequence and dynamics of peptide segments involved in conformational antibody epitopes is shown in Figure 2.7. Many of the peptides that are directly involved in CD4-binding site ligand interactions (Figure 2.7A) are either saturated with deuterium at the earliest time point (peptides 4 and 10 in Figure 2.7B) or are similarly disordered in the isolates for which data was available (e.g. peptides 7 and 8 in Figure 2.7B). However, peptide 12, which contains a number of CD4 contact residues and helix 5 is significantly more dynamic in 1157ip (Figure 2.7B). By ELISA, the CD4-binding site ligands CD4-IgG2 and IgG1-b12 bound strongly to the two clade B isolates, SF162 and HXB2 and relatively weakly to the clade C isolates (Figure 2.8). This pattern of differential binding across clades was particularly evident for IgG1-b12 and suggested that the observed differences in CD4-binding site ligand recognition of gp120 might be partly due to clade-specific primary sequence differences within the CD4-binding site (Figure 2.7C). Therefore, we collected SPR data for sCD4, CD4-IgG2, and IgG1-b12 binding to all four gp120s (Appendix B, Figure B.S21), but focused our comparison on the isolates 1084i and 1157ip, which are closely-related in their primary amino acid sequences (Figure 2.7C), yet exhibit dramatic differences in the stability of peptides both proximal (e.g. peptide 12 in Figure 2.7B) and distal (e.g inner domain peptides in Figure 2.3) to the CD4-binding site. This pair of isolates presents an opportunity to study the impact of gp120 dynamics on recognition by CD4-binding site ligands while limiting confounding amino acid changes.

CD4-IgG2 bound poorly to 1157ip gp120 as compared to 1084i by ELISA (Figure 2.8). These results were confirmed by SPR, which indicated that 1157ip had the weakest affinity for sCD4 and CD4-IgG2 of the four isolates, showing five-fold and two-fold weaker affinities for

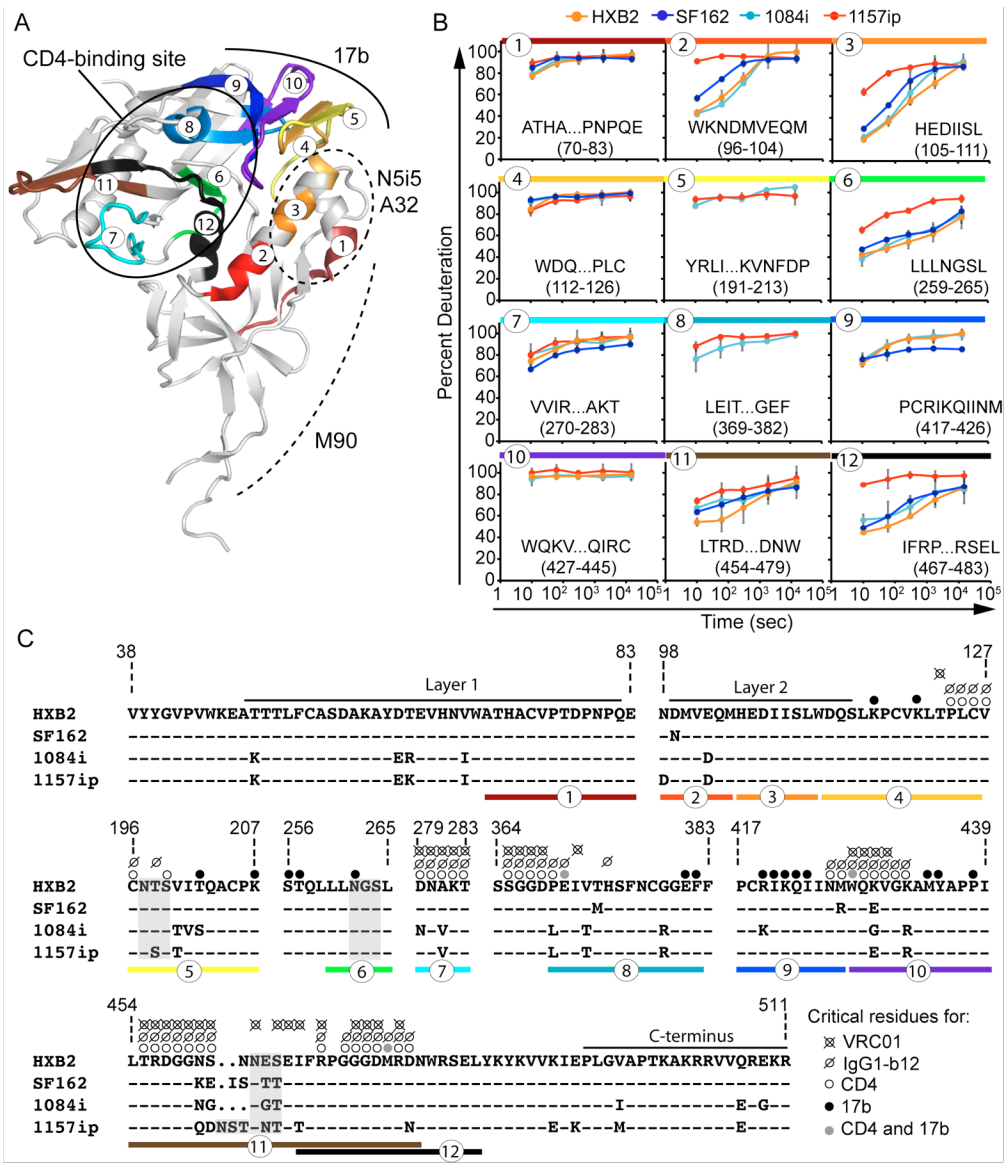

Figure 2.7. Summary of isolate-specific differences in conformational dynamics and primary sequence for peptides involved in conformation-dependent antibody epitopes. **(A)** Colors and numbers mapped onto the 3JWD crystal structure indicate peptides within conformation-dependent antibody epitopes that can be tracked by HDX-MS. The structure is annotated to indicate the CD4-binding site (targeted by sCD4, IgG1-b12, and VRC01) as well as N5i5, A32, M90, and 17b epitopes. **(B)** Deuteration profiles (% deuteration vs time) for peptides within conformation-dependent antibody epitopes. Plots are color-coded and numbered as in (A). **(C)** Amino acid alignment of the four isolates for regions of gp120 involved in conformation-dependent antibody binding. (-) indicates that the residue is conserved in a given isolate relative to HXB2; (.) indicates an insertion in a separate sequence. N5i5 and A32 recognize a similar epitope involving Layers 1 and 2 (279). Layer 1 and the C-terminus are thought to be involved in the M90 epitope (281, 300). Critical residues for CD4, IgG1-b12, VRC01, and 17b binding are indicated with dots as shown in the figure legend based on references (179, 188, 190). Peptides are indicated with colors and numbers as in (A) and (B).

sCD4 and CD4-IgG2, respectively, as compared to 1084i (Figure 2.9C and Table 2.4). IgG1-b12 binding to 1084i fit poorly to a 1:1 binding model, which complicated a direct comparison of 1084i and 1157ip binding to this antibody by SPR. The weak affinity of 1157ip for CD4-binding site ligands was largely due to slower rates of association (Figure 2.9A), although 1157ip also showed a slightly faster rate of dissociation from sCD4 as compared to 1084i (Figure 2.9B). Thus it appears that the increased conformational flexibility of 1157ip is associated with slower association rates, and an overall weaker affinity for CD4 mimetics (Figure 2.9C). This effect appears to be most prominent in CD4-binding site ligands that require contact with both the inner and outer domains of gp120 because while 1157ip bound to CD4-IgG2 at a very low level in ELISA, the potent and broad CD4 binding site antibody, VRC01, which primarily makes contact with the gp120 outer domain (190), bound to 1157ip at only a slightly reduced level relative to 1084i (Figure 2.8).

The few observable differences in the stability of peptides involved in the CD4-binding

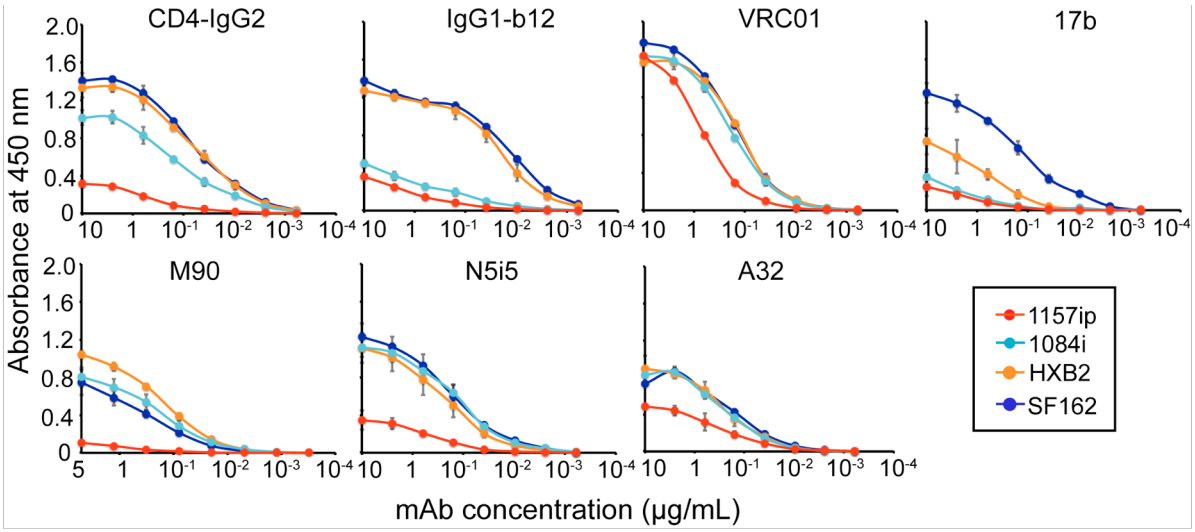

Figure 2.8. Conformation-dependent antibody binding to gp120 isolates by ELISA. Conformation-dependent antibodies specific for different regions of gp120 were tested: CD4-binding-site ligands (CD4-IgG2, IgG1-b12, and VRC01), conformational inner-domain antibodies (M90 and N5i5), and the co-receptor binding site antibody (17b). Each graph corresponds to a different antibody binding to the four gp120 isolates. The ELISA traces are color-coded by HIV isolate as shown in the legend. Antibody binding levels (measured as absorbance at 450 nm) versus antibody concentration are shown. Curves are representative of at least two independent experiments; error bars indicate standard deviation from duplicate measurements.

site across isolates (Figure 2.7) suggests that differences in conformational stability of regions outside of the CD4 binding site (for example, the gp120 inner domain) likely exert a strong influence on gp120's affinity for CD4 and binding-site targeted antibodies. This model is supported by previous work, which showed that layers 1, 2 and 3 of the inner domain – regions that are dramatically destabilized in 1157ip relative to the other isolates – significantly impact gp120 interactions with CD4 and CD4 mimetics (301-303).

Dynamics and the antigenicity of conformational inner domain epitopes

Because isolate-specific differences in gp120 stability were most apparent in the inner domain (Figures 2.3 and 2.7B), we measured binding of the four gp120s to antibodies that have been reported to target conformational epitopes within this region: M90, A32, and N5i5 (Figure 2.7A). M90 is thought to recognize a conformational epitope involving layer 1 and the N and C termini of gp120 (281, 300). N5i5 is a potent ADCC-active antibody that binds to a CD4-

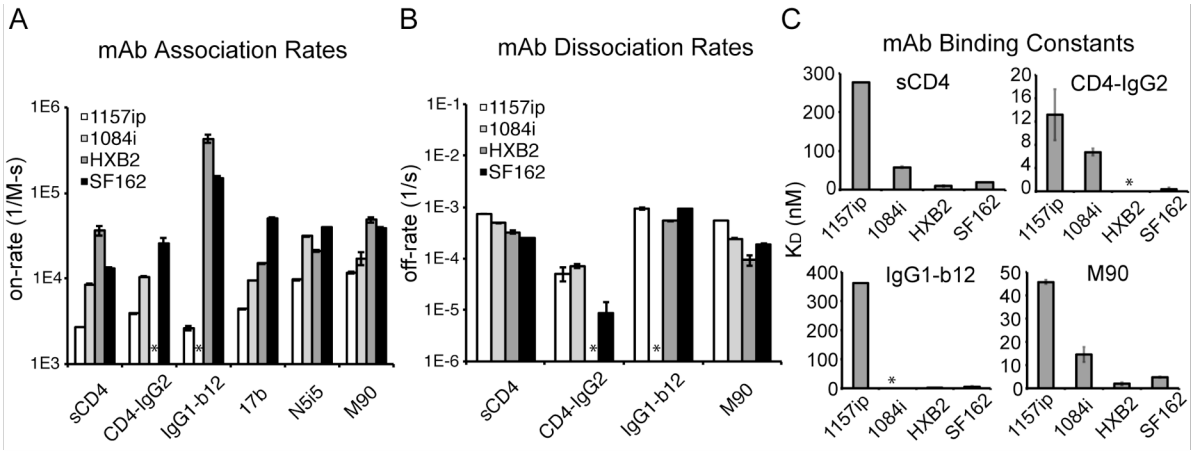

Figure 2.9. Summary of conformation-dependent antibody binding to gp120 measured by SPR. (A) Rate of association of the four gp120 proteins with immobilized sCD4 or captured antibodies. Because of slow dissociation rates for 17b and N5i5, only on-rates could be derived for these antibodies. **(B)** Rates of dissociation of the four gp120s from immobilized sCD4 or captured antibody ligands. Reliable off-rates could not be determined for 17b or N5i5. **(C)** Summary of binding constants for gp120 binding to immobilized sCD4 or captured antibody ligands. Large K_D values reflect weaker binding interactions. Raw data and fitted curves for gp120 binding to conformation-dependent ligands are presented as supplementary information. The (*) indicates that the experiment could not be reliably performed or that the signal could not be fit with a 1:1 binding model. Error bars indicate standard deviation calculated as described in materials and methods.

induced, discontinuous epitope similar to that of A32 (279) that includes layers 1 and 2 of the inner domain, and its contact residues are absolutely conserved in the isolates tested here (George Lewis, personal communication). Because of the high level of sequence conservation within the epitopes recognized by these antibodies, and in the N5i5 epitope, in particular, we were able to test the impact of gp120 dynamics on inner domain antigenicity with limited confounding effects from amino acid variability in the antibodies' epitopes (Figure 2.7C).

Antibodies M90, A32, and N5i5 bound well to 1084i, HXB2, and SF162 but only weakly to 1157ip gp120 by ELISA (Figure 2.8). These results were supported by SPR data, which showed that 1157ip bound to both N5i5 and M90 with the slowest on-rate of the four gp120s (Figure 2.9A). Additionally 1157ip had the fastest off-rate and weakest affinity for M90 of the four isolates (Figures 2.9B-C, Table 4, and Appendix B, Figure B.S21). The rate of N5i5 dissociation was too slow to obtain reliable estimates of the off-rate or binding affinity, even using dissociation times of greater than 1 hour (Appendix B, Figure B.S22). Overall, the relatively high degree of disorder within the 1157ip gp120 inner domain appears to correlate with a slower rate of association with and a weaker affinity for inner domain-specific, conformation-dependent antibodies.

Table 2.4. SPR binding parameters for conformation-dependent antibodies

		1157ip	1084i	HXB2	SF162
sCD4	ka (1/M-s)	$2.67(1) \times 10^{3}$*	$8.5(2) \times 10^{3}$	$37(5) \times 10^{3}$	$13.1(4) \times 10^{3}$
	kd (1/s)	$7.41(3) \times 10^{-4}$	$4.9(1) \times 10^{-4}$	$3.3(2) \times 10^{-4}$	$2.46(6) \times 10^{-4}$
	KD (nM)	277(1)	58(2)	9(2)	18.8(2)
CD4-IgG2	ka (1/M-s)	$3.91(8) \times 10^{3}$	$10.5(1) \times 10^{3}$	n.d.	$25(4) \times 10^{3}$
	kd (1/s)	$5(2) \times 10^{-5}$	$7.1(6) \times 10^{-5}$	n.d.	$0.9(5) \times 10^{-5}$
	KD (nM)	13(4)	6.8(6)	n.d.	0.4(3)
IgG1-b12	ka (1/M-s)	$2.6(1) \times 10^{3}$	-	$430(40) \times 10^{3}$	$150(10) \times 10^{3}$
	kd (1/s)	$9.4(5) \times 10^{-4}$	-	$5.4(1) \times 10^{-4}$	$9.2(2) \times 10^{-4}$
	KD (nM)	362(1)	-	1.3(1)	6.2(6)
M90	ka (1/M-s)	$1.18(4) \times 10^{4}$	$1.7(3) \times 10^{4}$	$4.9(4) \times 10^{4}$	$3.89(7) \times 10^{4}$
	kd (1/s)	$5.41(7) \times 10^{-4}$	$2.4(1) \times 10^{-4}$	$0.9(2) \times 10^{-4}$	$1.88(5) \times 10^{-4}$
	KD (nM)	45.7(8)	14(3)	1.9(6)	4.8(2)

*Error on the last significant figure is presented in parentheses as in Table 2
(-) Data fit poorly to a 1:1 binding model, n.d. experiment not done

Antibodies recognizing CD4-induced epitopes bind slowly to 1157ip in both the unliganded and CD4-bound states

HDX-MS analysis of sCD4-bound gp120 revealed that many regions of gp120 are stabilized as a result of sCD4 binding, including the bridging sheet microdomain and the gp120 inner domain (Figure 2.5). Notably, these same regions are targeted by antibodies such as 17b and N5i5, which preferentially recognize CD4-bound gp120 (179, 279, 304). Because HDX-MS indicated that differences in stability are maintained in sCD4-bound gp120 (Figure 2.5B), we sought to test the antigenicity of CD4-induced epitopes and the antigenic consequences of sCD4 binding across isolates using SPR.

As with N5i5, 17b off-rates were slow for all isolates (with the exception of 1084i), and we were limited to estimates of the on-rate for 1157ip, HXB2 and SF162 (Appendix B, Figure B.S23). Notably, 1157ip had the slowest rate of association with 17b in its unliganded state and was poorly recognized by 17b in ELISA (Figure 2.8), despite having well-conserved 17b-contact residues (Figure 2.7C). Many peptides containing residues critical for 17b binding were

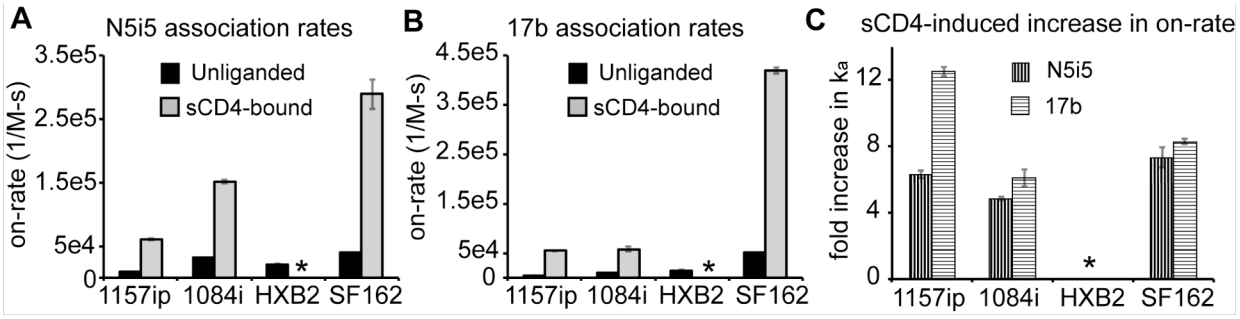

Figure 2.10. Changes in CD4i antibody binding to gp120 in the presence of sCD4 by SPR. (A) On-rates of N5i5 binding to the four gp120 isolates in the presence and absence of sCD4. Unliganded gp120 on-rates are shown in black, and sCD4-bound gp120 on-rates are shown in gray. **(B)** On-rates of 17b binding to the four gp120 isolates in the presence and absence of sCD4. Rates for unliganded and sCD4-bound gp120 are shown in black and gray, respectively. **(C)** Change in rates of association of 17b (horizontal stripes) and N5i5 (vertical stripes) with the gp120 isolates as a result of sCD4-binding. Data is presented as a fold-increase relative to the rate of association with unliganded gp120. (*) Indicates that the experiment could not be reliably performed. Error bars indicate standard deviation calculated as described in materials and methods.

saturated with deuterium at the earliest time point (peptides 4, 5, and 10 in Figure 2.7B) or were similarly disordered in the isolates for which data was available (peptides 8 in Figure 2.7B). Notably, SF162 exhibited stabilization in peptide 9 (Figure 2.7B) - which contains a number of residues critical for 17b binding (Figure 2.7C) - and bound strongly to 17b by ELISA and SPR relative to the other isolates (Figures 2.8 and 2.9). Conversely, peptide 6, which contains a residue critical for 17b binding at position 262 (HXB2 numbering) (179), was more disordered in 1157ip, as were peptides 2 and 3 (Figure 2.7B), which are directly linked to beta strands 2 and 3 of the bridging sheet (highlighted as peptides 4 and 5 in Figure 2.7A, respectively). Given the few differences in stability observed for peptides containing residues critical for 17b binding, it seems plausible that increased disorder observed in the inner domain of 1157ip is communicated to the bridging sheet, with implications for 17b binding to unliganded gp120.

Consistent with the stabilization of the 17b and N5i5 epitopes in sCD4-bound gp120 by HDX-MS (Figure 2.5 and Appendix B, Figure B.S24), we observed a dramatic increase in 17b and N5i5 binding to all four gp120s upon addition of sCD4 (Figure 2.10). It is worth noting that,

Table 2.5. SPR binding parameters for CD4i-epitope specific antibodies

		1157ip	1084i	HXB2	SF162
N5i5	ka (1/M-s)	$9.7(2) \times 10^3$	$31.2(4) \times 10^3$	$21.2(6) \times 10^3$	$39.4(2) \times 10^3$
	kd (1/s)	-	-	-	-
	KD (nM)	-	-	-	-
N5i5 + sCD4	ka (1/M-s)	$6.1(2) \times 10^4$	$15.1(3) \times 10^4$	n.d.	$29(2) \times 10^4$
	kd (1/s)	-	-	n.d.	-
	KD (nM)	-	-	n.d.	-
17b	ka (1/M-s)	$4.38(3) \times 10^3$	$9.5(1) \times 10^3$	$15.1(3) \times 10^3$	$50.6(7) \times 10^3$
	kd (1/s)	-	$2.72(1) \times 10^{-5}$	-	-
	KD (nM)	-	2.86(4)	-	-
17b + sCD4	ka (1/M-s)	$5.5(1) \times 10^4$	$5.8(5) \times 10^4$	n.d.	$41.9(6) \times 10^4$
	kd (1/s)	-	$1.3(1) \times 10^{-4}$	n.d.	-
	KD (nM)	-	2.2(4)	n.d.	-

* Error on the last significant figure is presented in parentheses as in Table 2
(-) Because of slow dissociation, it was not possible to reliably fit dissociation rates or binding constants for these interactions, n.d. experiment could not be reliably performed

in addition to epitope stabilization, tertiary structural changes, not readily detectable by HDX-MS, are also likely to contribute to the increase in 17b and N5i5 binding to sCD4-bound gp120. This may be especially true for 17b, as the lateral movement of V1/V2 upon sCD4 binding appears to lead to ordering of the bridging sheet and formation of the 17b epitope (142).

We investigated whether the differences in 17b and N5i5 reactivity across isolates observed in unliganded gp120 would be similarly apparent in the context of sCD4-bound gp120. SPR was used to measure the rate of gp120 binding to 17b and N5i5 in the presence of a 5-fold molar excess of sCD4. The rates of association with 17b and N5i5 increased for all isolates in the presence of sCD4, and the isolate rank order of fastest (SF162) and slowest (1157ip) rates of association with the two antibodies was identical in unliganded and sCD4-bound gp120 (Figure 2.10A-B and Table 2.5). Importantly, the increase in the rate of 1157ip binding to 17b and N5i5 upon addition of sCD4 was similar to that of the other isolates (Figure 2.10C), indicating that although 1157ip gp120 wasn't as dramatically stabilized by sCD4 as the other gp120s, it remains capable of binding to sCD4 and undergoing a transition to a CD4-induced state. Overall it appears that isolate-specific antigenic differences within CD4-induced epitopes are maintained in the sCD4-bound state, in agreement with the conformational stability profiles observed for the sCD4-bound gp120s by HDX-MS.

Consideration of potential caveats of sCD4-induced stabilization of gp120 by HDX-MS

Two factors we considered that could potentially complicate interpretation of the HDX-MS results for sCD4-bound gp120 are isolate-specific differences in kinetics and affinity of binding to sCD4 and isolate-specific variability in the fraction of "active" gp120 within a purified gp120 preparation. Because 1157ip has the weakest affinity for sCD4, we considered the possibility that the greater levels of deuterium uptake by this isolate in the presence of sCD4 reflect a difference in the amount of time a molecule of 1157ip would spend in the sCD4-bound state or a lower level of sCD4 occupancy at equilibrium. However, given the affinity values

calculated by SPR (Table 2.4) and the concentration of sCD4 used in complex formation, we estimate that only 0.01% more 1157ip would remain unbound at equilibrium as compared to 1084i (0.28% vs 0.27% unbound gp120 for 1157ip and 1084i, respectively), an insignificant difference. Similarly, using a standard first-order rate equation to model the exponential decay of the gp120-sCD4 complex, and the dissociation rates calculated by SPR (Table 2.4), after 12 seconds of deuteration, only 0.3% more dissociation would occur for 1157ip as compared to 1084i, yet we observed dramatic differences in deuterium uptake at this time point (Figure 2.5). Furthermore, we attempted to account for the weaker affinity of 1157ip for sCD4 by using a higher concentration of sCD4 in complex formation (5-fold molar excess) as compared to the other isolates (3-fold molar excess). The absence of additional stabilization in the 5-fold vs. 3-fold molar excess samples suggests that sCD4 is saturating the available 1157ip gp120 population. Thus differences in CD4 occupancy at equilibrium or kinetic differences in sCD4 dissociation are unlikely to explain the dramatic differences in stability observed for sCD4-bound 1157ip as compared to the other isolates.

Similarly, if purified 1157ip gp120 contained a relatively large fraction of inactive gp120, as a result of heterogeneity in disulfide bonding or glycosylation, for example, then addition of sCD4 would only weakly stabilize gp120 at the population-level (although it may be capable of dramatically stabilizing individual molecules of active gp120). However, there is no indication that such a population exists in 1157ip, for example, Kratky plots of 1157ip indicate that the gp120s have similar global structure (Appendix B, Figure B.S2). Furthermore, addition of sCD4 to 1157ip produces a similar increase in its rate of association with 17b and N5i5 as is observed for the other gp120s (Figure 2.10C). Because the rate of association is sensitive to the active concentration of analyte, this suggests that the fraction of gp120 that is active for sCD4 binding is similar among the four gp120s. Thus, we considered these caveats, but conclude that they are unlikely to be responsible for the observed isolate-specific differences in the stability and

antigenicity of sCD4-bound gp120. Instead, the differences appear to reflect inherent structural features of each gp120.

Discussion

Our understanding of the structural basis for antigenic and immunogenic differences among gp120 proteins from diverse isolates has been hindered by our inability to extract detailed structural information for intact Env glycoprotein constructs containing the variable loops and glycans, which are major determinants of isolate antigenicity and neutralization sensitivity. Crystal structures of truncated core constructs provide valuable information about the conserved elements of gp120 and their recognition by receptor and antibodies, but they do not elucidate how the conserved features are masked by the dominant variable elements or how these variable elements affect the conformation of distal, conserved epitopes in the context of full-length gp120 (305). Furthermore, x-ray crystallography cannot probe protein dynamics in solution, which may be an important determinant of Env antigenicity (145).

Here, we used HDX-MS and SAXS in combination with antibody binding studies to investigate the structural and antigenic variability among full-length, glycosylated gp120 proteins from diverse HIV-1 isolates in order to understand the role of structural differences such as variable loop position and conformational dynamics in modifying the antigenicity of gp120 proteins from diverse isolates. A comparison of the four full-length gp120s by SAXS (Figure 2.1 and Appendix B, Figure B.S2) indicated that the overall morphologies of the gp120 monomers were similar and that they were comparable to SF162 gp120 expressed in 293E and CHO cells, with the large V1/V2 loops likely occupying a similar position atop the gp120 core (142). Radii of gyration differed by only ~1Å and appeared to be in good agreement with expected sizes related to variable loop length and glycosylation. Kratky plots of the SAXS data also indicated that the gp120s were similarly ordered, and none of the isolates appeared to be unfolded or noticeably different in global structure by this measure (Appendix B, Figure B.S2).

Implications of Inner Domain Conformational Variability for CD4-reactivity

In contrast to the similar global organization observed for the gp120 monomers by SAXS, HDX-MS revealed significant differences in local dynamics among the four unliganded gp120 proteins (Figure 2.2). This is the first report, to our knowledge, of experimentally measured, naturally occurring structural heterogeneity among full-length, glycosylated gp120 monomers from diverse isolates. Many of the differences were concentrated in the inner domain and at the interface of inner and outer domains (Figures 2.3 and 2.4). This is consistent with previous computational (306) and structural studies, which suggest that the inner domain is capable of substantial structural variability. For example, layers 1 and 2 of the unliganded SIV core inner domain (307) adopt a conformation that is distinct from that observed in unliganded extended cores from multiple isolates (192) as well as CD4-bound HIV-1 isolates (25, 186). Similarly the inner domain exhibits substantial variability as compared to the relatively inert outer domain in the crystal structures of gp120 bound to antibodies b12 and F105 (188). Our observation that diverse, full-length gp120s can exhibit significant differences in structural order contrasts with a recent structural study of unliganded extended core constructs, which found that extended core proteins from diverse isolates were nearly superimposable (192). The results are not necessarily contradictory, however, given that variable loop truncation appears to favor a more uniform CD4-bound-like conformation (192). The crystal structures also lack glycosylation and are subject to packing constraints in the crystal, which could suppress isolate-specific differences in local dynamics and flexibility.

The gp120 inner domain is critical for maintaining gp120-gp41 interactions and mediating CD4 reactivity (35, 301, 303). In addition, recent work suggests that it is an important target for ADCC-active antibodies (279, 308). Site-directed mutagenesis studies have shown that residues in layers 1, 2, and 3 of the inner domain participate in a network of critical interactions in both soluble, monomeric gp120 and in the context of trimeric Env, and this

network is required for stabilizing the transition to the CD4-bound state and maintaining non-covalent gp120-gp41 interactions in the Env trimer (301-303). Our results are consistent with these reports and provide a direct probe of the structural ordering in layers 1, 2, and 3 of the gp120 inner domain as a result of CD4-binding. The key residues that have been shown to mediate the transition to the CD4-bound conformation are absolutely conserved among the four isolates studied here, including H66, P212, and S375 (301). Although these residues are present in the primary sequence, our HDX-MS results suggest that the regions containing these residues are ordered to different degrees in the four gp120s and are notably disordered in 1157ip (Figure 2.3). That disorder may preclude the formation of a stable bond network. Indeed, 1157ip had the weakest affinity for CD4-binding site ligands of the four isolates (Figures 2.8, 2.9), and HDX-MS analysis of the 1157ip gp120-sCD4 complex indicated that 1157ip was poorly stabilized in the presence of sCD4 relative to the other isolates (Figure 2.5). While addition of sCD4 stabilized the gp120s to different degrees, the pattern of sCD4-induced ordering was found to be conserved among the four isolates. Specifically, the CD4-binding site, bridging sheet and inner domain of gp120 were protected from deuterium uptake in all isolates in the presence of sCD4. CD4-induced ordering of the gp120 inner domain thus appears to be critical for viral entry, just as bridging sheet ordering is conserved and required for co-receptor binding (36).

Epitope dynamics and antibody binding

In order to determine whether the differences in structural dynamics we observed by HDX-MS were related to antigenic differences among the gp120 proteins, we measured antibody binding to the panel of full-length gp120s. Only subtle differences in linear epitope-specific antibody binding were observed across isolates (Figure 2.6) despite differences in the structural dynamics of the antibodies' epitopes among the four gp120s (Figure 2.3B). This contrasts somewhat with early studies in non-HIV systems, which concluded that linear epitope

flexibility correlates with improved recognition by antibodies. However, the conclusions of these previous studies were based on correlations between crystal structure temperature factors and the antigenicity of regions within a single protein, where antibodies raised against peptides from highly mobile protein elements bound to the protein better than antibodies to regions of the same protein with low B factors (309, 310). There are a number of potential caveats associated with this type analysis, including differences in the immunogenicity of peptide sequences and differences in tertiary structural context, which may alter antibody recognition. In contrast, our study looked at the binding of monoclonal antibodies to a common linear epitope, differentially stabilized among the gp120 proteins. While relatively minor differences in linear epitope recognition were observed, one exception was relatively poor recognition of SF162 gp120 by helix 1-specific antibodies. The stability of helix 1 as monitored by HDX-MS was similar in SF162, HXB2 and 1084i, thus the difference in linear epitope-specific antibody recognition of SF162 may reflect a difference in SF162 tertiary structure or possibly epitope occlusion by adjacent glycans.

Antibodies targeting discontinuous and conformational epitopes showed dramatic isolate-specific differences in gp120 binding (Figures 2.8 and 2.9). Importantly, the isolate with the most dynamic inner domain, 1157ip, was poorly recognized by every conformation-dependent antibody tested with an epitope that either wholly (A32, N5i5 and M90) or partially (IgG1-b12, sCD4, CD4-IgG2, and 17b) involves the inner domain. The potential importance of inner domain disorder in limiting the antigenicity of the CD4- and co-receptor-binding sites is further highlighted by the observation that many peptides in the CD4- and co-receptor binding sites were similarly disordered among the four isolates (Figure 2.7B). Notably, VRC01 binding to 1157ip was only slightly reduced as compared to other CD4 binding-site ligands (Figure 2.8). These data support a proposed model for the impressive breadth of VRC01 neutralization, which is that because VRC01 predominantly makes contact with the gp120 outer domain, it is

less sensitive to naturally-occurring structural heterogeneity within the gp120 inner domain (190, 311).

Increased conformational dynamics appeared to correlate with reduced binding by multiple antibodies with distinct specificities, thus it is unlikely that the effects we detect are simply due to amino acid changes within antibody contact sites. The contact residues of N5i5, in particular, were absolutely conserved among the four isolates (George Lewis, Personal Communication), yet substantial differences in N5i5 association with gp120 were observed among the four isolates. Additional support for the proposal that structural stabilization leads to improved recognition by conformation-dependent antibodies is found in the observation that sCD4-binding induces ordering within the epitopes targeted by N5i5 and 17b (Figure 2.5 and Appendix B, Figure B.S24), which correlates with increased N5i5 and 17b binding to sCD4-stabilized gp120 as compared to the relatively dynamic unliganded gp120 (Figure 2.10).

Overall the data suggest that antibodies recognizing discontinuous epitopes are sensitive to differences in the structural dynamics of elements both proximal and distal to the antibody binding site. The data presented here, and previous studies (142, 301) suggest that conformational epitopes in the CD4 binding site, bridging sheet and inner domain are coupled to one another. Thus, it is conceivable that enhanced conformational dynamics in specific regions of HIV-1 gp120 Env due to distal amino acid changes could provide an additional pathway for escape from neutralizing and ADCC-active antibodies targeting conserved, conformational epitopes – allowing for structural heterogeneity in regions where amino acid changes are not tolerated due to functional requirements.

It will be valuable to extend this work to trimeric Env constructs in order to test the influence of conformational dynamics within the Env trimer on the neutralization phenotype of virion-associated Env. However, such a study would depend on the identification of homogenous, native Env trimers that are suitable for structural comparisons among isolates. Such constructs remain elusive despite substantial effort (312). Soluble oligomeric gp140

ectodomain constructs, which are often thought to mimic the native Env trimer appear to exhibit substantial heterogeneity from one isolate to another (299), and in many cases, adopt non-native conformations especially within gp41 (Guttman et al., in preparation). At present, full-length gp120s are the most tractable system for comparing structural order among isolates. In many respects, full-length gp120 appears to recapitulate the subunit organization of gp120 in the context of the trimer (142) and can provide valuable insight into the structure-function relationship of HIV-1 Env. Furthermore, because monomeric gp120 is likely to be immunogenic in the course of natural HIV-1 infection due to the labile interactions between gp120 and gp41, which allow for gp120 shedding (146), and because monomeric gp120 proteins are commonly used vaccine immunogens, including in the RV144 trial, it is important to understand the structural factors that influence antibody reactivity to monomeric gp120 proteins as well as trimeric Env constructs.

Significance for gp120 as a prospective vaccine immunogen

The RV144 HIV-1 vaccine trial provided the first evidence that vaccine-induced protection against HIV-1 acquisition is possible and has rekindled interest in gp120 proteins as vaccine immunogens. Analysis of samples collected in the RV144 trial revealed that among other correlates of protection, ADCC activity was negatively associated with risk of infection in individuals with low levels of IgA antibodies (65). Notably, vaccinees with strong IgA responses to C1 in the gp120 inner domain were at greater risk of infection as compared to vaccinees without these antibodies, suggesting that IgA may inhibit ADCC-active antibody binding to this region. Thus it was proposed that inner domain-specific, ADCC-active IgG antibodies, similar to those A32-like antibodies commonly elicited during HIV-1 infection (308), may play an important role in protection from HIV-1 acquisition (313). We observe that the stability of the C1 region targeted by these antibodies varies among gp120 proteins from diverse isolates and the differences in stability correspond to differences in antibody binding to this region, including

N5i5, which potently mediates ADCC (279). In light of previous studies, our results suggest that conformational dynamics may play a role in facilitating evasion of antibodies targeting this functionally conserved gp120 epitope and highlight the potential importance of characterizing the local conformational stability of future gp120 vaccine immunogens.

The relationship between gp120 conformational flexibility, antigenicity, and immunogenicity is likely to be complex. The data presented here, and in previous studies (145) suggest that flexibility modifies gp120 antigenicity, however, antigenicity is not equivalent to immunogenicity, and it remains to be determined what effect flexibility may have on the immunogenicity of Env constructs. Indeed, previous work reveals that the opposing influences of stability and dynamics are both likely to influence epitope immunogenicity. For example, Dey and colleagues demonstrated that the immunogenicity of the gp120 coreceptor binding site can be enhanced using cavity-filled, disulfide-stabilized gp120 core proteins (314). Similarly, a single glycan deletion at the base of V2, which appears to shift the conformational equilibrium of Env towards a CD4-bound-like state (124) has been shown to elicit improved antibody titers with increased neutralization breadth in macaques (315). In contrast, a recent study by Liao et al. identified a conformationally-variable linear epitope in V2 to be an important immunogenic target of antibodies isolated from vaccinees in the RV144 trial (66). In the design of improved antibody-based HIV-1 vaccines, the appropriate balance between immunogen stability and flexibility should be carefully evaluated in the context of both immunogenicity (the ability to elicit high titers of antibodies) and quality (the ability to elicit broad and potent antibodies). Our results support a role for HDX-MS in testing the relationship between the local stability of immunogens, their recognition by antibodies, and their immunogenicity, with the goal of improving antibody-based HIV-1 vaccine efficacy.

ACKNOWLEDGEMENTS:

This work was supported by UAB CFAR grant P30-AI027767 through the CNIHR program for new HIV investigators (K.K.L.), and by NIH grants R00-GM080352, R01-GM099989 (K.K.L.), P01-RR000166 (Washington National Primate Research Center), R01-AI076170, and the Bill and Melinda Gates Foundation Collaboration for AIDS Vaccine Discovery (CAVD) grant OPP1033102 (S.L.H.). T.M.D. was supported by NIH training grant T32- AI 7509-12. Data collection at SSRL was supported by grant number P41-RR001209 from the National Center for Research Resources (NCRR), a component of the National Institutes of Health.

We acknowledge Tsutomu Matsui and Lester Carter at SSRL BL4-2 for valuable assistance with on-line FPLC SAXS data collection. We thank John Sumida and Mauro Acchione of the University of Washington Center for Intracellular Delivery of Biologics Analytical Biopharmacy core, supported by the Washington State Life Sciences Discovery Fund for helpful discussion and use of the Biacore T-100 instrument. We would like to acknowledge the contributors who generously provided materials that were important in carrying out these studies. We thank Yongjun Guan and George Lewis at the University of Maryland for providing the antibodies N5i5, B18, and C4 and for helpful discussions. The following reagents were obtained through the NIH AIDS Reagent Program, Division of AIDS, NIAID, NIH: HIV-1 Consensus Subtype B Env (15-mer) Peptides - Complete Set, HIV-1 gp120 monoclonal antibody (IgG1 b12) from Dr. Dennis Burton and Carlos Barbas, HIV-1 gp120 monoclonal antibodies 17b and A32 (cat #11438) from Dr. James E. Robinson, HIV-1 gp120 MAb (VRC01), from Dr. John Mascola, sCD4-183 from Pharmacia, Inc., Cat#11780, and CD4-IgG2 from Progenics Pharmaceuticals. The reagent CA13 (ARP #3119) was obtained from the Centre for AIDS Reagents, NIBSC HPA UK, supported by the EC FP6/7 Europrise Network of Excellence, and NGIN consortia and the Bill and Melinda Gates GHRC-CAVD Project and was donated by Ms. C. Arnold.

Chapter 3

Changes in Broadly Neutralizing Antibody Paratope Dynamics Over the Course of Affinity Maturation

Introduction

Diversity of sequence, structure, and specificity facilitate antibody recognition of diverse foreign antigens. This diversity is generated through the recombination of variable (V_H), diversity (D_H), joining (J_H) and constant (C_H) gene segments that code for the antibody heavy chain and the V_L, J_L, and C_L gene segments that code for the light chain (166). With many distinct copies of each gene segment in the human genome, there is substantial opportunity for combinatorial variability through this process (168). Non-templated incorporation of nucleotides at gene segment junctions and pairing of the heavy and light chains dramatically increase the structural diversity of the antibody paratope as well (316, 317). After contact with antigen, B cells undergo further diversification and selection during affinity maturation, in which the B cell receptor accumulates mutations that increase its affinity for a select epitope (318). It has been proposed that affinity maturation alters the conformational flexibility of the antibody paratope (170, 319). However, the site-specific changes in paratope stability are poorly defined, and it is unclear what role conformational flexibility may play in balancing the affinity and specificity with which an antibody binds to a complex viral antigen.

The factors that influence antibody binding affinity and specificity are of substantial interest for antibody-based HIV-1 vaccine design because of the enormous antigenic variability of the HIV-1 Envelope glycoprotein (Env), the sole target of neutralizing antibodies and the most diverse gene in the HIV-1 genome (26, 55). It is believed that an effective HIV-1 vaccine would

elicit so-called “broadly-neutralizing” antibodies (bNAbs) that are capable of recognizing diverse HIV-1 Env isolates (55, 203). These antibodies target structurally conserved epitopes on the Env trimer, and develop high affinity binding interactions in spite of variability within and surrounding the target epitope (81, 190). Nearly all bNAbs have undergone extensive somatic hypermutation, highlighting the importance of persistent stimulation by diverse antigens in bNAb development (164, 165). The changes acquired over the course of affinity maturation occur in both the complementarity determining regions (CDR) that make direct contact with the antigen and in the antibody framework regions (FWR) distal to the antigen-combining site (162, 163). Although FWR residues typically do not interact with antigen, mutations in this region have been shown to be critical for efficient binding and neutralization by mature bNAbs (163). It is hypothesized that mutations in these regions indirectly affect antibody binding by changing the stability, flexibility, or orientation of the CDR loops. However, the structural consquences of these mutations has never been directly examined.

While bNAbs are observed in 10-20% of infected individuals after more than two years of infection, we are currently unable to elicit these antibodies through vaccination (80, 81). Soluble Env immunogens elicit narrow antibody responses that are specific for the immunogen isolate, and exhibit little, if any, neutralizing activity against neutralization-resistant “Tier 2” isolates, which would likely be required of an effective antibody-based HIV-1 vaccine (55). A number of hypotheses have been presented as to why vaccination fails to generate broad neutralizing responses. Recently, it was proposed that bNAbs are not elicited through vaccination because Env immunogens bind poorly to the predicted germline precursors of known broadly neutralizing antibodies (162, 163, 320). In this way, bNAbs may not have an opportunity to develop because the germline B cells that give rise to broadly neutralizing B cell lineages are rarely activated to proliferate and undergo affinity maturation. However, there are rare examples of Env isolates that are capable of binding to bNAb germline precursors (66, 162, 321). It is of

primary interest to understand the structural basis for the poor recognition of Env immunogens by predicted bNAb germline precursors.

Here we tested the hypothesis that antibody paratope stability changes over the course of affinity maturation. Specifically, we hypothesized that predicted germline and early bNAb precursor antibodies would be more dynamic than mature bNAbs because flexibility has been associated with binding promiscuity. To maximize the likelihood that a germline B cell receptor would be able to recognize the nearly infinite set of possible foreign antigens, it would be favorable to possess some degree of binding promiscuity. We examined how local conformational dynamics may modify binding affinity and specificity (or lack thereof) in germline/early, intermediate and mature broadly neutralizing antibodies that target distinct epitopes on HIV-1 Env.

These hypotheses are based on previous reports, which observed that affinity maturation contributes to rigidification of the antibody paratope as the antibody becomes specific for a given antigen (319, 322). The relative conformational flexibility of germline antibodies is thought to permit expanded recognition of diverse antigens (170), although the interactions are thought to be of lower affinity than those of mature antibodies. Recent computational work demonstrated that germline antibodies likely do, in fact, exhibit non-specific binding behavior (323). In most cases, the polyspecificity of germline antibodies is likely traded for high affinity binding to a single epitope during B cell receptor maturation. In light of these observations, the question arises: how does breadth develop in HIV-1 bNAbs? Do these antibodies mature and rigidify to bind with high affinity to a very specific epitope that is structurally-conserved among HIV-1 isolates? Or do they mature to become relatively flexible in order to tolerate structural variability within their target epitope?

Hydrogen-deuterium exchange with mass spectrometry (HDX-MS) provides information on the stability of protein secondary structures and the degree of solvent accessibility (197). More dynamic, solvent-exposed regions take on deuterium rapidly, while structured, buried

regions of a protein take on deuterium relatively slowly (270). To better understand the conformational development of antibodies over the course of affinity maturation, we used HDX-MS to measure the local dynamics of antigen binding fragments (Fab) derived from germline and mature sequences for the bNAbs VRC03(182) and VRC26K, which was isolated from the HIV-infected individual CAP256 (324, 325). For VRC26K, we also measured the local conformational dynamics of an intermediate antibody sequence (VRC26D). Given the cross-sectional nature of many studies, and the randomness associated with V(D)J recombination, it is challenging to predict the "true" germline sequence for a mature antibody. The antibodies studied here were specifically selected because there was sufficient data from deep sequencing the donor B cell repertoires, to predict the germline and early/intermediate precursor sequences with a high level of confidence (183).

By measuring changes in conformational dynamics for two distinct bNAb specificities – CD4-binding site and V2-quaternary, for VRC03 and VRC26K, respectively – we hoped to address whether there are distinct changes in flexibility that occur on the pathway to the development of divergent broadly neutralizing antibody specificities. In addition, we hoped to better understand the structural basis for the weak recognition of Env immunogens by predicted germline and early precursors of broadly neutralizing antibodies. We observed that paratope stability does not increase monotonically throughout the course of affinity maturation. Rather, changes in conformational dynamics occur in a site-dependent manner with some regions becoming more dynamic in the mature antibody and others becoming more ordered. Additionally, VRC26 samples both high and low levels of conformational flexibility on its path toward optimal binding affinity and breadth. This work provides insight into biophysical mechanisms by which the human immune system may tailor the affinity and specificity of antibody binding to diverse foreign antigens.

Materials and Methods

Antigen Binding Fragments (Fab):

All Fabs were generously provided by Jason Gorman, Gordon Joyce, Peter Kwong, and John Mascola of the VRC, NIAID, NIH. Antibodies VRC03 and VRC26K were isolated from HIV-infected individuals with broad neutralizing activity by single-cell sorting techniques that have been previously described (VRC26 details are in preparation for publication) (30). Germline and early/intermediate precursor antibody sequences were predicted computationally using deep sequencing data from donor B cell repertoires (183). Fab fragments were prepared from full-length IgGs expressed and purified as previously described (182).

Hydrogen-Deuterium Exchange with Mass Spectrometry (HDX-MS):

Prior to HDX-MS, all Fabs were buffer-exchanged into an identical phosphate buffered saline solution (150 mM NaCl, 10 mM Phosphate, 1 mM EDTA, 0.02% Sodium Azide, pH 7.4). Deuteration of intact Fabs was carried out in triplicate, exactly as described in Chapter 2, with some minor modifications. Specifically, each exchange reaction was prepared with 7 µL of Fab at 1 mg/mL, 5 µL of a 20X-concentrated PBS solution and 88 µL of D_2O (Cambridge Isotopes). Fabs were allowed to exchange at room temperature for 3 sec, 12 sec, 1 min, 5 min, 30 min, 4 hr, and 20 hr prior to addition of the quench solution (4M Urea, 500 mM TCEP, 0.1% TFA, pH 2.5) and pepsin digestion on ice using a 2:1 mass ratio of pepsin:Fab for 5 minutes prior to flash freezing in liquid nitrogen. Pepsin fragments were resolved and analyzed as described in chapter 2. Undeuterated, “zero” second, and fully-deuterated controls were prepared as described previously (142). Exchanges for mature and germline/early/intermediate antibodies were prepared and analyzed side-by-side.

Data Analysis:

Rates of deuterium uptake for each observable peptide were analyzed in batch using HD-Examiner (Sierra Analytics) in combination with HX-Extreme (Mike Guttman), a batch-processing macro, which takes mass spectra from HD-Examiner and interfaces with HX-Express 2 (David Weis and Mike Guttman) to identify mass envelope centroids at each deuteration time point (326). Messy or overlapped mass spectral data was analyzed manually in MassLynx software (Waters) and centroids were calculated in HX-Express 2. Percent deuteration values were calculated using Equation 2.1. Heatmaps were prepared using PyMol Molecular Visualization Software (286).

Results

Conformational Dynamics in Germline and Mature VRC03:

Antibody dynamics has been shown to modify the affinity and specificity of antibodies in model systems (322). Here we tested the hypothesis that conformational dynamics plays a role in shaping antibody affinity and specificity in the context of the HIV-1 specific CD4-binding site-directed broadly neutralizing antibody, VRC03. We monitored changes in the conformational stability of VRC03 over the course of affinity maturation by comparing the local flexibility of Fabs derived from the predicted germline and mature VRC03 sequences using HDX-MS.

We observed peptic fragments corresponding to ~80% of the primary sequence by MS/MS for both germline (Appendix C, Figure C.S1) and mature (Appendix C, Figure C.S2) VRC03 Fabs. Amino acid changes in the variable domains led to distinct digestion patterns for germline and mature Fabs, which, in some cases complicated a direct comparison of the conformational dynamics in that region. However, there were 13 peptides that were similar between the germline and mature VRC03 sequences, and these could be used to compare differences in local conformational dynamics for 40% of the residues in the VRC03 heavy chain and 56% of the residues in the VRC03 light chain (Figure 3.1). There was only one peptide in

the VRC03 heavy chain variable domain (V_H) and three peptides in the light chain variable domain (V_L) that could be compared between germline and mature sequences. The remaining nine peptides provided good coverage in the Fab constant regions for both heavy (C_H1) and light chains (C_L).

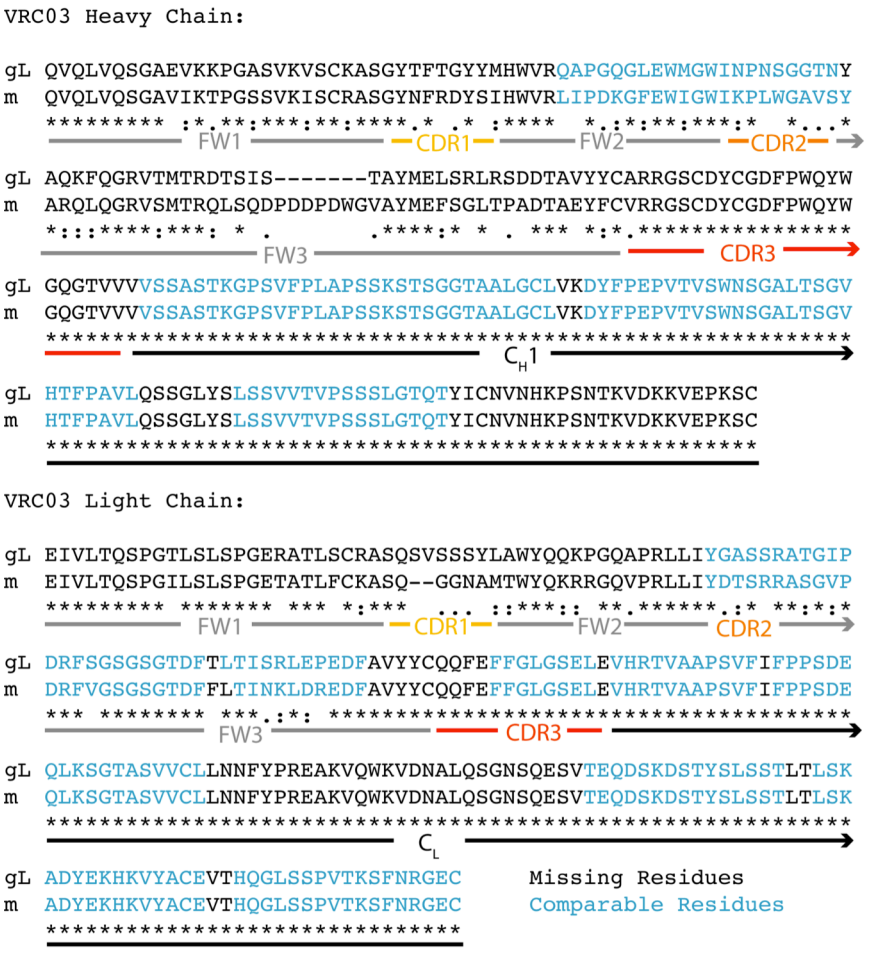

Figure 3.1. VRC03 Fab Residues Comparable by HDX-MS. A clustal-W alignment of the VRC03 germline and mature Fab sequences is shown for the heavy and light chains. The framework and complementarity determining regions of the VH and VL domains as well as the CH and CL domains are indicated below the alignment. Residues comparable by HDX-MS are indicated in blue, residues that can't be compared due to missing or dissimilar peptide fragments are indicated in black text.

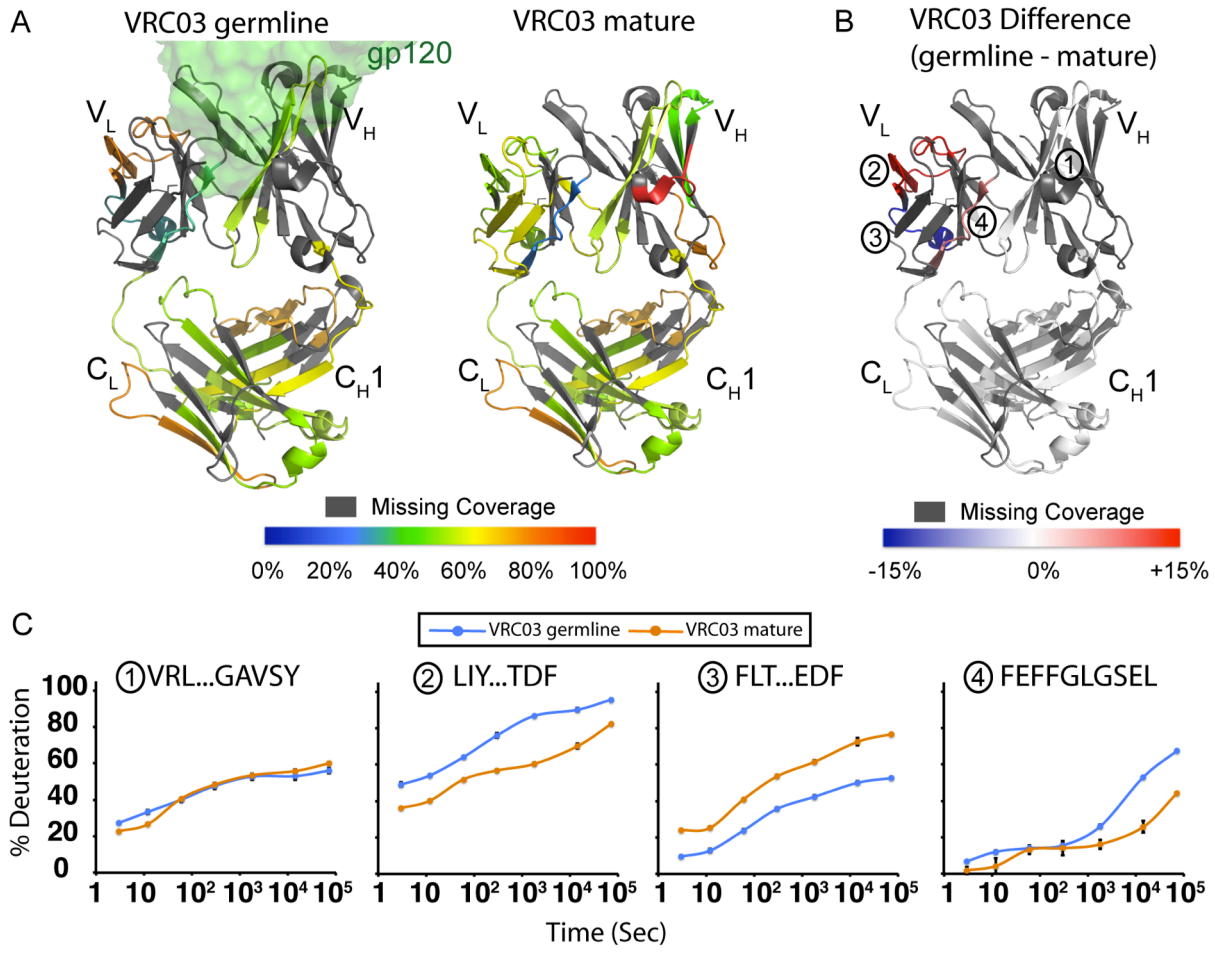

Figure 3.2. Germline and Mature VRC03 Deuteration Profiles. (A) Deuteration heatmaps: Colors mapped onto the VRC03 Fab structure (PDB 3SE8) indicate percent deuteration of peptides after 5 minutes of incubation in D_2O as shown in the legend. Gray indicates missing peptide coverage. The green surface displayed for VRC03 germline indicates the position of gp120 relative to the Fab variable loops in the mature VRC03-gp120 co-crystal structure. **(B)** Difference heatmaps: colors mapped onto the VRC03 Fab structure indicate the difference in deuterium uptake between VRC03 germline and mature after 5 minutes of incubation in D2O. Red colors indicate regions that are more deuterated in germline VRC03, blue colors are less deuterated; white indicates similar deuterium uptake, and gray is missing coverage. **(C)** Deuterium uptake plots show the percent deuteration vs time for comparable variable domain peptides. Blue lines: VRC03 germline, Yellow lines: VRC03 mature.

A comparison of heatmaps indicating percent deuteration of peptides throughout the VRC03 Fab revealed that the local stability of germline VRC03 was qualitatively similar to mature VRC03 (Figure 3.2A). The V_H peptide that could be compared in germline and mature VRC03 provided coverage of residues in the second framework region (FW2) and the second complementarity-determining region (CDRH2). These residues appeared to be similarly stable

in germline and mature VRC03 (Figure 3.2B and 3.2C). In contrast, there were measurable differences in deuterium uptake for the three V_L peptides, and these differences varied in a site-specific manner. While the two peptides that provided coverage of residues in the CDRL2 and CDRL3 loops were more rapidly deuterated in germline VRC03, a peptide from the light chain FW3 took on deuterium more slowly in the germline Fab (Figure 3.2B and 3.2C). Constant region peptides were deuterated at identical rates in germline and mature VRC03 (Figure 3.2B).

Overall this data suggests that conformational differences between germline and mature VRC03 are confined to the antibody variable domains. There were measurable differences in the dynamics of the VRC03 V_L domain, which supported a trend of increased CDR loop flexibility in the germline antibody. However, the germline Fab was not uniformly more dynamic, as a peptide from the light chain FW3 region was more stable in germline VRC03. These differences in stability were largely distal to the gp120 contact site. While it is possible that differences exist in the V_H domain as well, we were unable to detect these differences due to poor peptide coverage and differences in pepsin cleavage in this region.

Conformational Evolution of VRC26:

It is possible that the VH1-2*02 gene segment from which VRC03 is derived exhibits unique stability characteristics. Therefore, we explored conformational changes over the course of affinity maturation for a distinct antibody specificity descended from a distinct V_H gene segment. VRC26 is descended from V gene segment VH30-3*02, and targets a V2-quaternary epitope similar to PG9 and thus presents an opportunity to test the generalizability of changes in stability over the course of affinity maturation in a distinct antibody system. Additionally, because we have a more detailed understanding of the VRC26 developmental pathway, we have the opportunity to measure the flexibility of intermediates along the pathway to the mature bNAb. This allows us to test the hypothesis that a paratope becomes continually more stable as an antibody becomes increasingly specific for a foreign antigen. If this were true, we would

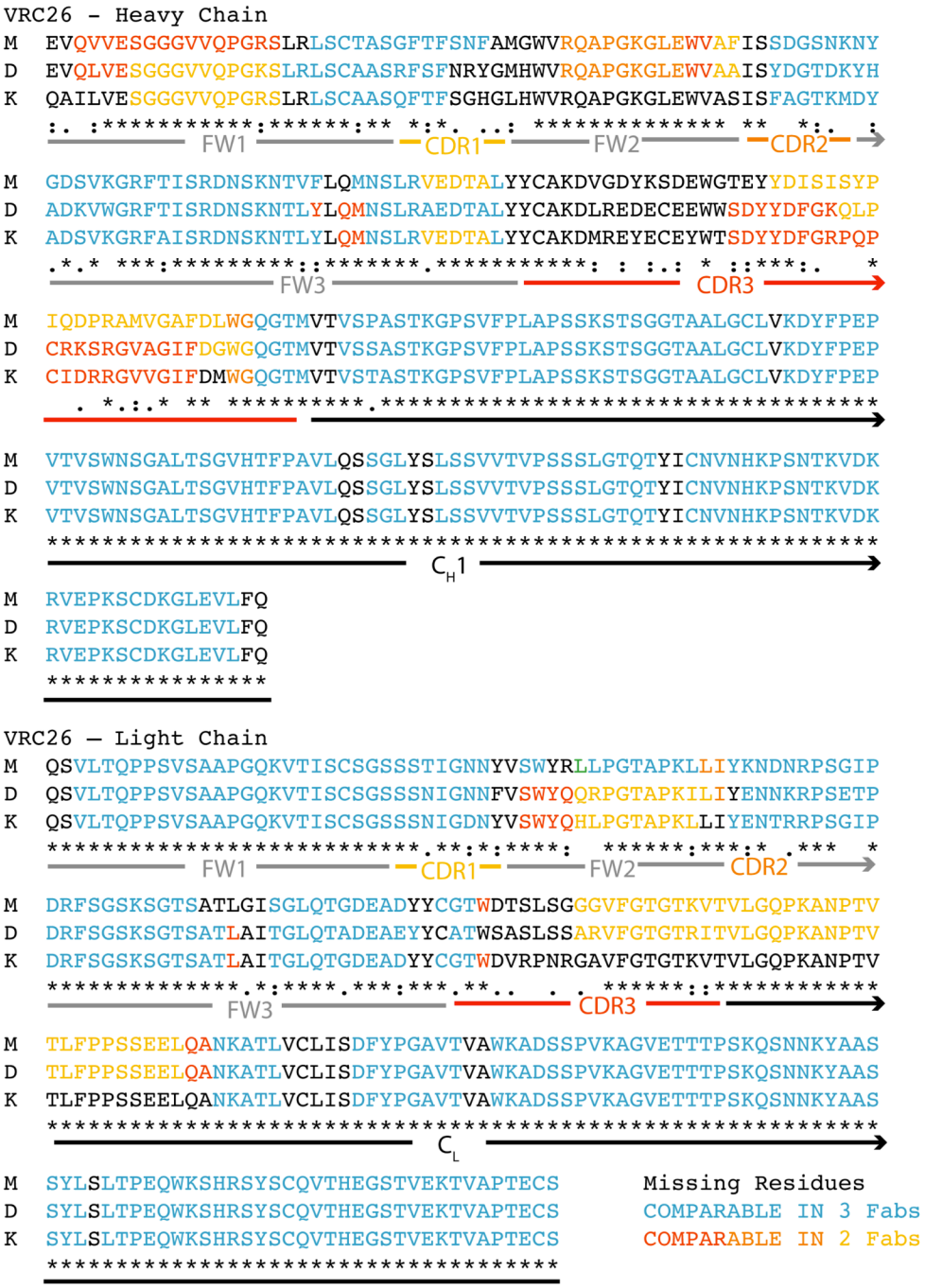

Figure 3.3. VRC26 Fab Residues Comparable by HDX-MS. A clustal-W alignment of the VRC26 early (M), intermediate (D), and mature (K) Fab sequences is shown for the heavy and light chains. The framework and complementarity determining regions of the VH and VL domains as well as the CH and CL domains are indicated below the alignment. Residues comparable among all three fabs by HDX-MS are indicated in blue, residues that can be compared between two fabs are indicated in red, orange or yellow text, and residues that can't be compared due to missing or dissimilar peptide fragments are indicated in black text.

expect the intermediate Fab to demonstrate an intermediate level of stability relative to the early and mature antibody sequences.

Here, we compared the conformational dynamics of early, intermediate, and mature versions of the antibody VRC26: VRC26M, VRC26D, and VRC26K, respectively. Pepsin digestion produced fragments corresponding to nearly 100% coverage of the antibodies' primary sequences (Appendix C, Figures C.S3-C.S5). Of these peptides, 16 were comparable between at least two Fabs, and 15 were comparable among all three Fabs – two in the VH domain, four in the VL domain, and the remainder in the constant region. We were able to compare the dynamics of residues corresponding to 83% of the heavy chain and 90% of the light chain sequence across at least two Fabs. However, only 60% of the heavy chain and 71% of the light chain sequence could be compared across all three Fabs, with the majority of these comparable residues occurring in the constant regions (Figure 3.3).

There were notable changes in post-translational modifications that were observed over the course of VRC26 somatic hypermutation. For example, VRC26M and VRC26D possess a DYYD sulfation motif in the CDRH3, but this motif is mutated to EYYD in VRC26K. We observed sulfotyrosine residues in MS/MS of VRC26M and VRC26D, but not for VRC26K. Similarly, there is an additional disulfide bond that is acquired over the course of somatic hypermutation within the CDRH3, which is present in VRC26D and VRC26K, but absent in VRC26M. Differences in sulfation had little impact on peptide dynamics (not shown). Differences in pepsin cleavage between VRC26M, D, and K prevented a direct comparison of peptide dynamics in the absence (VRC26M) and presence (VRC26D and K) of the additional disulfide bond.

Heatmaps indicating percent deuteration of peptides throughout the early, intermediate, and mature VRC26 revealed similar patterns of local stability throughout affinity maturation (Figure 3.4A). There were many similarities between VRC03 and VRC26, with regard to changes in conformational dynamics throughout affinity maturation. First, all of the measurable

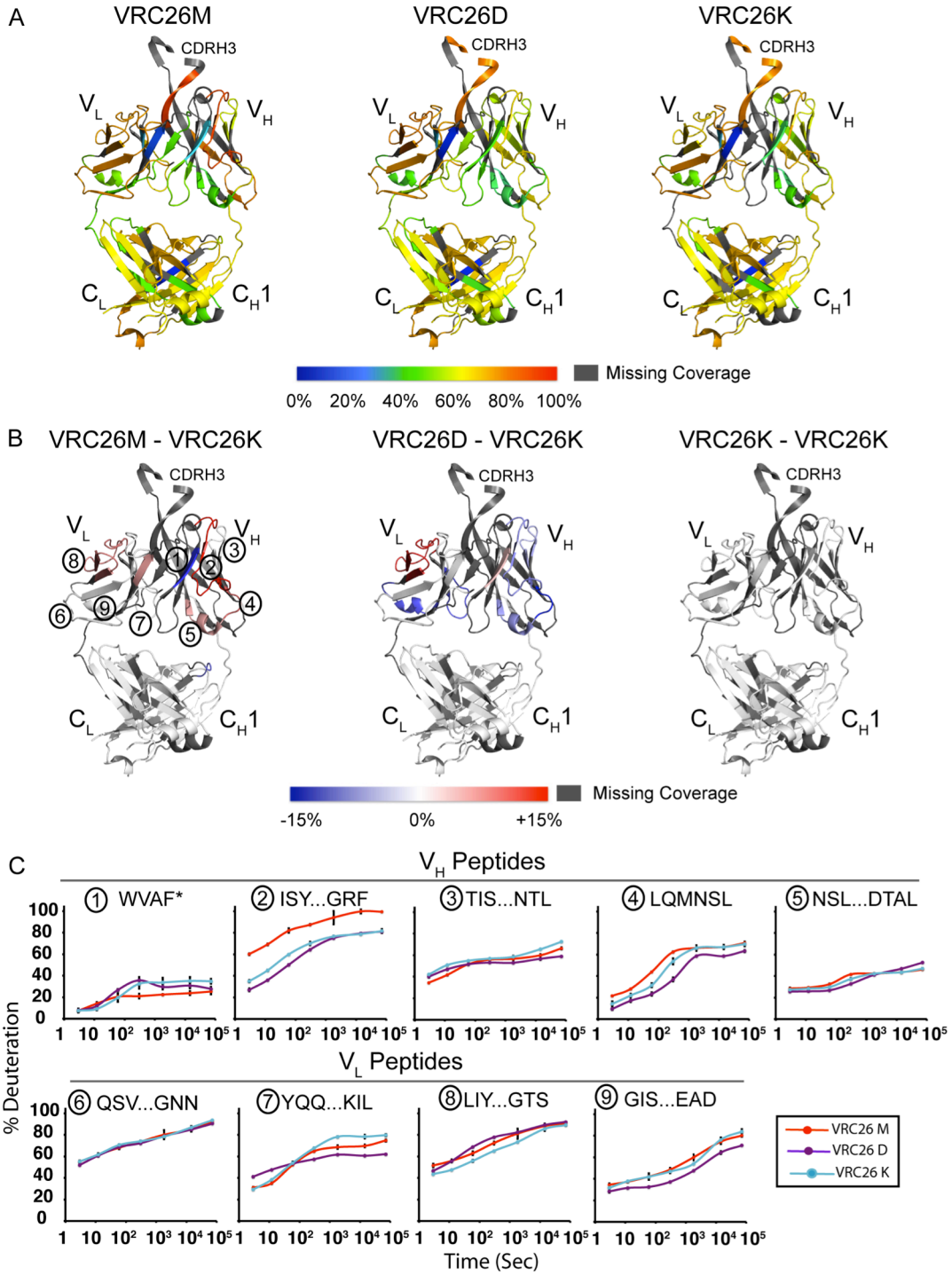

Figure 3.4. VRC26 Fab Deuteration Profiles. (A) Deuteration heatmaps: Colors mapped onto the VRC26-like Fab, PG9 structure (PDB 3U4E), indicate % deuteration of peptides after 5 minutes of incubation in D_2O. Gray indicates missing peptide coverage. **(B)** Difference heatmaps: colors mapped onto the PG9 Fab structure indicate the difference in deuterium uptake between early and mature (M-K, left), intermediate and mature (D-K, middle), and mature vs mature (K-K, right) after 5 minutes of incubation in D_2O. Red colors: more deuterated in the early/intermediate Fab relative to the mature Fab, blue colors: less deuterated in the early/intermediate Fab relative to the mature Fab; white: similar deuterium uptake, and gray: missing coverage. **(C)** Deuterium uptake plots show the % deuteration vs time for comparable variable domain peptides. Red lines: VRC26M (early), Purple lines: VRC26D (intermediate), and Blue lines: VRC26K (mature).

conformational differences between early, intermediate, and mature VRC26 Fabs were confined to the variable domains. Peptides from the constant regions were deuterated identically in all three Fabs (Figure 3.4B and 3.4C). In contrast, many - though not all - VH and VL peptides demonstrated substantial differences in deuterium uptake among the Fabs for which data was available. Second, as in VRC03, differences in conformational dynamics between early, intermediate, and late VRC26 appeared to vary in a site-specific manner. Some peptides demonstrated greater flexibility in the early Fab than in the mature, while others were more stable in the early Fab than in the mature VRC26K (Figure 3.4B and 3.4C).

Analyzing the intermediate VRC26D Fab conformational dynamics provided a unique opportunity to see whether changes in peptide flexibility from the early VRC26M to the mature VRC26K followed a monotonic path from flexible to stable. Contrary to expectations, many comparable peptides from V_H were observed to progress from being dynamic in VRC26M to stable in VRC26D to an intermediate stability in VRC26K (Peptides 2, 3, 4, 5, 7, and 9 in Figure 3.4B and 3.4C). However, a few peptides from V_L appeared to follow a different path in which the early and intermediate VRC26 showed high flexibility, and the mature VRC26K was substantially more stable (Peptide 8 in Figure 3.4B and 3.4C). Thus, as with the overall spatial trends of stabilization/destabilization observed from early to late VRC26, it seems that the conformational path to the mature Fab varies in a site-specific manner as well. However, there is a predominant trend from high, to low, to intermediate stability over the course of affinity maturation, which suggests that the antibody samples different levels of stability in order to identify an optimal level that facilitates efficient recognition of diverse foreign antigens.

Discussion

Here we attempted to address the question of whether Fab conformational dynamics evolves over the course of affinity maturation, in order to understand the role paratope flexibility may play in defining the affinity and specificity with which an antibody recognizes a foreign

antigen. To this end, we measured changes in the local stability of two distinct HIV-1 bNAb specificities over the course of affinity maturation. Our results suggest that the evolution of paratope stability does not occur in a uniform, unidirectional fashion, but rather appears to occur in a site-specific manner along a non-linear path in which paratope stability is optimized to maximize antigen recognition.

For both VRC03 and VRC26, a majority of comparable peptides were similarly or more dynamic in the germline/early Fab than in the mature Fab. There were a limited number of variable domain peptides that could be compared in VRC03 (n=4), so it is possible that with increased peptide coverage, this trend would change. However, of the 23 variable domain peptides in VRC26 that were comparable between the early VRC26M and a later Fab, 14 of them were similarly dynamic, and 5 were distinctly more dynamic in VRC26M. There were critical gaps in the data within the CDRH3 that prevented a comparison of VRC26M to other Fabs. Additionally, differences in peptide amino acid sequences could conceivably contribute to observed differences in rates of deuterium uptake. Therefore, it will be valuable to explicitly test the impact of amino acid sequence on the intrinsic rates of HDX, by comparing the observed rates to theoretical rates of deuterium uptake for each peptide sequence. Overall, these data support previous observations from model systems that early/germline antibodies are relatively dynamic as compared to their mature descendants (322). As in other protein-ligand systems, the increased flexibility of early/germline antibodies may favor increased polyreactivity (327), which been proposed for germline antibodies based on in silico analyses (323). However, it has yet to be explicitly demonstrated that predicted germline bNAb precursors are more promiscuous binders than mature bNAbs. In light of our work, if flexibility is associated with polyreactivity, we would expect the predicted germline/early sequences of VRC03 and VRC26 to be more polyreactive than the mature antibody sequences.

The results from VRC26, for which we were able to measure the stability of an intermediate Fab, suggest that there may be an increase in conformational dynamics for many

Fab peptides in the mature antibody relative to the intermediate VRC26D. We currently do not know when VRC26 developed its broadly neutralizing activity or whether the increase in flexibility between VRC26D and VRC26K correlated with a change from isolate-specific to broad neutralization activity. Previous work from Klein et al. identified a destabilizing A61P mutation in the framework region of bNAb 3BNC60, which disrupted a beta sheet and decreased the melting temperature of the Fab but increased the breadth and potency of 3BNC60 neutralization (163). Thus, it is possible that bNAbs may be uniquely dynamic relative to other mature antibody specificities, and that the increased flexibility of bNAbs contributes to their breadth of antigen binding. It will be valuable in future work to study the changes in antibody flexibility during the transition from isolate-specific to broadly-neutralizing activity. It would also be informative to explore differences in stabilization associated with antigen binding over the course of affinity maturation.

Overall, this work supports previous observations that germline/early antibodies are more conformationally dynamic than mature antibodies. It remains unclear whether this flexibility contributes to germline BCR polyreactivity or whether increased flexibility and/or polyreactivity is inversely associated with affinity for Env immunogens. The identification of a successful antibody-based vaccine against HIV-1 will require potent stimulation of germline B cells for subsequent affinity maturation into broadly neutralizing antibody specificities. This work provides an understanding of changes in antibody stability over the course of affinity maturation, and the biophysical factors that should be considered in rationally designing an optimal vaccine to stimulate the development of broadly neutralizing antibodies from germline precursor B cells.

Acknowledgements:

We would like to thank Jason Gorman, Gordon Joyce, Peter Kwong, and John Mascola of the VRC, NIAID, NIH for their very generous contribution of the Fabs studied in these experiments.

Chapter 4

Discussion and Conclusions

The design of an effective antibody-based vaccine will depend on the identification of immunogens that can bind BCR with high affinity and stimulate the development of long lived plasma cells and memory B cells expressing antibodies with broad neutralizing activity. In the work presented here, I have attempted to understand the molecular factors that hinder and enhance antibody binding to soluble Env immunogens. In chapter 1, I tested the impact of glycosylation, cleavage of gp160 into gp120 and gp41, and oligomerization state on soluble gp140 Env immunogen recognition by the newly discovered broadly neutralizing antibodies PG9 and PG16. More recently, I tested the role that gp120 (chapter 2) and antibody (chapter 3) conformational dynamics may play in modifying Env – antibody interactions. In the context of recent work from other groups, these findings suggest novel avenues for future research, which will ideally inform the design of enhanced immunogens to better guide B cell development toward desired bNAb specificities.

The Glycan-Dependent Quaternary Epitope Recognized by mAbs PG9 and PG16:

Our understanding of the epitope recognized by the antibodies PG9 and PG16 has improved dramatically in recent years. The results in chapter 1 revealed that the epitope targeted by PG9 is efficiently presented in the context of monomeric gp140 proteins, while PG16 exhibited greater specificity for the native Env trimer. The results for PG9 suggested that the antibodies do not absolutely require that the epitope be presented by the native trimer, although they may recognize it preferentially in that context. Indeed, subsequent x-ray

crystallography studies identified minimal scaffold proteins containing glycosylated V1/V2 loops that are capable of binding efficiently to PG9 and PG16 (132, 328). This work revealed intimate contacts between the long CDR3 loop of PG9 with a conserved beta sheet structure and glycans in the V2 loop. Both PG9 and PG16 make contact with a Man5GlcNAc2 glycan at position N160, but the antibodies differ in their recognition of a second glycan: PG9 appears to preferentially bind a high mannose glycan at position N156, whereas PG16 preferentially recognizes a complex-type, sialylated glycan at position N173 (132, 328). The N156 and N173 glycans are described as "spatially equivalent" because although they occur at different positions in the primary sequence, the glycans occupy similar positions in the three dimensional structure, which satisfy similar requirements for PG9 and PG16 binding. Although PG9 may be capable of recognizing complex-type glycans in the N156/N173 position as well, mutations in the PG16 light chain appear to favor efficient recognition of sialylated glycans (132). From these data and the data in chapter 1, it seems that certain Env isolates are naturally capable of binding to PG9 and PG16 with high affinity, even as gp120 or minimal scaffold proteins.

Additionally, recent structural work provides insight into the mechanism by which PG9 and PG16 achieve broad neutralization in spite of their recognition of the highly variable V2 loop. Breadth of neutralization appears to be accomplished by targeting a conserved glycan-peptide-glycan epitope, in which glycan structures are limited to a relatively small number of possible patterns as defined by host-cell glycosylation machinery, and where peptide interactions are mediated by many sequence-independent contacts involving backbone hydrogen bonds between the PG9/PG16 CDRH3 and a structurally-conserved beta sheet in V2 (132, 328). Recent work indicates that the V2 epitope targeted by PG9/PG16 is likely to be structurally heterogenous (66). This suggests that the beta-sheet conformation observed in crystal structures may be induced by PG9/PG16 binding. However, it is also possible that the V1/V2 loops may be stabilized in a beta-sheet structure, similar to that observed in the V1/V2 scaffolds, by quaternary contacts in the context of the native trimer. Trimer-dependent

stabilization of V1/V2 secondary structure may contribute to the quaternary "preference" of PG9 and PG16. Furthermore, the structural variability of the V2 loop may explain why certain isolates are naturally well-suited to interaction with PG9/PG16 even in the context of gp120 proteins, as these isolates may possess inherently stable V2 beta-sheet structures.

An alternative or complementary explanation for the "quaternary preference" of PG9 and PG16 is that the antibodies recognize an epitope that is made up of more than Env subunit. Data presented in chapter 1 and the initial description of PG9 and PG16 suggested that this was an unlikely explanation, however recent work suggests that these observations were likely based on experimental artifacts. For example, monomeric gp140 proteins bound to PG9/PG16 even better than trimeric gp140s in chapter 1, but these trimeric gp140 constructs were recently shown to be disulfide-linked oligomers, rather than trimers (141). Nevertheless, the PG9/PG16 epitope was sufficiently presented within monomeric gp140 proteins to be efficiently bound by PG9 and PG16. Similarly, in the initial description of PG9 and PG16, the authors used a mixed trimer experiment in which they transfected cells with different ratios of wild-type gp160 and a gp160 N160A mutant that could not bind PG9/PG16 (30). It is important to note that this assumes that that the quaternary preference of these antibodies is due to bivalent recognition of two independent, identical epitopes involving N160. These mixed-trimer experiments could not address the increasingly likely model that PG9/PG16 bind in a monovalent fashion to the N160 glycan from one protomer and other non-N160 elements from an adjacent protomer. Indeed, data from chapter 1 demonstrated that the quaternary preference of PG9/PG16 was unlikely to be explained by bivalent antibody binding to two separate protomers.

The hypothesis that PG9 and PG16 recognize a complex epitope composed of elements from at least two adjacent subunits is supported by recent electron microscopy and small-angle x-ray scattering experiments. This work showed that PG9 binds to the crown of soluble trimeric Env constructs, with one F(ab) molecule bound at the three-fold axis of each trimer (198, 329). These low-resolution structural experiments do not definitively demonstrate interactions

between PG9 and elements from multiple protomers, but such interactions are very likely given that the variable loops from the three protomers are thought to converge within crown of the Env trimer (19). And while a single protomer may achieve many of the contacts required for successful binding of PG9/PG16, as has been demonstrated by multiple, independent studies (132, 133, 328, 330), including this one, it seems likely that additional contacts are satisfied in the context of the trimer that make PG9/PG16 binding even more efficient. The molecular explanation for the quaternary epitope preference of PG9/PG16 is not fully resolved and the specific details of this interaction may, in fact, vary among isolates. The work presented in chapter 1 and recently published data have helped to clarify the nature of the PG9/PG16 epitope, which has provided valuable insight into mechanisms of broad neutralization, molecular features of the "native" Env trimer, and desirable features of future Env immunogens.

The Authenticity of gp140 Trimers:

The existence of PG9/PG16 - antibodies that are capable of neutralizing diverse HIV-1 Env isolates, but which bind poorly to most soluble Env trimers - provides important evidence that most soluble Env immunogens do not accurately recapitulate the structure of the native, virion-associated Env trimer. Importantly, PG9-like antibodies with distinct specificities have now been isolated from a number of donors (29, 30, 154, 324). The existence of multiple quaternary antibody specificities from a number of individuals suggests that the quaternary epitope is frequently immunogenic and a relevant target for vaccine design.

In chapter 1, I observed that PG9 and PG16 bound well to uncleaved monomeric gp140 proteins but bound relatively poorly to oligomeric gp140. This was an unexpected finding in light of the reported quaternary preference of PG9/PG16. As discussed above, recent work has provided a possible explanation for the poor reactivity of PG9/PG16 with oligomeric gp140. Using SAXS and dynamic and static light scattering (DLS and SLS) Guttman et al. observed that many oligomeric gp140 proteins that are commonly assumed to be trimeric (including the

gp140 constructs used in chapter 1) are likely to be dimeric (141). Notably, these gp140 oligomers resembled aberrant, disulfide linked gp120 dimers as measured by HDX-MS (141). Work from other groups has shown that the gp120 dimer interface likely involves the gp120 N/C-termini and the V2 loop (139). Thus, given the similarities observed between gp120 dimers and gp140 oligomers, it is likely that the gp140 oligomers that were assumed to be trimeric, were likely to be dimeric, and that the PG9/PG16 epitope within the V2 loop may have been poorly accessible within the dimer interface. It is understandable, then, that PG9 would bind poorly to oligomeric gp140 constructs relative to monomeric gp140 proteins.

Recent work surrounding PG9 and PG16 has also provided insight into questions surrounding the "true" glycosylation pattern of HIV-1 Env. It has been proposed that our lack of success in designing an effective antibody-based HIV-1 vaccine is due, in part, to the fact that Env immunogens may not accurately reproduce the "true" glycosylation pattern observed on HIV-1 Env (131, 133, 134, 331). Earlier reports suggested that native Env trimers on the surface of infectious virions possessed high-mannose glycans exclusively (131). However, given the preference of PG16 for complex-type glycans observed by crystallography (132), it appears that an antibody elicited over the course of a natural infection matured to efficiently target sialylated glycans on Env. This suggests that although the majority of glycans on native Env may be high-mannose, at least a few critical residues are processed into complex-type sugars.

PG9 and PG16 have demonstrated themselves to be valuable reagents for testing the authenticity of Env immunogens (198). However, equating PG9/PG16 binding with the presence of a native Env trimer is certainly flawed, given that we and others have observed efficient PG9/PG16 binding to non-native and non-trimeric constructs (132, 328, 330). Quaternary-epitope "specific" antibody binding studies will facilitate the identification of improved gp140 Env immunogens, however PG9 is not sufficiently specific for the native trimer to make it a definitive test of the native-like structure. Other V2-directed antibodies appear to be truly

specific for the native Env trimer (for example, mAb 2909) and may be useful reagents for characterizing candidate Env immunogens (29). In future work, it will be valuable to understand differences and similarities in the detailed epitopes recognized by 2909-like antibodies and PG9/PG16, as this will clarify the nature of the quaternary epitope. In combination with biophysical techniques to characterize gp140 trimer shape, size, stability, and structure, 2909- and PG9-like antibodies will facilitate the identification of soluble, trimeric Env immunogens that effectively recapitulate the structure and antigenicity of the native Env trimer.

Conformational Stability in Immunogen Design:

Two biophysical techniques have proven to be valuable for studying unmodified gp120 and gp140 proteins: HDX-MS and SAXS. These techniques were used in chapter 2 to identify conformational differences among diverse gp120 proteins that may modify gp120-antibody interactions. The differences in stability and antigenicity observed in chapter 2 were largely confined to the gp120 inner domain. Recent work has shown that this region is stabilized in the context of gp140 monomers, likely due to interactions with gp41 (141). In light of this, it is possible that isolate-specific inner domain conformational differences would be less dramatic in the context of gp140 trimers, due to stabilization at the gp120-gp41 interface. Conversely, interactions between variable loops are likely to be critical in proper trimer formation (33, 192). Whereas the variable loops were highly dynamic in the context of gp120, becoming saturated with deuterium at the earliest time point, it is that the loops will be more structured in the context of the gp140 trimer. This may allow subtle differences in variable loop structure to be measured in gp140 trimers that could not be observed in the context of monomeric gp120. In order to address whether changes in conformational dynamics mediate viral escape from neutralizing antibody specificities, it will be critical to extend our studies to diverse trimeric Env constructs in future work.

A number of previous studies have attempted to understand the relationship between flexibility and antigenicity (309, 332, 333). In general, flexible regions of a protein are observed to be more antigenic; however, the association is confounded because surface-exposed loops, which are accessible to antibody binding, are often more dynamic than stable peptide segments within the protein core, which would be poorly accessible and poorly antigenic. In addition, most previous work has focused on the antigenicity of differentially-stabilized linear epitopes. The results presented in chapter 2 suggest that dynamics may have a larger impact on antibody binding to conformational epitopes than to linear epitopes. The role of conformational dynamics in modifying protein immunogenicity has only begun to be examined (334), likely due to the dearth of techniques to easily measure this aspect of protein structure. The role of stability in Env immunogenicity was previously tested using cavity-filled, disulfide-stabilized gp120 core proteins by Dey and colleagues, who observed that stabilized core constructs elicited better antibody responses to the co-receptor binding site (314). Because most HIV-1 bNAbs target conformational epitopes on gp120, it is of exceptional relevance to better understand the relationship between structural dynamics and the immunogenicity of conformational epitopes.

The 1157ip gp120 described in chapter 2 may prove to be a valuable reagent to further test the role of dynamics in modifying immunogenicity. In chapter 2, we identified 1157ip as a uniquely dynamic gp120 protein, and we observed that it was poorly recognized by antibodies targeting conformational epitopes. However, it is well established that antigenicity does not predict immunogenicity, and it remains to be determined if the 1157ip gp120 has a distinct immunogenic profile relative to more stable gp120 proteins. In future work, it will be informative to identify the residues responsible for the relative disorder of 1157ip. This would make it possible to compare the immunogenicity of the wild-type and stabilized 1157ip gp120 proteins. I would hypothesize that the stabilized 1157ip gp120 would elicit better antibody responses to conformational epitopes in the gp120 inner domain. The wild-type and stabilized 1157ip gp120 proteins would also make it possible to test whether disorder influences the ability of ADCC-

active antibodies to activate cell-killing. Additionally, these two reagents may be useful in antibody depletion experiments to screen for inner-domain specific, conformation-dependent antibodies similar to A32 in plasma from infected individuals, in a manner analogous to the D368R mutant that has facilitated the identification of individuals with CD4-binding site-directed antibodies (335). Differentially-stabilized gp120s with minimal sequence differences would be valuable reagents for answering a number of important questions in HIV-1 vaccine design, and the identification of 1157ip gp120 as being uniquely disordered in solution provides a critical starting point to begin developing such reagents.

Dynamics and Evolvability of HIV-1 Env:

Protein stability has been linked with increased evolvability – increased potential for evolution – as a result of an increased tolerance for destabilizing mutations on the evolutionary path towards new protein sequences, specificities, or functions (336-338). Because rapid evolution is a central component of the immune evasion strategy of HIV-1 Env, understanding the factors that facilitate diversification may provide insight into the limitations of this process and potential targets for intervention. In future work, it would be valuable to study the conformational stability of native, virion-associated Env constructs, using HDX-MS, for example, to test the role of stability in facilitating Env evolution. Other techniques, such as single-molecule fluorescence resonance energy transfer, with site-specific labeling, may also provide useful information about frequency of conformational fluctuations in the quaternary structure of the Env trimer as a separate measure of trimer stability (339).

There is a critical difference between the evolvability of Env and the evolvability of other proteins from previous studies: Env evolution occurs in the presence of neutralizing antibodies. In this context, protein stability may be unfavorable for protein evolvability, as it may facilitate nAb binding and neutralization and would thus reduce Env fitness. An alternative technique by which a protein may tolerate extensive mutagenesis is through disorder. Highly flexible,

disordered loops can tolerate mutagenesis because the altered residues do not participate in bonding networks that are critical for protein stability (340). Furthermore, in light of data from chapter 2, dynamic regions may be poorly recognized by antibodies, which would be beneficial for Env fitness and facilitate Env evolution in the unfriendly environment of a humoral immune response. The numerous disulfide bonds in gp120 may also contribute to the Env evolvability – providing a degree of baseline stability and maintaining a core structure, while allowing the loops of gp120 to sample a wide variety of sequences and structures. Glycosylation provides an alternative mechanism of immune evasion by limiting antibody access, and may also contribute to the evolvability of HIV-1 Env. Thus it is unclear what molecular features – stability, flexibility, disulfide bonding, glycosylation, etc. – contribute to the high degree of evolvability in HIV-1 Env. Experimental evolution of differentially stabilized or differentially glycosylated Env trimers is a rich avenue for future investigation, which may reveal targets for novel inhibitors to limit the ease of HIV-1 escape from humoral immunity.

Protein Dynamics and Binding Specificity:

We observed in chapter 3 that antibody conformational dynamics changes throughout affinity maturation. In light of previous work in other systems, which showed that protein stability increases ligand binding specificity (327, 341), we hypothesized that germline antibodies would be measurably more flexible than mature antibodies in order to maximize the likelihood of binding to diverse foreign antigens. In contrast, we reasoned that mature antibodies may be more structured, as they have "differentiated" and become optimized for binding to a specific antigen (319, 322). However, the data suggests that it is not a linear path from a highly dynamic germline antibody to a stable mature antibody. This may be due to the fact that the antibodies studied in chapter 3 are broadly neutralizing antibodies, which have not been optimized for binding to a single antigen, but a diverse array of circulating Env isolates. It raises the question of whether broadly neutralizing antibodies such as VRC03 and VRC26 are exceptionally

dynamic relative to other mature antibodies. To address this question, it would be informative to measure the conformational dynamics of antibody intermediates on the pathway to the development of bNAb specificity. One could compare an antibody intermediate with isolate specific neutralizing activity to the mature bNAb to see whether the bNAb has increased its promiscuity by acquiring mutations that increase flexibility. Alternatively, it may be informative to compare the conformational flexibility of mature antibodies of differing breadth. To minimize confounding sequence changes, this comparison would ideally be limited to antibodies derived from the same germline gene segments. Understanding conformational features of both germline and mature broadly neutralizing antibodies would be valuable to address basic questions in immunology and biochemistry, and it would ideally facilitate the design of improved immunogens to guide B cell development.

Future Directions for HIV-1 Vaccine Design:

There are currently many Env immunogens that have been designed to effectively present bNAb epitopes and to bind to these antibodies with high affinity. Our work suggests that there is some potential to improve upon these immunogens through addition of glycans, screening and elimination of non-native soluble Env trimers, directed stabilization, among other methods. However, these immunogens will be ineffective, unless they are designed to activate the naïve human immune system to develop a broadly neutralizing response. Such work as this is currently underway by Peter Kwong and others, who have proposed using a sequential immunization strategy, to mimic the viral evolution that may have guided the humoral immune system towards the development of broadly neutralizing antibodies in an HIV-1 infected individual (165, 321). Along these lines, other groups are designing immunogens to bind germline BCR of broadly neutralizing antibodies (320, 342). We have dramatically improved our understanding of factors governing macromolecular interactions and methods to rationally manipulate these interactions (343). The next, most critical step, towards the development of an

effective HIV-1 vaccine will be to learn how to tailor these macromolecular interactions to effectively communicate with the human immune system.

Summary and Conclusions:

Overall, this work reveals the importance of subtle structural modifications in regulating interactions between antibodies and soluble Env immunogens. The identification of these modifications opens potential paths towards the design of enhanced Env immunogens and provides insight into feasible methods of characterizing the authenticity of existing immunogens. In particular, the observation that naturally-occurring differences in the stability of gp120 proteins may contribute to antigenic differences provides novel evidence that HIV-1 may use conformational dynamics to evade humoral immunity. This work demonstrates the importance of complementary studies of Env immunogen dynamics in addition to classical, high-resolution techniques that provide static structural information. Critically, it suggests novel methods of manipulating immunogen antigenicity, and perhaps immunogenicity, through targeted stabilization or destabilization. The design of an effective HIV-1 vaccine will require a coordinated effort from disparate scientific fields, and in the end, time will continue to prove that we are indeed a global community, and the life of that first person infected with HIV-1 group M will have been directly linked not only to those 70 million people who have since become infected, but also to the global community of researchers and health workers who will be required to successfully halt the HIV-1 pandemic.

Appendix A:

Chapter 1 Supplementary Information

Table A.S1. SPR methods for PG9, PG16 and 447-52D Fab binding to amine- coupled gp140.

gp140	Immobilization of gp140 (Ligand)			Fab (Analyte)				
	Conc (μg/mL)	Buffer	Immobilized Level (RU)	Fab	Concentration (nM)	Injection Time (s)	Dissociation Time (s)	Maximum Observed Response (RU)
Q168a2 monomer	10	10 mM sodium acetate, pH 5.0	1673	**PG9**	1000, 500, 250, 125, 62.5, 31.2, 15.6	420	1200	45
				PG16	2000, 1000, 500, 250, 125, 62.5, 31.2, 15.6	420	420	28
				447-52D	500, 250, 125, 62.5, 31.2, 15.6, 7.8	420	420	60
Q168a2 trimer	10	10 mM sodium acetate, pH 5.5	3270	**PG9**	1000, 500, 250, 125, 62.5, 31.2, 15.6	420	1200	37
				PG16	2000, 1000, 500, 250, 125, 62.5	420	420	23
				447-52D	1000, 500, 250, 125, 62.5, 31.2, 15.6, 7.8	420	420	350
Q259d2.17 monomer	30	10 mM sodium acetate, pH 4.7	1670	**PG9**	1000, 500, 250, 125, 62.5, 31.2, 15.6	420	1200	40
				PG16	1000, 500, 250, 125, 62.5, 31.2, 15.6	300	420	9
				447-52D	1000, 500, 250, 125, 62.5, 31.2, 15.6	300	420	170
Q259d2.17 trimer	10	10 mM sodium acetate, pH 5.0	3099	**PG9**	1000, 500, 250, 125, 62.5, 31.2, 15.6, 7.8	420	1200	9
				PG16	2000, 1000, 500, 250, 125, 62.5, 31.2, 15.6	420	420	6
				447-52D	1000, 500, 250, 125, 62.5, 31.2, 15.6, 7.8	420	420	430
Q461e2 trimer	10	10 mM sodium acetate, pH 5.0	2588	**PG9**	1000, 500, 250, 125, 62.5, 31.2	420	420	23
				PG16	2000	420	420	8
				447-52D	1000, 500, 250, 125, 62.5, 31.2, 15.6, 7.8	420	420	240
Q769h5 monomer	20	10 mM sodium acetate, pH 5.0	1342	**PG9**	1000, 500, 250, 125, 62.5, 31.2, 15.6, 7.8	420	1200	5
				PG16	1000, 500, 250, 125, 62.5, 31.2, 15.6, 7.8	420	600	2
				447-52D	500	420	1200	70
Q769h5 trimer	10	10 mM sodium acetate, pH 5.0	3078	**PG9**	1000, 500, 250, 125, 62.5, 31.2, 15.6, 7.8	420	1200	8
				PG16	2000, 1000, 500, 250, 125, 62.5, 31.2, 15.6	420	420	3
				447-52D	1000, 500, 250, 125, 62.5, 31.2, 15.6, 7.8	420	420	205
SF162 K160N monomer	50	10 mM sodium acetate, pH 5.0	1707	**PG9**	1000, 500, 250, 125, 62.5, 31.2 and 15.6	420	600	115
				PG16	1000, 500, 250, 125, 62.5, 31.2 and 15.6	300	300	68
				447-52D	ND			
SF162 K160N trimer	50	10 mM sodium acetate, pH 5.0	3132	**PG9**	1000, 500, 250, 125, 62.5, 31.2 and 15.6	420	600	100
				PG16	1000, 500, 250, 125, 62.5, 31.2 and 15.6	300	300	60
				447-52D	ND			
SF162 trimer	30	10 mM sodium acetate, pH 5.0	3166	**PG9**	1000, 500, 250, 125, 62.5, 31.2 and 15.6	420	1200	1
				PG16	1000, 500, 250, 125, 62.5, 31.2 and 15.6	300	420	1
				447-52D	1000, 500, 250, 125, 62.5, 31.2 and 15.6	300	420	870

Figure A.S1. Characterization of purified Env gp140 proteins

(A) SDS PAGE

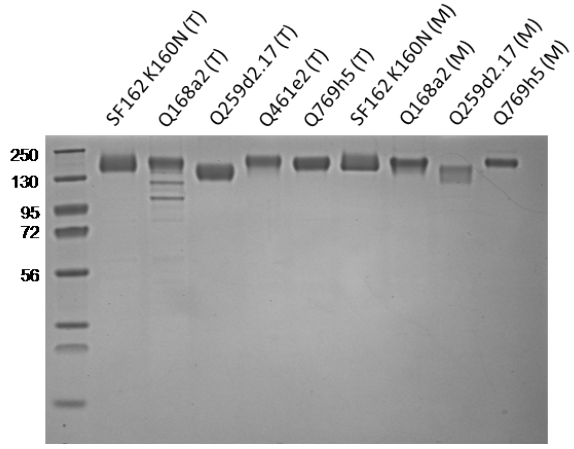

SimplyBlue-stained SDS 4-12% PAGE gel of the indicated purified Env proteins used. 2 µg/lane

B) Analytical SEC

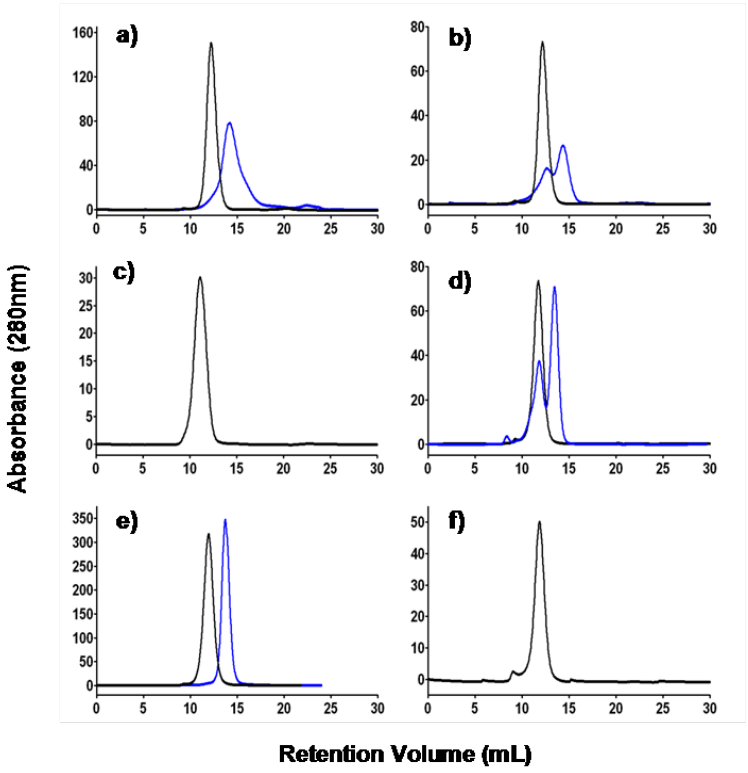

80-420 µg of Env was loaded on a SEC and a flow rate of 1 mL/min, in 1X PBS. Individual monomer and trimer peaks overlaid to show resolution. a) Q168a2, b) Q259d2.17, c) Q461e2, d) Q769h5, e) SF162 K160N, f) SF162 wt. Black: Trimeric gp140; blue: Monomeric gp140

Appendix B:

Chapter 2 Supplementary Information

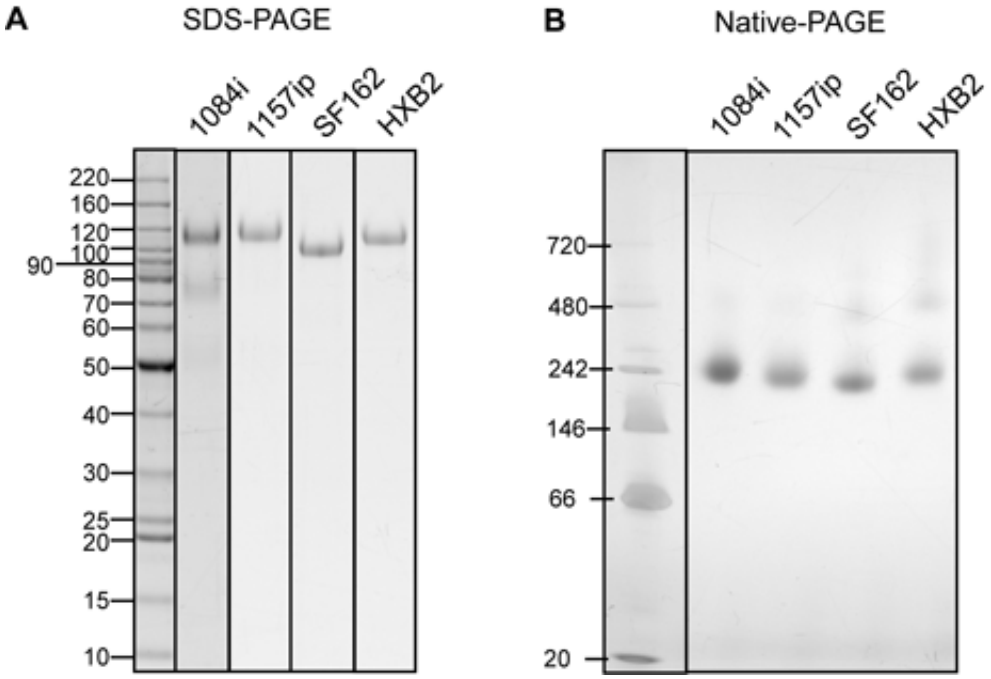

Figure B.S1. SDS- and Native-PAGE analysis of purified gp120 proteins. (A) SDS-PAGE analysis of purified gp120 proteins. (B) Blue Native-PAGE analysis of purified monomeric gp120.

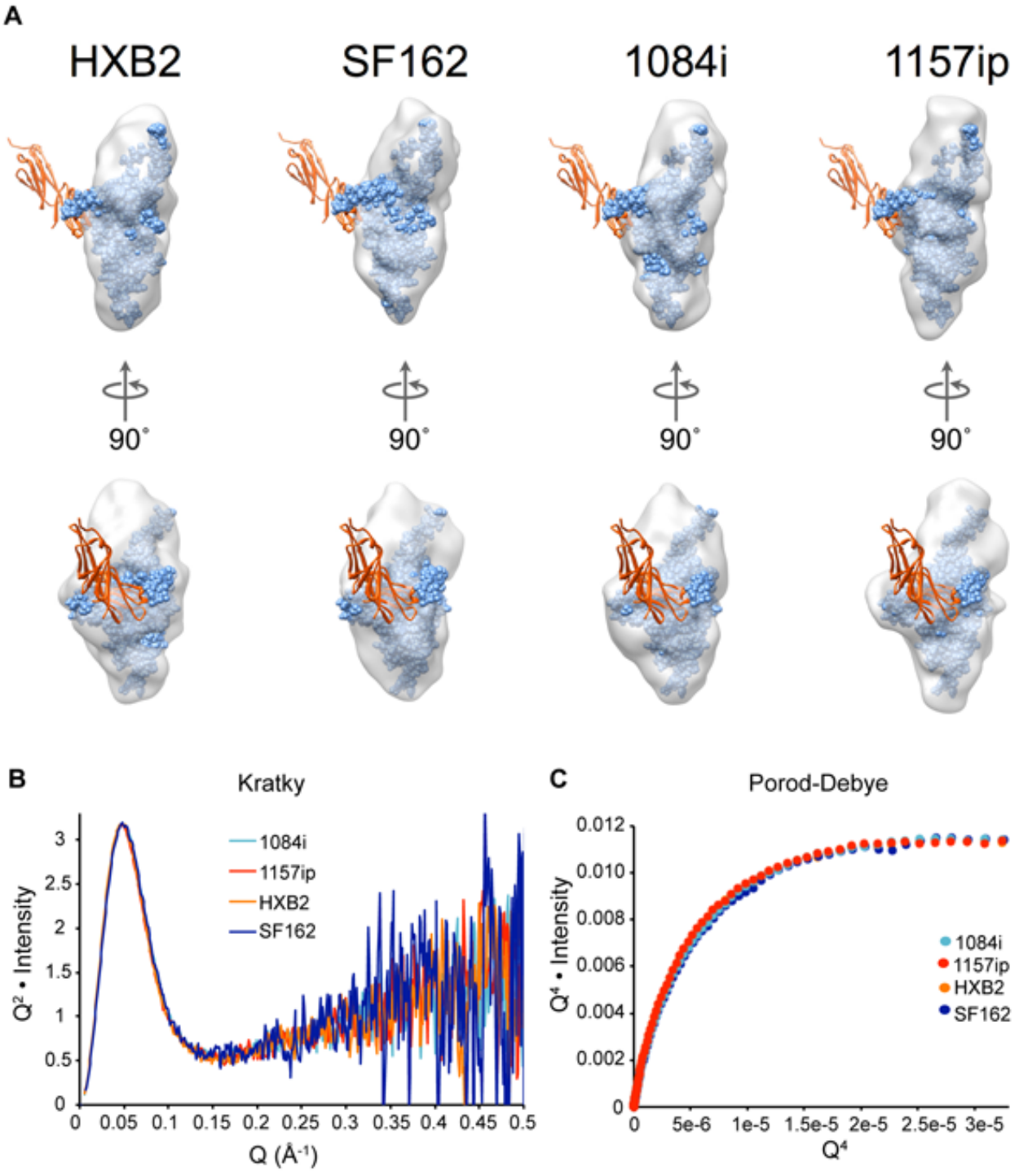

Figure B.S2. SAXS reconstruction, Kratky plot, and Porod-Debye analysis of SAXS data. **(A)** DAMMIN reconstructions of the four full-length gp120 monomers (gray density) overlayed with a space-filling model of the gp120 core (3JWD) (35) including the V3 loop from (2B4C) (187) (blue spheres) (B) Kratky and (C) Porod-Debye analysis of SAXS data. Each isolate is represented by a different color, as shown in the legend. The data are superimposable for all for gp120s, indicating similar degrees of globular structure.

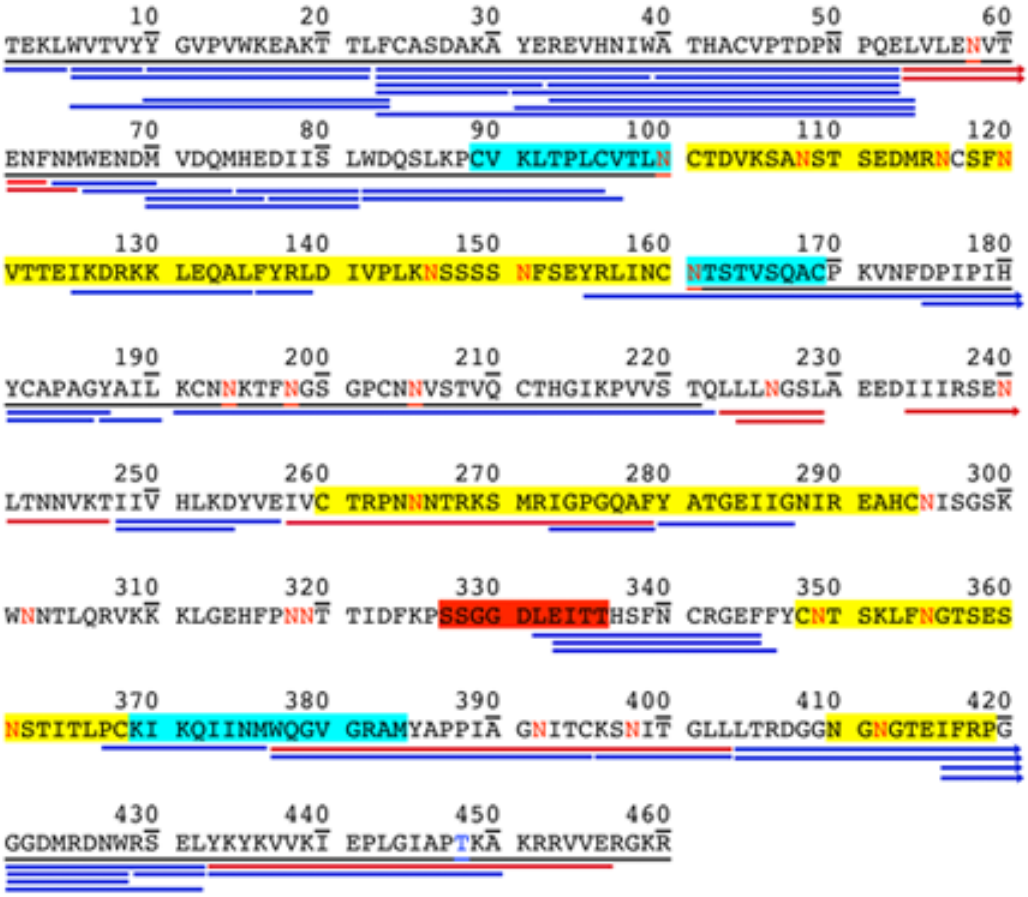

Figure B.S3. Pepsin digestion map for 1084i gp120. The mature 1084i gp120 amino sequence is indicated (with numbering based on mature 1084i). Inner domain elements are underlined (thin black line), variable loops are indicated in yellow, bridging sheet elements highlighted in cyan, and CD4 binding loop in red. Red text indicates sites of PNGS, blue text indicates O-linked glycosylation site. Blue and red lines beneath the sequence indicate peptides and glycopeptides, respectively, that are observable in HDX-MS analysis.

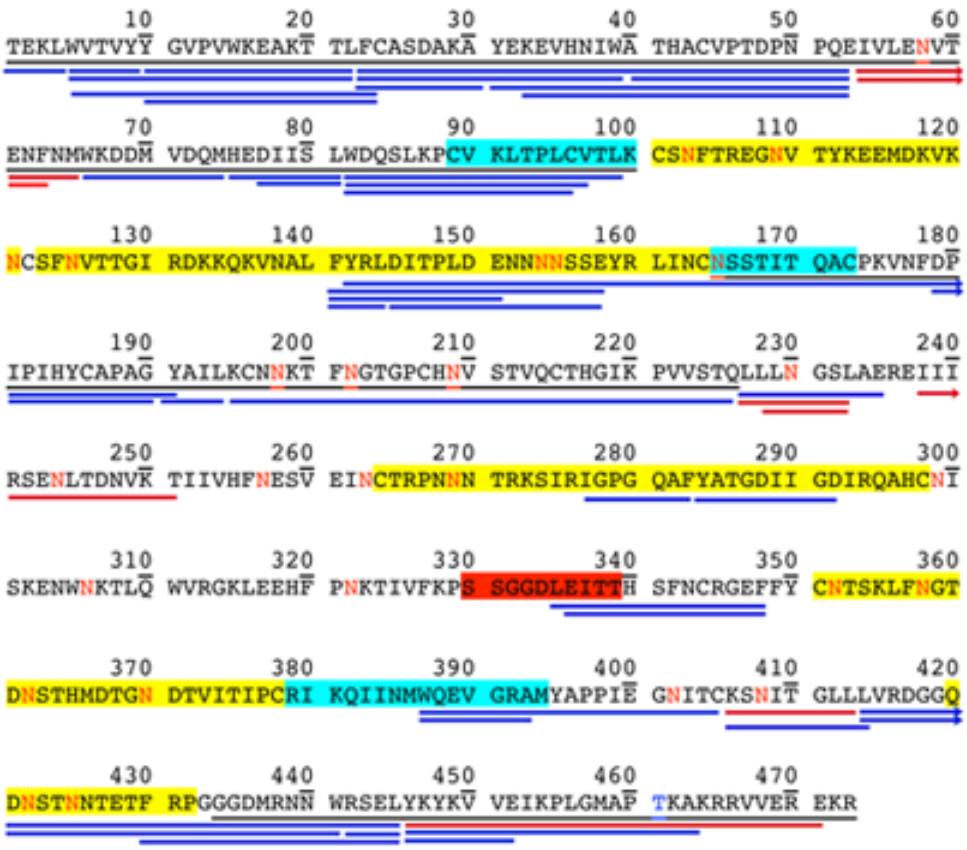

Figure B.S4. Pepsin digestion map for 1157ip gp120. The mature 1157ip gp120 amino sequence is indicated (with numbering based on mature 1157ip). Inner domain elements are underlined (thin black line), variable loops are indicated in yellow, bridging sheet elements highlighted in cyan, and CD4 binding loop in red. Red text indicates sites of PNGS, blue text indicates O-linked glycosylation site. Blue and red lines beneath the sequence indicate peptides and glycopeptides, respectively, that are observable in HDX-MS analysis.

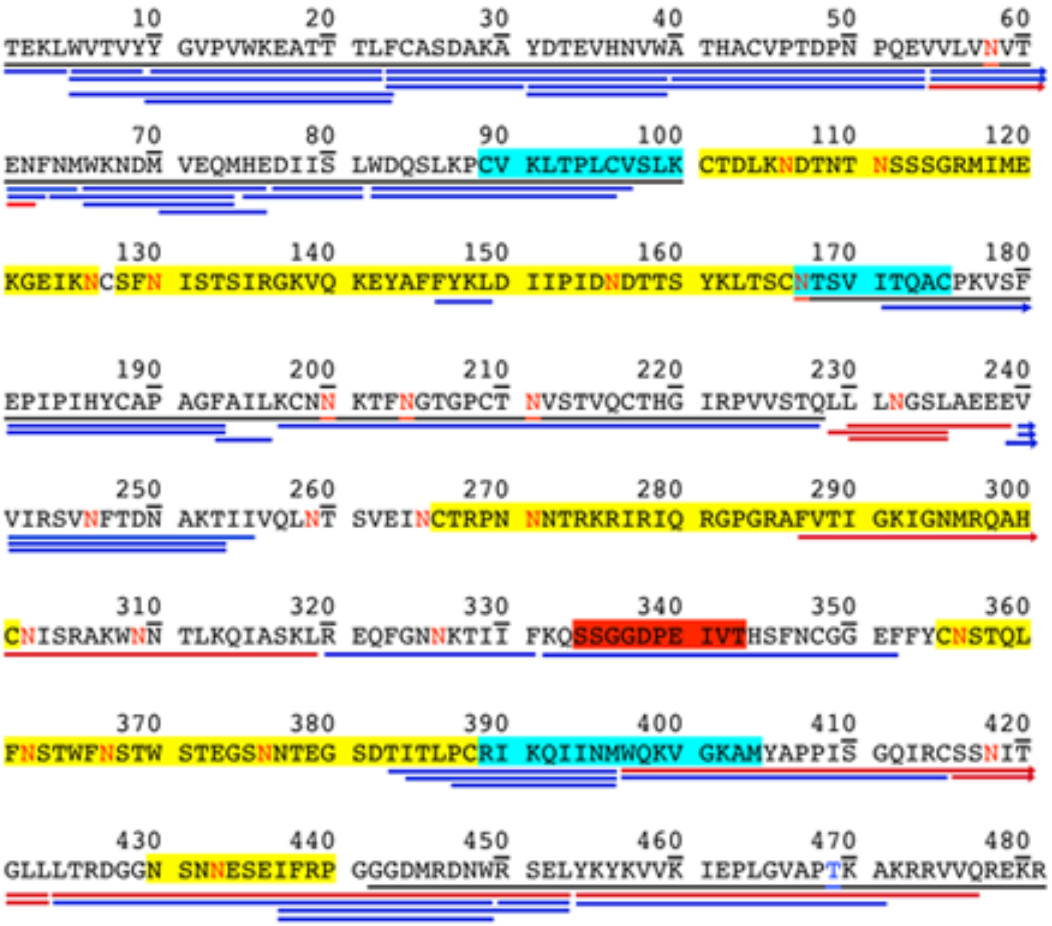

Figure B.S5. Pepsin digestion map for HXB2 gp120. The mature HXB2 gp120 amino sequence is indicated (with numbering based on mature HXB2). Inner domain elements are underlined (thin black line), variable loops are indicated in yellow, bridging sheet elements highlighted in cyan, and CD4 binding loop in red. Red text indicates sites of PNGS, blue text indicates O-linked glycosylation site. Blue and red lines beneath the sequence indicate peptides and glycopeptides, respectively, that are observable in HDX-MS analysis.

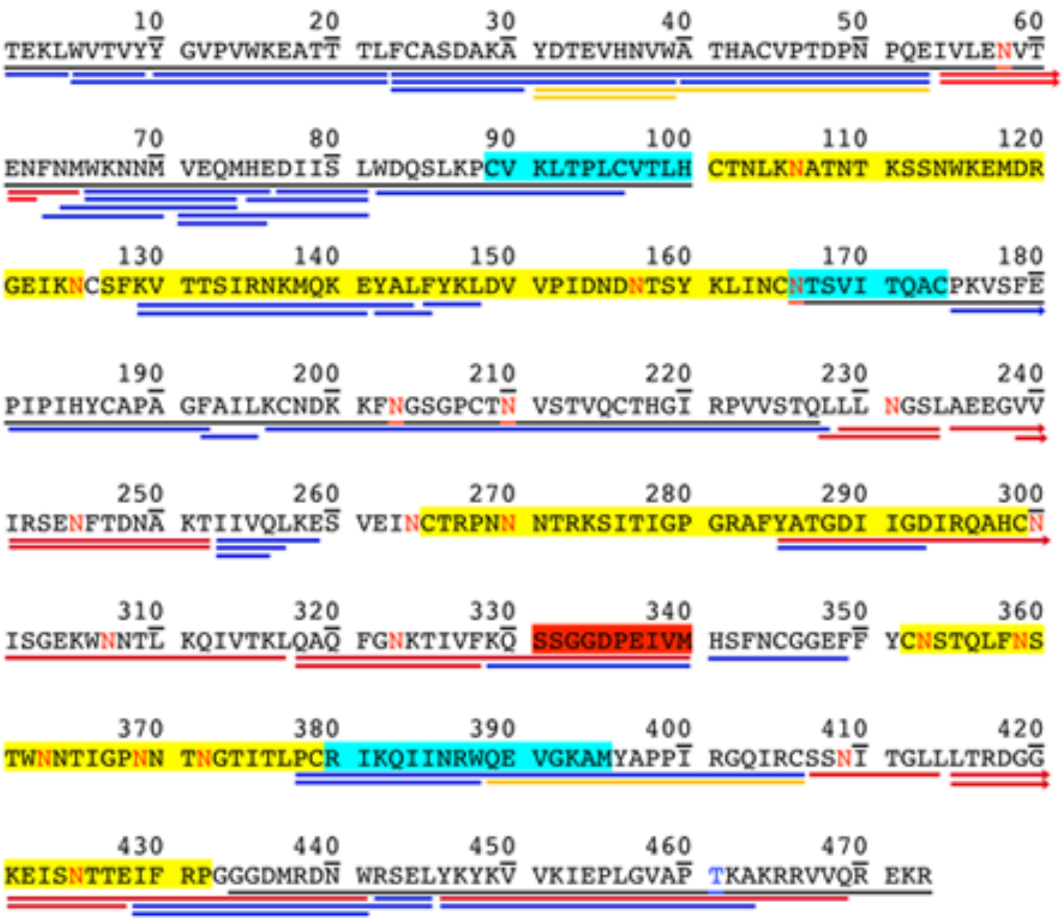

Figure B.S6. Pepsin digestion map for SF162 gp120. The mature SF162 gp120 amino sequence is indicated (with numbering based on mature SF162). Inner domain elements are underlined (thin black line), variable loops are indicated in yellow, bridging sheet elements highlighted in cyan, and CD4 binding loop in red. Red text indicates sites of PNGS, blue text indicates O-linked glycosylation site. Blue and red lines beneath the sequence indicate peptides and glycopeptides, respectively, that are observable in HDX-MS analysis. Yellow lines indicate coverage by subtraction of overlapping peptides.

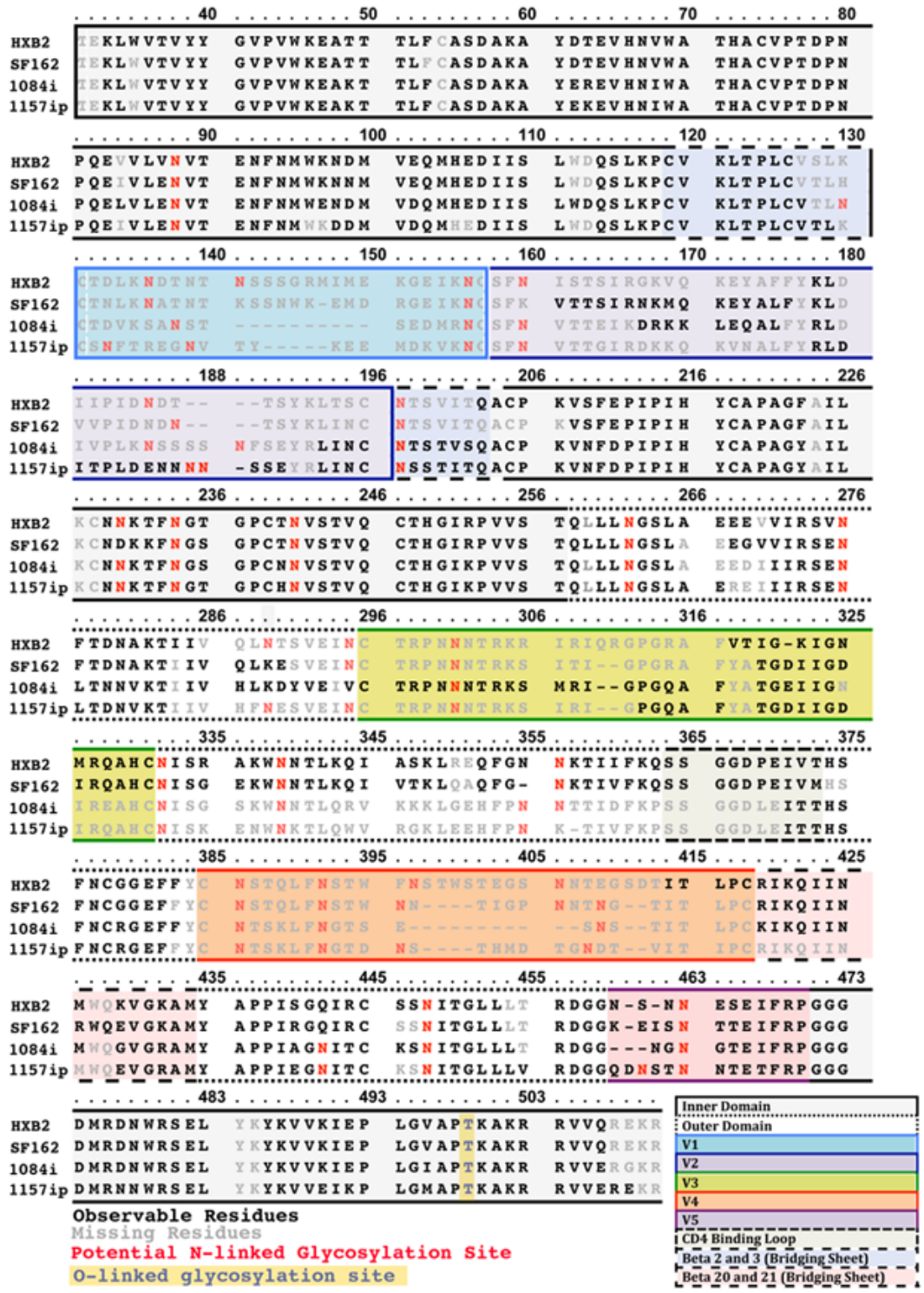

Figure B.S7. Sequence coverage of all peptides for every isolate. The four isolates are aligned to HXB2 and numbered based on standard HXB2 numbering. HDX-MS-observable residues are indicated in black; residues that cannot be measured as a result of missing peptide coverage or rapid back-exchange (N-terminal residues of peptic fragments) are indicated in grey. Variable loops, bridging sheet elements, and CD4-binding loop are colored as described in the inset.

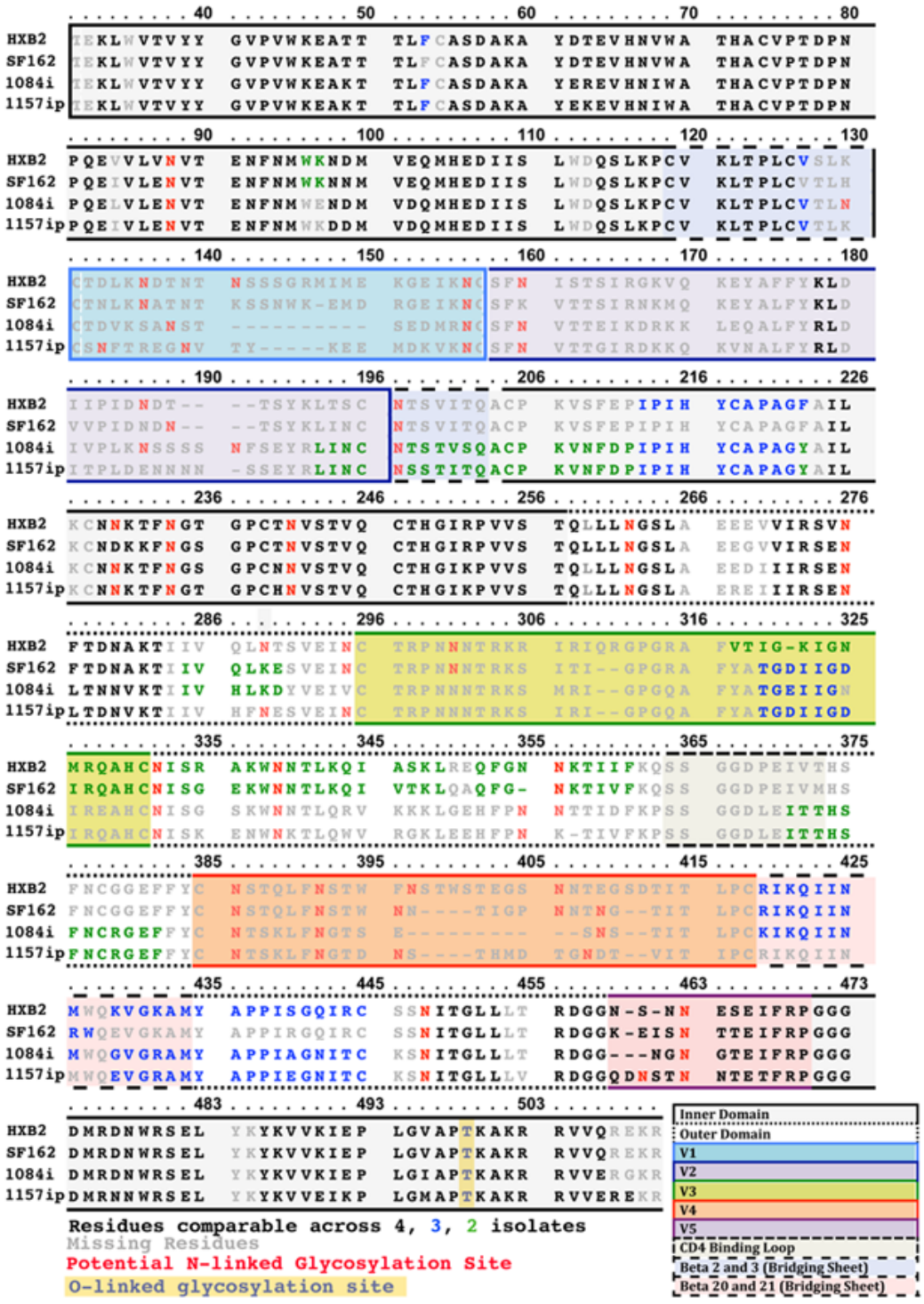

Figure B.S8. Sequence coverage of peptides that are comparable across isolates. The four isolates are aligned to HXB2 and numbered based on standard HXB2 numbering. Black, blue and green text indicates residues that are comparable across 4, 3 and 2 isolates, respectively; residues that cannot be compared across isolates as a result of missing peptide coverage or rapid back-exchange (N-terminal residues of peptic fragments) are indicated in grey. Variable loops, bridging sheet elements, and CD4-binding loop are colored as described in the inset.

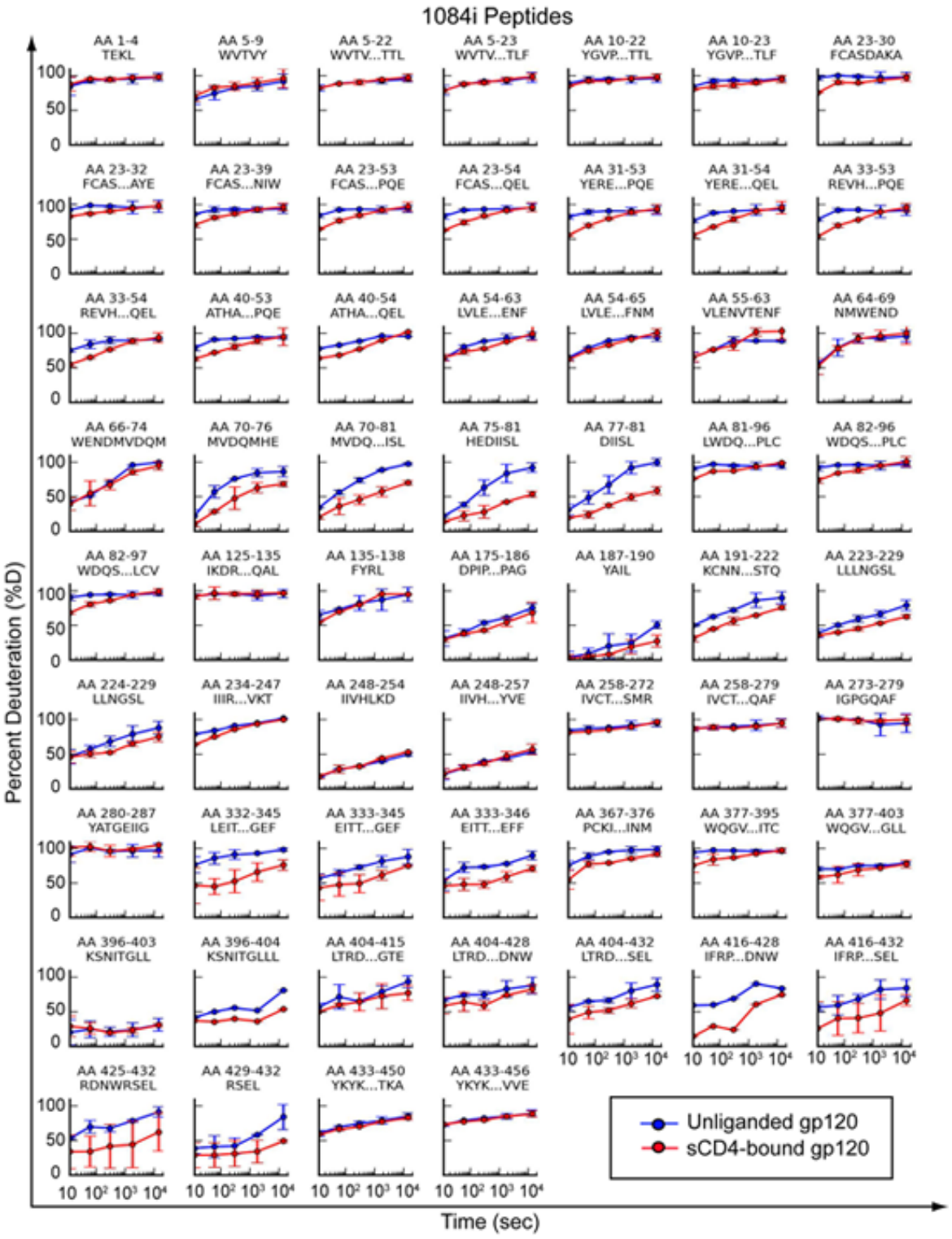

Figure B.S9. Deuteration plots of all unique 1084i peptides (+/-) sCD4. Deuterium uptake plots with percent deuteration vs time are shown for each unique peptide observed for 1084i gp120. Data for unliganded gp120 is shown in blue, while data for sCD4-bound gp120 is shown in red. Amino acid sequence and position of each peptide (using the same numbering as in Figure S3) are indicated above each plot.

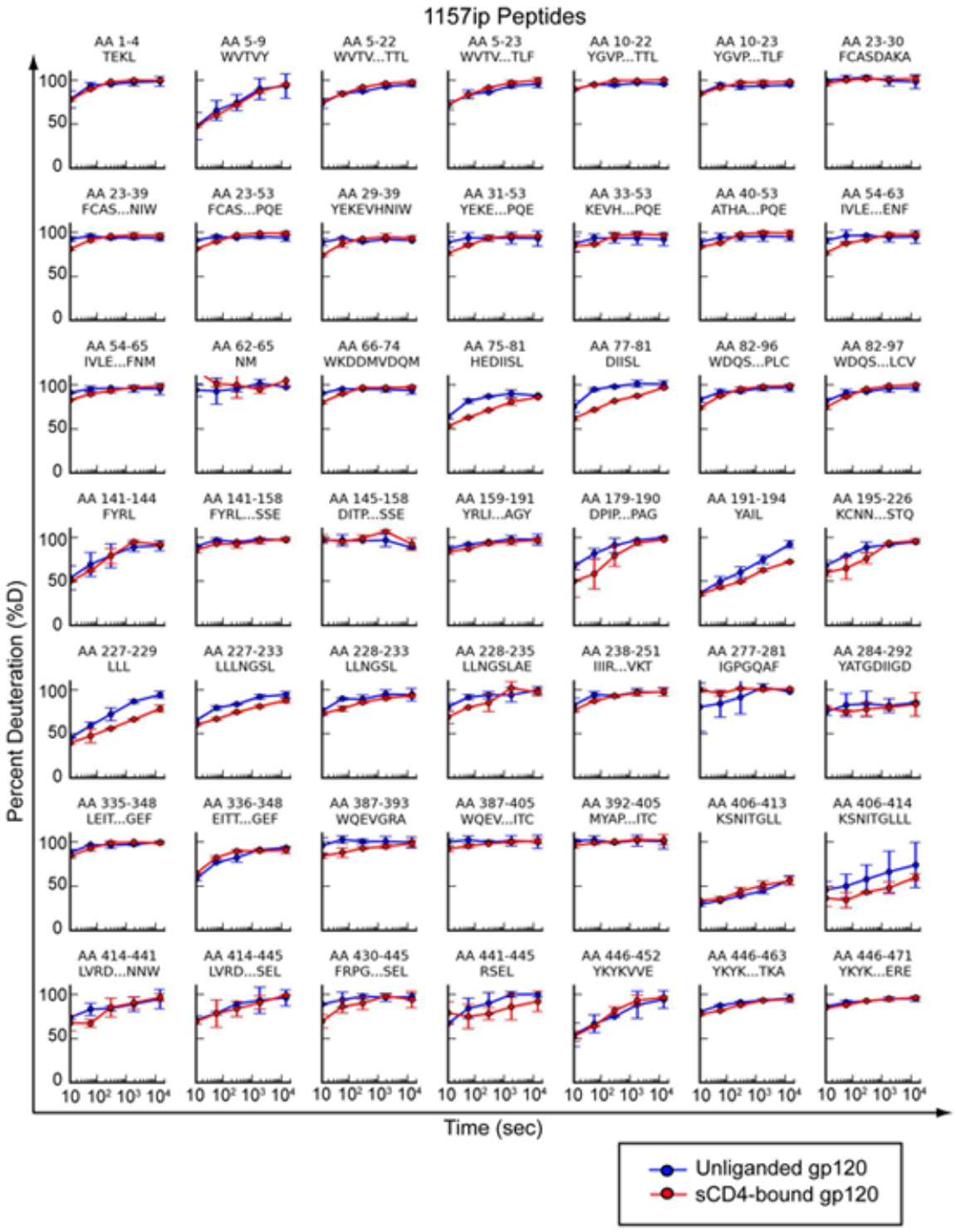

Figure B.S10. Deuteration plots of all unique 1157ip peptides (+/-) sCD4. Deuterium uptake plots with percent deuteration vs. time are shown for each unique peptide observed for 1157ip gp120. Data for unliganded gp120 is shown in blue, while data for sCD4-bound gp120 is shown in red. Amino acid sequence and position of each peptide (using the same numbering as in Figure S4) are indicated above each plot.

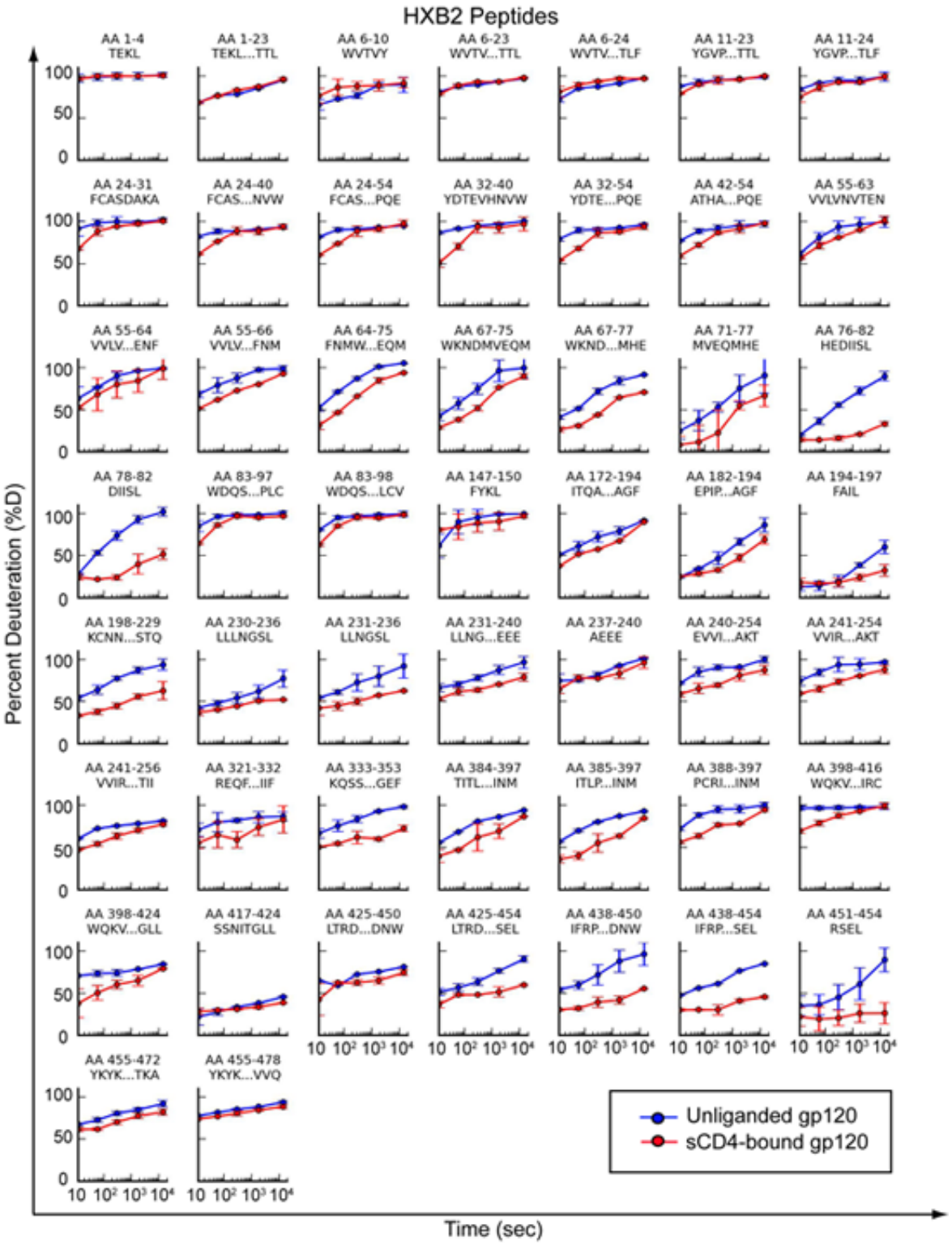

Figure B.S11. Deuteration plots of all unique HXB2 peptides (+/-) sCD4. Deuterium uptake plots with percent deuteration over time are shown for each unique peptide observed for HXB2 gp120. Data for unliganded gp120 is shown in blue, while data for sCD4-bound gp120 is shown in red. Amino acid sequence and position of each peptide (using the same numbering scheme as in Figure S5) are indicated above each plot.

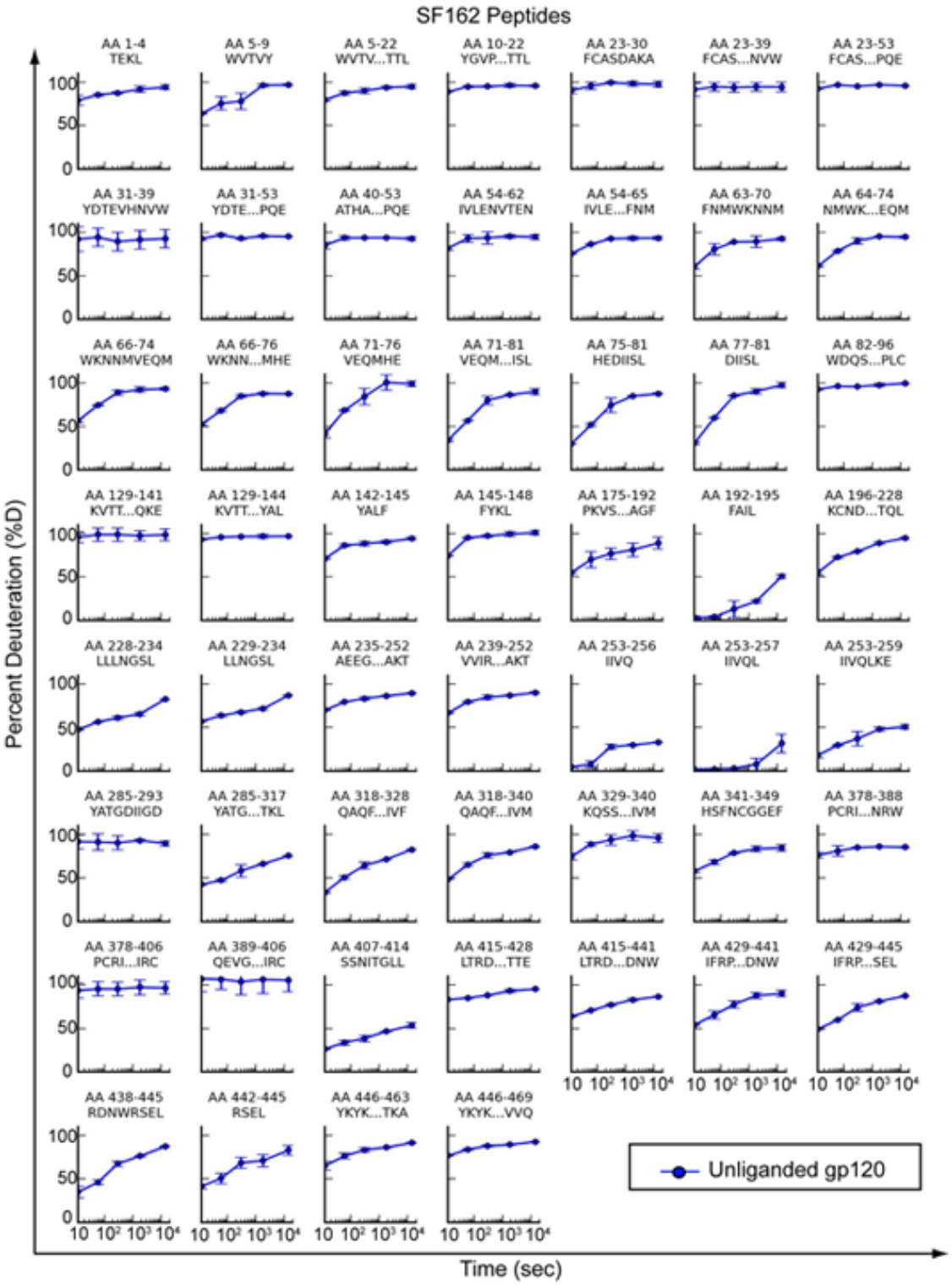

Figure B.S12. Deuteration plots of all unique SF162 peptides. Deuterium uptake plots with percent deuteration over time are shown for each unique peptide observed for SF162 gp120. Data for unliganded gp120 is shown in blue, data was not collected for sCD4-bound SF162, as it has been previously characterized. Amino acid sequence and position of each peptide (using the same numbering scheme as in Figure S6) are indicated above each plot.

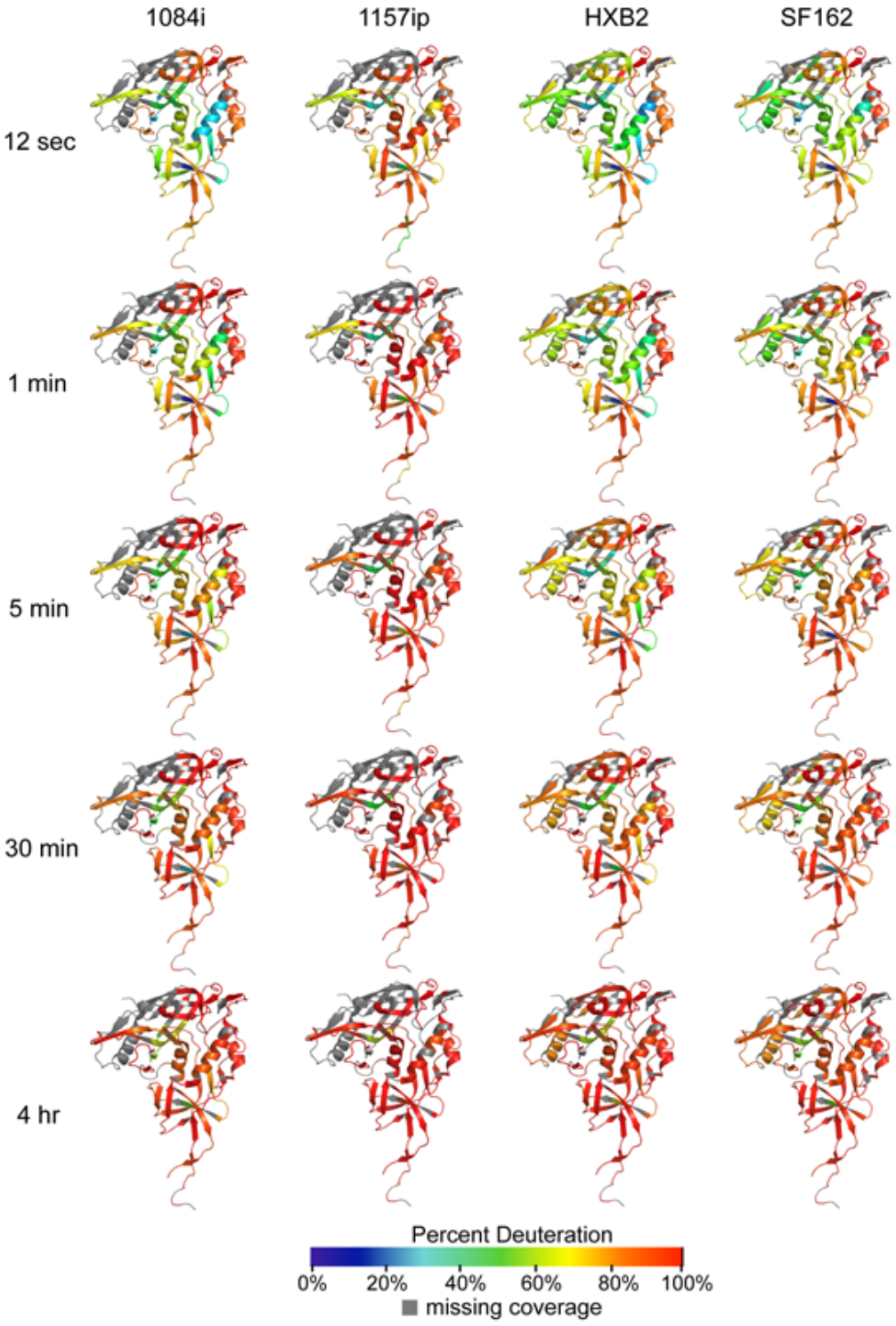

Figure B.S13. Heat map summary of HDX-MS data. Colors mapped onto gp120 core (PDB ID: 3JWD) (35) indicate percent deuteration of peptides throughout gp120 at each deuteration time point (12 sec, 1 min, 5 min, 30 min, 4 hr) for each of the four unliganded gp120 proteins. Deuteration levels are indicated in the legend, with red colors corresponding to high levels of deuterium uptake (dynamic regions) and blue colors corresponding to low levels of deuteration (ordered or "protected" regions). Regions where peptide information is missing are indicated in gray.

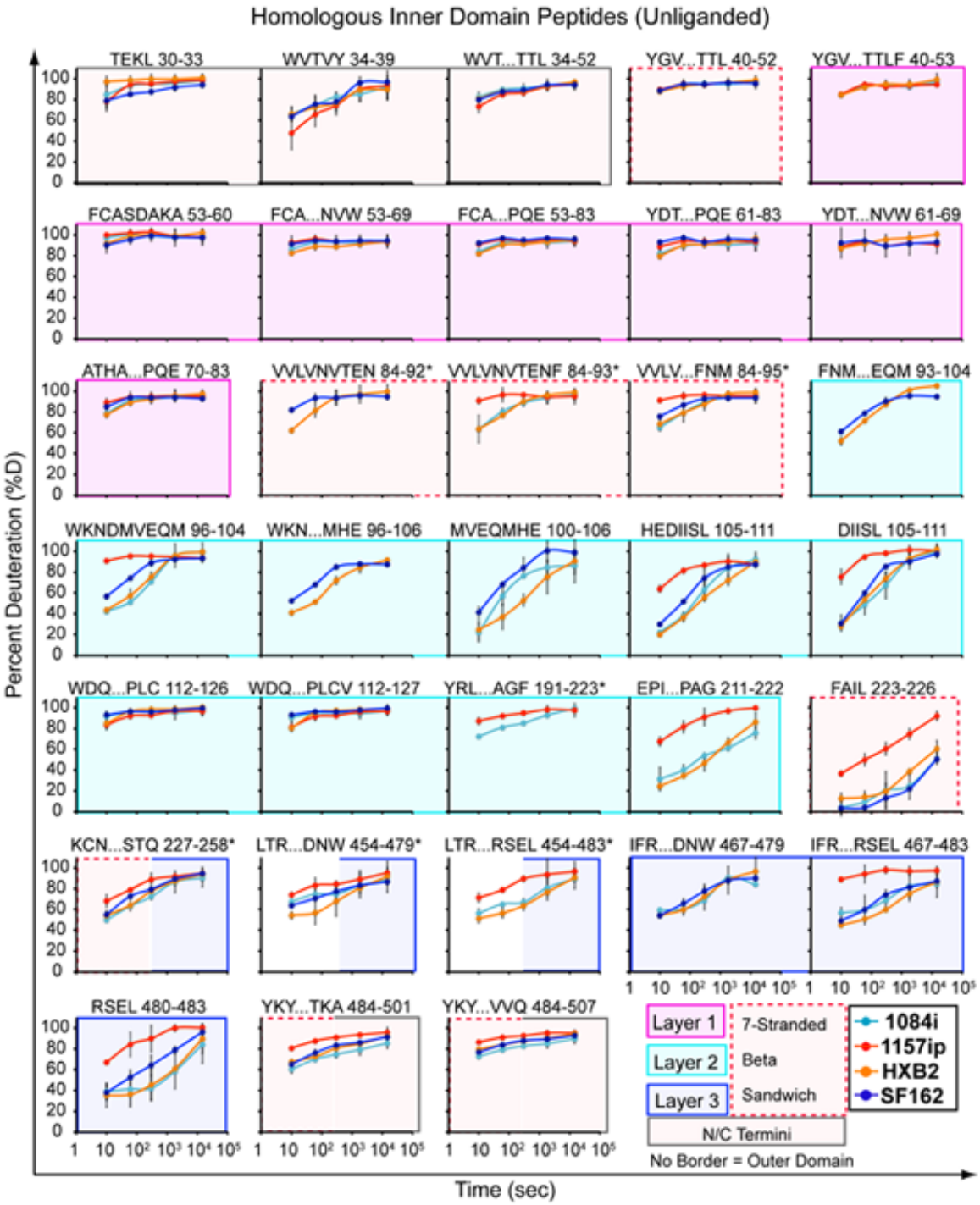

Figure B.S14. Deuteration plots for all comparable inner domain peptides (unliganded gp120). Each graph shows deuterium uptake (% deuteration) over time for peptides throughout the gp120 inner domain, which are either identical or homologous among at least two gp120 isolates. The peptide sequence and amino acid position (both according to HXB2) are indicated for each graph. Each line on the graph corresponds to the deuterium uptake for a different isolate, as indicated in the figure legend. The position of each peptide in the context of the gp120 inner domain is indicated by the colored boxes surrounding the graphs, as defined in the figure legend. Half-boxes indicate peptides that occupy a sequence spanning two separate regions. (*) indicates glycopeptides.

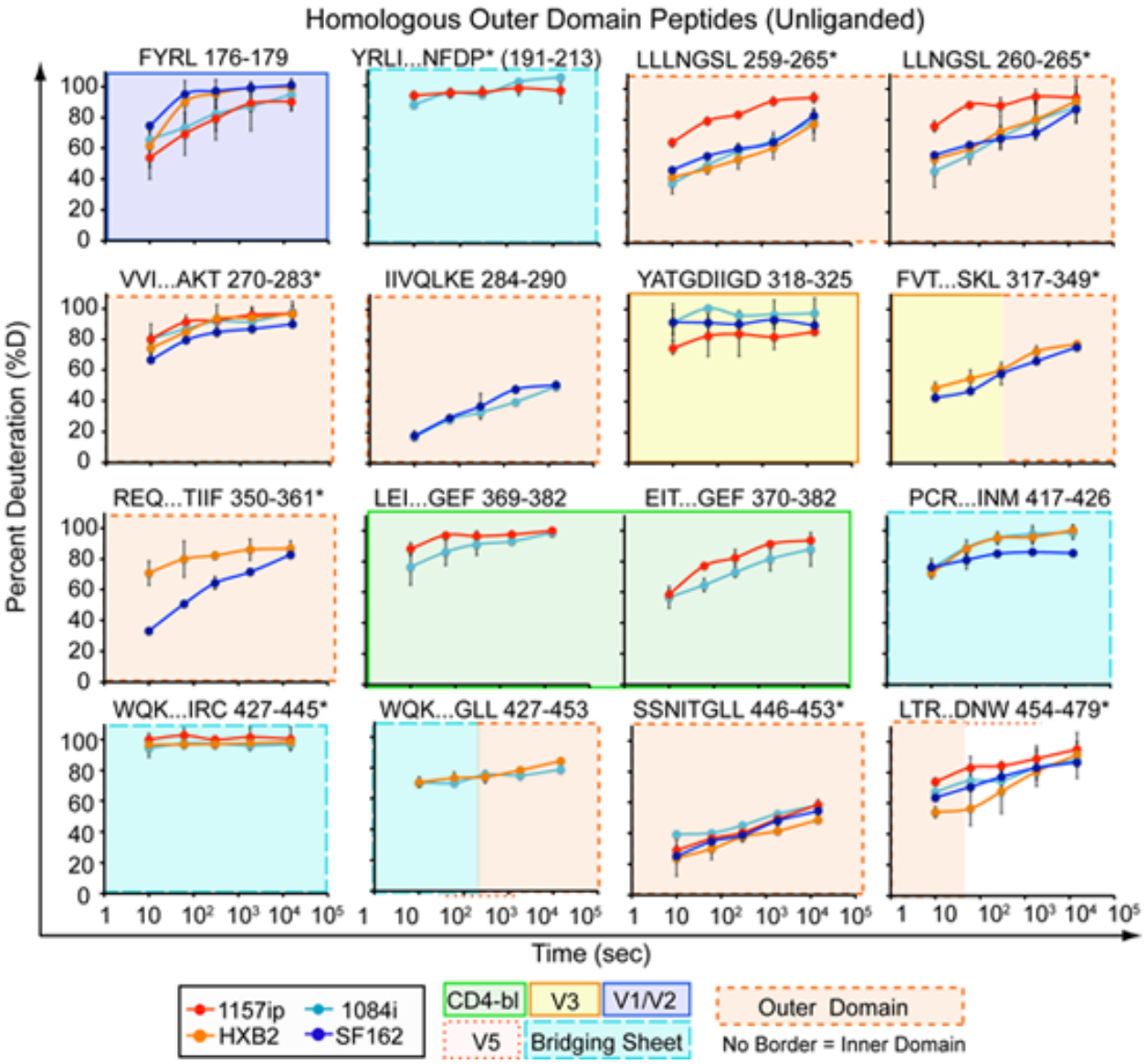

Figure B.S15. Deuteration plots for all comparable outer domain/variable loop/bridging sheet peptides (unliganded gp120). Each graph shows deuterium uptake (% deuteration) over time for peptides throughout the gp120 outer domain, variable loops, or bridging sheet, which are either identical or homologous among at least two gp120 isolates. The peptide sequence and amino acid position (both according to HXB2, unless a peptide for HXB2 was not observed) are indicated for each graph. Each line on the graph corresponds to the deuterium uptake for a different isolate, as indicated in the figure legend. The position of each peptide in the context of the gp120 inner domain is indicated by the colored boxes surrounding the graphs, as defined in the figure legend. Partial-boxes indicate peptides that occupy a sequence spanning two separate regions. (*) indicates glycopeptides.

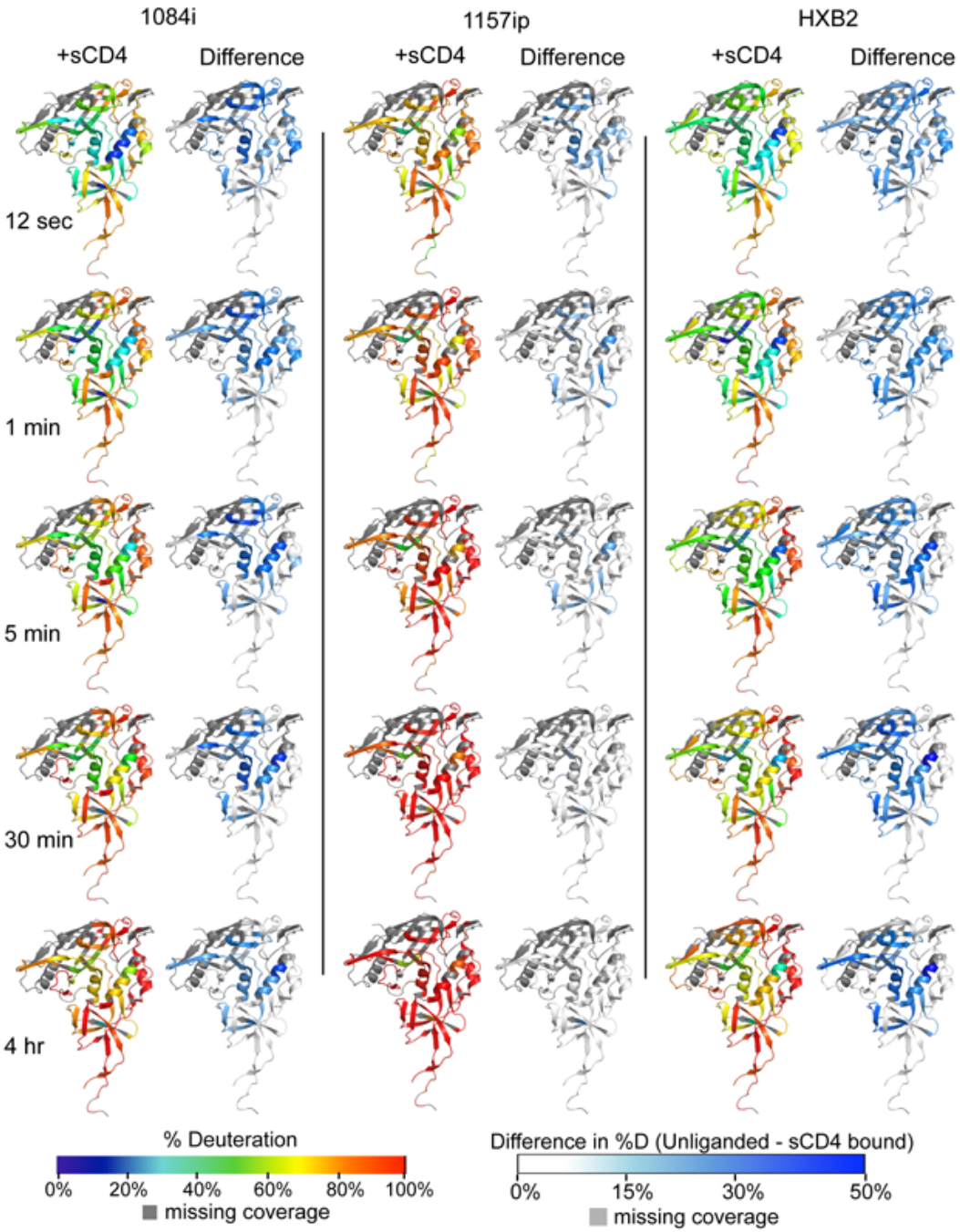

Figure B.S16. Heat map summary of sCD4-bound gp120 deuteration and difference maps. Data for each gp120 isolate (1084i, 1157ip, and HXB2) is presented in a separate column, and each row reflects a different time point (12 sec, 1 min, 5 min, 30 min, and 4 hr). Within each column, the colors mapped onto gp120 core (PDB ID: 3JWD) (35) indicate percent deuteration (left) or difference in percent deuteration relative to unliganded gp120 (right). Deuteration levels are indicated in the legend on the left, with red colors corresponding to high levels of deuterium uptake (dynamic regions) and blue colors corresponding to low levels of deuteration (ordered or "protected" regions). Regions where peptide information is missing are indicated in gray. Deuteration difference values are indicated in the legend on the right, where white colors reflect regions that are similarly deuterated in unliganded and sCD4-bound gp120 and blue colors reflect regions that are stabilized as a result of sCD4-binding.

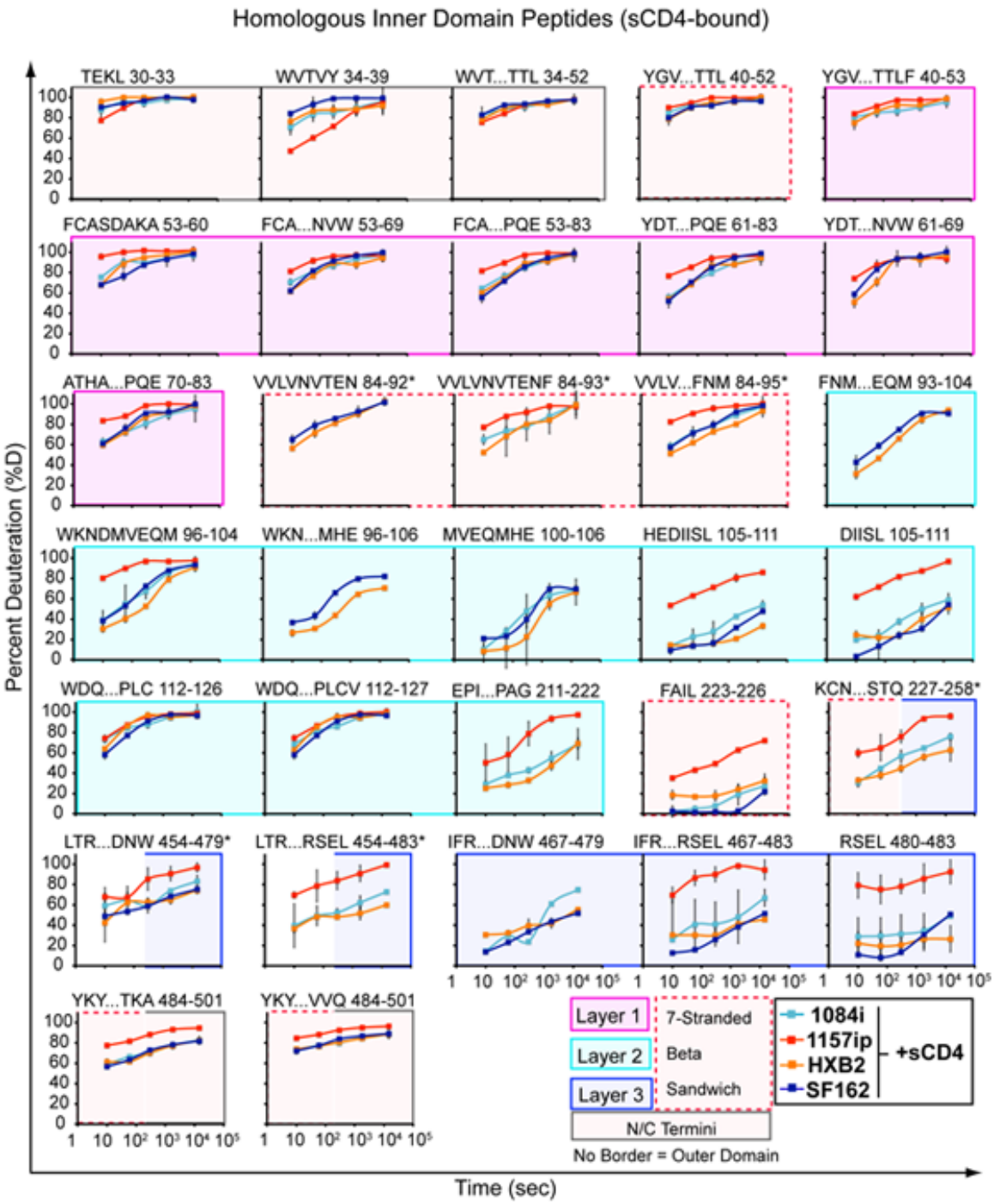

Figure B.S17. Deuteration plots for all comparable inner domain peptides (sCD4-bound gp120). Each graph shows deuterium uptake (% deuteration) over time for peptides throughout the gp120 inner domain in sCD4-bound gp120, which are either identical or homologous among at least two gp120 isolates. The peptide sequence and amino acid position (both according to HXB2, unless a peptide for HXB2 was not observed) are indicated for each graph. Each line on the graph corresponds to the deuterium uptake for a different isolate, as indicated in the figure legend. The position of each peptide in the context of the gp120 inner domain is indicated by the colored boxes surrounding the graphs, as defined in the figure legend. Half-boxes indicate peptides that occupy a sequence spanning two separate regions. (*) indicates glycopeptides.

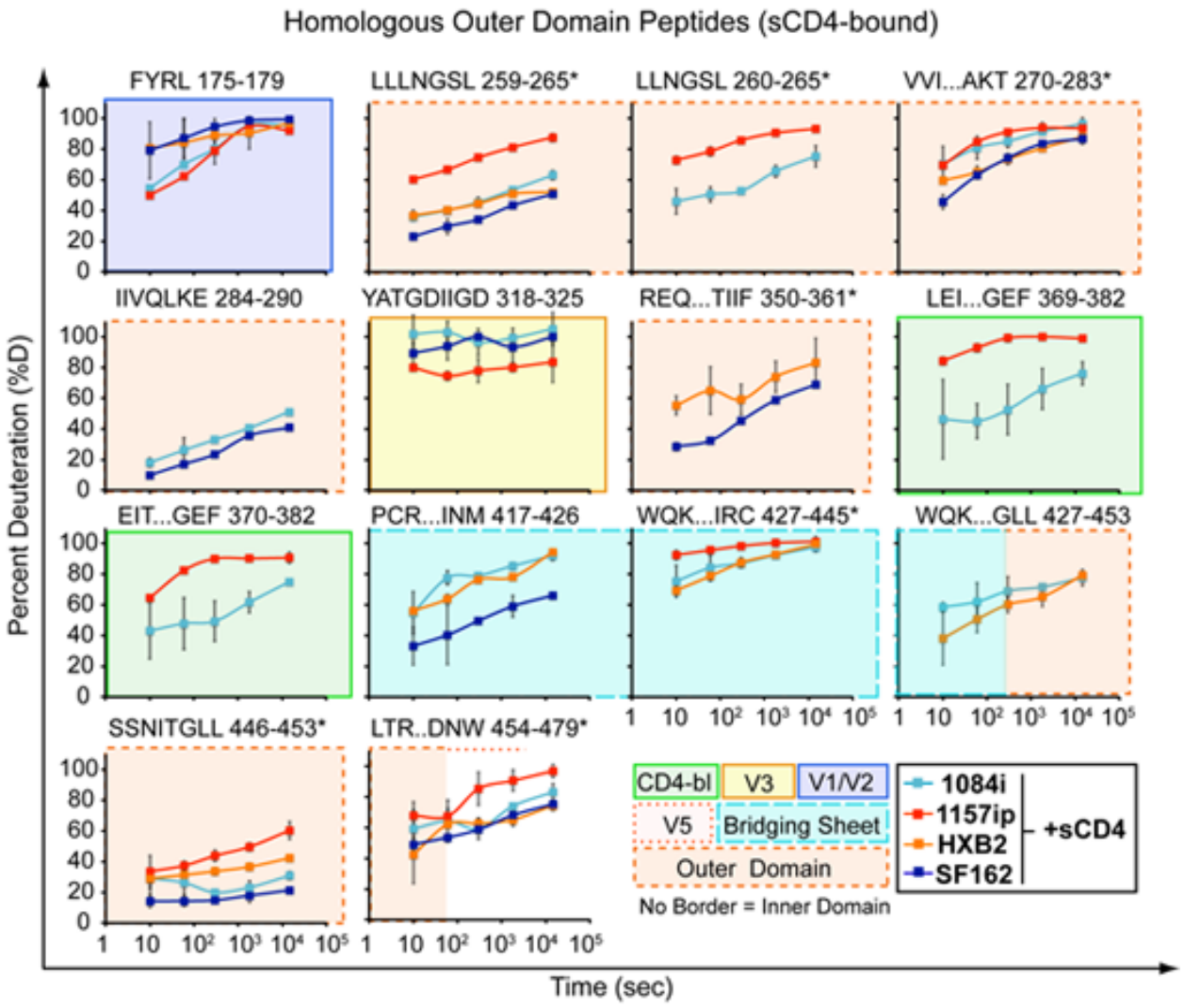

Figure B.S18. Deuteration plots for all comparable outer domain/variable loop/bridging sheet peptides (sCD4-bound gp120) Each graph shows deuterium uptake (% deuteration) over time for peptides throughout the gp120 outer domain, variable loops or bridging sheet, which are either identical or homologous among at least two gp120 isolates. The peptide sequence and amino acid position (both according to HXB2) are indicated for each graph. Each line on the graph corresponds to the deuterium uptake for a different isolate, as indicated in the figure legend. The position of each peptide in the context of the gp120 inner domain is described by the colored boxes surrounding the graphs, as defined in the figure legend. Partial-boxes indicate peptides that occupy a sequence spanning two separate regions. (*) indicates glycopeptides.

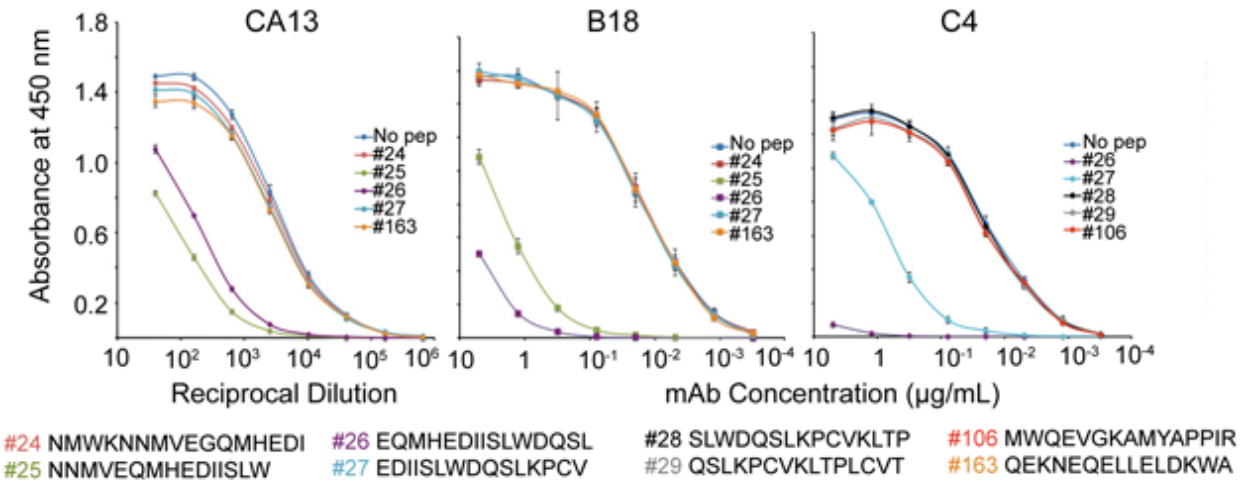

Figure B.S19. Linear epitope-specific antibody peptide competition ELISA. Antibody binding curves are shown for mAbs CA13, C4, and B18 binding to SF162 gp120 in the presence or absence of competing peptides. Peptide competition for antibody binding to gp120 is reflected by a shift in the binding curve to lower levels relative to the "no pep" control. For each antibody binding curve, the different lines indicate antibody binding in the presence of a different peptide as described in the inset for each binding curve. The x-axis for CA13 shows reciprocal dilution of antibody supernatant, and the x-axis for the B18 and C4 curves shows monoclonal antibody concentration. The identity of each peptide number is defined below the graphs. Axes show antibody binding levels (measured as absorbance at 450 nm) vs antibody concentration.

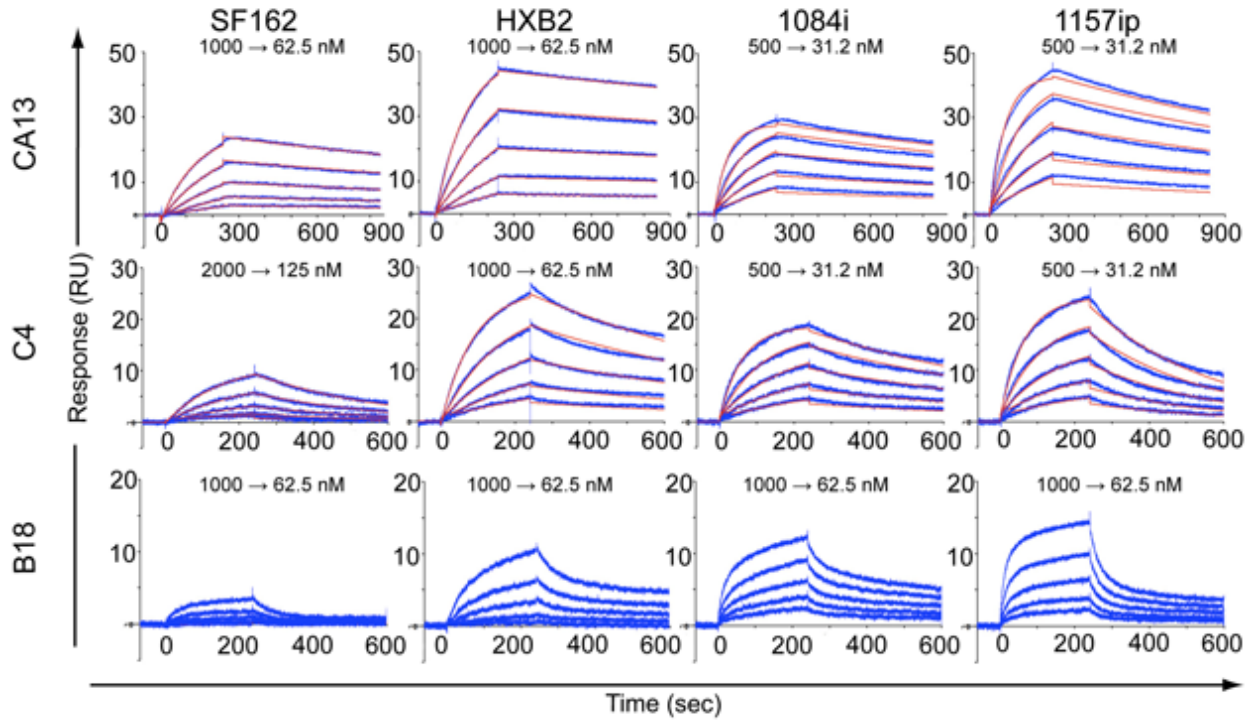

Figure B.S20. Linear epitope-specific antibody SPR binding curves. Double-reference subtracted SPR binding curves are shown for gp120 binding to captured linear-epitope specific antibodies CA13, C4, or B18 over a series of gp120 concentrations (indicated above each graph). Raw data is shown in blue, and best-fit 1:1 binding model curves are in red. Each column shows data for a different gp120 isolate, and each row shows data for a different antibody. Y-axis is SPR response (in RU) and x-axis is time. Note changes in gp120 concentration range and scale for the Y-axis for each antibody.

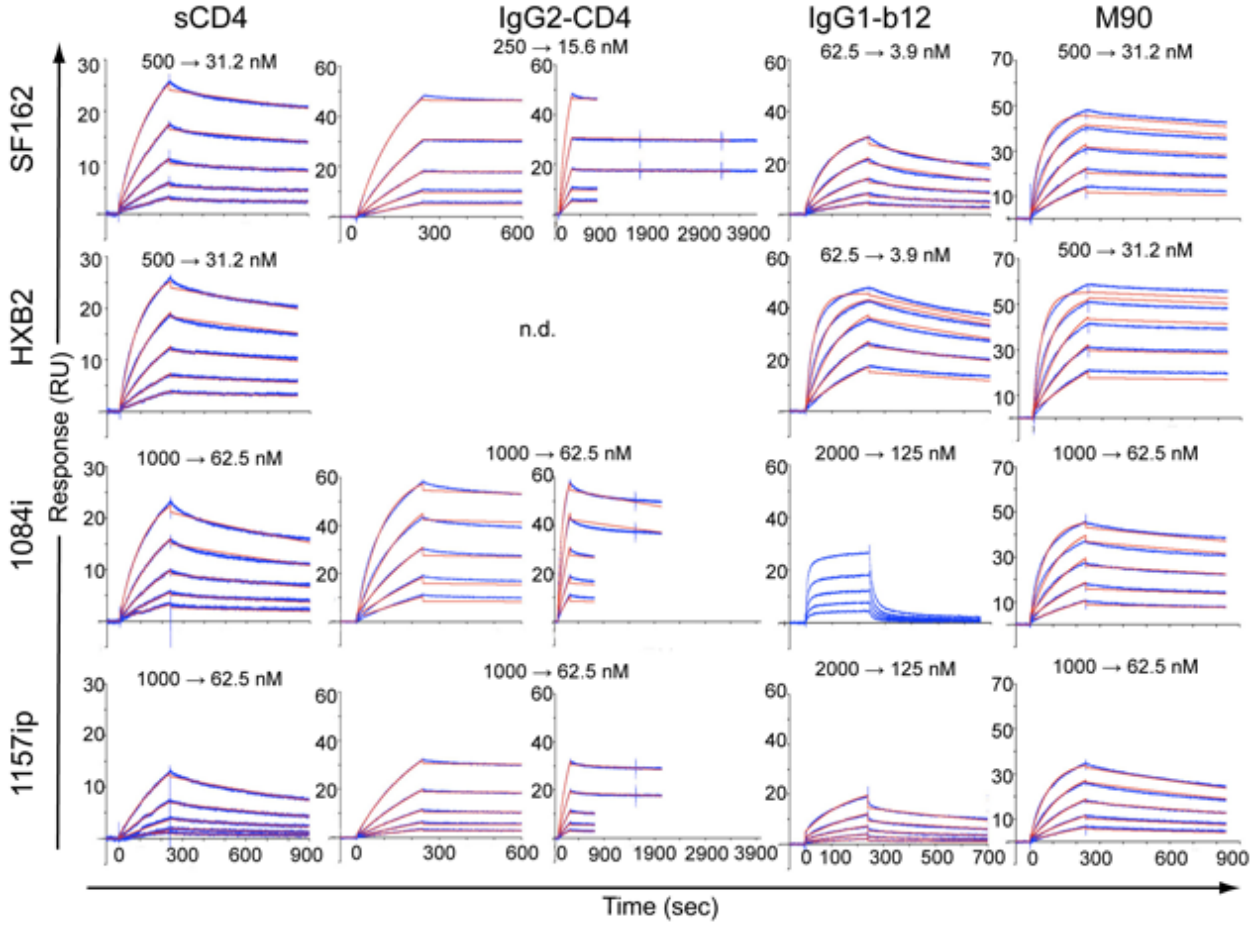

Figure B.S21. Conformation-dependent antibody SPR binding curves. Double-reference subtracted SPR binding curves are shown for gp120 binding to immobilized (sCD4) or captured conformation-dependent ligands CD4-IgG2, IgG1-b12, and M90 over a series of gp120 concentrations (indicated above each graph, note changes in concentration range among the isolates). Raw data is shown in blue, and best-fit 1:1 binding model curves are in red. Each column shows data for a different gp120 ligand, and each row shows data for a different isolate. Y-axis is SPR response (in RU) and x-axis is time. Note changes in scale for the Y-axis for each ligand. Because IgG2-CD4 dissociation was relatively slow, a longer dissociation phase was used. The early time scale (0-600 sec) is shown on the left, and the full time scale is shown on the right (0-3900 sec).

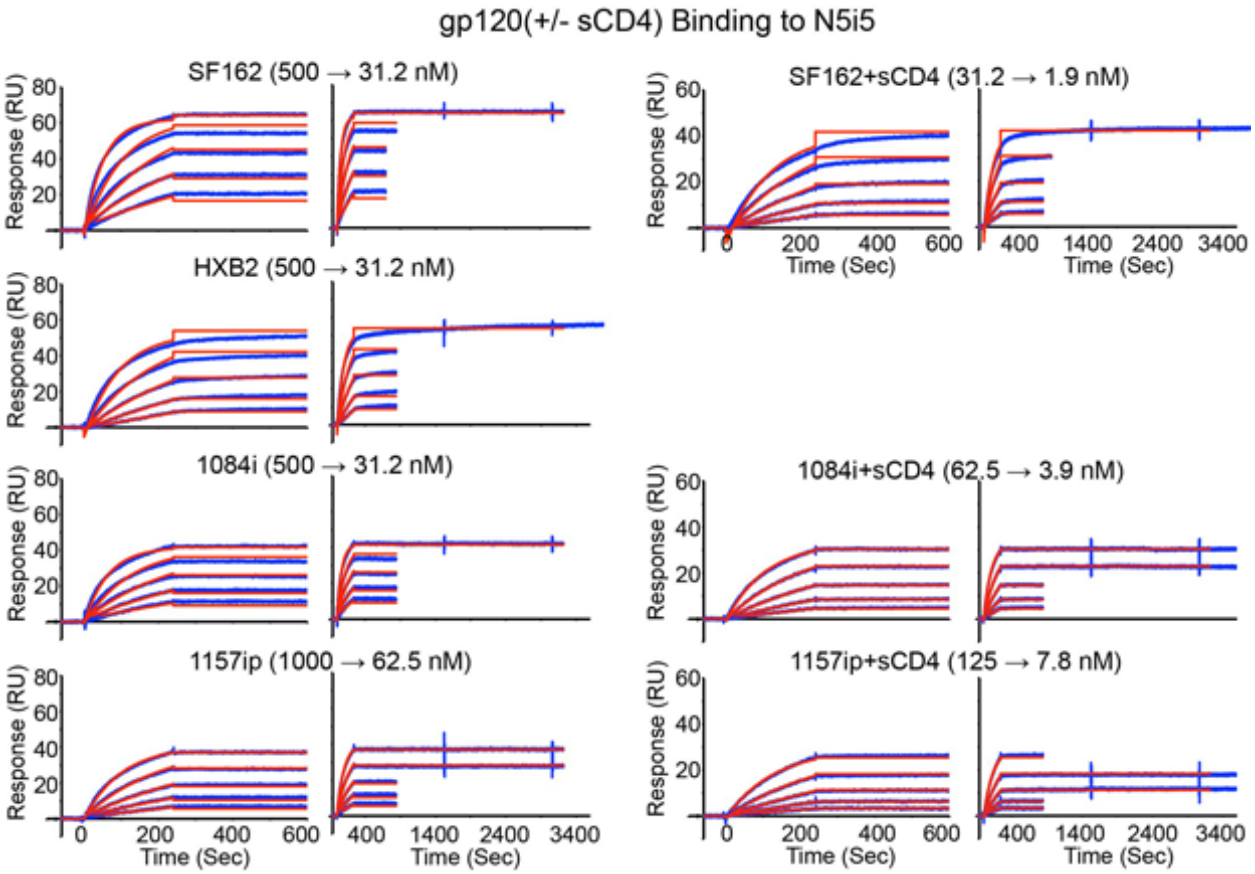

Figure B.S22. N5i5 SPR binding curves +/- sCD4. Double-reference subtracted SPR binding curves are shown for gp120 (in the presence or absence of 625 nM sCD4) binding to immobilized N5i5 over a series of gp120 concentrations (indicated above each graph). Raw data is shown in blue, and best-fit curves for a 1:1 binding model with the dissociation rate fixed at 0 s^{-1} are in red. Each row shows data for a different gp120 isolate, and each column shows data for that isolate in the absence (left) or presence (right) of sCD4. Y-axis is SPR response (in RU) and x-axis is time. Note changes in scale for the Y-axis, and differences in gp120 concentration series used in the experiment. Because N5i5 dissociation was slow, a longer dissociation phase was used. Within each column, the early time scale (0-600 sec) is shown on the left, and the full time scale is shown on the right (0-3900 sec).

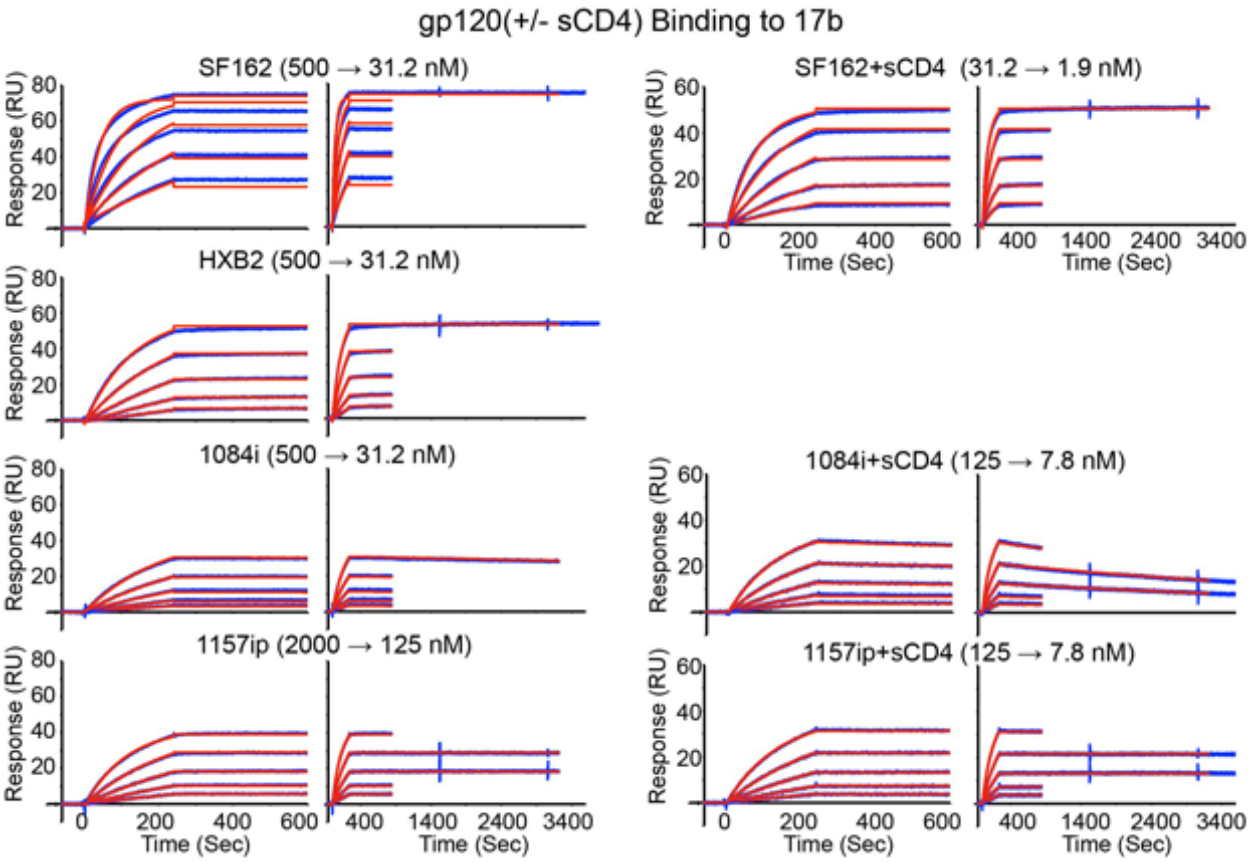

Figure B.S23. 17b SPR binding curves +/- sCD4. Double-reference subtracted SPR binding curves are shown for gp120 (in the presence or absence of 625 nM sCD4) binding to immobilized 17b over a series of gp120 concentrations (indicated above each graph). Raw data is shown in blue, and best-fit curves for a 1:1 binding model with the dissociation rate fixed at 0 s^{-1} are in red. In the case of 1084i, there was sufficient dissociation to fit the dissociation rate as well using a standard 1:1 binding model. Each row shows data for a different gp120 isolate, and each column shows data for that isolate in the absence (left) or presence (right) of sCD4. Y-axis is SPR response (in RU) and x-axis is time. Note changes in scale for the Y-axis and gp120 concentration series used in the experiment. Because 17b dissociation was slow, a longer dissociation phase was used. Within each column, the early time scale (0-600 sec) is shown on the left, and the full time scale is shown on the right (0-3900 sec).

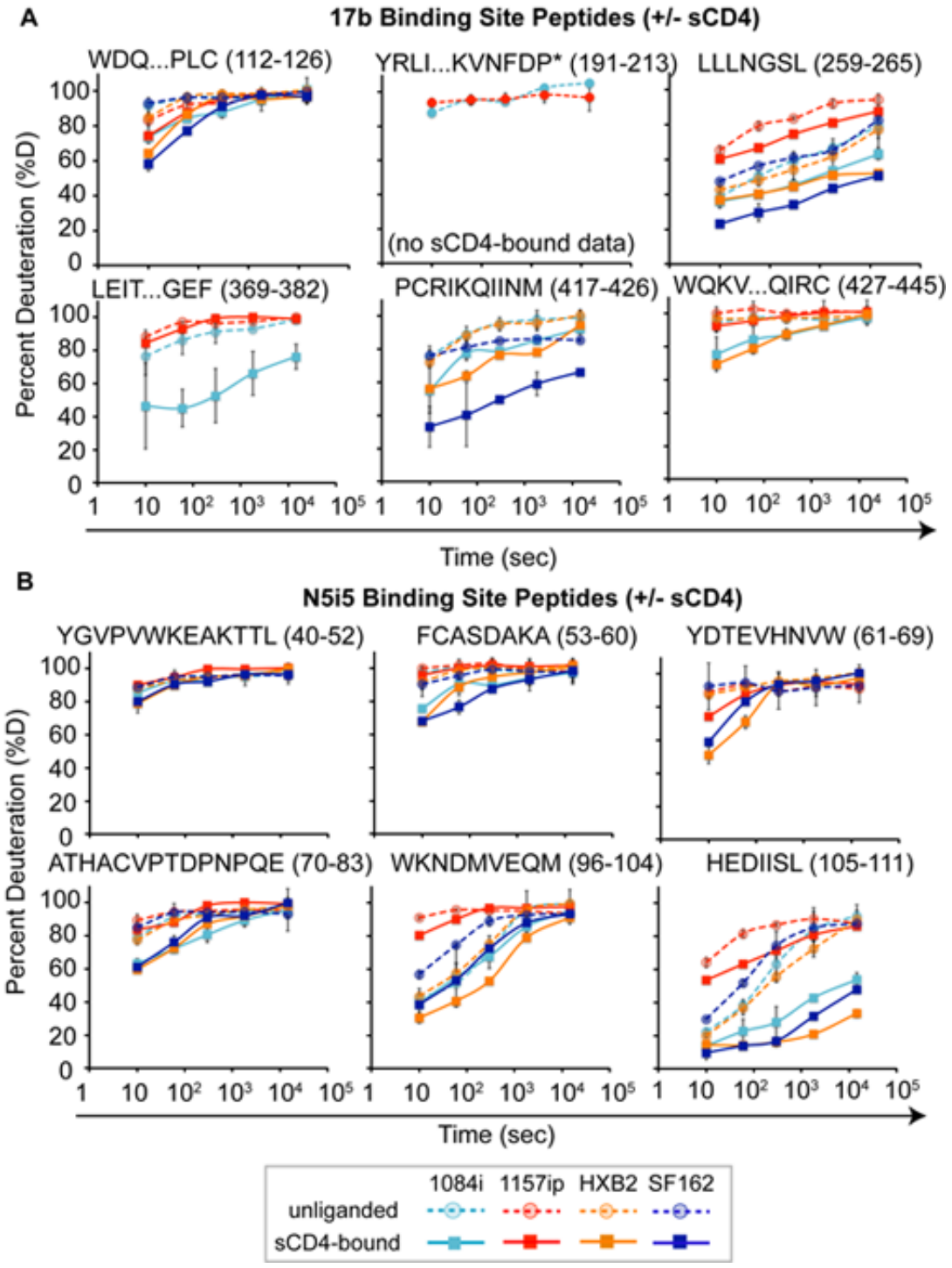

Figure B.S24. sCD4-induced stabilization of peptides within 17b and N5i5 epitopes. Percent deuteration plots for peptides containing CD4-induced antibody contact residues are shown for peptides in the 17b (A) and N5i5 (B) epitopes in the presence and absence of sCD4. Dashed lines with circles indicate data for unliganded gp120, solid lines with squares indicate data for sCD4-bound gp120. Each isolate is represented by a different color as indicated in the figure legend. It can be seen that CD4i antibody epitopes are differentially stabilized in the different gp120 isolates as a result of sCD4 binding.

Table B.S1. Summary of SPR Experimental Details

Ligand	Immobilization	Density (RU)	Analyte	Flow rate (ul/min)	Concentration Series (nM)	On (sec)	Off 1 (sec)	Off 2 (sec)	Off 2 Concs (nM)	Fitted Concs.
sCD4	EDC/NHS	85	HXB2	40	1000 -> 7.8	240	600	n/a	n/a	500 -> 31.2
		85	SF162	40	1000 -> 15.6	240	780	n/a	n/a	500 -> 31.2
		185	1084i	40	1000 -> 15.6	240	660	n/a	n/a	1000 -> 62
		185	1157ip	40	1000 -> 15.6	240	780	n/a	n/a	1000 -> 62
IgG2-CD4	G α H Fc cap*	80	HXB2		n.d.	n.d.	n.d.	n.d.	n.d.	n.d.
		80	SF162	40	250 -> 3.9	240	720	3600	125, 62.5	250 -> 15.6
		80	1084i	40	2000 -> 31.2	240	720	1800	1000, 500	1000 -> 62
		80	1157ip	40	2000 -> 31.2	240	720	1800	1000, 500	1000 -> 62
IgG1-b12	G α H Fc cap	50	HXB2	50	500 -> 3.9	240	480	n/a	n/a	62 -> 3.9
		75	SF162	40	250 -> 3.9	240	720	3600	125, 62.5	62 -> 3.9
		75	1084i	40	2000 -> 31.2	240	720	1800	1000, 500	not 1:1
		75	1157ip	40	2000 -> 31.2	240	720	1800	1000, 500	2000 -> 125
17b	G α H Fc cap	60	HXB2	40	1000 -> 31.2	240	600	4200	1000, 500	500 -> 31.2*
		60	SF162	40	1000 -> 31.2	240	600	4200	1000, 500	500 -> 31.2*
		60	1084i	40	2000 -> 31.2	240	600	3600	1000, 500	1000 -> 31.2
		60	1157ip	40	2000 -> 31.2	240	600	3600	1000, 500	2000 -> 125*
17b	G α H Fc cap	50	HXB2 + sCD4	40	n.d.	n.d.	n.d.	n.d.	n.d.	n.d.
		50	SF162 + sCD4	40	125 -> 1.9	240	720	4500	62.5, 31.2	31.2 -> 1.9*
		50	1084i + sCD4	40	125 -> 1.9	240	720	4500	62.5, 31.2	125 -> 7.8
		50	1157ip + sCD4	40	125 -> 1.9	240	720	4500	62.5, 31.2	125 -> 7.8*
N5i5	G α H Fc cap	60	HXB2	40	1000 -> 31.2	240	600	4200	1000, 500	500 -> 31.2*
		60	SF162	40	1000 -> 31.2	240	600	4200	1000, 500	500 -> 31.2*
		60	1084i	40	2000 -> 31.2	240	600	3600	1000, 500	500 -> 31.2*
		60	1157ip	40	2000 -> 31.2	240	600	3600	1000, 500	1000 -> 62.5*
N5i5	G α H Fc cap	50	HXB2 +sCD4	40	n.d.	n.d.	n.d.	n.d.	n.d.	n.d.
		50	SF162 + sCD4	40	125 -> 1.9	240	720	4500	62.5, 31.2	31.2 -> 1.9*
		50	1084i + sCD4	40	125 -> 1.9	240	720	4500	62.5, 31.2	62.5 -> 3.9*
		50	1157ip + sCD4	40	125 -> 1.9	240	720	4500	62.5, 31.2	125 -> 7.8*
M90	G α M Fc cap**	50	HXB2	40	2000 -> 31.2	240	660	n/a	n/a	500 -> 31.2
		50	SF162	40	2000 -> 31.2	240	660	n/a	n/a	500 -> 31.2
		50	1084i	40	2000 -> 31.2	240	660	n/a	n/a	1000 -> 62.5
		50	1157ip	40	2000 -> 31.2	240	660	n/a	n/a	1000 -> 62.5
B18	G α M Fc cap	75	HXB2	40	2000 -> 31.2	240	900	n/a	n/a	not 1:1
		75	SF162	40	1000 -> 31.2	240	720	n/a	n/a	not 1:1
		75	1084i	40	2000 -> 31.2	240	900	n/a	n/a	not 1:1
		75	1157ip	40	2000 -> 31.2	240	900	n/a	n/a	not 1:1
C4	G α M Fc cap	75	HXB2	40	2000 -> 31.2	240	900	n/a	n/a	1000 -> 62.5
		75	SF162	40	1000 -> 31.2	240	720	n/a	n/a	1000 -> 62.5
		75	1084i	40	2000 -> 31.2	240	900	n/a	n/a	500 -> 31.2
		75	1157ip	40	2000 -> 31.2	240	900	n/a	n/a	500 -> 31.2
CA13	G α M Fc cap	70	HXB2	40	2000 -> 31.2	240	900	n/a	n/a	2000 -> 125
		70	SF162	40	2000 -> 31.2	240	720	n/a	n/a	1000 -> 62.5
		70	1084i	40	4000 -> 31.2	240	900	n/a	n/a	1000 -> 62.5
		70	1157ip	40	4000 -> 31.2	240	900	n/a	n/a	1000 -> 62.5

* Goat anti-human, Fc-specific antibody capture
** Goat anti-mouse, Fc-specific antibody capture
n.d. experiment not done

Table B.S2. Chi^2 error of 1:1 binding vs. fixed dissociation rate (kd = 0 s^{-1}) fits to CD4i antibody SPR data

		Float kd		Fixed kd = 0 s^{-1}	
	Isolate	ka (1/M-s)	Chi2	ka (1/M-s)	Chi2
17b	HXB2	1.52(4) ×10^4*	0.405(7)	1.51(3) ×10^4	0.36(6)
	SF162	5.06(8) ×10^4	4.4(8)	5.06(7) ×10^4	4.4(8)
	1084i	9.5(1) ×10^3	0.32(9)	-	-
	1157ip	4.43(3) ×10^3	0.114(1)	4.38(3) ×10^3	0.121(2)
17b + sCD4	HXB2	-	-	-	-
	SF162	4.24(5) ×10^5	0.332(2)	4.19(6) ×10^5	0.323(1)
	1084i	5.8(5) ×10^4	0.17(9)	-	-
	1157ip	5.59(9) ×10^4	0.07(2)	5.5(1) ×10^4	0.08(2)
N5i5	HXB2	2.2(1) ×10^4	3.0(3)	2.12(6) ×10^4	3.28(4)
	SF162	3.94(3) ×10^4	4.01(9)	3.94(2) ×10^4	3.98(8)
	1084i	3.11(2) ×10^4	1.5(4)	3.12(4) ×10^4	1.50(3)
	1157ip	9.6(2) ×10^3	0.51(5)	9.7(2) ×10^3	0.50(7)
N5i5 + sCD4	HXB2	-	-	-	-
	SF162	2.8(1) ×10^5	1.2(2)	2.9(2) ×10^5	1.2(2)
	1084i	1.6(1) ×10^5	0.3(3)	1.51(3) ×10^5	0.1(4)
	1157ip	6.1(2) ×10^4	0.21(1)	6.1(2) ×10^4	0.214(9)

(-) experiment was not performed or the fixed kd model was not applied
* error on the last significant figure is presented in parentheses as in Table 2 from the main text.

Supporting Methods for Peptide Competition ELISA

Peptides for the peptide competition ELISA were obtained from the NIH AIDS Reagent Program (Consensus Subtype B Env 15-mer peptide set, #9480). The peptide competition ELISA was carried out exactly as described for the standard ELISA in the main text, with a few modifications. SF162 gp120 was plated at 50 ng/well in PBS at 4^{o}C overnight. All peptides were resuspended in dimethyl sulfoxide (DMSO) just prior to use. During the blocking step, antibodies C4 and B18 at 5 μg/mL (or a 1:40 dilution for the CA13 supernatant) were incubated for 1 hour at room temperature with a 40-fold molar excess of peptide. After washing the plate, the antibody/peptide mixture was diluted in a 4-fold concentration series into antibody dilution buffer containing a constant concentration of peptide (~1.2 μM). Matched volumes of DMSO were added to the "no peptide" control samples. Following incubation of the primary antibody for 1 hour at room temperature, washing, secondary antibody, and development were carried out exactly as described for the standard ELISA.

Appendix C:

Chapter 3 Supplementary Information

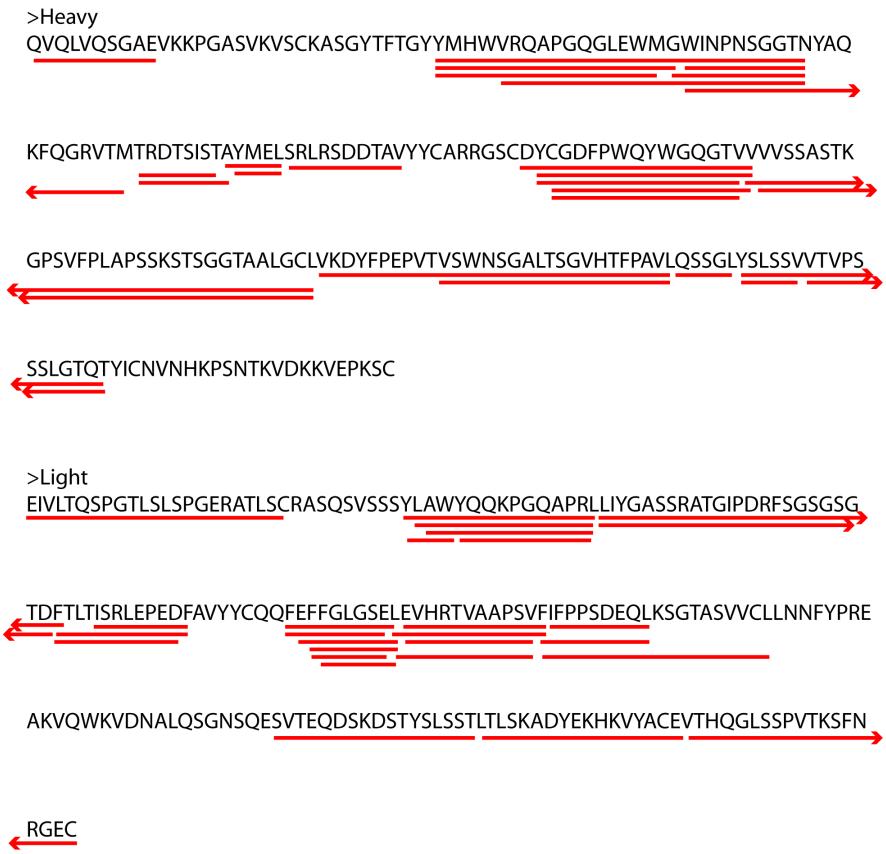

Figure C.S1. Peptide coverage map for VRC03 germline Fab. The primary amino acid sequence for the Fab region of the VRC03 germline heavy and light chains is shown. Red lines beneath the sequence indicate pepsin fragments identified by tandem mass spectrometry.

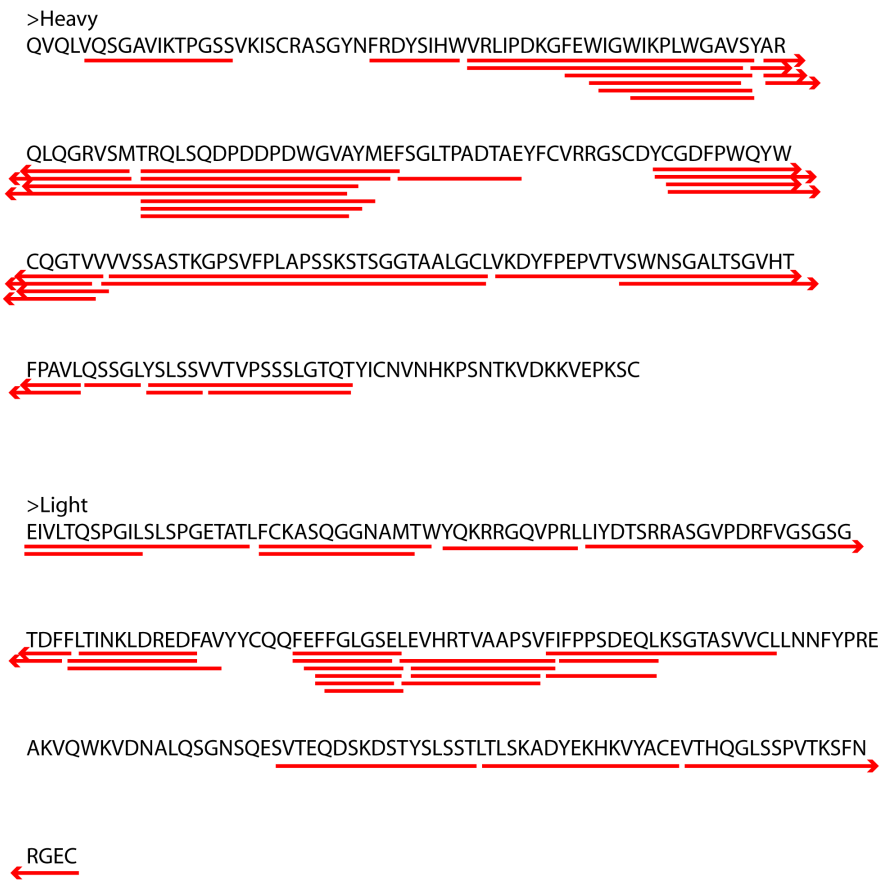

Figure C.S2. Peptide coverage map for VRC03 mature Fab. The primary amino acid sequence for the Fab region of the VRC03 mature heavy and light chains is shown. Red lines beneath the sequence indicate pepsin fragments identified by tandem mass spectrometry.

Figure C.S3. Peptide coverage map for VRC26M (early) Fab. The primary amino acid sequence for the Fab region of the VRC26M heavy and light chains is shown. Red lines beneath the sequence indicate pepsin fragments identified by tandem mass spectrometry. The blue box highlights an ammonia loss on the glutamine residue.

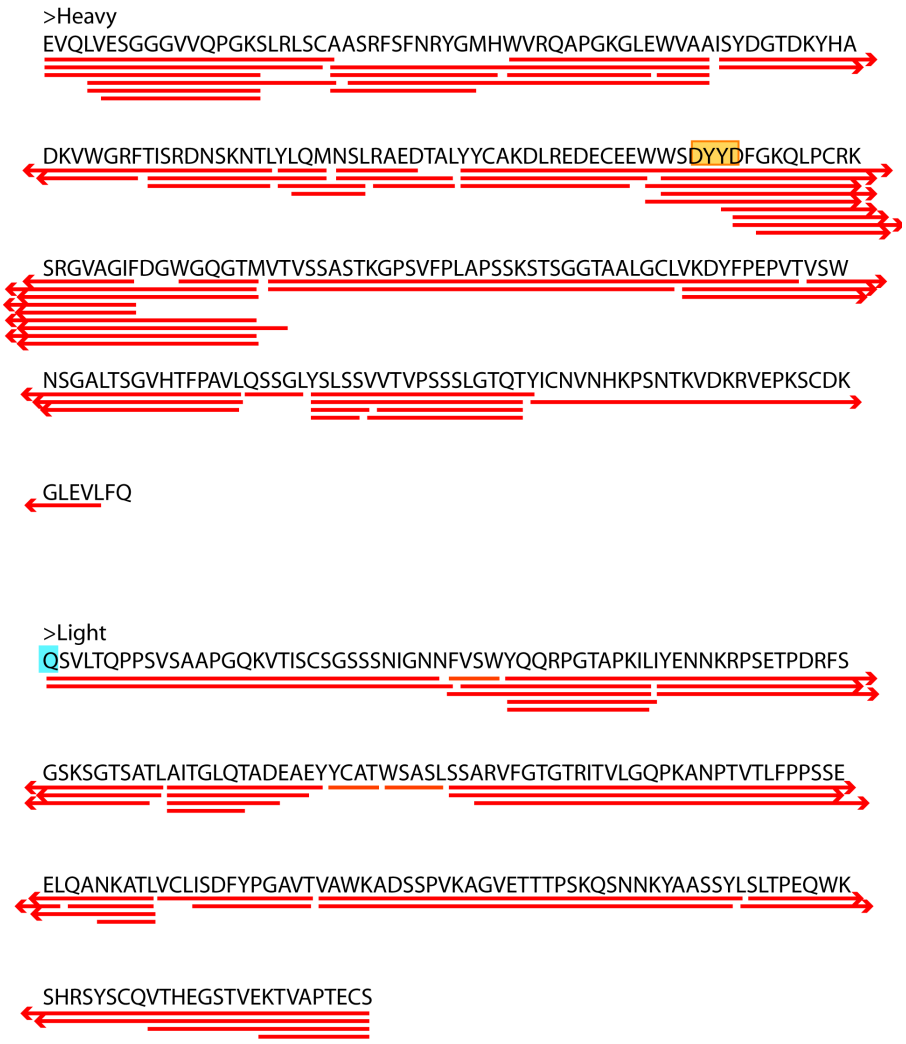

Figure C.S4. Peptide coverage map for VRC26D (intermediate) Fab. The primary amino acid sequence for the Fab region of the VRC26D heavy and light chains is shown. Red lines beneath the sequence indicate pepsin fragments identified by tandem mass spectrometry. Yellow box indicates the sulfation motif. The blue box highlights an ammonia loss on the glutamine residue.

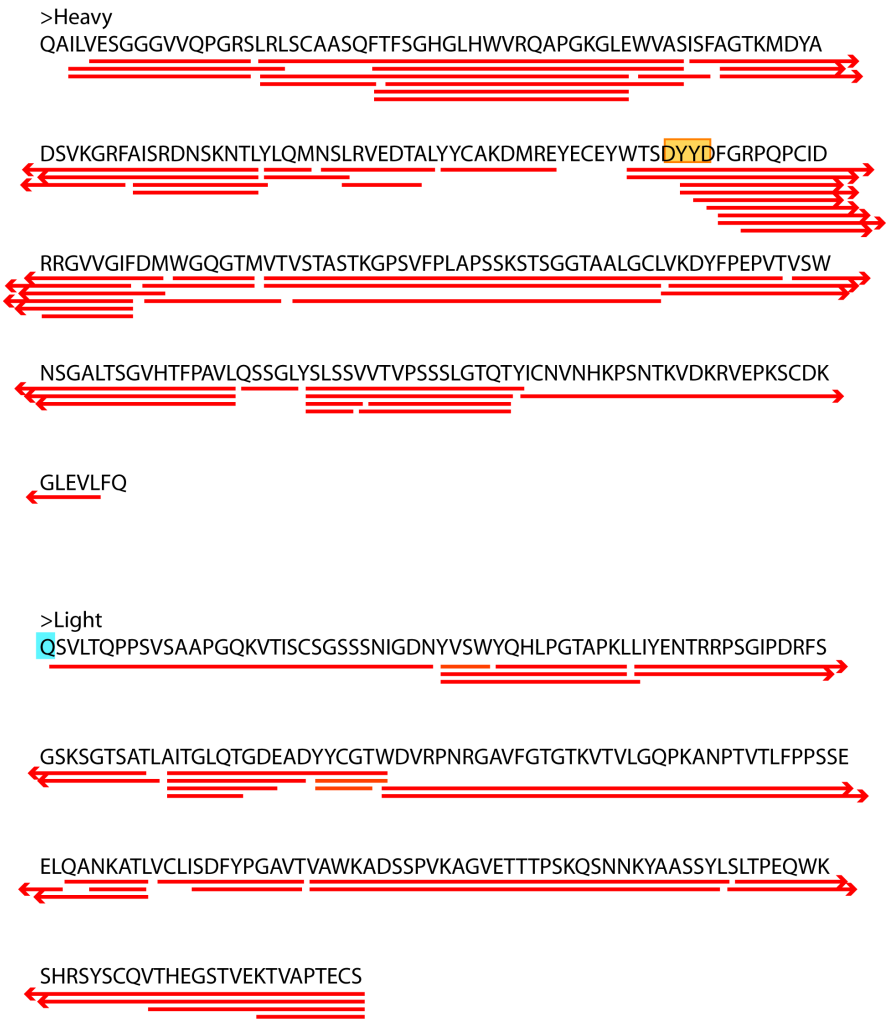

Figure C.S5. Peptide coverage map for VRC26K (mature) Fab. The primary amino acid sequence for the Fab region of the VRC26K heavy and light chains is shown. Red lines beneath the sequence indicate pepsin fragments identified by tandem mass spectrometry. The yellow box highlights the sulfation motif. Blue box indicates an ammonia loss on the glutamine residue.

References

1. **Barré-Sinoussi F**, **Chermann JC**, **Rey F**, **Nugeyre MT**, **Chamaret S**, **Gruest J**, **Dauguet C**, **Axler-Blin C**, **Vézinet-Brun F**, **Rouzioux C**, **Rozenbaum W**, **Montagnier L**. 1983. Isolation of a T-lymphotropic retrovirus from a patient at risk for acquired immune deficiency syndrome (AIDS). Science **220**:868–871.
2. **Gallo RC**, **Sarin PS**, **Gelmann EP**, **Robert-Guroff M**, **Richardson E**, **Kalyanaraman VS**, **Mann D**, **Sidhu GD**, **Stahl RE**, **Zolla-Pazner S**, **Leibowitch J**, **Popovic M**. 1983. Isolation of human T-cell leukemia virus in acquired immune deficiency syndrome (AIDS). Science **220**:865–867.
3. **Centers for Disease Control (CDC)**. 1981. Kaposi's sarcoma and Pneumocystis pneumonia among homosexual men--New York City and California. MMWR Morb. Mortal. Wkly. Rep. **30**:305–308.
4. **Centers for Disease Control (CDC)**. 1982. A cluster of Kaposi's sarcoma and Pneumocystis carinii pneumonia among homosexual male residents of Los Angeles and Orange Counties, California. MMWR Morb. Mortal. Wkly. Rep. **31**:305–307.
5. **UNAIDS JUNPOHA**. 2013. Global Report 1–272.
6. **Levy JA**. 2007. HIV and The Pathogenesis of AIDS, 3rd ed. American Society for Microbiology Press, Washington, D.C.
7. **Hu WS**, **Temin HM**. 1990. Genetic consequences of packaging two RNA genomes in one retroviral particle: pseudodiploidy and high rate of genetic recombination. Proc. Natl. Acad. Sci. U.S.A. **87**:1556–1560.
8. **Sundquist WI**, **Kräusslich H-G**. 2012. HIV-1 assembly, budding, and maturation. Cold Spring Harb Perspect Med **2**:a006924.
9. **Freed EO**. 2004. HIV-1 and the host cell: an intimate association. Trends in Microbiology **12**:170–177.
10. **Montagnier L**, **Clavel F**, **Krust B**, **Chamaret S**, **Rey F**, **Barré-Sinoussi F**, **Chermann JC**. 1985. Identification and antigenicity of the major envelope glycoprotein of lymphadenopathy-associated virus. Virology **144**:283–289.
11. **Allan JS**, **Coligan JE**, **Barin F**, **McLane MF**, **Sodroski JG**, **Rosen CA**, **Haseltine WA**, **Lee TH**, **Essex M**. 1985. Major glycoprotein antigens that induce antibodies in AIDS patients are encoded by HTLV-III. Science **228**:1091–1094.
12. **Wyatt R**. 1998. The HIV-1 Envelope Glycoproteins: Fusogens,

Antigens, and Immunogens. Science **280**:1884–1888.
13. **Checkley MA**, **Luttge BG**, **Freed EO**. 2011. HIV-1 envelope glycoprotein biosynthesis, trafficking, and incorporation. Journal of Molecular Biology **410**:582–608.
14. **Zhu P**, **Liu J**, **Bess J**, **Chertova E**, **Lifson JD**, **Grisé H**, **Ofek GA**, **Taylor KA**, **Roux KH**. 2006. Distribution and three-dimensional structure of AIDS virus envelope spikes. Nature **441**:847–852.
15. **Malim MH**, **Emerman M**. 2008. HIV-1 accessory proteins--ensuring viral survival in a hostile environment. Cell Host and Microbe **3**:388–398.
16. **Harris RS**, **Hultquist JF**, **Evans DT**. 2012. The restriction factors of human immunodeficiency virus. Journal of Biological Chemistry **287**:40875–40883.
17. **Center RJ**, **Leapman RD**, **Lebowitz J**, **Arthur LO**, **Earl PL**, **Moss B**. 2002. Oligomeric structure of the human immunodeficiency virus type 1 envelope protein on the virion surface. J. Virol. **76**:7863–7867.
18. **Wyatt R**, **Kwong PD**, **Desjardins E**, **Sweet RW**, **Robinson J**, **Hendrickson WA**, **Sodroski JG**. 1998. The antigenic structure of the HIV gp120 envelope glycoprotein. Nature **393**:705–711.
19. **Merk A**, **Subramaniam S**. 2013. HIV-1 envelope glycoprotein structure. Current Opinion in Structural Biology 1–9.
20. **Wilen CB**, **Tilton JC**, **Doms RW**. 2012. HIV: cell binding and entry. Cold Spring Harb Perspect Med **2**.
21. **Barin F**, **McLane MF**, **Allan JS**, **Lee TH**, **Groopman JE**, **Essex M**. 1985. Virus envelope protein of HTLV-III represents major target antigen for antibodies in AIDS patients. Science **228**:1094–1096.
22. **Klasse PJ**. 2012. The molecular basis of HIV entry. Cell Microbiol **14**:1183–1192.
23. **Yang X**, **Kurteva S**, **Ren X**, **Lee S**, **Sodroski J**. 2005. Stoichiometry of envelope glycoprotein trimers in the entry of human immunodeficiency virus type 1. J. Virol. **79**:12132–12147.
24. **Magnus C**, **Rusert P**, **Bonhoeffer S**, **Trkola A**, **Regoes RR**. 2009. Estimating the Stoichiometry of Human Immunodeficiency Virus Entry.
25. **Kwong PD**, **Wyatt R**, **Robinson J**, **Sweet RW**, **Sodroski J**, **Hendrickson WA**. 1998. Structure of an HIV gp120 envelope glycoprotein in complex with the CD4 receptor and a neutralizing

human antibody. Nature **393**:648–659.
26. **Korber B**, **Gaschen B**, **Yusim K**, **Thakallapally R**, **Kesmir C**, **Detours V**. 2001. Evolutionary and immunological implications of contemporary HIV-1 variation. Br. Med. Bull. **58**:19–42.
27. **Hu G**, **Liu J**, **Taylor KA**, **Roux KH**. 2011. Structural Comparison of HIV-1 Envelope Spikes with and without the V1/V2 Loop. J. Virol. **85**:2741–2750.
28. **White TA**, **Bartesaghi A**, **Borgnia MJ**, **Meyerson JR**, **la Cruz de MJV**, **Bess JW**, **Nandwani R**, **Hoxie JA**, **Lifson JD**, **Milne JLS**, **Subramaniam S**. 2010. Molecular Architectures of Trimeric SIV and HIV-1 Envelope Glycoproteins on Intact Viruses: Strain-Dependent Variation in Quaternary Structure. PLoS Pathogens **6**:e1001249.
29. **Gorny MK**, **Stamatatos L**, **Volsky B**, **Revesz K**, **Williams C**, **Wang X-H**, **Cohen S**, **Staudinger R**, **Zolla-Pazner S**. 2005. Identification of a new quaternary neutralizing epitope on human immunodeficiency virus type 1 virus particles. J. Virol. **79**:5232–5237.
30. **Walker LM**, **Phogat SK**, **Chan-Hui PY**, **Wagner D**, **Phung P**, **Goss JL**, **Wrin T**, **Simek MD**, **Fling S**, **Mitcham JL**, **Lehrman JK**, **Priddy FH**, **Olsen OA**, **Frey SM**, **Hammond PW**, **Protocol G Principal Investigators**, **Kaminsky S**, **Zamb T**, **Moyle M**, **Koff WC**, **Poignard P**, **Burton DR**. 2009. Broad and Potent Neutralizing Antibodies from an African Donor Reveal a New HIV-1 Vaccine Target. Science **326**:285–289.
31. **Land A**, **Zonneveld D**, **Braakman I**. 2003. Folding of HIV-1 envelope glycoprotein involves extensive isomerization of disulfide bonds and conformation-dependent leader peptide cleavage. FASEB J. **17**:1058–1067.
32. Visual Science. Visual Science.
33. **Liu J**, **Bartesaghi A**, **Borgnia MJ**, **Sapiro G**, **Subramaniam S**. 2008. Molecular architecture of native HIV-1 gp120 trimers. Cellular and Molecular Immunology **455**:109–113.
34. **Binley JM**, **Ban YEA**, **Crooks ET**, **Eggink D**, **Osawa K**, **Schief WR**, **Sanders RW**. 2010. Role of Complex Carbohydrates in Human Immunodeficiency Virus Type 1 Infection and Resistance to Antibody Neutralization. J. Virol. **84**:5637–5655.
35. **Pancera M**, **Majeed S**, **Ban YEA**, **Chen L**, **Huang CC**, **Kong L**, **Kwon YD**, **Stuckey J**, **Zhou T**, **Robinson JE**, **Schief WR**, **Sodroski J**, **Wyatt R**, **Kwong PD**. 2010. Structure of HIV-1

gp120 with gp41-interactive region reveals layered envelope architecture and basis of conformational mobility. Proceedings of the National Academy of Sciences **107**:1166–1171.

36. **Decker JM**, **Bibollet-Ruche F**, **Wei X**, **Wang S**, **Levy DN**, **Wang W**, **Delaporte E**, **Peeters M**, **Derdeyn CA**, **Allen S**, **Hunter E**, **Saag MS**, **Hoxie JA**, **Hahn BH**, **Kwong PD**, **Robinson JE**, **Shaw GM**. 2005. Antigenic conservation and immunogenicity of the HIV coreceptor binding site. J. Exp. Med. **201**:1407–1419.
37. **Buzon V**, **Natrajan G**, **Schibli D**, **Campelo F**, **Kozlov MM**, **Weissenhorn W**. 2010. Crystal structure of HIV-1 gp41 including both fusion peptide and membrane proximal external regions. PLoS Pathogens **6**:e1000880.
38. **Tran EEH**, **Borgnia MJ**, **Kuybeda O**, **Schauder DM**, **Bartesaghi A**, **Frank GA**, **Sapiro G**, **Milne JLS**, **Subramaniam S**. 2012. Structural Mechanism of Trimeric HIV-1 Envelope Glycoprotein Activation. PLoS Pathogens **8**:e1002797.
39. **Rolland M**, **Nickle DC**, **Mullins JI**. 2007. HIV-1 group M conserved elements vaccine. PLoS Pathogens **3**:e157.
40. **Arts EJ**, **Hazuda DJ**. 2012. HIV-1 antiretroviral drug therapy. Cold Spring Harb Perspect Med **2**:a007161.
41. **Guay LA**, **Musoke P**, **Fleming T**, **Bagenda D**, **Allen M**, **Nakabiito C**, **Sherman J**, **Bakaki P**, **Ducar C**, **Deseyve M**, **Emel L**, **Mirochnick M**, **Fowler MG**, **Mofenson L**, **Miotti P**, **Dransfield K**, **Bray D**, **Mmiro F**, **Jackson JB**. 1999. Intrapartum and neonatal single-dose nevirapine compared with zidovudine for prevention of mother-to-child transmission of HIV-1 in Kampala, Uganda: HIVNET 012 randomised trial. The Lancet **354**:795–802.
42. **Kilewo C**, **Karlsson K**, **Ngarina M**, **Massawe A**, **Lyamuya E**, **Swai A**, **Lipyoga R**, **Mhalu F**, **Biberfeld G**, **Mitra Plus Study Team**. 2009. Prevention of mother-to-child transmission of HIV-1 through breastfeeding by treating mothers with triple antiretroviral therapy in Dar es Salaam, Tanzania: the Mitra Plus study. J. Acquir. Immune Defic. Syndr. **52**:406–416.
43. **Cohen MS**, **Chen YQ**, **McCauley M**, **Gamble T**, **Hosseinipour MC**, **Kumarasamy N**, **Hakim JG**, **Kumwenda J**, **Grinsztejn B**, **Pilotto JHS**, **Godbole SV**, **Mehendale S**, **Chariyalertsak S**, **Santos BR**, **Mayer KH**, **Hoffman IF**, **Eshleman SH**, **Piwowar-Manning E**, **Wang L**, **Makhema J**, **Mills LA**, **de Bruyn G**, **Sanne I**, **Eron J**, **Gallant J**, **Havlir D**, **Swindells S**, **Ribaudo H**, **Elharrar V**, **Burns D**, **Taha TE**, **Nielsen-Saines K**, **Celentano D**, **Essex**

M, **Fleming TR**, **HPTN 052 Study Team**. 2011. Prevention of HIV-1 infection with early antiretroviral therapy. N Engl J Med **365**:493–505.

44. **Grant RM**, **Lama JR**, **Anderson PL**, **McMahan V**, **Liu AY**, **Vargas L**, **Goicochea P**, **Casapía M**, **Guanira-Carranza JV**, **Ramirez-Cardich ME**, **Montoya-Herrera O**, **Fernández T**, **Veloso VG**, **Buchbinder SP**, **Chariyalertsak S**, **Schechter M**, **Bekker L-G**, **Mayer KH**, **Kallás EG**, **Amico KR**, **Mulligan K**, **Bushman LR**, **Hance RJ**, **Ganoza C**, **Defechereux P**, **Postle B**, **Wang F**, **McConnell JJ**, **Zheng J-H**, **Lee J**, **Rooney JF**, **Jaffe HS**, **Martinez AI**, **Burns DN**, **Glidden DV**, **iPrEx Study Team**. 2010. Preexposure chemoprophylaxis for HIV prevention in men who have sex with men. N Engl J Med **363**:2587–2599.

45. **Baeten JM**, **Donnell D**, **Ndase P**, **Mugo NR**, **Campbell JD**, **Wangisi J**, **Tappero JW**, **Bukusi EA**, **Cohen CR**, **Katabira E**, **Ronald A**, **Tumwesigye E**, **Were E**, **Fife KH**, **Kiarie J**, **Farquhar C**, **John-Stewart G**, **Kakia A**, **Odoyo J**, **Mucunguzi A**, **Nakku-Joloba E**, **Twesigye R**, **Ngure K**, **Apaka C**, **Tamooh H**, **Gabona F**, **Mujugira A**, **Panteleeff D**, **Thomas KK**, **Kidoguchi L**, **Krows M**, **Revall J**, **Morrison S**, **Haugen H**, **Emmanuel-Ogier M**, **Ondrejcek L**, **Coombs RW**, **Frenkel L**, **Hendrix C**, **Bumpus NN**, **Bangsberg D**, **Haberer JE**, **Stevens WS**, **Lingappa JR**, **Celum C**, **Partners PrEP Study Team**. 2012. Antiretroviral prophylaxis for HIV prevention in heterosexual men and women. N Engl J Med **367**:399–410.

46. **Thigpen MC**, **Kebaabetswe PM**, **Paxton LA**, **Smith DK**, **Rose CE**, **Segolodi TM**, **Henderson FL**, **Pathak SR**, **Soud FA**, **Chillag KL**, **Mutanhaurwa R**, **Chirwa LI**, **Kasonde M**, **Abebe D**, **Buliva E**, **Gvetadze RJ**, **Johnson S**, **Sukalac T**, **Thomas VT**, **Hart C**, **Johnson JA**, **Malotte CK**, **Hendrix CW**, **Brooks JT**, **TDF2 Study Group**. 2012. Antiretroviral preexposure prophylaxis for heterosexual HIV transmission in Botswana. N Engl J Med **367**:423–434.

47. **Bailey RC**, **Moses S**, **Parker CB**, **Agot K**, **Maclean I**, **Krieger JN**, **Williams CFM**, **Campbell RT**, **Ndinya-Achola JO**. 2007. Male circumcision for HIV prevention in young men in Kisumu, Kenya: a randomised controlled trial. Lancet **369**:643–656.

48. **Jia Z**, **Mao Y**, **Zhang F**, **Ruan Y**, **Ma Y**, **Li J**, **Guo W**, **Liu E**, **Dou Z**, **Zhao Y**, **Wang L**, **Li Q**, **Xie P**, **Tang H**, **Han J**, **Jin X**, **Xu J**, **Xiong R**, **Zhao D**, **Li P**, **Wang X**, **Wang L**, **Qing Q**, **Ding Z**, **Chen**

RY, **Liu Z**, **Shao Y**. 2013. Antiretroviral therapy to prevent HIV transmission in serodiscordant couples in China (2003-11): a national observational cohort study. Lancet **382**:1195–1203.

49. **Lockman S**, **Shapiro RL**, **Smeaton LM**, **Wester C**, **Thior I**, **Stevens L**, **Chand F**, **Makhema J**, **Moffat C**, **Asmelash A**, **Ndase P**, **Arimi P**, **van Widenfelt E**, **Mazhani L**, **Novitsky V**, **Lagakos S**, **Essex M**. 2007. Response to antiretroviral therapy after a single, peripartum dose of nevirapine. N Engl J Med **356**:135–147.
50. **Carr A**, **Cooper DA**. 2000. Adverse effects of antiretroviral therapy. The Lancet **356**:1423–1430.
51. **Larson HJ**, **Ghinai I**. 2011. Lessons from polio eradication. Cellular and Molecular Immunology **473**:446–447.
52. **Moss WJ**, **Griffin DE**. 2006. Global measles elimination. Nat Rev Micro **4**:900–908.
53. **Lehtinen M**, **Paavonen J**, **Wheeler CM**, **Jaisamrarn U**, **Garland SM**, **Castellsagué X**, **Skinner SR**, **Apter D**, **Naud P**, **Salmerón J**, **Chow S-N**, **Kitchener H**, **Teixeira JC**, **Hedrick J**, **Limson G**, **Szarewski A**, **Romanowski B**, **Aoki FY**, **Schwarz TF**, **Poppe WAJ**, **De Carvalho NS**, **Germar MJV**, **Peters K**, **Mindel A**, **De Sutter P**, **Bosch FX**, **David M-P**, **Descamps D**, **Struyf F**, **Dubin G**, **HPV PATRICIA Study Group**. 2012. Overall efficacy of HPV-16/18 AS04-adjuvanted vaccine against grade 3 or greater cervical intraepithelial neoplasia: 4-year end-of-study analysis of the randomised, double-blind PATRICIA trial. Lancet Oncol. **13**:89–99.
54. **Long EF**, **Owens DK**. 2011. The cost-effectiveness of a modestly effective HIV vaccine in the United States. Vaccine **29**:6113–6124.
55. **Mascola JR**, **Montefiori DC**. 2010. The Role of Antibodies in HIV Vaccines. Annu. Rev. Immunol. **28**:413–444.
56. **Berman PW**, **Gregory TJ**, **Riddle L**, **Nakamura GR**, **Champe MA**, **Porter JP**, **Wurm FM**, **Hershberg RD**, **Cobb EK**, **Eichberg JW**. 1990. Protection of chimpanzees from infection by HIV-1 after vaccination with recombinant glycoprotein gp120 but not gp160. Nature **345**:622–625.
57. **Berman PW**, **Murthy KK**, **Wrin T**, **Vennari JC**, **Cobb EK**, **Eastman DJ**, **Champe M**, **Nakamura GR**, **Davison D**, **Powell MF**, **Bussiere J**, **Francis DP**, **Matthews T**, **Gregory TJ**, **Obijeski JF**. 1996. Protection of MN-rgp120-immunized

chimpanzees from heterologous infection with a primary isolate of human immunodeficiency virus type 1. J INFECT DIS **173**:52–59.

58. **Flynn NM**, **Forthal DN**, **Harro CD**, **Judson FN**, **Mayer KH**, **Para MF**, **rgp120 HIV Vaccine Study Group**. 2005. Placebo-controlled phase 3 trial of a recombinant glycoprotein 120 vaccine to prevent HIV-1 infection. J INFECT DIS **191**:654–665.
59. **Pitisuttithum P**, **Gilbert P**, **Gurwith M**, **Heyward W**, **Martin M**, **van Griensven F**, **Hu D**, **Tappero JW**, **Choopanya K**, **Bangkok Vaccine Evaluation Group**. 2006. Randomized, double-blind, placebo-controlled efficacy trial of a bivalent recombinant glycoprotein 120 HIV-1 vaccine among injection drug users in Bangkok, Thailand. J INFECT DIS **194**:1661–1671.
60. **Wrin T**, **Nunberg JH**. 1994. HIV-1MN recombinant gp120 vaccine serum, which fails to neutralize primary isolates of HIV-1, does not antagonize neutralization by antibodies from infected individuals. AIDS **8**:1622–1623.
61. **Gilbert P**, **Wang M**, **Wrin T**, **Petropoulos C**, **Gurwith M**, **Sinangil F**, **D'Souza P**, **Rodriguez Chavez IR**, **DeCamp A**, **Giganti M**, **Berman PW**, **Self SG**, **Montefiori DC**. 2010. Magnitude and Breadth of a Nonprotective Neutralizing Antibody Response in an Efficacy Trial of a Candidate HIV-1 gp120 Vaccine. Journal of Infectious ….
62. **Buchbinder SP**, **Mehrotra DV**, **Duerr A**, **Fitzgerald DW**, **Mogg R**, **Li D**, **Gilbert PB**, **Lama JR**, **Marmor M**, **del Rio C**, **McElrath MJ**, **Casimiro DR**, **Gottesdiener KM**, **Chodakewitz JA**, **Corey L**, **Robertson MN**. 2008. Efficacy assessment of a cell-mediated immunity HIV-1 vaccine (the Step Study): a double-blind, randomised, placebo-controlled, test-of-concept trial. The Lancet **372**:1881–1893.
63. **Nitayaphan S**, **Pitisuttithum P**, **Karnasuta C**, **Eamsila C**, **de Souza M**, **Morgan P**, **Polonis V**, **Benenson M**, **VanCott T**, **Ratto-Kim S**, **Kim J**, **Thapinta D**, **Garner R**, **Bussaratid V**, **Singharaj P**, **el-Habib R**, **Gurunathan S**, **Heyward W**, **Birx D**, **McNeil J**, **Brown AE**, **Thai AIDS Vaccine Evaluation Group**. 2004. Safety and immunogenicity of an HIV subtype B and E prime-boost vaccine combination in HIV-negative Thai adults. J INFECT DIS **190**:702–706.
64. **Rerks-Ngarm S**, **Pitisuttithum P**, **Nitayaphan S**, **Kaewkungwal J**, **Chiu J**, **Paris R**, **Premsri N**, **Namwat C**, **de Souza M**, **Adams E**, **Benenson M**, **Gurunathan S**, **Tartaglia J**, **McNeil JG**,

Francis DP, **Stablein D**, **Birx DL**, **Chunsuttiwat S**, **Khamboonruang C**, **Thongcharoen P**, **Robb ML**, **Michael NL**, **Kunasol P**, **Kim JH**. 2009. Vaccination with ALVAC and AIDSVAX to Prevent HIV-1 Infection in Thailand. N Engl J Med **361**:2209–2220.

65. **Haynes BF**, **Gilbert PB**, **McElrath MJ**, **Zolla-Pazner S**, **Tomaras GD**, **Alam SM**, **Evans DT**, **Montefiori DC**, **Karnasuta C**, **Sutthent R**, **Liao H-X**, **DeVico AL**, **Lewis GK**, **Williams C**, **Pinter A**, **Fong Y**, **Janes H**, **DeCamp A**, **Huang Y**, **Rao M**, **Billings E**, **Karasavvas N**, **Robb ML**, **Ngauy V**, **de Souza MS**, **Paris R**, **Ferrari G**, **Bailer RT**, **Soderberg KA**, **Andrews C**, **Berman PW**, **Frahm N**, **De Rosa SC**, **Alpert MD**, **Yates NL**, **Shen X**, **Koup RA**, **Pitisuttithum P**, **Kaewkungwal J**, **Nitayaphan S**, **Rerks-Ngarm S**, **Michael NL**, **Kim JH**. 2012. Immune-correlates analysis of an HIV-1 vaccine efficacy trial. N Engl J Med **366**:1275–1286.

66. **Liao H-X**, **Bonsignori M**, **Alam SM**, **McLellan JS**, **Tomaras GD**, **Moody MA**, **Kozink DM**, **Hwang K-K**, **Chen X**, **Tsao C-Y**, **Liu P**, **Lu X**, **Parks RJ**, **Montefiori DC**, **Ferrari G**, **Pollara J**, **Rao M**, **Peachman KK**, **Santra S**, **Letvin NL**, **Karasavvas N**, **Yang Z-Y**, **Dai K**, **Pancera M**, **Gorman J**, **Wiehe K**, **Nicely NI**, **Rerks-Ngarm S**, **Nitayaphan S**, **Kaewkungwal J**, **Pitisuttithum P**, **Tartaglia J**, **Sinangil F**, **Kim JH**, **Michael NL**, **Kepler TB**, **Kwong PD**, **Mascola JR**, **Nabel GJ**, **Pinter A**, **Zolla-Pazner S**, **Haynes BF**. 2013. Vaccine induction of antibodies against a structurally heterogeneous site of immune pressure within HIV-1 envelope protein variable regions 1 and 2. Immunity **38**:176–186.

67. **Rolland M**, **Edlefsen PT**, **Larsen BB**, **Tovanabutra S**, **Sanders-Buell E**, **Hertz T**, **deCamp AC**, **Carrico C**, **Menis S**, **Magaret CA**, **Ahmed H**, **Juraska M**, **Chen L**, **Konopa P**, **Nariya S**, **Stoddard JN**, **Wong K**, **Zhao H**, **Deng W**, **Maust BS**, **Bose M**, **Howell S**, **Bates A**, **Lazzaro M**, **O'Sullivan A**, **Lei E**, **Bradfield A**, **Ibitamuno G**, **Assawadarachai V**, **O'Connell RJ**, **deSouza MS**, **Nitayaphan S**, **Rerks-Ngarm S**, **Robb ML**, **McLellan JS**, **Georgiev I**, **Kwong PD**, **Carlson JM**, **Michael NL**, **Schief WR**, **Gilbert PB**, **Mullins JI**, **Kim JH**. 2012. Increased HIV-1 vaccine efficacy against viruses with genetic signatures in Env V2. Cellular and Molecular Immunology **490**:417–420.

68. **Deeks SG**, **Walker BD**. 2007. Human immunodeficiency virus controllers: mechanisms of durable virus control in the absence of

antiretroviral therapy. Immunity **27**:406–416.
69. **Davenport MP**, **Petravic J**. 2010. CD8+ T cell control of HIV--a known unknown. PLoS Pathogens **6**:e1000728.
70. **Korber BT**, **Letvin NL**, **Haynes BF**. 2009. T-cell vaccine strategies for human immunodeficiency virus, the virus with a thousand faces. J. Virol. **83**:8300–8314.
71. **Siliciano RF**, **Greene WC**. 2011. HIV latency. Cold Spring Harb Perspect Med **1**:a007096.
72. **Shibata R**, **Igarashi T**, **Haigwood N**, **Buckler White A**, **Ogert R**, **Ross W**, **Willey R**, **Cho MW**, **Martin MA**. 1999. Neutralizing antibody directed against the HIV-1 envelope glycoprotein can completely block HIV-1/SIV chimeric virus infections of macaque monkeys. Nature Medicine **5**:204–210.
73. **Parren PW**, **Marx PA**, **Hessell AJ**, **Luckay A**, **Harouse J**, **Cheng-Mayer C**, **Moore JP**, **Burton DR**. 2001. Antibody protects macaques against vaginal challenge with a pathogenic R5 simian/human immunodeficiency virus at serum levels giving complete neutralization in vitro. J. Virol. **75**:8340–8347.
74. **Hessell AJ**, **Poignard P**, **Hunter M**, **Hangartner L**, **Tehrani DM**, **Bleeker WK**, **Parren PWHI**, **Marx PA**, **Burton DR**. 2009. Effective, low-titer antibody protection against low-dose repeated mucosal SHIV challenge in macaques. Nature Medicine 1–5.
75. **Hessell AJ**, **Rakasz EG**, **Poignard P**, **Hangartner L**, **Landucci G**, **Forthal DN**, **Koff WC**, **Watkins DI**, **Burton DR**. 2009. Broadly Neutralizing Human Anti-HIV Antibody 2G12 Is Effective in Protection against Mucosal SHIV Challenge Even at Low Serum Neutralizing Titers. PLoS Pathogens **5**:e1000433.
76. **Plotkin SA**. 2001. Immunologic correlates of protection induced by vaccination. Pediatr. Infect. Dis. J. **20**:63–75.
77. **Pantophlet R**, **Burton DR**. 2006. GP120: target for neutralizing HIV-1 antibodies. Annu. Rev. Immunol. **24**:739–769.
78. **Bar KJ**, **Tsao C-Y**, **Iyer SS**, **Decker JM**, **Yang Y**, **Bonsignori M**, **Chen X**, **Hwang K-K**, **Montefiori DC**, **Liao H-X**, **Hraber P**, **Fischer W**, **Li H**, **Wang S**, **Sterrett S**, **Keele BF**, **Ganusov VV**, **Perelson AS**, **Korber BT**, **Georgiev I**, **McLellan JS**, **Pavlicek JW**, **Gao F**, **Haynes BF**, **Hahn BH**, **Kwong PD**, **Shaw GM**. 2012. Early low-titer neutralizing antibodies impede HIV-1 replication and select for virus escape. PLoS Pathogens **8**:e1002721.
79. **McMichael AJ**, **Borrow P**, **Tomaras GD**, **Goonetilleke N**, **Haynes BF**. 2009. The immune response during acute HIV-1

infection: clues for vaccine development. Nature Publishing Group **10**:11–23.

80. **Mikell I**, **Sather DN**, **Kalams SA**, **Altfeld M**, **Alter G**, **Stamatatos L**. 2011. Characteristics of the Earliest Cross-Neutralizing Antibody Response to HIV-1. PLoS Pathogens **7**:e1001251.
81. **Walker LM**, **Simek MD**, **Priddy F**, **Gach JS**, **Wagner D**, **Zwick MB**, **Phogat SK**, **Poignard P**, **Burton DR**. 2010. A Limited Number of Antibody Specificities Mediate Broad and Potent Serum Neutralization in Selected HIV-1 Infected Individuals. PLoS Pathogens **6**:e1001028.
82. **Piantadosi A**, **Panteleeff D**, **Blish CA**, **Baeten JM**, **Jaoko W**, **McClelland RS**, **Overbaugh J**. 2009. Breadth of Neutralizing Antibody Response to Human Immunodeficiency Virus Type 1 Is Affected by Factors Early in Infection but Does Not Influence Disease Progression. J. Virol. **83**:10269–10274.
83. **Doria-Rose NA**, **Klein RM**, **Daniels MG**, **O'Dell S**, **Nason M**, **Lapedes A**, **Bhattacharya T**, **Migueles SA**, **Wyatt RT**, **Korber BT**, **Mascola JR**, **Connors M**. 2010. Breadth of Human Immunodeficiency Virus-Specific Neutralizing Activity in Sera: Clustering Analysis and Association with Clinical Variables. J. Virol. **84**:1631–1636.
84. **Sather DN**, **Armann J**, **Ching LK**, **Mavrantoni A**, **Sellhorn G**, **Caldwell Z**, **Yu X**, **Wood B**, **Self S**, **Kalams S**, **Stamatatos L**. 2008. Factors Associated with the Development of Cross-Reactive Neutralizing Antibodies during Human Immunodeficiency Virus Type 1 Infection. J. Virol. **83**:757–769.
85. **Cortez V**, **Odem-Davis K**, **McClelland RS**, **Jaoko W**, **Overbaugh J**. 2012. HIV-1 superinfection in women broadens and strengthens the neutralizing antibody response. PLoS Pathogens **8**:e1002611.
86. **van Gils MJ**, **Euler Z**, **Schweighardt B**, **Wrin T**, **Schuitemaker H**. 2009. Prevalence of cross-reactive HIV-1-neutralizing activity in HIV-1-infected patients with rapid or slow disease progression. AIDS **23**:2405–2414.
87. **Moore PL**, **Gray ES**, **Wibmer CK**, **Bhiman JN**, **Nonyane M**, **Sheward DJ**, **Hermanus T**, **Bajimaya S**, **Tumba NL**, **Abrahams M-R**, **Lambson BE**, **Ranchobe N**, **Ping L**, **Ngandu N**, **Abdool Karim Q**, **Abdool Karim SS**, **Swanstrom RI**, **Seaman MS**, **Williamson C**, **Morris L**. 2012. Evolution of an HIV glycan-dependent broadly neutralizing antibody epitope through immune

escape. Nature Medicine **18**:1688–1692.
88. **Wei X**, **Decker JM**, **Wang S**, **Hui H**, **Kappes JC**, **Wu X**, **Salazar-Gonzalez JF**, **Salazar MG**, **Kilby JM**, **Saag MS**, **Komarova NL**, **Nowak MA**, **Hahn BH**, **Kwong PD**, **Shaw GM**. 2003. Antibody neutralization and escape by HIV-1. Nature **422**:307–312.
89. **Bosch KA**, **Rainwater S**, **Jaoko W**, **Overbaugh J**. 2010. Temporal analysis of HIV envelope sequence evolution and antibody escape in a subtype A-infected individual with a broad neutralizing antibody response. Virology **398**:115–124.
90. **Bunnik EM**, **Pisas L**, **van Nuenen AC**, **Schuitemaker H**. 2008. Autologous Neutralizing Humoral Immunity and Evolution of the Viral Envelope in the Course of Subtype B Human Immunodeficiency Virus Type 1 Infection. J. Virol. **82**:7932–7941.
91. **Rong R**, **Li B**, **Lynch RM**, **Haaland RE**, **Murphy MK**, **Mulenga J**, **Allen SA**, **Pinter A**, **Shaw GM**, **Hunter E**, **Robinson JE**, **Gnanakaran S**, **Derdeyn CA**. 2009. Escape from Autologous Neutralizing Antibodies in Acute/Early Subtype C HIV-1 Infection Requires Multiple Pathways. PLoS Pathogens **5**:e1000594.
92. **Euler Z**, **van Gils MJ**, **Bunnik EM**, **Phung P**, **Schweighardt B**, **Wrin T**, **Schuitemaker H**. 2010. Cross-Reactive Neutralizing Humoral Immunity Does Not Protect from HIV Type 1 Disease Progression. J INFECT DIS **201**:1045–1053.
93. **van Gils MJ**, **Bunnik EM**, **Burger JA**, **Jacob Y**, **Schweighardt B**, **Wrin T**, **Schuitemaker H**. 2010. Rapid escape from preserved cross-reactive neutralizing humoral immunity without loss of viral fitness in HIV-1-infected progressors and long-term nonprogressors. J. Virol. **84**:3576–3585.
94. **Wu X**, **Wang C**, **O'Dell S**, **Li Y**, **Keele BF**, **Yang Z**, **Imamichi H**, **Doria-Rose N**, **Hoxie JA**, **Connors M**, **Shaw GM**, **Wyatt RT**, **Mascola JR**. 2012. Selection pressure on HIV-1 envelope by broadly neutralizing antibodies to the conserved CD4-binding site. J. Virol. **86**:5844–5856.
95. **Lynch RM**, **Tran L**, **Wu X**, **Li Y**, **Lee B**, **Mascola J**. 2012. Characterizing the fitness cost of viral escape from the HIV-1 broadly neutralizing monoclonal antibody VRC01. Retrovirology **9**:P87.
96. **Abrahams M-R**, **Anderson JA**, **Giorgi EE**, **Seoighe C**, **Mlisana K**, **Ping LH**, **Athreya GS**, **Treurnicht FK**, **Keele BF**, **Wood N**, **Salazar-Gonzalez JF**, **Bhattacharya T**, **Chu H**, **Hoffman I**, **Galvin S**, **Mapanje C**, **Kazembe P**, **Thebus R**, **Fiscus S**, **Hide**

W, **Cohen MS**, **Karim SA**, **Haynes BF**, **Shaw GM**, **Hahn BH**, **Korber BT**, **Swanstrom R**, **Williamson C**, **CAPRISA Acute Infection Study Team**, **Center for HIV-AIDS Vaccine Immunology Consortium**. 2009. Quantitating the multiplicity of infection with human immunodeficiency virus type 1 subtype C reveals a non-poisson distribution of transmitted variants. J. Virol. **83**:3556–3567.

97. **Haaland RE**, **Hawkins PA**, **Salazar-Gonzalez J**, **Johnson A**, **Tichacek A**, **Karita E**, **Manigart O**, **Mulenga J**, **Keele BF**, **Shaw GM**, **Hahn BH**, **Allen SA**, **Derdeyn CA**, **Hunter E**. 2009. Inflammatory genital infections mitigate a severe genetic bottleneck in heterosexual transmission of subtype A and C HIV-1. PLoS Pathogens **5**:e1000274.

98. **Salazar-Gonzalez JF**, **Bailes E**, **Pham KT**, **Salazar MG**, **Guffey MB**, **Keele BF**, **Derdeyn CA**, **Farmer P**, **Hunter E**, **Allen S**, **Manigart O**, **Mulenga J**, **Anderson JA**, **Swanstrom R**, **Haynes BF**, **Athreya GS**, **Korber BTM**, **Sharp PM**, **Shaw GM**, **Hahn BH**. 2008. Deciphering human immunodeficiency virus type 1 transmission and early envelope diversification by single-genome amplification and sequencing. J. Virol. **82**:3952–3970.

99. **Eichberg JW**, **Murthy KK**, **Ward RH**, **Prince AM**. 1992. Prevention of HIV infection by passive immunization with HIVIG or CD4-IgG. AIDS Res. Hum. Retroviruses **8**:1515.

100. **Burton DR**, **Hessell AJ**, **Keele BF**, **Klasse PJ**, **Ketas TA**, **Moldt B**, **Dunlop DC**, **Poignard P**, **Doyle LA**, **Cavacini L**, **Veazey RS**, **Moore JP**. 2011. Limited or no protection by weakly or nonneutralizing antibodies against vaginal SHIV challenge of macaques compared with a strongly neutralizing antibody. Proceedings of the National Academy of Sciences **108**:11181–11186.

101. **Lynch JB**, **Nduati R**, **Blish CA**, **Richardson BA**, **Mabuka JM**, **Jalalian-Lechak Z**, **John-Stewart G**, **Overbaugh J**. 2011. The Breadth and Potency of Passively Acquired Human Immunodeficiency Virus Type 1-Specific Neutralizing Antibodies Do Not Correlate with the Risk of Infant Infection. J. Virol. **85**:5252–5261.

102. **Wu X**, **Parast AB**, **Richardson BA**, **Nduati R**, **John-Stewart G**, **Mbori-Ngacha D**, **Rainwater SMJ**, **Overbaugh J**. 2006. Neutralization escape variants of human immunodeficiency virus type 1 are transmitted from mother to infant. J. Virol. **80**:835–844.

103. **Ronen K**, **McCoy CO**, **Matsen FA**, **Boyd DF**, **Emery S**, **Odem-Davis K**, **Jaoko W**, **Mandaliya K**, **McClelland RS**, **Richardson BA**, **Overbaugh J**. 2013. HIV-1 Superinfection Occurs Less Frequently Than Initial Infection in a Cohort of High-Risk Kenyan Women. PLoS Pathogens **9**:e1003593.
104. **Redd AD**, **Mullis CE**, **Serwadda D**, **Kong X**, **Martens C**, **Ricklefs SM**, **Tobian AAR**, **Xiao C**, **Grabowski MK**, **Nalugoda F**, **Kigozi G**, **Laeyendecker O**, **Kagaayi J**, **Sewankambo N**, **Gray RH**, **Porcella SF**, **Wawer MJ**, **Quinn TC**. 2012. The rates of HIV superinfection and primary HIV incidence in a general population in Rakai, Uganda. J INFECT DIS **206**:267–274.
105. **Piantadosi A**, **Chohan B**, **Chohan V**, **McClelland RS**, **Overbaugh J**. 2007. Chronic HIV-1 infection frequently fails to protect against superinfection. PLoS Pathogens **3**:e177.
106. **Blish CA**, **Dogan OC**, **Derby NR**, **Nguyen M-A**, **Chohan B**, **Richardson BA**, **Overbaugh J**. 2008. Human immunodeficiency virus type 1 superinfection occurs despite relatively robust neutralizing antibody responses. J. Virol. **82**:12094–12103.
107. **Siliciano RF**, **Finzi D**, **Blankson J**, **Siliciano JD**, **Margolick JB**, **Chadwick K**, **Pierson T**, **Smith K**, **Lisziewicz J**, **Lori F**, **Flexner C**, **Quinn TC**, **Chaisson RE**, **Rosenberg E**, **Walker B**, **Gange S**, **Gallant J**. 1999. Latent infection of CD4+ T cells provides a mechanism for lifelong persistence of HIV-1, even in patients on effective combination therapy - Nature Medicine. Nature Medicine **5**:512–517.
108. **Perelson AS**, **Essunger P**, **Cao Y**, **Vesanen M**, **Hurley A**, **Saksela K**, **Markowitz M**, **Ho DD**. 1997. Decay characteristics of HIV-1-infected compartments during combination therapy. Nature **387**:188–191.
109. **Malim MH**, **Bieniasz PD**. 2012. HIV Restriction Factors and Mechanisms of Evasion. Cold Spring Harb Perspect Med **2**:a006940.
110. **Overbaugh J**, **Morris L**. 2012. The Antibody Response against HIV-1. Cold Spring Harb Perspect Med **2**:a007039.
111. **Klatt NR**, **Brenchley JM**. 2010. Th17 cell dynamics in HIV infection. Current Opinion in HIV and AIDS **5**:135–140.
112. **Hu W-S**, **Hughes SH**. 2012. HIV-1 reverse transcription. Cold Spring Harb Perspect Med **2**.
113. **Coffin J**, **Swanstrom R**. 2013. HIV pathogenesis: dynamics and genetics of viral populations and infected cells. Cold Spring Harb

Perspect Med **3**:a012526.
114. **Worobey M**, **Gemmel M**, **Teuwen DE**, **Haselkorn T**, **Kunstman K**, **Bunce M**, **Muyembe J-J**, **Kabongo J-MM**, **Kalengayi RM**, **Van Marck E**, **Gilbert MTP**, **Wolinsky SM**. 2008. Direct evidence of extensive diversity of HIV-1 in Kinshasa by 1960. Cellular and Molecular Immunology **455**:661–664.
115. **Keele BF**. 2006. Chimpanzee Reservoirs of Pandemic and Nonpandemic HIV-1. Science **313**:523–526.
116. **Gao F**, **Bailes E**, **Robertson DL**, **Chen Y**, **Rodenburg CM**, **Michael SF**, **Cummins LB**, **Arthur LO**, **Peeters M**, **Shaw GM**, **Sharp PM**, **Hahn BH**. 1999. Origin of HIV-1 in the chimpanzee Pan troglodytes troglodytes. Nature **397**:436–441.
117. LANL HIV Sequence Database. Los Alamos National Laboratory.
118. **Sharp PM**, **Hahn BH**. 2011. Origins of HIV and the AIDS Pandemic. Cold Spring Harbor perspectives ….
119. **Gilbert MTP**, **Rambaut A**, **Wlasiuk G**, **Spira TJ**, **Pitchenik AE**, **Worobey M**. 2007. When HIV spread afar. Proceedings of the National Academy of Sciences **104**:18351–18352.
120. **Gaschen B**. 2002. Diversity Considerations in HIV-1 Vaccine Selection. Science **296**:2354–2360.
121. **Seaman MS**, **Janes H**, **Hawkins N**, **Grandpre LE**, **Devoy C**, **Giri A**, **Coffey RT**, **Harris L**, **Wood B**, **Daniels MG**, **Bhattacharya T**, **Lapedes A**, **Polonis VR**, **McCutchan FE**, **Gilbert PB**, **Self SG**, **Korber BT**, **Montefiori DC**, **Mascola JR**. 2010. Tiered Categorization of a Diverse Panel of HIV-1 Env Pseudoviruses for Assessment of Neutralizing Antibodies. J. Virol. **84**:1439–1452.
122. **Berger EA**, **Murphy PM**, **Farber JM**. 1999. Chemokine receptors as HIV-1 coreceptors: roles in viral entry, tropism, and disease. Annu. Rev. Immunol. **17**:657–700.
123. **Harouse JM**, **Kunsch C**, **Hartle HT**, **Laughlin MA**, **Hoxie JA**, **Wigdahl B**, **Gonzalez-Scarano F**. 1989. CD4-independent infection of human neural cells by human immunodeficiency virus type 1. J. Virol. **63**:2527–2533.
124. **Kolchinsky P**, **Kiprilov E**, **Bartley P**, **Rubinstein R**, **Sodroski J**. 2001. Loss of a single N-linked glycan allows CD4-independent human immunodeficiency virus type 1 infection by altering the position of the gp120 V1/V2 variable loops. J. Virol. **75**:3435–3443.
125. **Leonard CK**, **Spellman MW**, **Riddle L**, **Harris RJ**, **Thomas JN**, **Gregory TJ**. 1990. Assignment of intrachain disulfide bonds and

characterization of potential glycosylation sites of the type 1 recombinant human immunodeficiency virus envelope glycoprotein (gp120) expressed in Chinese hamster ovary cells. J. Biol. Chem. **265**:10373–10382.

126. **Benjelloun F**, **Lawrence P**, **Verrier B**, **Genin C**, **Paul S**. 2012. Role of human immunodeficiency virus type 1 envelope structure in the induction of broadly neutralizing antibodies. J. Virol. **86**:13152–13163.

127. **Wang W**, **Nie J**, **Prochnow C**, **Truong C**, **Jia Z**, **Wang S**, **Chen XS**, **Wang Y**. 2013. A systematic study of the N-glycosylation sites of HIV-1 envelope protein on infectivity and antibody-mediated neutralization. Retrovirology **10**:14.

128. **Go EP**, **Chang Q**, **Liao H-X**, **Sutherland LL**, **Alam SM**, **Haynes BF**, **Desaire H**. 2009. Glycosylation Site-Specific Analysis of Clade C HIV-1 Envelope Proteins. J. Proteome Res. **8**:4231–4242.

129. **Go EP**, **Irungu J**, **Zhang Y**, **Dalpathado DS**, **Liao H-X**, **Sutherland LL**, **Alam SM**, **Haynes BF**, **Desaire H**. 2008. Glycosylation Site-Specific Analysis of HIV Envelope Proteins (JR-FL and CON-S) Reveals Major Differences in Glycosylation Site Occupancy, Glycoform Profiles, and Antigenic Epitopes' Accessibility. J. Proteome Res. **7**:1660–1674.

130. **Go EP**, **Hewawasam G**, **Liao HX**, **Chen H**, **Ping LH**, **Anderson JA**, **Hua DC**, **Haynes BF**, **Desaire H**. 2011. Characterization of Glycosylation Profiles of HIV-1 Transmitted/Founder Envelopes by Mass Spectrometry. J. Virol. **85**:8270–8284.

131. **Doores KJ**, **Bonomelli C**, **Harvey DJ**, **Vasiljevic S**, **Dwek RA**, **Burton DR**, **Crispin M**, **Scanlan CN**. 2010. Envelope glycans of immunodeficiency virions are almost entirely oligomannose antigens. Proceedings of the National Academy of Sciences **107**:13800–13805.

132. **Pancera M**, **Shahzad-Ul-Hussan S**, **Doria-Rose NA**, **McLellan JS**, **Bailer RT**, **Dai K**, **Loesgen S**, **Louder MK**, **Staupe RP**, **Yang Y**, **Zhang B**, **Parks R**, **Eudailey J**, **Lloyd KE**, **Blinn J**, **Alam SM**, **Haynes BF**, **Amin MN**, **Wang L-X**, **Burton DR**, **Koff WC**, **Nabel GJ**, **Mascola JR**, **Bewley CA**, **Kwong PD**. 2013. Structural basis for diverse N-glycan recognition by HIV-1-neutralizing V1-V2-directed antibody PG16. Nat Struct Mol Biol **20**:804–813.

133. **Doores KJ**, **Burton DR**. 2010. Variable Loop Glycan

Dependency of the Broad and Potent HIV-1-Neutralizing Antibodies PG9 and PG16. J. Virol. **84**:10510–10521.

134. **Kong L**, **Sheppard NC**, **Stewart-Jones GBE**, **Robson CL**, **Chen H**, **Xu X**, **Krashias G**, **Bonomelli C**, **Scanlan CN**, **Kwong PD**, **Jeffs SA**, **Jones IM**, **Sattentau QJ**. 2010. Expression-System-Dependent Modulation of HIV-1 Envelope Glycoprotein Antigenicity and Immunogenicity. Journal of Molecular Biology **403**:131–147.

135. **Willey RL**, **Bonifacino JS**, **Potts BJ**, **Martin MA**, **Klausner RD**. 1988. Biosynthesis, cleavage, and degradation of the human immunodeficiency virus 1 envelope glycoprotein gp160. Proc. Natl. Acad. Sci. U.S.A. **85**:9580–9584.

136. **Guo HG**, **Veronese FM**, **Tschachler E**, **Pal R**, **Kalyanaraman VS**, **Gallo RC**, **Reitz MS**. 1990. Characterization of an HIV-1 point mutant blocked in envelope glycoprotein cleavage. Virology **174**:217–224.

137. **Pancera M**, **Wyatt R**. 2005. Selective recognition of oligomeric HIV-1 primary isolate envelope glycoproteins by potently neutralizing ligands requires efficient precursor cleavage. Virology **332**:145–156.

138. **Owens RJ**, **Compans RW**. 1990. The human immunodeficiency virus type 1 envelope glycoprotein precursor acquires aberrant intermolecular disulfide bonds that may prevent normal proteolytic processing. Virology **179**:827–833.

139. **Finzi A**, **Pacheco B**, **Zeng X**, **Kwon YD**, **Kwong PD**, **Sodroski J**. 2010. Conformational characterization of aberrant disulfide-linked HIV-1 gp120 dimers secreted from overexpressing cells. Journal of Virological Methods **168**:155–161.

140. **Yuan W**, **Craig S**, **Yang X**, **Sodroski J**. 2005. Inter-subunit disulfide bonds in soluble HIV-1 envelope glycoprotein trimers. Virology.

141. **Guttman M**, **Lee KK**. 2013. A Functional Interaction between gp41 and gp120 Is Observed for Monomeric but Not Oligomeric, Uncleaved HIV-1 Env gp140. J. Virol. **87**:11462–11475.

142. **Guttman M**, **Kahn M**, **Garcia NK**, **Hu S-L**, **Lee KK**. 2012. Solution structure, conformational dynamics, and CD4-induced activation in full-length, glycosylated, monomeric HIV gp120. J. Virol. **86**:8750–8764.

143. **Schiffner T**, **Kong L**, **Duncan CJA**, **Back JW**, **Benschop JJ**, **Shen X**, **Huang PS**, **Stewart-Jones GB**, **Destefano J**, **Seaman**

MS, **Tomaras GD**, **Montefiori DC**, **Schief WR**, **Sattentau QJ**. 2013. Immune Focusing and Enhanced Neutralization Induced by HIV-1 gp140 Chemical Cross-Linking. J. Virol. **87**:10163–10172.

144. **Kong L**, **Huang CC**, **Coales SJ**, **Molnar KS**, **Skinner J**, **Hamuro Y**, **Kwong PD**. 2010. Local Conformational Stability of HIV-1 gp120 in Unliganded and CD4-Bound States as Defined by Amide Hydrogen/Deuterium Exchange. J. Virol. **84**:10311–10321.

145. **Kwong PD**, **Doyle ML**, **Casper DJ**, **Cicala C**, **Leavitt SA**, **Majeed S**, **Steenbeke TD**, **Venturi M**, **Chaiken I**, **Fung M**, **Katinger H**, **Parren PWIH**, **Robinson J**, **Van Ryk D**, **Wang L**, **Burton DR**, **Freire E**, **Wyatt R**, **Sodroski J**, **Hendrickson WA**, **Arthos J**. 2002. HIV-1 evades antibody-mediated neutralization through conformational masking of receptor-binding sites. Nature **420**:678–682.

146. **Moore JP**, **McKeating JA**, **Weiss RA**, **Sattentau QJ**. 1990. Dissociation of gp120 from HIV-1 virions induced by soluble CD4. Science **250**:1139–1142.

147. **Moore PL**, **Crooks ET**, **Porter L**, **Zhu P**, **Cayanan CS**, **Grisé H**, **Corcoran P**, **Zwick MB**, **Franti M**, **Morris L**, **Roux KH**, **Burton DR**, **Binley JM**. 2006. Nature of nonfunctional envelope proteins on the surface of human immunodeficiency virus type 1. J. Virol. **80**:2515–2528.

148. **Crooks ET**, **Tong T**, **Osawa K**, **Binley JM**. 2011. Enzyme digests eliminate nonfunctional Env from HIV-1 particle surfaces, leaving native Env trimers intact and viral infectivity unaffected. J. Virol. **85**:5825–5839.

149. **Tong T**, **Crooks ET**, **Osawa K**, **Binley JM**. 2012. HIV-1 virus-like particles bearing pure env trimers expose neutralizing epitopes but occlude nonneutralizing epitopes. J. Virol. **86**:3574–3587.

150. **Sattentau QJ**, **Moore JP**. 1995. Human immunodeficiency virus type 1 neutralization is determined by epitope exposure on the gp120 oligomer. J. Exp. Med. **182**:185–196.

151. **Tong T**, **Osawa K**, **Robinson JE**, **Crooks ET**, **Binley JM**. 2013. Topological analysis of HIV-1 glycoproteins expressed in situ on virus surfaces reveals tighter packing but greater conformational flexibility than for soluble gp120. J. Virol. **87**:9233–9249.

152. **McCaffrey RA**, **Saunders C**, **Hensel M**, **Stamatatos L**. 2004. N-linked glycosylation of the V3 loop and the immunologically silent face of gp120 protects human immunodeficiency virus type 1 SF162 from neutralization by anti-gp120 and anti-gp41

antibodies. J. Virol. **78**:3279–3295.
153. **Doores KJ**, **Fulton Z**, **Hong V**, **Patel MK**, **Scanlan CN**, **Wormald MR**, **Finn MG**, **Burton DR**, **Wilson IA**, **Davis BG**. 2010. A nonself sugar mimic of the HIV glycan shield shows enhanced antigenicity. Proceedings of the National Academy of Sciences **107**:17107–17112.
154. **Walker LM**, **Huber M**, **Doores KJ**, **Falkowska E**, **Pejchal R**, **Julien J-P**, **Wang S-K**, **Ramos A**, **Chan-Hui P-Y**, **Moyle M**, **Mitcham JL**, **Hammond PW**, **Olsen OA**, **Phung P**, **Fling S**, **Wong C-H**, **Phogat S**, **Wrin T**, **Simek MD**, **Principal Investigators PG**, **Koff WC**, **Wilson IA**, **Burton DR**, **Poignard P**. 2011. Broad neutralization coverage of HIV by multiple highly potent antibodies. Cellular and Molecular Immunology **477**:466–470.
155. **Trkola A**, **Purtscher M**, **Muster T**, **Ballaun C**, **Buchacher A**, **Sullivan N**, **Srinivasan K**, **Sodroski J**, **Moore JP**, **Katinger H**. 1996. Human monoclonal antibody 2G12 defines a distinctive neutralization epitope on the gp120 glycoprotein of human immunodeficiency virus type 1. J. Virol. **70**:1100–1108.
156. **Buchacher A**, **Predl R**, **Strutzenberger K**, **Steinfellner W**, **Trkola A**, **Purtscher M**, **Gruber G**, **Tauer C**, **Steindl F**, **Jungbauer A**. 1994. Generation of human monoclonal antibodies against HIV-1 proteins; electrofusion and Epstein-Barr virus transformation for peripheral blood lymphocyte immortalization. AIDS Res. Hum. Retroviruses **10**:359–369.
157. **Zwick MB**, **Jensen R**, **Church S**, **Wang M**, **Stiegler G**, **Kunert R**, **Katinger H**, **Burton DR**. 2005. Anti-Human Immunodeficiency Virus Type 1 (HIV-1) Antibodies 2F5 and 4E10 Require Surprisingly Few Crucial Residues in the Membrane-Proximal External Region of Glycoprotein gp41 To Neutralize HIV-1.
158. **Alam SM**, **McAdams M**, **Boren D**, **Rak M**, **Scearce RM**, **Gao F**, **Camacho ZT**, **Gewirth D**, **Kelsoe G**, **Chen P**, **Haynes BF**. 2007. The role of antibody polyspecificity and lipid reactivity in binding of broadly neutralizing anti-HIV-1 envelope human monoclonal antibodies 2F5 and 4E10 to glycoprotein 41 membrane proximal envelope epitopes. J. Immunol. **178**:4424–4435.
159. **Alam SM**, **Morelli M**, **Dennison SM**, **Liao H-X**, **Zhang R**, **Xia S-M**, **Rits-Volloch S**, **Sun L**, **Harrison SC**, **Haynes BF**, **Chen B**. 2009. Role of HIV membrane in neutralization by two broadly neutralizing antibodies. Proceedings of the National Academy of

Sciences **106**:20234–20239.
160. **Chen Y**, **Zhang J**, **Hwang K-K**, **Bouton-Verville H**, **Xia S-M**, **Newman A**, **Ouyang Y-B**, **Haynes BF**, **Verkoczy L**. 2013. Common tolerance mechanisms, but distinct cross-reactivities associated with gp41 and lipids, limit production of HIV-1 broad neutralizing antibodies 2F5 and 4E10. The Journal of Immunology **191**:1260–1275.
161. **Klein JS**, **Bjorkman PJ**. 2010. Few and Far Between: How HIV May Be Evading Antibody Avidity. PLoS Pathogens **6**:e1000908.
162. **Hoot S**, **McGuire AT**, **Cohen KW**, **Strong RK**, **Hangartner L**, **Klein F**, **Diskin R**, **Scheid JF**, **Sather DN**, **Burton DR**, **Stamatatos L**. 2013. Recombinant HIV envelope proteins fail to engage germline versions of anti-CD4bs bNAbs. PLoS Pathogens **9**:e1003106.
163. **Klein F**, **Diskin R**, **Scheid JF**, **Gaebler C**, **Mouquet H**, **Georgiev IS**, **Pancera M**, **Zhou T**, **Incesu R-B**, **Fu BZ**, **Gnanapragasam PNP**, **Oliveira TY**, **Seaman MS**, **Kwong PD**, **Bjorkman PJ**, **Nussenzweig MC**. 2013. Somatic mutations of the immunoglobulin framework are generally required for broad and potent HIV-1 neutralization. Cell **153**:126–138.
164. **Kwong PD**, **Mascola JR**. 2012. Human Antibodies that Neutralize HIV-1: Identification, Structures, and B Cell Ontogenies. Immunity **37**:412–425.
165. **Klein F**, **Mouquet H**, **Dosenovic P**, **Scheid JF**, **Scharf L**, **Nussenzweig MC**. 2013. Antibodies in HIV-1 vaccine development and therapy. Science **341**:1199–1204.
166. **Schatz DG**, **Oettinger MA**. 1992. V (D) J recombination: molecular biology and regulation. Annual review of ….
167. **Janeway CA**, **Travers P**, **Walport M**, **Shlomchik M**. 2005. Immunobiology: The Immune System in Health &.
168. **Schatz DG**, **Ji Y**. 2011. Recombination centres and the orchestration of V(D)J recombination. Nature Publishing Group **11**:251–263.
169. **Grawunder U**, **West RB**, **Lieber MR**. 1998. Antigen receptor gene rearrangement. Current Opinion in Immunology.
170. **Jimenez R**, **Salazar G**, **Baldridge KK**, **Romesberg FE**. 2003. Flexibility and molecular recognition in the immune system. Proc. Natl. Acad. Sci. U.S.A. **100**:92–97.
171. **Adhikary R**, **Yu W**, **Oda M**, **Zimmermann J**, **Romesberg FE**. 2012. Protein dynamics and the diversity of an antibody

response. Journal of Biological Chemistry **287**:27139–27147.
172. **Hu S-L**, **Stamatatos L**. 2007. Prospects of HIV Env modification as an approach to HIV vaccine design. Curr. HIV Res. **5**:507–513.
173. **Schief WR**, **Ban Y-EA**, **Stamatatos L**. 2009. Challenges for structure-based HIV vaccine design. Current Opinion in HIV and AIDS **4**:431–440.
174. **Kwong PD**, **Mascola JR**, **Nabel GJ**. 2009. Mining the B Cell Repertoire for Broadly Neutralizing Monoclonal Antibodies to HIV-1. Cell Host and Microbe **6**:292–294.
175. **Burton DR**, **Barbas CF**, **Persson MA**, **Koenig S**, **Chanock RM**, **Lerner RA**. 1991. A large array of human monoclonal antibodies to type 1 human immunodeficiency virus from combinatorial libraries of asymptomatic seropositive individuals. Proc. Natl. Acad. Sci. U.S.A. **88**:10134–10137.
176. **Burton DR**, **Pyati J**, **Koduri R**, **Sharp SJ**, **Thornton GB**, **Parren PW**, **Sawyer LS**, **Hendry RM**, **Dunlop N**, **Nara PL**. 1994. Efficient neutralization of primary isolates of HIV-1 by a recombinant human monoclonal antibody. Science **266**:1024–1027.
177. **Muster T**, **Steindl F**, **Purtscher M**, **Trkola A**, **Klima A**, **Himmler G**, **Rüker F**, **Katinger H**. 1993. A conserved neutralizing epitope on gp41 of human immunodeficiency virus type 1. J. Virol. **67**:6642–6647.
178. **PURTSCHER M**, **Trkola A**, **GRUBER G**, **BUCHACHER A**, **PREDL R**, **STEINDL F**, **TAUER C**, **BERGER R**, **BARRETT N**, **JUNGBAUER A**, **Katinger H**. 1994. A broadly neutralizing human monoclonal antibody against gp41 of human immunodeficiency virus type 1. AIDS Res. Hum. Retroviruses **10**:1651–1658.
179. **Thali M**, **Moore JP**, **Furman C**, **Charles M**, **Ho DD**, **Robinson J**, **Sodroski J**. 1993. Characterization of conserved human immunodeficiency virus type 1 gp120 neutralization epitopes exposed upon gp120-CD4 binding. J. Virol. **67**:3978–3988.
180. **Trkola A**, **Dragic T**, **Arthos J**, **Binley JM**, **Olson WC**, **Allaway GP**, **Cheng-Mayer C**, **Robinson J**, **Maddon PJ**, **Moore JP**. 1996. CD4-dependent, antibody-sensitive interactions between HIV-1 and its co-receptor CCR-5. Nature **384**:184–187.
181. **Gorny MK**, **Conley AJ**, **Karwowska S**, **Buchbinder A**, **Xu JY**, **Emini EA**, **Koenig S**, **Zolla-Pazner S**. 1992. Neutralization of

diverse human immunodeficiency virus type 1 variants by an anti-V3 human monoclonal antibody. J. Virol. **66**:7538–7542.

182. **Wu X**, **Yang Z-Y**, **Li Y**, **Hogerkorp C-M**, **Schief WR**, **Seaman MS**, **Zhou T**, **Schmidt SD**, **Wu L**, **Xu L**, **Longo NS**, **McKee K**, **O'Dell S**, **Louder MK**, **Wycuff DL**, **Feng Y**, **Nason M**, **Doria-Rose N**, **Connors M**, **Kwong PD**, **Roederer M**, **Wyatt RT**, **Nabel GJ**, **Mascola JR**. 2010. Rational design of envelope identifies broadly neutralizing human monoclonal antibodies to HIV-1. Science **329**:856–861.

183. **Wu X**, **Zhou T**, **Zhu J**, **Zhang B**, **Georgiev I**, **Wang C**, **Chen X**, **Longo NS**, **Louder M**, **McKee K**, **O'Dell S**, **Perfetto S**, **Schmidt SD**, **Shi W**, **Wu L**, **Yang Y**, **Yang ZY**, **Yang Z**, **Zhang Z**, **Bonsignori M**, **Crump JA**, **Kapiga SH**, **Sam NE**, **Haynes BF**, **Simek M**, **Burton DR**, **Koff WC**, **Doria-Rose NA**, **Connors M**, **NISC Comparative Sequencing Program**, **Mullikin JC**, **Nabel GJ**, **Roederer M**, **Shapiro L**, **Kwong PD**, **Mascola JR**. 2011. Focused Evolution of HIV-1 Neutralizing Antibodies Revealed by Structures and Deep Sequencing. Science **333**:1593–1602.

184. **Diskin R**, **Scheid JF**, **Marcovecchio PM**, **West AP**, **Klein F**, **Gao H**, **Gnanapragasam PNP**, **Abadir A**, **Seaman MS**, **Nussenzweig MC**, **Bjorkman PJ**. 2011. Increasing the potency and breadth of an HIV antibody by using structure-based rational design. Science **334**:1289–1293.

185. **Scheid JF**, **Mouquet H**, **Ueberheide B**, **Diskin R**, **Klein F**, **Oliveira TYK**, **Pietzsch J**, **Fenyo D**, **Abadir A**, **Velinzon K**, **Hurley A**, **Myung S**, **Boulad F**, **Poignard P**, **Burton DR**, **Pereyra F**, **Ho DD**, **Walker BD**, **Seaman MS**, **Bjorkman PJ**, **Chait BT**, **Nussenzweig MC**. 2011. Sequence and structural convergence of broad and potent HIV antibodies that mimic CD4 binding. Science **333**:1633–1637.

186. **Kwong PD**, **Wyatt R**, **Majeed S**, **Robinson J**, **Sweet RW**, **Sodroski J**, **Hendrickson WA**. 2000. Structures of HIV-1 gp120 envelope glycoproteins from laboratory-adapted and primary isolates. Structure **8**:1329–1339.

187. **Huang CC**. 2005. Structure of a V3-Containing HIV-1 gp120 Core. Science **310**:1025–1028.

188. **Chen L**, **Do Kwon Y**, **Zhou T**, **Wu X**, **O'Dell S**, **Cavacini L**, **Hessell AJ**, **Pancera M**, **Tang M**, **Xu L**, **Yang ZY**, **Zhang MY**, **Arthos J**, **Burton DR**, **Dimitrov DS**, **Nabel GJ**, **Posner MR**, **Sodroski J**, **Wyatt R**, **Mascola JR**, **Kwong PD**. 2009. Structural

Basis of Immune Evasion at the Site of CD4 Attachment on HIV-1 gp120. Science **326**:1123–1127.

189. **Diskin R**, **Marcovecchio PM**, **Bjorkman PJ**. 2010. Structure of a clade C HIV-1 gp120 bound to CD4 and CD4-induced antibody reveals anti-CD4 polyreactivity. Nature Publishing Group **17**:608–613.

190. **Zhou T**, **Georgiev I**, **Wu X**, **Yang ZY**, **Dai K**, **Finzi A**, **Do Kwon Y**, **Scheid JF**, **Shi W**, **Xu L**, **Yang Y**, **Zhu J**, **Nussenzweig MC**, **Sodroski J**, **Shapiro L**, **Nabel GJ**, **Mascola JR**, **Kwong PD**. 2010. Structural Basis for Broad and Potent Neutralization of HIV-1 by Antibody VRC01. Science **329**:811–817.

191. **Zhou T**, **Xu L**, **Dey B**, **Hessell AJ**, **Van Ryk D**, **Xiang S-H**, **Yang X**, **Zhang M-Y**, **Zwick MB**, **Arthos J**, **Burton DR**, **Dimitrov DS**, **Sodroski J**, **Wyatt R**, **Nabel GJ**, **Kwong PD**. 2007. Structural definition of a conserved neutralization epitope on HIV-1 gp120. Cellular and Molecular Immunology **445**:732–737.

192. **Kwon YD**, **Finzi A**, **Wu X**, **Dogo-Isonagie C**, **Lee LK**, **Moore LR**, **Schmidt SD**, **Stuckey J**, **Yang Y**, **Zhou T**, **Zhu J**, **Vicic DA**, **Debnath AK**, **Shapiro L**, **Bewley CA**, **Mascola JR**, **Sodroski JG**, **Kwong PD**. 2012. Unliganded HIV-1 gp120 core structures assume the CD4-bound conformation with regulation by quaternary interactions and variable loops. Proceedings of the National Academy of Sciences **109**:5663–5668.

193. **Moore JP**, **McCutchan FE**, **Poon SW**, **Mascola J**, **Liu J**, **Cao Y**, **Ho DD**. 1994. Exploration of antigenic variation in gp120 from clades A through F of human immunodeficiency virus type 1 by using monoclonal antibodies. J. Virol. **68**:8350–8364.

194. **Smith DH**, **Winters-Digiacinto P**, **Mitiku M**, **O'Rourke S**, **Sinangil F**, **Wrin T**, **Montefiori DC**, **Berman PW**. 2010. Comparative immunogenicity of HIV-1 clade C envelope proteins for prime/boost studies. PLoS ONE **5**:e12076.

195. **Mertens HDT**, **Svergun DI**. 2010. Structural characterization of proteins and complexes using small-angle X-ray solution scattering. Journal of Structural Biology **172**:128–141.

196. **Engen JR**. 2009. Analysis of Protein Conformation and Dynamics by Hydrogen/Deuterium Exchange MS. Anal. Chem. **81**:7870–7875.

197. **Englander SW**. 2006. Hydrogen exchange and mass spectrometry: A historical perspective. J Am Soc Mass Spectrom **17**:1481–1489.

198. **Sanders RW**, **Derking R**, **Cupo A**, **Julien J-P**, **Yasmeen A**, **de Val N**, **Kim HJ**, **Blattner C**, **la Peña de AT**, **Korzun J**, **Golabek M**, **de Los Reyes K**, **Ketas TJ**, **van Gils MJ**, **King CR**, **Wilson IA**, **Ward AB**, **Klasse PJ**, **Moore JP**. 2013. A Next-Generation Cleaved, Soluble HIV-1 Env Trimer, BG505 SOSIP.664 gp140, Expresses Multiple Epitopes for Broadly Neutralizing but Not Non-Neutralizing Antibodies. PLoS Pathogens **9**:e1003618.
199. **Li Y**, **Svehla K**, **Mathy NL**, **Voss G**, **Mascola JR**, **Wyatt R**. 2006. Characterization of antibody responses elicited by human immunodeficiency virus type 1 primary isolate trimeric and monomeric envelope glycoproteins in selected adjuvants. J. Virol. **80**:1414–1426.
200. **Liao H-X**, **Tsao C-Y**, **Alam SM**, **Muldoon M**, **Vandergrift N**, **Ma B-J**, **Lu X**, **Sutherland LL**, **Scearce RM**, **Bowman C**, **Parks R**, **Chen H**, **Blinn JH**, **Lapedes A**, **Watson S**, **Xia S-M**, **Foulger A**, **Hahn BH**, **Shaw GM**, **Swanstrom R**, **Montefiori DC**, **Gao F**, **Haynes BF**, **Korber B**. 2013. Antigenicity and immunogenicity of transmitted/founder, consensus, and chronic envelope glycoproteins of human immunodeficiency virus type 1. J. Virol. **87**:4185–4201.
201. **Ofek G**, **Guenaga FJ**, **Schief WR**, **Skinner J**, **Baker D**, **Wyatt R**, **Kwong PD**. 2010. Elicitation of structure-specific antibodies by epitope scaffolds. Proceedings of the National Academy of Sciences **107**:17880–17887.
202. **Correia BE**, **Ban Y-EA**, **Holmes MA**, **Xu H**, **Ellingson K**, **Kraft Z**, **Carrico C**, **Boni E**, **Sather DN**, **Zenobia C**, **Burke KY**, **Bradley-Hewitt T**, **Bruhn-Johannsen JF**, **Kalyuzhniy O**, **Baker D**, **Strong RK**, **Stamatatos L**, **Schief WR**. 2010. Computational design of epitope-scaffolds allows induction of antibodies specific for a poorly immunogenic HIV vaccine epitope. Structure **18**:1116–1126.
203. **Hoxie JA**. 2010. Toward an Antibody-Based HIV-1 Vaccine. Annu. Rev. Med. **61**:135–152.
204. **Beddows S**, **Franti M**, **Dey AK**, **Kirschner M**, **Iyer SPN**, **Fisch DC**, **Ketas T**, **Yuste E**, **Desrosiers RC**, **Klasse PJ**, **Maddon PJ**, **Olson WC**, **Moore JP**. 2007. A comparative immunogenicity study in rabbits of disulfide-stabilized, proteolytically cleaved, soluble trimeric human immunodeficiency virus type 1 gp140, trimeric cleavage-defective gp140 and monomeric gp120. Virology **360**:329–340.

205. **Beddows S**, **Schülke N**, **Kirschner M**, **Barnes K**, **Franti M**, **Michael E**, **Ketas T**, **Sanders RW**, **Maddon PJ**, **Olson WC**, **Moore JP**. 2005. Evaluating the immunogenicity of a disulfide-stabilized, cleaved, trimeric form of the envelope glycoprotein complex of human immunodeficiency virus type 1. J. Virol. **79**:8812–8827.
206. **Blish CA**, **Sather DN**, **Sellhorn G**, **Stamatatos L**, **Sun Y**, **Srivastava I**, **Barnett SW**, **Cleveland B**, **Overbaugh J**, **Hu SL**. 2010. Comparative Immunogenicity of Subtype A Human Immunodeficiency Virus Type 1 Envelope Exhibiting Differential Exposure of Conserved Neutralization Epitopes. J. Virol. **84**:2573–2584.
207. **Derby NR**, **Kraft Z**, **Kan E**, **Crooks ET**, **Barnett SW**, **Srivastava IK**, **Binley JM**, **Stamatatos L**. 2006. Antibody Responses Elicited in Macaques Immunized with Human Immunodeficiency Virus Type 1 (HIV-1) SF162-Derived gp140 Envelope Immunogens: Comparison with Those Elicited during Homologous Simian/Human Immunodeficiency Virus SHIVSF162P4 and Heterologous HIV-1 Infection. J. Virol. **80**:8745–8762.
208. **Dey B**, **Pancera M**, **Svehla K**, **Shu Y**, **Xiang SH**, **Vainshtein J**, **Li Y**, **Sodroski J**, **Kwong PD**, **Mascola JR**, **Wyatt R**. 2007. Characterization of Human Immunodeficiency Virus Type 1 Monomeric and Trimeric gp120 Glycoproteins Stabilized in the CD4-Bound State: Antigenicity, Biophysics, and Immunogenicity. J. Virol. **81**:5579–5593.
209. **Doria-Rose NA**, **Learn GH**, **Rodrigo AG**, **Nickle DC**, **Li F**, **Mahalanabis M**, **Hensel MT**, **McLaughlin S**, **Edmonson PF**, **Montefiori D**, **Barnett SW**, **Haigwood NL**, **Mullins JI**. 2005. Human immunodeficiency virus type 1 subtype B ancestral envelope protein is functional and elicits neutralizing antibodies in rabbits similar to those elicited by a circulating subtype B envelope. J. Virol. **79**:11214–11224.
210. **Forsell MNE**, **Dey B**, **Mörner A**, **Svehla K**, **O'Dell S**, **Hogerkorp C-M**, **Voss G**, **Thorstensson R**, **Shaw GM**, **Mascola JR**, **Karlsson Hedestam GB**, **Wyatt RT**. 2008. B cell recognition of the conserved HIV-1 co-receptor binding site is altered by endogenous primate CD4. PLoS Pathogens **4**:e1000171.
211. **Grundner C**, **Li Y**, **Louder M**, **Mascola J**, **Yang X**, **Sodroski J**, **Wyatt R**. 2005. Analysis of the neutralizing antibody response elicited in rabbits by repeated inoculation with trimeric HIV-1

envelope glycoproteins. Virology **331**:33–46.
212. **Haigwood NL**, **Nara PL**, **Brooks E**, **Van Nest GA**, **Ott G**, **Higgins KW**, **Dunlop N**, **Scandella CJ**, **Eichberg JW**, **Steimer KS**. 1992. Native but not denatured recombinant human immunodeficiency virus type 1 gp120 generates broad-spectrum neutralizing antibodies in baboons. J. Virol. **66**:172–182.
213. **Kraft Z**, **Strouss K**, **Sutton WF**, **Cleveland B**, **Tso FY**, **Polacino P**, **Overbaugh J**, **Hu SL**, **Stamatatos L**. 2008. Characterization of Neutralizing Antibody Responses Elicited by Clade A Envelope Immunogens Derived from Early Transmitted Viruses. J. Virol. **82**:5912–5921.
214. **Mörner A**, **Douagi I**, **Forsell MNE**, **Sundling C**, **Dosenovic P**, **O'Dell S**, **Dey B**, **Kwong PD**, **Voss G**, **Thorstensson R**, **Mascola JR**, **Wyatt RT**, **Karlsson Hedestam GB**. 2009. Human immunodeficiency virus type 1 env trimer immunization of macaques and impact of priming with viral vector or stabilized core protein. J. Virol. **83**:540–551.
215. **Nkolola JP**, **Peng H**, **Settembre EC**, **Freeman M**, **Grandpre LE**, **Devoy C**, **Lynch DM**, **La Porte A**, **Simmons NL**, **Bradley R**, **Montefiori DC**, **Seaman MS**, **Chen B**, **Barouch DH**. 2010. Breadth of neutralizing antibodies elicited by stable, homogeneous clade A and clade C HIV-1 gp140 envelope trimers in guinea pigs. J. Virol. **84**:3270–3279.
216. **VanCott TC**, **Mascola JR**, **Kaminski RW**, **Kalyanaraman V**, **Hallberg PL**, **Burnett PR**, **Ulrich JT**, **Rechtman DJ**, **Birx DL**. 1997. Antibodies with specificity to native gp120 and neutralization activity against primary human immunodeficiency virus type 1 isolates elicited by immunization with oligomeric gp160. J. Virol. **71**:4319–4330.
217. **Wu L**, **Yang Z-Y**, **Xu L**, **Welcher B**, **Winfrey S**, **Shao Y**, **Mascola JR**, **Nabel GJ**. 2006. Cross-clade recognition and neutralization by the V3 region from clade C human immunodeficiency virus-1 envelope. Vaccine **24**:4995–5002.
218. **Yang X**, **Wyatt R**, **Sodroski J**. 2001. Improved elicitation of neutralizing antibodies against primary human immunodeficiency viruses by soluble stabilized envelope glycoprotein trimers. J. Virol. **75**:1165–1171.
219. **Simek MD**, **Rida W**, **Priddy FH**, **Pung P**, **Carrow E**, **Laufer DS**, **Lehrman JK**, **Boaz M**, **Tarragona-Fiol T**, **Miiro G**, **Birungi J**, **Pozniak A**, **McPhee DA**, **Manigart O**, **Karita E**, **Inwoley A**,

Jaoko W, **DeHovitz J**, **Bekker LG**, **Pitisuttithum P**, **Paris R**, **Walker LM**, **Poignard P**, **Wrin T**, **Fast PE**, **Burton DR**, **Koff WC**. 2009. Human Immunodeficiency Virus Type 1 Elite Neutralizers: Individuals with Broad and Potent Neutralizing Activity Identified by Using a High-Throughput Neutralization Assay together with an Analytical Selection Algorithm. J. Virol. **83**:7337–7348.

220. **Beddows S**, **Lister S**, **Cheingsong R**, **Bruck C**, **Weber J**. 1999. Comparison of the antibody repertoire generated in healthy volunteers following immunization with a monomeric recombinant gp120 construct derived from a CCR5/CXCR4-using human immunodeficiency virus type 1 isolate with sera from naturally infected individuals. J. Virol. **73**:1740–1745.

221. **Berman PW**, **Matthews TJ**, **Riddle L**, **Champe M**, **Hobbs MR**, **Nakamura GR**, **Mercer J**, **Eastman DJ**, **Lucas C**, **Langlois AJ**. 1992. Neutralization of multiple laboratory and clinical isolates of human immunodeficiency virus type 1 (HIV-1) by antisera raised against gp120 from the MN isolate of HIV-1. J. Virol. **66**:4464–4469.

222. **Haigwood NL**, **Shuster JR**, **Moore GK**, **Lee H**, **Skiles PV**, **Higgins KW**, **Barr PJ**, **George-Nascimento C**, **Steimer KS**. 1990. Importance of hypervariable regions of HIV-1 gp120 in the generation of virus neutralizing antibodies. AIDS Res. Hum. Retroviruses **6**:855–869.

223. **HANSON CV**. 1994. Measuring Vaccine-Induced HIV Neutralization: Report of a Workshop. AIDS Res. Hum. Retroviruses **10**:645–648.

224. **Keefer MC**, **Graham BS**, **McElrath MJ**, **Matthews TJ**, **Stablein DM**, **Corey L**, **Wright PF**, **Lawrence D**, **Fast PE**, **Weinhold K**, **Hsieh RH**, **Chernoff D**, **Dekker C**, **Dolin R**. 1996. Safety and immunogenicity of Env 2-3, a human immunodeficiency virus type 1 candidate vaccine, in combination with a novel adjuvant, MTP-PE/MF59. NIAID AIDS Vaccine Evaluation Group. AIDS Res. Hum. Retroviruses **12**:683–693.

225. **Mascola JR**, **Snyder SW**, **Weislow OS**, **Belay SM**, **Belshe RB**, **Schwartz DH**, **Clements ML**, **Dolin R**, **Graham BS**, **Gorse GJ**, **Keefer MC**, **McElrath MJ**, **Walker MC**, **Wagner KF**, **McNeil JG**, **McCutchan FE**, **Burke DS**. 1996. Immunization with envelope subunit vaccine products elicits neutralizing antibodies against laboratory-adapted but not primary isolates of human immunodeficiency virus type 1. The National Institute of Allergy

and Infectious Diseases AIDS Vaccine Evaluation Group. J INFECT DIS **173**:340–348.

226. **Nara PL**, **Robey WG**, **Pyle SW**, **Hatch WC**, **Dunlop NM**, **Bess JW**, **Kelliher JC**, **Arthur LO**, **Fischinger PJ**. 1988. Purified envelope glycoproteins from human immunodeficiency virus type 1 variants induce individual, type-specific neutralizing antibodies. J. Virol. **62**:2622–2628.

227. **Steimer KS**, **Haigwood NL**. 1992. Immunization of primates with native, recombinant HIV-SF2 gp120 generates broadly effective neutralizing antibodies directed to conformational epitopes. AIDS Res. Hum. Retroviruses **8**:1391.

228. **VanCott TC**, **Mascola JR**, **Loomis-Price LD**, **Sinangil F**, **Zitomersky N**, **McNeil J**, **Robb ML**, **Birx DL**, **Barnett S**. 1999. Cross-subtype neutralizing antibodies induced in baboons by a subtype E gp120 immunogen based on an R5 primary human immunodeficiency virus type 1 envelope. J. Virol. **73**:4640–4650.

229. **Phogat S**, **Wyatt R**. 2007. Rational modifications of HIV-1 envelope glycoproteins for immunogen design. Curr. Pharm. Des. **13**:213–227.

230. **Dey AK**, **David KB**, **Lu M**, **Moore JP**. 2009. Biochemical and biophysical comparison of cleaved and uncleaved soluble, trimeric HIV-1 envelope glycoproteins. Virology **385**:275–281.

231. **Robinson JE**, **Franco K**, **Elliott DH**, **Maher MJ**, **Reyna A**, **Montefiori DC**, **Zolla-Pazner S**, **Gorny MK**, **Kraft Z**, **Stamatatos L**. 2010. Quaternary Epitope Specificities of Anti-HIV-1 Neutralizing Antibodies Generated in Rhesus Macaques Infected by the Simian/Human Immunodeficiency Virus SHIVSF162P4. J. Virol. **84**:3443–3453.

232. **Changela A**, **Wu X**, **Yang Y**, **Zhang B**, **Zhu J**, **Nardone GA**, **O'Dell S**, **Pancera M**, **Gorny MK**, **Phogat S**, **Robinson JE**, **Stamatatos L**, **Zolla-Pazner S**, **Mascola JR**, **Kwong PD**. 2011. Crystal Structure of Human Antibody 2909 Reveals Conserved Features of Quaternary Structure-Specific Antibodies That Potently Neutralize HIV-1. J. Virol. **85**:2524–2535.

233. **Wu X**, **Changela A**, **O'Dell S**, **Schmidt SD**, **Pancera M**, **Yang Y**, **Zhang B**, **Gorny MK**, **Phogat S**, **Robinson JE**, **Stamatatos L**, **Zolla-Pazner S**, **Kwong PD**, **Mascola JR**. 2011. Immunotypes of a Quaternary Site of HIV-1 Vulnerability and Their Recognition by Antibodies. J. Virol. **85**:4578–4585.

234. **Sellhorn G**, **Caldwell Z**, **Mineart C**, **Stamatatos L**. 2009.

Improving the expression of recombinant soluble HIV Envelope glycoproteins using pseudo-stable transient transfection. Vaccine **28**:430–436.

235. **Platt EJ**, **Wehrly K**, **Kuhmann SE**, **Chesebro B**, **Kabat D**. 1998. Effects of CCR5 and CD4 cell surface concentrations on infections by macrophagetropic isolates of human immunodeficiency virus type 1. J. Virol. **72**:2855–2864.
236. **Gorny MK**, **Xu JY**, **Karwowska S**, **Buchbinder A**, **Zolla-Pazner S**. 1993. Repertoire of neutralizing human monoclonal antibodies specific for the V3 domain of HIV-1 gp120. J. Immunol. **150**:635–643.
237. **Blish CA**, **Nedellec R**, **Mandaliya K**, **Mosier DE**, **Overbaugh J**. 2007. HIV-1 subtype A envelope variants from early in infection have variable sensitivity to neutralization and to inhibitors of viral entry. AIDS **21**:693–702.
238. **Cheng-Mayer C**, **Quiroga M**, **Tung JW**, **Dina D**, **Levy JA**. 1990. Viral determinants of human immunodeficiency virus type 1 T-cell or macrophage tropism, cytopathogenicity, and CD4 antigen modulation. J. Virol. **64**:4390–4398.
239. **Saunders CJ**, **McCaffrey RA**, **Zharkikh I**, **Kraft Z**, **Malenbaum SE**, **Burke B**, **Cheng-Mayer C**, **Stamatatos L**. 2005. The V1, V2, and V3 regions of the human immunodeficiency virus type 1 envelope differentially affect the viral phenotype in an isolate-dependent manner. J. Virol. **79**:9069–9080.
240. **Earl PL**, **Moss B**. 1993. Mutational analysis of the assembly domain of the HIV-1 envelope glycoprotein. AIDS Res. Hum. Retroviruses **9**:589–594.
241. **Srivastava IK**, **Stamatatos L**, **Kan E**, **Vajdy M**, **Lian Y**, **Hilt S**, **Martin L**, **Vita C**, **Zhu P**, **Roux KH**, **Vojtech L**, **C Montefiori D**, **Donnelly J**, **Ulmer JB**, **Barnett SW**. 2003. Purification, characterization, and immunogenicity of a soluble trimeric envelope protein containing a partial deletion of the V2 loop derived from SF162, an R5-tropic human immunodeficiency virus type 1 isolate. J. Virol. **77**:11244–11259.
242. **Durocher Y**, **Perret S**, **Kamen A**. 2002. High-level and high-throughput recombinant protein production by transient transfection of suspension-growing human 293-EBNA1 cells. Nucleic Acids Res. **30**:E9.
243. **Blay WM**, **Kasprzyk T**, **Misher L**, **Richardson BA**, **Haigwood NL**. 2007. Mutations in envelope gp120 can impact proteolytic

processing of the gp160 precursor and thereby affect neutralization sensitivity of human immunodeficiency virus type 1 pseudoviruses. J. Virol. **81**:13037–13049.

244. **Long EM**, **Rainwater SMJ**, **Lavreys L**, **Mandaliya K**, **Overbaugh J**. 2002. HIV type 1 variants transmitted to women in Kenya require the CCR5 coreceptor for entry, regardless of the genetic complexity of the infecting virus. AIDS Res. Hum. Retroviruses **18**:567–576.

245. **Herrera C**, **Klasse PJ**, **Michael E**, **Kake S**, **Barnes K**, **Kibler CW**, **Campbell-Gardener L**, **Si Z**, **Sodroski J**, **Moore JP**, **Beddows S**. 2005. The impact of envelope glycoprotein cleavage on the antigenicity, infectivity, and neutralization sensitivity of Env-pseudotyped human immunodeficiency virus type 1 particles. Virology **338**:154–172.

246. **Herrera C**, **Spenlehauer C**, **Fung MS**, **Burton DR**, **Beddows S**, **Moore JP**. 2003. Nonneutralizing Antibodies to the CD4-Binding Site on the gp120 Subunit of Human Immunodeficiency Virus Type 1 Do Not Interfere with the Activity of a Neutralizing Antibody against the Same Site. J. Virol. **77**:1084–1091.

247. **Poignard P**, **Moulard M**, **Golez E**, **Vivona V**, **Franti M**, **Venturini S**, **Wang M**, **Parren PWHI**, **Burton DR**. 2003. Heterogeneity of envelope molecules expressed on primary human immunodeficiency virus type 1 particles as probed by the binding of neutralizing and nonneutralizing antibodies. J. Virol. **77**:353–365.

248. **Srivastava IK**, **Stamatatos L**, **Legg H**, **Kan E**, **Fong A**, **Coates SR**, **Leung L**, **Wininger M**, **Donnelly JJ**, **Ulmer JB**, **Barnett SW**. 2002. Purification and characterization of oligomeric envelope glycoprotein from a primary R5 subtype B human immunodeficiency virus. J. Virol. **76**:2835–2847.

249. **Srivastava IK**, **VanDorsten K**, **Vojtech L**, **Barnett SW**, **Stamatatos L**. 2003. Changes in the immunogenic properties of soluble gp140 human immunodeficiency virus envelope constructs upon partial deletion of the second hypervariable region. J. Virol. **77**:2310–2320.

250. **Binley JM**, **Sanders RW**, **Master A**, **Cayanan CS**, **Wiley CL**, **Schiffner L**, **Travis B**, **Kuhmann S**, **Burton DR**, **Hu S-L**, **Olson WC**, **Moore JP**. 2002. Enhancing the proteolytic maturation of human immunodeficiency virus type 1 envelope glycoproteins. J. Virol. **76**:2606–2616.

251. **Xu H**, **Song L**, **Kim M**, **Holmes MA**, **Kraft Z**, **Sellhorn G**, **Reinherz EL**, **Stamatatos L**, **Strong RK**. 2009. Interactions between Lipids and Human Anti-HIV Antibody 4E10 Can Be Reduced without Ablating Neutralizing Activity. J. Virol. **84**:1076–1088.
252. **Rich RL**, **Myszka DG**. 2008. Survey of the year 2007 commercial optical biosensor literature. J. Mol. Recognit. **21**:355–400.
253. **Pejchal R**, **Walker LM**, **Stanfield RL**, **Phogat SK**, **Koff WC**, **Poignard P**, **Burton DR**, **Wilson IA**. 2010. Structure and function of broadly reactive antibody PG16 reveal an H3 subdomain that mediates potent neutralization of HIV-1. Proceedings of the National Academy of Sciences **107**:11483–11488.
254. **Lasky LA**, **Groopman JE**, **Fennie CW**, **Benz PM**, **Capon DJ**, **Dowbenko DJ**, **Nakamura GR**, **Nunes WM**, **Renz ME**, **Berman PW**. 1986. Neutralization of the AIDS retrovirus by antibodies to a recombinant envelope glycoprotein. Science **233**:209–212.
255. **Alam SM**, **Liao H-X**, **Tomaras GD**, **Bonsignori M**, **Tsao C-Y**, **Hwang K-K**, **Chen H**, **Lloyd KE**, **Bowman C**, **Sutherland L**, **Jeffries TL**, **Kozink DM**, **Stewart S**, **Anasti K**, **Jaeger FH**, **Parks R**, **Yates NL**, **Overman RG**, **Sinangil F**, **Berman PW**, **Pitisuttithum P**, **Kaewkungwal J**, **Nitayaphan S**, **Karasavva N**, **Rerks-Ngarm S**, **Kim JH**, **Michael NL**, **Zolla-Pazner S**, **Santra S**, **Letvin NL**, **Harrison SC**, **Haynes BF**. 2013. Antigenicity and immunogenicity of RV144 vaccine AIDSVAX clade E envelope immunogen is enhanced by a gp120 N-terminal deletion. J. Virol. **87**:1554–1568.
256. **Scarlatti G**, **Tresoldi E**, **Björndal A**, **Fredriksson R**, **Colognesi C**, **Deng HK**, **Malnati MS**, **Plebani A**, **Siccardi AG**, **Littman DR**, **Fenyö EM**, **Lusso P**. 1997. In vivo evolution of HIV-1 co-receptor usage and sensitivity to chemokine-mediated suppression. Nature Medicine **3**:1259–1265.
257. **Haim H**, **Si Z**, **Madani N**, **Wang L**, **Courter JR**, **Princiotto A**, **Kassa A**, **DeGrace M**, **McGee-Estrada K**, **Mefford M**, **Gabuzda D**, **Smith AB**, **Sodroski J**. 2009. Soluble CD4 and CD4-Mimetic Compounds Inhibit HIV-1 Infection by Induction of a Short-Lived Activated State. PLoS Pathogens **5**:e1000360.
258. **Starcich BR**, **Hahn BH**, **Shaw GM**, **McNeely PD**, **Modrow S**, **Wolf H**, **Parks ES**, **Parks WP**, **Josephs SF**, **Gallo RC**. 1986. Identification and characterization of conserved and variable regions in the envelope gene of HTLV-III/LAV, the retrovirus of

AIDS. Cell **45**:637–648.
259. **Wyatt R**, **Moore J**, **Accola M**, **Desjardin E**, **Robinson J**, **Sodroski J**. 1995. Involvement of the V1/V2 variable loop structure in the exposure of human immunodeficiency virus type 1 gp120 epitopes induced by receptor binding. J. Virol. **69**:5723–5733.
260. **Rong R**, **Bibollet-Ruche F**, **Mulenga J**, **Allen S**, **Blackwell JL**, **Derdeyn CA**. 2007. Role of V1V2 and Other Human Immunodeficiency Virus Type 1 Envelope Domains in Resistance to Autologous Neutralization during Clade C Infection. J. Virol. **81**:1350–1359.
261. **Pinter A**, **Honnen WJ**, **He Y**, **Gorny MK**, **Zolla-Pazner S**, **Kayman SC**. 2004. The V1/V2 domain of gp120 is a global regulator of the sensitivity of primary human immunodeficiency virus type 1 isolates to neutralization by antibodies commonly induced upon infection. J. Virol. **78**:5205–5215.
262. **Sethi A**, **Tian J**, **Derdeyn CA**, **Korber B**, **Gnanakaran S**. 2013. A Mechanistic Understanding of Allosteric Immune Escape Pathways in the HIV-1 Envelope Glycoprotein. PLoS Comput Biol **9**:e1003046.
263. **Cheng-Mayer C**, **Weiss C**, **Seto D**, **Levy JA**. 1989. Isolates of human immunodeficiency virus type 1 from the brain may constitute a special group of the AIDS virus. Proc. Natl. Acad. Sci. U.S.A. **86**:8575–8579.
264. **Shaw GM**, **Hahn BH**, **Arya SK**, **Groopman JE**, **Gallo RC**, **Wong-Staal F**. 1984. Molecular characterization of human T-cell leukemia (lymphotropic) virus type III in the acquired immune deficiency syndrome. Science **226**:1165–1171.
265. **Grisson RD**, **Chenine A-L**, **Yeh L-Y**, **He J**, **Wood C**, **Bhat GJ**, **Xu W**, **Kankasa C**, **Ruprecht RM**. 2004. Infectious molecular clone of a recently transmitted pediatric human immunodeficiency virus clade C isolate from Africa: evidence of intraclade recombination. J. Virol. **78**:14066–14069.
266. **Song RJ**, **Chenine AL**, **Rasmussen RA**, **Ruprecht CR**, **Mirshahidi S**, **Grisson RD**, **Xu W**, **Whitney JB**, **Goins LM**, **Ong H**, **Li PL**, **Shai-Kobiler E**, **Wang T**, **McCann CM**, **Zhang H**, **Wood C**, **Kankasa C**, **Secor WE**, **McClure HM**, **Strobert E**, **Else JG**, **Ruprecht RM**. 2006. Molecularly Cloned SHIV-1157ipd3N4: a Highly Replication- Competent, Mucosally Transmissible R5 Simian-Human Immunodeficiency Virus Encoding HIV Clade C

env. J. Virol. **80**:8729–8738.
267. **Rambo RP**, **Tainer JA**. 2010. Bridging the solution divide: comprehensive structural analyses of dynamic RNA, DNA, and protein assemblies by small-angle X-ray scattering. Current Opinion in Structural Biology **20**:128–137.
268. **Putnam CD**, **Hammel M**, **Hura GL**, **Tainer JA**. 2007. X-ray solution scattering (SAXS) combined with crystallography and computation: defining accurate macromolecular structures, conformations and assemblies in solution. Quart. Rev. Biophys. **40**.
269. **Svergun DI**, **Koch MHJ**. 2002. Advances in structure analysis using small-angle scattering in solution. Current Opinion in Structural Biology **12**:654–660.
270. **Morgan CR**, **Engen JR**. 2001. Investigating Solution-Phase Protein Structure and Dynamics by Hydrogen Exchange Mass Spectrometry. John Wiley & Sons, Inc., Hoboken, NJ, USA.
271. **Cheng-Mayer C**, **Liu R**, **Landau NR**, **Stamatatos L**. 1997. Macrophage tropism of human immunodeficiency virus type 1 and utilization of the CC-CKR5 coreceptor. J. Virol. **71**:1657–1661.
272. **Siddappa NB**, **Watkins JD**, **Wassermann KJ**, **Song R**, **Wang W**, **Kramer VG**, **Lakhashe S**, **Santosuosso M**, **Poznansky MC**, **Novembre FJ**, **Villinger F**, **Else JG**, **Montefiori DC**, **Rasmussen RA**, **Ruprecht RM**. 2010. R5 Clade C SHIV Strains with Tier 1 or 2 Neutralization Sensitivity: Tools to Dissect Env Evolution and to Develop AIDS Vaccines in Primate Models. PLoS ONE **5**:e11689.
273. **Zhang H**, **Rola M**, **West JT**, **Tully DC**, **Kubis P**, **He J**, **Kankasa C**, **Wood C**. 2010. Functional properties of the HIV-1 subtype C envelope glycoprotein associated with mother-to-child transmission. Virology **400**:164–174.
274. **Ching LK**, **Vlachogiannis G**, **Bosch KA**, **Stamatatos L**. 2008. The First Hypervariable Region of the gp120 Env Glycoprotein Defines the Neutralizing Susceptibility of Heterologous Human Immunodeficiency Virus Type 1 Isolates to Neutralizing Antibodies Elicited by the SF162gp140 Immunogen. J. Virol. **82**:949–956.
275. **Barbas CF**, **Björling E**, **Chiodi F**, **Dunlop N**, **Cababa D**, **Jones TM**, **Zebedee SL**, **Persson MA**, **Nara PL**, **Norrby E**. 1992. Recombinant human Fab fragments neutralize human type 1

immunodeficiency virus in vitro. Proc. Natl. Acad. Sci. U.S.A. **89**:9339–9343.

276. **Roben P**, **Moore JP**, **Thali M**, **Sodroski J**, **Barbas CF**, **Burton DR**. 1994. Recognition properties of a panel of human recombinant Fab fragments to the CD4 binding site of gp120 that show differing abilities to neutralize human immunodeficiency virus type 1. J. Virol. **68**:4821–4828.

277. **Moore JP**, **Thali M**, **Jameson BA**, **Vignaux F**, **Lewis GK**, **Poon SW**, **Charles M**, **Fung MS**, **Sun B**, **Durda PJ**. 1993. Immunochemical analysis of the gp120 surface glycoprotein of human immunodeficiency virus type 1: probing the structure of the C4 and V4 domains and the interaction of the C4 domain with the V3 loop. J. Virol. **67**:4785–4796.

278. **Garlick RL**, **Kirschner RJ**, **Eckenrode FM**, **Tarpley WG**, **Tomich CS**. 1990. Escherichia coli expression, purification, and biological activity of a truncated soluble CD4. AIDS Res. Hum. Retroviruses **6**:465–479.

279. **Guan Y**, **Pazgier M**, **Sajadi MM**, **Kamin-Lewis R**, **Al-Darmarki S**, **Flinko R**, **Lovo E**, **Wu X**, **Robinson JE**, **Seaman MS**, **Fouts TR**, **Gallo RC**, **DeVico AL**, **Lewis GK**. 2013. Diverse specificity and effector function among human antibodies to HIV-1 envelope glycoprotein epitopes exposed by CD4 binding. Proceedings of the National Academy of Sciences **110**:E69–78.

280. **Abacioglu YH**, **Fouts TR**, **Laman JD**, **Claassen E**, **Pincus SH**, **Moore JP**, **Roby CA**, **Kamin-Lewis R**, **Lewis GK**. 1994. Epitope mapping and topology of baculovirus-expressed HIV-1 gp160 determined with a panel of murine monoclonal antibodies. AIDS Res. Hum. Retroviruses **10**:371–381.

281. **di Marzo Veronese F**, **Rahman R**, **Pal R**, **Boyer C**, **Romano J**, **Kalyanaraman VS**, **Nair BC**, **Gallo RC**, **Sarngadharan MG**. 1992. Delineation of immunoreactive, conserved regions in the external glycoprotein of the human immunodeficiency virus type 1. AIDS Res. Hum. Retroviruses **8**:1125–1132.

282. **Guo W**, **Cleveland B**, **Davenport TM**, **Lee KK**, **Hu S-L**. 2013. Purification of recombinant vaccinia virus-expressed monomeric HIV-1 gp120 to apparent homogeneity. Protein Expression and Purification **90**:34–39.

283. **Fang J**, **Rand KD**, **Beuning PJ**, **Engen JR**. 2010. False EX1 signatures caused by sample carryover during HX MS analyses. International Journal of Mass Spectrometry 1–7.

284. **Weis DD**, **Engen JR**, **Kass IJ**. 2006. Semi-automated data processing of hydrogen exchange mass spectra using HX-Express. J Am Soc Mass Spectrom **17**:1700–1703.
285. **Guttman M**, **Scian M**, **Lee KK**. 2011. Tracking hydrogen/deuterium exchange at glycan sites in glycoproteins by mass spectrometry. Anal. Chem. **83**:7492–7499.
286. **DeLano WL**. 2002. The PyMOL Molecular Graphics System. DeLano Scientific, San Carlos, CA.
287. **Smolsky IL**, **Liu P**, **Niebuhr M**, **Ito K**, **Weiss TM**, **Tsuruta H**. 2007. Biological small-angle X-ray scattering facility at the Stanford Synchrotron Radiation Laboratory. J Appl Crystallogr **40**:s453–s458.
288. **Petoukhov MV**, **Konarev PV**, **Kikhney AG**, **Svergun DI**. 2007. ATSAS2.1 – towards automated and web-supported small-angle scattering data analysis. J Appl Crystallogr **40**:s223–s228.
289. **Konarev PV**, **Volkov VV**, **Sokolova AV**, **Koch MHJ**, **Svergun DI**. 2003. PRIMUS: a Windows PC-based system for small-angle scattering data analysis. J Appl Crystallogr **36**:1277–1282.
290. **Petoukhov MV**, **Svergun DI**. 2007. Analysis of X-ray and neutron scattering from biomacromolecular solutions. Current Opinion in Structural Biology **17**:562–571.
291. **Svergun DI**. 1991. Mathematical methods in small-angle scattering data analysis. J Appl Crystallogr **24**:485–492.
292. **Svergun DI**. 1992. Determination of the regularization parameter in indirect-transform methods using perceptual criteria. J Appl Crystallogr **25**:495–503.
293. **Svergun DI**. 1999. Restoring low resolution structure of biological macromolecules from solution scattering using simulated annealing. Biophysical Journal **76**:2879–2886.
294. **Volkov VV**, **Svergun DI**. 2003. Uniqueness of ab initioshape determination in small-angle scattering. J Appl Crystallogr **36**:860–864.
295. **Rambo RP**, **Tainer JA**. 2011. Characterizing flexible and intrinsically unstructured biological macromolecules by SAS using the Porod-Debye law. Biopolymers **95**:559–571.
296. **Hamuro Y**, **Coales SJ**, **Molnar KS**, **Tuske SJ**, **Morrow JA**. 2008. Specificity of immobilized porcine pepsin in H/D exchange compatible conditions. Rapid Commun. Mass Spectrom. **22**:1041–1046.
297. **Myszka DG**, **Sweet RW**, **Hensley P**, **Brigham-Burke M**, **Kwong**

PD, **Hendrickson WA**, **Wyatt R**, **Sodroski J**, **Doyle ML**. 2000. Energetics of the HIV gp120-CD4 binding reaction. Proc. Natl. Acad. Sci. U.S.A. **97**:9026–9031.

298. **Atassi MZ**. 1975. Antigenic structure of myoglobin: the complete immunochemical anatomy of a protein and conclusions relating to antigenic structures of proteins. Immunochemistry **12**:423–438.

299. **Jeffs SA**, **Goriup S**, **Kebble B**, **Crane D**, **Bolgiano B**, **Sattentau Q**, **Jones S**, **Holmes H**. 2004. Expression and characterisation of recombinant oligomeric envelope glycoproteins derived from primary isolates of HIV-1. Vaccine **22**:1032–1046.

300. **Wyatt R**, **Desjardin E**, **Olshevsky U**, **Nixon C**, **Binley J**, **Olshevsky V**, **Sodroski J**. 1997. Analysis of the interaction of the human immunodeficiency virus type 1 gp120 envelope glycoprotein with the gp41 transmembrane glycoprotein. J. Virol. **71**:9722–9731.

301. **Finzi A**, **Xiang S-H**, **Pacheco B**, **Wang L**, **Haight J**, **Kassa A**, **Danek B**, **Pancera M**, **Kwong PD**, **Sodroski J**. 2010. Topological layers in the HIV-1 gp120 inner domain regulate gp41 interaction and CD4-triggered conformational transitions. Mol. Cell **37**:656–667.

302. **Désormeaux A**, **Coutu M**, **Medjahed H**, **Pacheco B**, **Herschhorn A**, **Gu C**, **Xiang S-H**, **Mao Y**, **Sodroski J**, **Finzi A**. 2013. The highly conserved layer-3 component of the HIV-1 gp120 inner domain is critical for CD4-required conformational transitions. J. Virol. **87**:2549–2562.

303. **Kassa A**, **Madani N**, **Schön A**, **Haim H**, **Finzi A**, **Xiang S-H**, **Wang L**, **Princiotto A**, **Pancera M**, **Courter J**, **Smith AB**, **Freire E**, **Kwong PD**, **Sodroski J**. 2009. Transitions to and from the CD4-bound conformation are modulated by a single-residue change in the human immunodeficiency virus type 1 gp120 inner domain. J. Virol. **83**:8364–8378.

304. **Xiang S-H**, **Doka N**, **Choudhary RK**, **Sodroski J**, **Robinson JE**. 2002. Characterization of CD4-induced epitopes on the HIV type 1 gp120 envelope glycoprotein recognized by neutralizing human monoclonal antibodies. AIDS Res. Hum. Retroviruses **18**:1207–1217.

305. **Drummer HE**, **Hill MK**, **Maerz AL**, **Wood S**, **Ramsland PA**, **Mak J**, **Poumbourios P**. 2013. Allosteric Modulation of the HIV-1 gp120-gp41 Association Site by Adjacent gp120 Variable Region 1 (V1) N-Glycans Linked to Neutralization Sensitivity. PLoS

Pathogens **9**:e1003218.
306. **Korkut A**, **Hendrickson WA**. 2012. Structural plasticity and conformational transitions of HIV envelope glycoprotein gp120. PLoS ONE **7**:e52170.
307. **Chen B**, **Vogan EM**, **Gong H**, **Skehel JJ**, **Wiley DC**, **Harrison SC**. 2005. Structure of an unliganded simian immunodeficiency virus gp120 core. Cellular and Molecular Immunology **433**:834–841.
308. **Ferrari G**, **Pollara J**, **Kozink D**, **Harms T**, **Drinker M**, **Freel S**, **Moody MA**, **Alam SM**, **Tomaras GD**, **Ochsenbauer C**, **Kappes JC**, **Shaw GM**, **Hoxie JA**, **Robinson JE**, **Haynes BF**. 2011. An HIV-1 gp120 envelope human monoclonal antibody that recognizes a C1 conformational epitope mediates potent antibody-dependent cellular cytotoxicity (ADCC) activity and defines a common ADCC epitope in human HIV-1 serum. J. Virol. **85**:7029–7036.
309. **Tainer JA**, **Getzoff ED**, **Alexander H**, **Houghten RA**, **Olson AJ**, **Lerner RA**, **Hendrickson WA**. 1984. The reactivity of anti-peptide antibodies is a function of the atomic mobility of sites in a protein. Nature **312**:127–134.
310. **Westhof E**, **Altschuh D**, **Moras D**, **Bloomer AC**, **Mondragon A**, **Klug A**, **Van Regenmortel MHV**. 1984. Correlation between segmental mobility and the location of antigenic determinants in proteins. Nature **311**:123–126.
311. **Li Y**, **O'Dell S**, **Walker LM**, **Wu X**, **Guenaga J**, **Feng Y**, **Schmidt SD**, **McKee K**, **Louder MK**, **Ledgerwood JE**, **Graham BS**, **Haynes BF**, **Burton DR**, **Wyatt RT**, **Mascola JR**. 2011. Mechanism of Neutralization by the Broadly Neutralizing HIV-1 Monoclonal Antibody VRC01. J. Virol. **85**:8954–8967.
312. **Forsell MN**, **Schief WR**, **Wyatt RT**. 2009. Immunogenicity of HIV-1 envelope glycoprotein oligomers. Current Opinion in HIV and AIDS **4**:380–387.
313. **Tomaras GD**, **Ferrari G**, **Shen X**, **Alam SM**, **Liao H-X**, **Pollara J**, **Bonsignori M**, **Moody MA**, **Fong Y**, **Chen X**, **Poling B**, **Nicholson CO**, **Zhang R**, **Lu X**, **Parks R**, **Kaewkungwal J**, **Nitayaphan S**, **Pitisuttithum P**, **Rerks-Ngarm S**, **Gilbert PB**, **Kim JH**, **Michael NL**, **Montefiori DC**, **Haynes BF**. 2013. Vaccine-induced plasma IgA specific for the C1 region of the HIV-1 envelope blocks binding and effector function of IgG. Proceedings of the National Academy of Sciences.

314. **Dey B**, **Svehla K**, **Xu L**, **Wycuff D**, **Zhou T**, **Voss G**, **Phogat A**, **Chakrabarti BK**, **Li Y**, **Shaw G**, **Kwong PD**, **Nabel GJ**, **Mascola JR**, **Wyatt RT**. 2009. Structure-Based Stabilization of HIV-1 gp120 Enhances Humoral Immune Responses to the Induced Co-Receptor Binding Site. PLoS Pathogens **5**:e1000445.
315. **Li Y**, **Cleveland B**, **Klots I**, **Travis B**, **Richardson BA**, **Anderson D**, **Montefiori D**, **Polacino P**, **Hu SL**. 2008. Removal of a Single N-Linked Glycan in Human Immunodeficiency Virus Type 1 gp120 Results in an Enhanced Ability To Induce Neutralizing Antibody Responses. J. Virol. **82**:638–651.
316. **Alt FW**, **Baltimore D**. 1982. Joining of immunoglobulin heavy chain gene segments: implications from a chromosome with evidence of three D-JH fusions.
317. **Lieber MR**, **Hesse JE**, **Mizuuchi K**, **Gellert M**. 1988. Lymphoid V(D)J recombination: nucleotide insertion at signal joints as well as coding joints. Proc. Natl. Acad. Sci. U.S.A. **85**:8588–8592.
318. **Tarlinton D**, **Good-Jacobson K**. 2013. Diversity among memory B cells: origin, consequences, and utility. Science **341**:1205–1211.
319. **Zimmermann J**, **Oakman EL**, **Thorpe IF**, **Shi X**, **Abbyad P**, **Brooks CL**, **Boxer SG**, **Romesberg FE**. 2006. Antibody evolution constrains conformational heterogeneity by tailoring protein dynamics. Proc. Natl. Acad. Sci. U.S.A. **103**:13722–13727.
320. **McGuire AT**, **Hoot S**, **Dreyer AM**, **Lippy A**, **Stuart A**, **Cohen KW**, **Jardine J**, **Menis S**, **Scheid JF**, **West AP**, **Schief WR**, **Stamatatos L**. 2013. Engineering HIV envelope protein to activate germline B cell receptors of broadly neutralizing anti-CD4 binding site antibodies. Journal of Experimental Medicine.
321. **Liao H-X**, **Lynch R**, **Zhou T**, **Gao F**, **Alam SM**, **Boyd SD**, **Fire AZ**, **Roskin KM**, **Schramm CA**, **Zhang Z**, **Zhu J**, **Shapiro L**, **NISC Comparative Sequencing Program**, **Becker J**, **Benjamin B**, **Blakesley R**, **Bouffard G**, **Brooks S**, **Coleman H**, **Dekhtyar M**, **Gregory M**, **Guan X**, **Gupta J**, **Han J**, **Hargrove A**, **Ho S-L**, **Johnson T**, **Legaspi R**, **Lovett S**, **Maduro Q**, **Masiello C**, **Maskeri B**, **McDowell J**, **Montemayor C**, **Mullikin J**, **Park M**, **Riebow N**, **Schandler K**, **Schmidt B**, **Sison C**, **Stantripop M**, **Thomas J**, **Thomas P**, **Vemulapalli M**, **Young A**, **Mullikin JC**, **Gnanakaran S**, **Hraber P**, **Wiehe K**, **Kelsoe G**, **Yang G**, **Xia S-M**, **Montefiori DC**, **Parks R**, **Lloyd KE**, **Scearce RM**, **Soderberg**

KA, **Cohen M**, **Kamanga G**, **Louder MK**, **Tran LM**, **Chen Y**, **Cai F**, **Chen S**, **Moquin S**, **Du X**, **Joyce MG**, **Srivatsan S**, **Zhang B**, **Zheng A**, **Shaw GM**, **Hahn BH**, **Kepler TB**, **Korber BTM**, **Kwong PD**, **Mascola JR**, **Haynes BF**. 2013. Co-evolution of a broadly neutralizing HIV-1 antibody and founder virus. Cellular and Molecular Immunology.

322. **Jimenez R**, **Salazar G**, **Yin J**, **Joo T**, **Romesberg FE**. 2004. Protein dynamics and the immunological evolution of molecular recognition. Proc. Natl. Acad. Sci. U.S.A. **101**:3803–3808.

323. **Willis JR**, **Briney BS**, **DeLuca SL**, **Crowe JE**, **Meiler J**. 2013. Human germline antibody gene segments encode polyspecific antibodies. PLoS Comput Biol **9**:e1003045.

324. **Moore PL**, **Gray ES**, **Sheward D**, **Madiga M**, **Ranchobe N**, **Lai Z**, **Honnen WJ**, **Nonyane M**, **Tumba N**, **Hermanus T**, **Sibeko S**, **Mlisana K**, **Abdool Karim SS**, **Williamson C**, **Pinter A**, **Morris L**, **CAPRISA 002 Study**. 2011. Potent and broad neutralization of HIV-1 subtype C by plasma antibodies targeting a quaternary epitope including residues in the V2 loop. J. Virol. **85**:3128–3141.

325. **Moore PL**, **Sheward D**, **Nonyane M**, **Ranchobe N**, **Hermanus T**, **Gray ES**, **Abdool Karim SS**, **Williamson C**, **Morris L**. 2013. Multiple pathways of escape from HIV broadly cross-neutralizing V2-dependent antibodies. J. Virol. **87**:4882–4894.

326. **Guttman M**, **Weis DD**, **Engen JR**, **Lee KK**. 2013. Analysis of Overlapped and Noisy Hydrogen/Deuterium Exchange Mass Spectra. J Am Soc Mass Spectrom.

327. **Park H**, **Lee S**, **Suh J**. 2005. Structural and dynamical basis of broad substrate specificity, catalytic mechanism, and inhibition of cytochrome P450 3A4. J. Am. Chem. Soc. **127**:13634–13642.

328. **McLellan JS**, **Pancera M**, **Carrico C**, **Gorman J**, **Julien J-P**, **Khayat R**, **Louder R**, **Pejchal R**, **Sastry M**, **Dai K**, **O'Dell S**, **Patel N**, **Shahzad-Ul-Hussan S**, **Yang Y**, **Zhang B**, **Zhou T**, **Zhu J**, **Boyington JC**, **Chuang G-Y**, **Diwanji D**, **Georgiev I**, **Kwon YD**, **Lee D**, **Louder MK**, **Moquin S**, **Schmidt SD**, **Yang Z-Y**, **Bonsignori M**, **Crump JA**, **Kapiga SH**, **Sam NE**, **Haynes BF**, **Burton DR**, **Koff WC**, **Walker LM**, **Phogat S**, **Wyatt R**, **Orwenyo J**, **Wang L-X**, **Arthos J**, **Bewley CA**, **Mascola JR**, **Nabel GJ**, **Schief WR**, **Ward AB**, **Wilson IA**, **Kwong PD**. 2011. Structure of HIV-1 gp120 V1/V2 domain with broadly neutralizing antibody PG9. Cellular and Molecular Immunology **480**:336–343.

329. **Julien J-P**, **Lee JH**, **Cupo A**, **Murin CD**, **Derking R**, **Hoffenberg**

S, **Caulfield MJ**, **King CR**, **Marozsan AJ**, **Klasse PJ**, **Sanders RW**, **Moore JP**, **Wilson IA**, **Ward AB**. 2013. Asymmetric recognition of the HIV-1 trimer by broadly neutralizing antibody PG9. Proceedings of the National Academy of Sciences **110**:4351–4356.

330. **Kovacs JM**, **Nkolola JP**, **Peng H**, **Cheung A**, **Perry J**, **Miller CA**, **Seaman MS**, **Barouch DH**, **Chen B**. 2012. HIV-1 envelope trimer elicits more potent neutralizing antibody responses than monomeric gp120. Proceedings of the National Academy of Sciences **109**:12111–12116.
331. **Raska M**, **Takahashi K**, **Czernekova L**, **Zachova K**, **Hall S**, **Moldoveanu Z**, **Elliott MC**, **Wilson L**, **Brown R**, **Jancova D**, **Barnes S**, **Vrbkova J**, **Tomana M**, **Smith PD**, **Mestecky J**, **Renfrow MB**, **Novak J**. 2010. Glycosylation patterns of HIV-1 gp120 depend on the type of expressing cells and affect antibody recognition. Journal of Biological Chemistry **285**:20860–20869.
332. **Fieser TM**, **Tainer JA**, **Geysen HM**, **Houghten RA**, **Lerner RA**. 1987. Influence of protein flexibility and peptide conformation on reactivity of monoclonal anti-peptide antibodies with a protein alpha-helix. Proc. Natl. Acad. Sci. U.S.A. **84**:8568–8572.
333. **MOORE GR**, **WILLIAMS RJP**. 1984. Protein antigenicity and protein mobility. Nature **312**:706–706.
334. **Oomen CJ**, **Hoogerhout P**, **Bonvin AMJJ**, **Kuipers B**, **Brugghe H**, **Timmermans H**, **Haseley SR**, **van Alphen L**, **Gros P**. 2003. Immunogenicity of peptide-vaccine candidates predicted by molecular dynamics simulations. Journal of Molecular Biology **328**:1083–1089.
335. **Li Y**, **Migueles SA**, **Welcher B**, **Svehla K**, **Phogat A**, **Louder MK**, **Wu X**, **Shaw GM**, **Connors M**, **Wyatt RT**, **Mascola JR**. 2007. Broad HIV-1 neutralization mediated by CD4-binding site antibodies. Nature Medicine **13**:1032–1034.
336. **Romero PA**, **Arnold FH**. 2009. Exploring protein fitness landscapes by directed evolution : Abstract : Nature Reviews Molecular Cell Biology. Nature Reviews Molecular Cell Biology.
337. **Bloom JD**, **Labthavikul ST**, **Otey CR**, **Arnold FH**. 2006. Protein stability promotes evolvability. Proc. Natl. Acad. Sci. U.S.A. **103**:5869–5874.
338. **Bloom JD**, **Wilke CO**, **Arnold FH**, **Adami C**. 2004. Stability and the evolvability of function in a model protein. Biophysical Journal **86**:2758–2764.

339. **Schuler B**, **Eaton WA**. 2008. Protein folding studied by single-molecule FRET. Current Opinion in Structural Biology **18**:16–26.
340. **Tokuriki N**, **Tawfik DS**. 2009. Protein dynamism and evolvability. Science **324**:203–207.
341. **Zimmerman AW**, **van Moerkerk HT**, **Veerkamp JH**. 2001. Ligand specificity and conformational stability of human fatty acid-binding proteins. Int. J. Biochem. Cell Biol. **33**:865–876.
342. **Jardine J**, **Julien J-P**, **Menis S**, **Ota T**, **Kalyuzhniy O**, **McGuire A**, **Sok D**, **Huang P-S**, **MacPherson S**, **Jones M**, **Nieusma T**, **Mathison J**, **Baker D**, **Ward AB**, **Burton DR**, **Stamatatos L**, **Nemazee D**, **Wilson IA**, **Schief WR**. 2013. Rational HIV immunogen design to target specific germline B cell receptors. Science **340**:711–716.
343. **Azoitei ML**, **Correia BE**, **Ban Y-EA**, **Carrico C**, **Kalyuzhniy O**, **Chen L**, **Schroeter A**, **Huang P-S**, **McLellan JS**, **Kwong PD**, **Baker D**, **Strong RK**, **Schief WR**. 2011. Computation-guided backbone grafting of a discontinuous motif onto a protein scaffold. Science **334**:373–376.